ORAL MICROBIOME AND INFLAMMATION CONNECTION TO SYSTEMIC HEALTH

EDITED BY: Tomomi Hashizume-Takizawa, Ana Carolina Morandini, Loreto Abusleme and Sinem Esra Sahingur

PUBLISHED IN: Frontiers in Cellular and Infection Microbiology

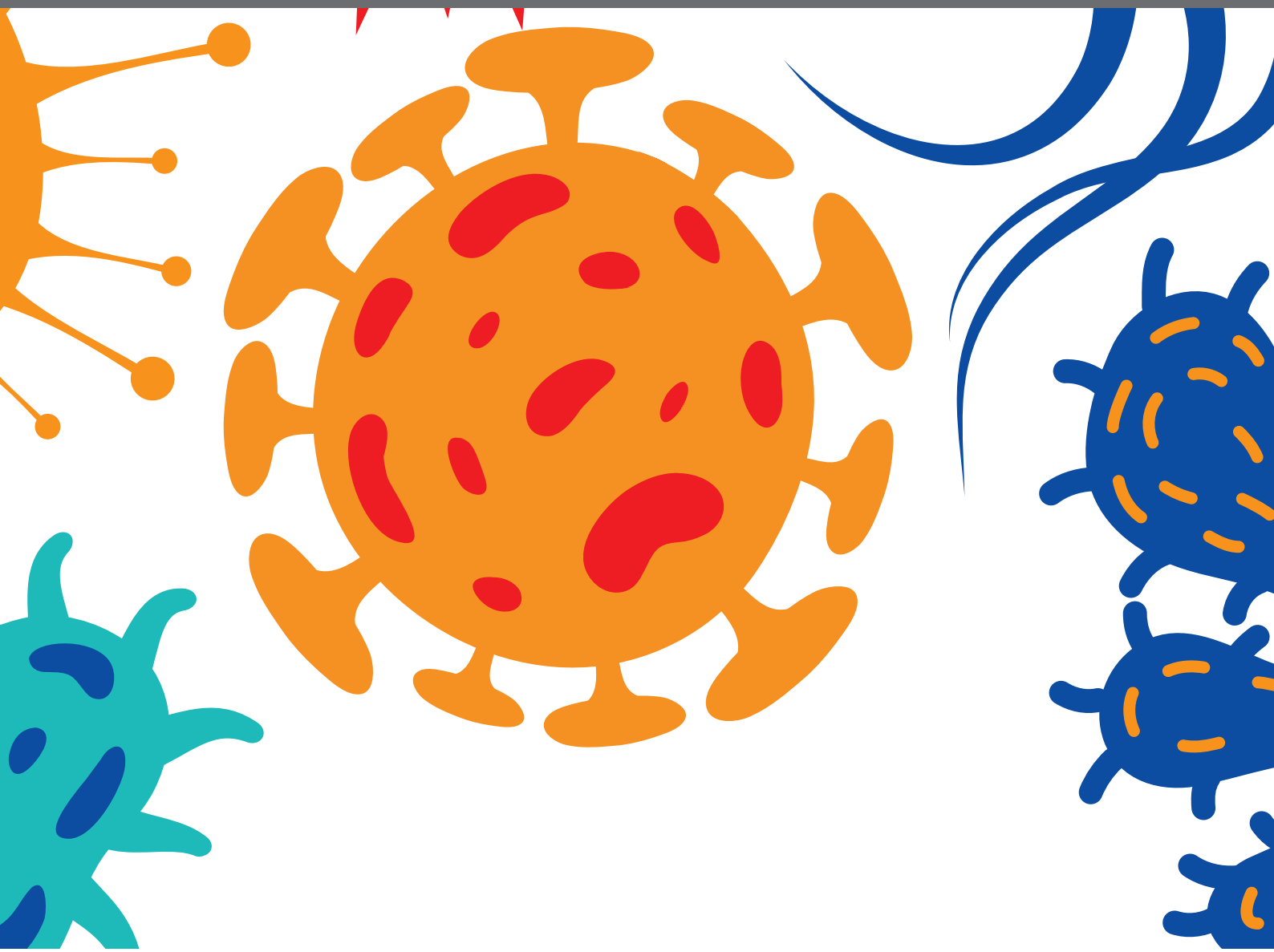

frontiers Research Topics

frontiers

ISSN 1664-8714
ISBN 978-2-88971-932-7
DOI 10.3389/978-2-88971-932-7

About Frontiers

Frontiers is more than just an open-access publisher of scholarly articles: it is a pioneering approach to the world of academia, radically improving the way scholarly research is managed. The grand vision of Frontiers is a world where all people have an equal opportunity to seek, share and generate knowledge. Frontiers provides immediate and permanent online open access to all its publications, but this alone is not enough to realize our grand goals.

Frontiers Journal Series

The Frontiers Journal Series is a multi-tier and interdisciplinary set of open-access, online journals, promising a paradigm shift from the current review, selection and dissemination processes in academic publishing. All Frontiers journals are driven by researchers for researchers; therefore, they constitute a service to the scholarly community. At the same time, the Frontiers Journal Series operates on a revolutionary invention, the tiered publishing system, initially addressing specific communities of scholars, and gradually climbing up to broader public understanding, thus serving the interests of the lay society, too.

Dedication to Quality

Each Frontiers article is a landmark of the highest quality, thanks to genuinely collaborative interactions between authors and review editors, who include some of the world's best academicians. Research must be certified by peers before entering a stream of knowledge that may eventually reach the public - and shape society; therefore, Frontiers only applies the most rigorous and unbiased reviews.
Frontiers revolutionizes research publishing by freely delivering the most outstanding research, evaluated with no bias from both the academic and social point of view. By applying the most advanced information technologies, Frontiers is catapulting scholarly publishing into a new generation.

What are Frontiers Research Topics?

Frontiers Research Topics are very popular trademarks of the Frontiers Journals Series: they are collections of at least ten articles, all centered on a particular subject. With their unique mix of varied contributions from Original Research to Review Articles, Frontiers Research Topics unify the most influential researchers, the latest key findings and historical advances in a hot research area! Find out more on how to host your own Frontiers Research Topic or contribute to one as an author by contacting the Frontiers Editorial Office: frontiersin.org/about/contact

ORAL MICROBIOME AND INFLAMMATION CONNECTION TO SYSTEMIC HEALTH

Topic Editors:
Tomomi Hashizume-Takizawa, Nihon University, Japan
Ana Carolina Morandini, Augusta University, United States
Loreto Abusleme, University of Chile, Chile
Sinem Esra Sahingur, University of Pennsylvania, United States

Citation: Hashizume-Takizawa, T., Morandini, A. C., Abusleme, L., Sahingur, S. E., eds. (2021). Oral Microbiome and Inflammation Connection to Systemic Health. Lausanne: Frontiers Media SA. doi: 10.3389/978-2-88971-932-7

Table of Contents

frontiers in Cellular and Infection Microbiology

EDITORIAL
published: 02 November 2021
doi: 10.3389/fcimb.2021.780182

Editorial: Oral Microbiome and Inflammation Connection to Systemic Health

Loreto Abusleme[1,2*†], *Ana Carolina Morandini*[3,4†], *Tomomi Hashizume-Takizawa*[5†] *and Sinem Esra Sahingur*[6†]

[1] Laboratory of Oral Microbiology, Department of Pathology and Oral Medicine, Faculty of Dentistry, University of Chile, Santiago, Chile, [2] Laboratory for Craniofacial Translational Research, Faculty of Dentistry, University of Chile, Santiago, Chile, [3] Department of Oral Biology and Diagnostic Sciences, Dental College of Georgia at Augusta University, GA, United States, [4] Department of Periodontics, Dental College of Georgia at Augusta University, GA, United States, [5] Department of Microbiology and Immunology, Nihon University School of Dentistry at Matsudo, Chiba, Japan, [6] Department of Periodontics, School of Dental Medicine, University of Pennsylvania, PA, United States

Keywords: oral bacteria, systemic diseases, inflammation, oral microbiome, dysbiosis

Editorial on the Research Topic

Oral Microbiome and Inflammation Connection to Systemic Health

OPEN ACCESS

Edited and reviewed by:
Ulvi Kahraman Gürsoy, University of Turku, Finland

***Correspondence:**
Loreto Abusleme
loreto.abusleme@odontologia.uchile.cl

[†]These authors have contributed equally to this work

Specialty section:
This article was submitted to Bacteria and Host, a section of the journal Frontiers in Cellular and Infection Microbiology

Received: *20 September 2021*
Accepted: *18 October 2021*
Published: *02 November 2021*

Citation:
Abusleme L, Morandini AC, Hashizume-Takizawa T and Sahingur SE (2021) Editorial: Oral Microbiome and Inflammation Connection to Systemic Health. Front. Cell. Infect. Microbiol. 11:780182. doi: 10.3389/fcimb.2021.780182

In recent years, our current understanding of the interplay between the oral microbiome and the host immune response has expanded considerably, becoming increasingly complex. Significant progress has been made towards studying how host microbial interactions can shape the clinical outcomes in health and disease. We now appreciate that these microbes are also taking part of diverse microbial assemblies inhabiting the oral cavity. One of the critical factors that has contributed to this knowledge is the wide utilization of next-generation sequencing techniques, which have allowed to unravel the complexity of oral microbial communities from a more ecological perspective. For instance, the study by Saito et al. utilizing a very large data-set of over 1,000 oral samples, have uncovered relevant differences between salivary and tooth-associated plaque microbial communities. They also showed that microbial diversity and abundance of *Treponema* and *Selenomonas* were increased as periodontal disease progresses and describe novel bacterial interactions during disease.

The influence of environmental factors on the oral microbiome has been a critical question in the field that continues to be interrogated. The study by Jia et al. examined the effect of cigarette smoking on the oral microbiota in a Chinese cohort of 316 healthy subjects. The results showed that smokers had significantly higher diversity and select bacterial species were associated with cigarette smoking. Further analyses showed increased levels of *Actinomyces* and *Veillonella* and expression of acid production-related pathways in smokers. The study concluded that cigarette smoking may affect oral health by creating an acidic environment that alters bacterial abundance and metabolic function.

We have also gained a much broader view of the importance of the oral microbiome and how its dysbiosis may play a crucial role in the pathogenesis of not only local diseases but in several systemic conditions. Huang et al. presented relevant data of the salivary microbiome of 293 patients with progressive histological stages of gastric carcinogenesis. Patients with gastric cancer had increased pro-inflammatory bacteria; whereas the genera *Haemophilus* and *Neisseria* were decreased, which may lead

to accumulation of carcinogens. Their findings suggest that oral bacteria may be involved in the pathogenesis of gastric carcinogenesis and propose potential diagnostic bacterial biomarkers for gastric cancer. Examining other systemic condition, He et al. showed how the oral microbial dysbiosis was associated with the pathogenesis of Immunoglobin A Nephropathy (IgAN), the most common type of glomerulonephritis. Data include the profile of the most abundant oral microbiota species in diseased patients *versus* controls indicating the shared and specific species between the two groups. The authors also showed correlative studies between oral microbiota and clinical sub-phenotypes of the disease defining predictive functional profiles that may be more associated with IgAN.

Translocation of oral microorganisms to distant sites is also another critical aspect that may constitute a direct mechanism by which select oral bacteria impact systemic health. In the study by Bordagaray et al. the authors reported the potential dissemination of bacteria associated with apical periodontitis to the bloodstream. *Porphyromonas* spp. were frequently detected in tissues and root canals exudates from apical lesions. Total bacteria and *P. endodontalis*, but not *P. gingivalis*, were detected in peripheral blood mononuclear cells (PBMCs) from patients, suggesting that *P. endodontalis* may disseminate from the apical lesion to the systemic bloodstream by PBMCs. On a related topic, the relationship of oral bacteria and the overall bone metabolism is starting to be explored. Hirohashi et al. addressed a technical issue in their study, regarding the possibility to use tetracycline as a fluorescent dye to evaluate bone loss caused by the tetracycline-sensitive oral bacteria, *Streptococcus mutans*. Their findings revealed that tetracycline can be utilized in the measurement of bone loss induced by drug-sensitive bacteria, and that *S. mutans* triggers a reduction of bone mass possibly by reducing bone formation activity.

The study of host-microbial interactions between oral microorganisms and stromal or immune cells is at the center of the mechanistic understanding of how select oral pathobionts play a role in the pathogenesis of oral and systemic conditions. Oral bacteria associated with periodontal diseases have been the most thoroughly characterized in a variety of pathological settings. *Porphyromonas gingivalis* is a prominent example, and the study by Elsayed et al. assessed the role of this organism in the vulnerability to senescence in human primary isolated gingival keratinocytes and bone marrow-derived dendritic cells (DCs) from young (yDCs) and old (oDCs) mice. The authors found increased senescence, impaired maturation of DCs and proliferation of $CD4^+$ T cells upon oDCs or yDCs+Pg stimulation. A characterization of exosomes of DCs (control and DCs+Pg) revealed a differential regulation of miRNAs in the *Pg* challenged group alongside an enrichment of the fimbrial adhesin protein mfa1 and pro-inflammatory cytokines. The study concluded that *P. gingivalis* can induce premature senescence through direct cellular invasion and by stimulating secretion of exosomes that promote paracrine immune senescence in bystander cells. Focusing on another periodontal organism, *Treponema denticola*, the study by Malone et al. evaluated the influence of this bacterium on the actin filaments of periodontal ligament (PDL) cells. The authors elegantly described mechanistic interactions between *T. denticola* and human PDL cells, showing that this periodontopathogen drives a pathological response characterized by upregulation of RASA4, depolymerization of actin filaments, and a subsequent increase in MMP-2 activity. Authors speculate that these contributions shed light on new potential targets for *T. denticola*-PDL interactions that may influence periodontal tissue homeostasis. The study of Li et al. examined the interplay of another periodontal bacteria, *Fusobacterium nucleatum* in combination with a recognized respiratory pathogen, *Pseudomonas aeruginosa*, and analyzed how these two organisms interacted with pulmonary epithelial cells. Co-infection of both organisms or pre-treatment with *F. nucleatum* resulted in increased bacterial invasion and inflammatory cytotoxicity of pulmonary epithelial cells. These findings provide novel insights on the mechanisms behind the deterioration of lung function associated to these two organisms.

We would like to thank all authors in this collection for their valuable contributions. We hope this Research Topic continues to stimulate the generation of new knowledge dedicated to unravel influence of the oral microbiome on systemic health.

AUTHOR CONTRIBUTIONS

All authors listed have made a substantial, direct, and intellectual contribution to the work and approved it for publication.

FUNDING

This work was funded in part by ANID/Chilean National Fund for Scientific and Technologic Development (FONDECYT), grant #11180505 (to LA), and grants R01DE025037 and R01DE027374 from the National Institute of Dental and Craniofacial Research/National Institutes of Health (to SES).

Conflict of Interest: The authors declare that the research was conducted in the absence of any commercial or financial relationships that could be construed as a potential conflict of interest.

frontiers in Cellular and Infection Microbiology

ORIGINAL RESEARCH
published: 29 January 2021
doi: 10.3389/fcimb.2020.604596

Oral Microbiome Analysis in Prospective Genome Cohort Studies of the Tohoku Medical Megabank Project

Sakae Saito[1], Yuichi Aoki[1,2], Toru Tamahara[1,3], Maki Goto[1], Hiroyuki Matsui[1,3], Junko Kawashima[1], Inaho Danjoh[1,4], Atsushi Hozawa[1,4], Shinichi Kuriyama[1,4,5], Yoichi Suzuki[1,6], Nobuo Fuse[1,4], Shigeo Kure[1,4], Riu Yamashita[1,7], Osamu Tanabe[1,8], Naoko Minegishi[1,4,9], Kengo Kinoshita[1,2,9], Akito Tsuboi[1,3,4], Ritsuko Shimizu[1,4] and Masayuki Yamamoto[1,4,9]**

[1] Tohoku Medical Megabank Organization, Tohoku University, Sendai, Japan, [2] Graduate School of Information Sciences, Tohoku University, Sendai, Japan, [3] Graduate School of Dentistry, Tohoku University, Sendai, Japan, [4] Graduate School of Medicine, Tohoku University, Sendai, Japan, [5] International Research Institute of Disaster Science, Tohoku University, Sendai, Japan, [6] Department of Clinical Genetics, Ageo Central General Hospital, Ageo, Japan, [7] Exploratory Oncology Research & Clinical Trial Center, National Cancer Center, Kashiwa, Japan, [8] Biosample Research Center, Radiation Effects Research Foundation, Hiroshima, Japan, [9] Advanced Research Center for Innovations in Next-Generation Medicine, Tohoku University, Sendai, Japan

A baseline oral microbiome study of the Tohoku Medical Megabank Organization (TMM) was planned to characterize the profile of the oral microbiome in the Japanese population. The study also aimed to clarify risk factors for multifactorial diseases by integrated analysis of the oral microbiome and host genome/omics information. From 2013 to 2016, we collected three types of oral biospecimens, saliva, supragingival plaque, and tongue swab, from a total of 25,101 participants who had a dental examination in TMM. In this study, we used two independent cohorts; the Community-Based Cohort and Birth and Three-Generation Cohort as discovery and validation cohorts, respectively, and we selected participants examined by a single dentist. We found through the 16S ribosomal RNA gene sequencing analysis of 834 participants of the Community-Based Cohort Study that there are differences in the microbial composition and community structure between saliva and plaque. The species diversities in both saliva and plaque were increased in correlation with the severity of periodontal disease. These results were nicely reproduced in the analysis of 455 participants of the Birth and Three-Generation Cohort Study. In addition, strong positive and negative associations of microbial taxa in both plaque and saliva with periodontitis-associated biofilm formation were detected by co-occurrence network analysis. The classes *Actinobacteria* and *Bacilli*, including oral health-associated bacterial species, showed a positive correlation in saliva. These results revealed differences in microbial composition and community structure between saliva

OPEN ACCESS

Edited by:
Tomomi Hashizume-Takizawa, Nihon University, Japan

Reviewed by:
Gena D. Tribble, University of Texas Health Science Center at Houston, United States
Toru Takeshita, Kyushu University, Japan

***Correspondence:**
Ritsuko Shimizu
rshimizu@med.tohoku.ac.jp
Masayuki Yamamoto
masiyamamoto@med.tohoku.ac.jp

Specialty section:
This article was submitted to Microbiome in Health and Disease, a section of the journal Frontiers in Cellular and Infection Microbiology

Received: *09 September 2020*
Accepted: *07 December 2020*
Published: *29 January 2021*

Citation:
Saito S, Aoki Y, Tamahara T, Goto M, Matsui H, Kawashima J, Danjoh I, Hozawa A, Kuriyama S, Suzuki Y, Fuse N, Kure S, Yamashita R, Tanabe O, Minegishi N, Kinoshita K, Tsuboi A, Shimizu R and Yamamoto M (2021) Oral Microbiome Analysis in Prospective Genome Cohort Studies of the Tohoku Medical Megabank Project. Front. Cell. Infect. Microbiol. 10:604596. doi: 10.3389/fcimb.2020.604596

and plaque and a correlation between microbial species and the severity of periodontal disease. We expect that the large database of the oral microbiome in the TMM biobank will help in the discovery of novel targets for the treatment and prevention of oral diseases, as well as for the discovery of therapeutic and/or preventive targets of systemic diseases.

Keywords: 16S ribosomal RNA, saliva, dental plaque, microbiome, periodontal disease, prospective cohort, oral health

INTRODUCTION

A prospective genome cohort study with long-term observational data for large healthy populations is a key activity to elucidate the pathogenesis of multigenic and multifactorial diseases (Donnelly, 2008; McCarthy et al., 2008; Plomin et al., 2009). Multifactorial diseases developed by an interaction between genetic and environmental factors are common in the general population and account for many chronic diseases (Plomin et al., 2009). The Tohoku Medical Megabank (TMM) project was established to conduct large-scale prospective genome cohort studies in Miyagi and Iwate Prefectures after devastating damage resulted from the Great East Japan Earthquake in 2011. The project was conducted by the Tohoku Medical Megabank Organization (ToMMo) and Iwate Tohoku Medical Megabank Organization (IMM). The aim of this project is to contribute to the health maintenance of residents in the tsunami devastated area and to form a solid foundation of personalized healthcare by strategically constructing two prospective genome cohorts and an integrated biobank (Fuse et al., 2019).

We are conducting two prospective genome cohort studies in the TMM project (Kuriyama et al., 2016). One is a population-based cohort study called the TMM Community-Based Cohort Study (TMM CommCohort Study) targeting adult individuals (aged 20 and older), and this study recruited a total of 87,865 participants from 2013 to 2016 (Hozawa et al., 2020). The other is a birth and three-generation cohort study called the TMM Birth and Three-Generation Cohort Study (TMM BirThree Cohort Study), which has a family-based prospective study design, including newborns and their parents, siblings, grandparents, and extended family members. In the TMM BirThree Cohort Study, we recruited 73,529 participants, including 22,493 mothers and 23,143 newborn children, from 2013 to 2017 (Kuriyama et al., 2019).

In the TMM biobank, all biospecimens and clinical information collected from cohort participants have been registered and rendered for systematic storage. The TMM biobank aims to be an integrated biobank in which ordinal analyses are conducted by an analytical center affiliated with the biobank. At first, data are shared by the users, and if samples are still necessary, the biobank shares biological samples. Therefore, multiomics analyses, such as genomics, transcriptomics, epigenomics, proteomics and metabolomics, have been performed using these biospecimen resources in the biobank (Takai-Igarashi et al., 2017; Minegishi et al., 2019). By 2019, ToMMo performed whole-genome sequencing of over 80,000 participants and constructed a Japanese whole-genome reference panel that provides information on the frequency of genetic variations in the Japanese population (Tadaka et al., 2018; Yasuda et al., 2019).

Based on the Japanese genome reference panel data, we designed a custom single nucleotide polymorphism (SNP) array aiming to conveniently collect the SNP genotype data for all cohort participants by means of microarray technology. ToMMo has also been conducting a comprehensive metabolome analysis of blood plasma and has finished the analysis of approximately 15,000 participants (Koshiba et al., 2018). The multiomics data analyzed in the TMM project are available in a public database, the Japanese Multi Omics Reference Panel (jMorp), which provides comprehensive information on human life sciences (Tadaka et al., 2018).

As part of the TMM cohort study, we planned to clarify how symbiotic microbiota influences our health and wellness. Therefore, a large-scale human microbiome analysis was conducted to identify profiles of symbiotic microbiota, which are environmental factors in the human body. The human microbiome, which is one of the regulatory factors determining our body constitution and disease susceptibility, varies significantly, depending on the population and living environment. Recently, the integrated Human Microbiome Project (iHMP) explored the temporal dynamics of the microbiome and host by a multiomics approach and described the interrelationship between microbiota and diseases, including diabetes (Zhou et al., 2019) and inflammatory bowel disease (Lloyd-Price et al., 2019), and preterm birth (Fettweis et al., 2019).

In this study, we focused on the oral microbiome, the second largest and diverse microbiota harboring more than 700 species of bacteria (Kilian, 2018), and developed an oral metagenomics as one of the TMM multiomics analysis pipelines. The oral microbiota has been shown to be involved in the onset of various oral diseases, such as caries, periodontal disease, and cancer, by producing various noxious metabolites in the oral cavity (Willis and Gabaldón, 2020). Oral microbiomes seem to play critical roles in modulating the host response not only in the oral cavity but also in the whole body by acting as pathogens and/or changing metabolic pathways in the host (Leishman et al., 2012; Zheng et al., 2015). Accumulating lines of evidence support the notion that oral microbiota are closely related to systemic diseases (Graves et al., 2019; Willis and Gabaldón, 2020), including rheumatoid arthritis (Chen et al., 2018), adverse pregnancy outcomes (Cobb et al., 2017), and cardiovascular disease (Bryan et al., 2017). Therefore, comprehensive analysis of the microbiome together with the host genome and metabolome is a cutting-edge strategy for public health surveillance and disease risk prediction.

In this report, we introduce how we have conducted a baseline oral microbiome study in the ToMMo project. We also present the results of 16S ribosomal RNA (rRNA) gene analysis using saliva and plaque of 1,289 cohort participants, in which 834 were from the TMM CommCohort Study, and 455 were from the TMM BirThree Cohort Study. The former and the latter were exploited as discovery and validation cohorts, respectively. Our datasets revealed the differences in microbial composition and community structure between saliva and plaque and indicate the correlation between microbial species in saliva and the severity of periodontal disease.

MATERIALS AND METHODS

Study Population, Design, and Samples

The cohort studies of the TMM project were approved by the ethics committees of Tohoku University and Iwate Medical University. The ToMMo baseline oral microbiome study was approved by the ethics committee of Tohoku University. All adult participants signed an informed consent form, and informed consent was obtained from a parent of minors.

We recruited participants from the baseline oral microbiome study at seven Community Support Centers in Miyagi Prefecture. On the day of the visit, participants completed an informed consent form, physiological measurements, oral examination and biospecimen collection. The details of all assessments, collections, and measurements were as previously reported (Kuriyama et al., 2016; Hozawa et al., 2020). We organized a team of 133 dentists who were given specific instructions regarding the oral examination methods in the ToMMo cohort studies. Details of oral examinations included dental and periodontal statuses, including third molar, occlusal, and oral hygiene statuses, conditions of soft tissue, frenal attachment, oral tori, and temporomandibular junction function.

A dental questionnaire was administered as reported (Tsuboi et al., 2020). Supragingival plaques were collected from right and left molar teeth [#16 and #26 under the Fédération Dentaire Internationale (FDI) Two-Digit system] by a sterile Gracey curette and suspended in 1 ml saline in a standardized tube. If the index first molar was missing, the sample was obtained from the second molar teeth instead. If both the first and second molars were absent, the sample was collected from the premolar teeth closest to the missing index teeth. Up to 2 ml of unstimulated whole mouth saliva was collected into a 50-ml sterile tube. A tongue swab specimen was collected from the surface of the tongue using a spoon-shaped plastic scraper, and then the scraper was dipped into 1 ml saline in a standard tube. Collection was conducted between 9 am and noon or 1 pm and 4 pm, and biospecimens were immediately frozen at -80°C.

Oral supragingival plaque, saliva and tongue swab biospecimens were transported on dry ice to the TMM biobank located at Tohoku University and immediately deidentified (Takai-Igarashi et al., 2017). Saliva was thawed once at 4°C and divided into half if there were more than 200 µl. One-half of the saliva was centrifuged at 3,000 × g for 10 min in a microcentrifuge tube and separated into the cell-free supernatant saliva and the cell containing sediment. Six types of oral biospecimens, *i.e.*, whole saliva without centrifugation, supernatant saliva, salivary sediment, supragingival plaque from right molar teeth, supragingival plaque from left molar teeth and tongue swab, were registered in the TMM biobank and stored at -80°C. LabVantage laboratory information management system (LIMS) (ver. 6 and ver. 8; LabVantage Solutions, Somerset, NJ) was used to manage the biospecimen information and to leave audit trails in the TMM biobank.

Oral Microbiome Analysis

To analyze the saliva and plaque microbiota, we selected participants who met the following criteria: *i*) aged between 45 and 69 years, *ii*) had more than 20 teeth, and *iii*) underwent a dental examination and biospecimen collection by one dentist at the Sendai Community Support Center. In this study, we selected samples collected by one dentist. Therefore, unexpected variation of data derived from differences in minor maneuver seemed to be prevented. Of the 1,919 participants that met these three criteria, 1,349 participants were randomly selected for the microbiome analysis. There were 1,349 and 1,345 analyzed samples for supragingival plaque from right molar teeth and whole saliva, respectively. In this study, we defined four severity categories of periodontal disease by the percentage of teeth with periodontal pocket depth (PPD) ≥ 4 mm: healthy (0%), mild (> 0% and ≤ 20%), moderate (> 20% and ≤ 50%), and severe (> 50%).

Amplification and Sequencing

The composition and diversity of the oral microbiome were assessed by high-throughput sequencing of 16S rRNA gene amplicons by using the Illumina MiSeq Platform (Illumina, Inc., San Diego, CA). The plaque and saliva samples from 1,349 participants were subjected to DNA extraction using the PowerSoil DNA Isolation Kit (MO BIO, Carlsbad, CA) according to the manufacturer's protocol. Sequencing libraries were prepared using a two-step PCR method for targeting the V4 region (typically 258 or 259 bp) of the 16S rRNA gene as previously described (Sato et al., 2015). In brief, the first PCR was conducted using gene-specific primers, followed by the second PCR using separate indexing primers that fused Illumina sequencing adaptors plus dual barcodes to the sample amplicons. Ex Taq DNA Polymerase (TaKaRa Bio Inc., Japan) was used for PCR amplification. The pooled library was then quantified using the Qubit 2.0 Fluorometer and dsDNA HS Assay Kit (Life Technologies, Carlsbad, CA) and diluted to a final concentration of 12 pM with 50% PhiX. Sequencing was performed using the MiSeq Reagent Kit v3 (Illumina, Inc.) by a 300 bp paired-end sequencing protocol according to the manufacturer's instructions, and 28.15 million paired-end reads were obtained in total. The samples had a mean read pair count of 20,934 and 22,228 and a maximum read pair count of 66,325 and 76,399 in saliva and plaque, respectively.

Amplicon Sequence Variants

Sequence data for the 16S rRNA gene amplicons were analyzed using the QIIME2 platform, version 2018.11 (Bolyen et al., 2019).

For all paired reads, the first 20 bases of both sequences were trimmed to remove primer sequences, the bases after position 200 were truncated to remove low-quality sequence data, and potential amplicon sequencing errors were corrected using DADA2 (Callahan et al., 2016) to produce an amplicon sequence variant (ASV) dataset. The resultant ASVs were aligned using MAFFT (Katoh and Standley, 2013) and then used to construct a phylogenetic tree with FastTree2 (Price et al., 2010).

The α- and β-diversity metrics were estimated from a subsampled ASV dataset, with 10,000 sequences per sample. Each ASV was identified using a Naïve Bayes classifier trained on 16S rRNA gene sequences from the Greengenes dataset (release 13_8) (Bokulich et al., 2018). All reads were assigned to total 232 and 259 ASVs at the species level in saliva and plaque, respectively.

Principal coordinate analysis (PCoA) and other statistical analyses were performed using custom R and Python scripts. ASVs detected one or more times in less than 500 samples were defined as minor. The dataset of 1,289 participants who had over 10,000 high-quality reads per person in the saliva and plaque, excluding withdrawal of the consent before February 3, 2020, have been released in the jMorp database (https://jmorp.megabank.tohoku.ac.jp/) and the Integrated Database of Tohoku Medical Megabank (dbTMM; http://www.dist.megabank.tohoku.ac.jp/index.html).

Statistics

All statistical analyses were performed using R 3.5.3 (https://www.r-project.org/) or SAS 9.4 software (SAS Institute Inc., Cary, NC). Probability values $p < 0.05$ were considered to indicate statistical significance. Co-occurrence network analysis was performed based on the relative abundance of ASVs using Cytoscape 3.7.2 software (http://www.cytoscape.org/). Nodes and edges were filtered by correlation value (Spearman's correlation coefficient ≥ 0.4 or ≤ -0.4, $p < 0.05$) and visualized.

RESULTS

Study Design and Sample Collection

The ToMMo baseline oral microbiome study was performed on the participants of the TMM cohort studies. During the first half of the baseline survey (October 2013–May 2016), this study targeted more than 25,000 participants who received a dental checkup either in the TMM CommCohort Study or in the TMM BirThree Cohort Study. The oral cavity has various microbial habitats, such as teeth, buccal mucosa, soft and hard palates, and tongue, each of which forms a species-rich unique microbiota (Kilian, 2018).

In the ToMMo baseline oral microbiome study, we recruited participants at seven Community Support Centers (Kesennuma, Osaki, Ishinomaki, Tagajo, Sendai, Iwanuma, and Shiroishi) in Miyagi Prefecture, which were established for the voluntary recruitment and health assessment of participants. On the day of the visit, participants completed an informed consent form and physiological measurements, oral examination and biospecimen collection were performed as reported (Kuriyama et al., 2016; Hozawa et al., 2020). A comprehensive whole mouth oral examination was performed by trained dentists, and details of oral examinations and dental questionnaires were as previously reported (Tsuboi et al., 2020).

We aimed to obtain three types of oral biospecimens, *i.e.*, saliva, dental plaque, and tongue swab, from participants. Saliva contains microbiota exfoliated from various habitats of the oral cavity and is a suitable sample for evaluating the entire oral microbiome. Dental plaque exists close to the foci of caries and periodontal diseases, two major diseases of the oral cavity, and is deeply involved in the development and progression of these diseases. The tongue is the largest microbial habitat in the oral cavity, and various kinds of microbial species, both aerobic or anaerobic, inhabit the tongue coating. Therefore, we collected supragingival plaque from right and left molar teeth, unstimulated whole mouth saliva, and tongue swab specimens from a total of 25,101 participants in this study (**Table 1**). These collections were conducted by trained dentists, and biospecimens were immediately frozen at -80°C. These oral biospecimens were transported to the TMM biobank and immediately deidentified (Takai-Igarashi et al., 2017).

The age distribution of the participants is shown in **Figure 1A**. The average age was 54.9 ± 15.1 years, with a range from 5 to 90 years, and the group of participants aged 61–70 years was the largest, accounting for 33.3% of the participants. There were 17,263 and 7,751 participants in the TMM CommCohort Study and in the TMM BirThree Cohort Study, respectively (**Figure 1B**).

Several studies have reported that the human microbiota varies greatly by geographical location and/or ethnicity (Gupta et al., 2017). Therefore, constructing a Japanese reference database covering the microbiota inhabiting multiple sites in the oral cavity is important for research on diseases affected by oral microbiota in the Japanese population. In particular, this database is essential for studying oral diseases. To analyze the saliva and plaque microbiotas, we randomly selected 1,349 participants from 1,919 participants who met the following criteria: *i*) between 45 and 69 years of age, *ii*) more than 20 teeth and *iii*) underwent a dental examination and biospecimen collection by one dentist at the Sendai Community Support Center.

TABLE 1 | Overview of the oral biospecimens in the ToMMo baseline oral microbiome study.

		Number of times to visit to the Community Support Centers			
		1st visit	2nd visit	3rd visit	Total
Participants with oral biospecimens		25,014	86	1	25,101
Saliva	Whole	24,868	85	1	24,954
	Supernatant	24,423	83	0	24,506
	Sediment	24,464	84	0	24,548
Supragingival plaque	Right molar tooth	24,889	82	1	24,972
	Left molar tooth	24,876	82	1	24,959
Tongue swab		24,988	82	1	25,071

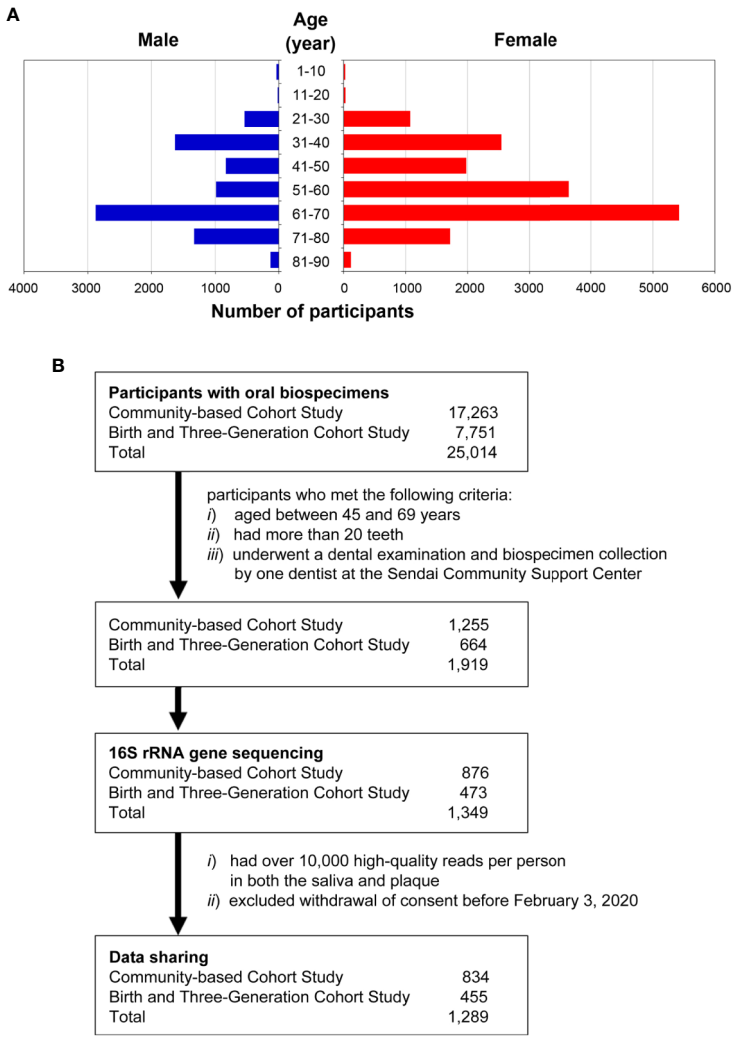

FIGURE 1 | Overview of the participants in the ToMMo baseline oral microbiome study. **(A)** Sex and age distribution of the participants (n = 24,913) in the ToMMo baseline oral microbiome study. Of the 25,014 individuals from which oral biospecimens were collected, 101 were excluded due to missing information regarding gender, date of birth, or dental examination. **(B)** Number of participants registered in the TMM CommCohort Study and in the TMM BirThree Cohort Study. The flow chart shows the criteria for selecting the participants whose data were analyzed by 16S rRNA gene sequencing.

There were 1,349 and 1,345 analyzed samples for supragingival plaque from right molar teeth and whole saliva, respectively. We designed two-phase discovery and validation analyses to identify microbial taxa of interest for oral disease states using two closely related but independent cohorts: the TMM CommCohort Study as the discovery cohort and the TMM BirThree Cohort Study as the validation cohort. Of the 1,349 analyzed participants, 876 participants were from the TMM CommCohort Study, and 473 participants were from the TMM BirThree Cohort Study (**Figure 1B**).

Species Diversity (α-Diversity) Correlates With Periodontal Disease Severity in Oral Microbiota

With the aim of building a database of the human microbiome in the TMM project, we established a new pipeline for microbiome 16S rRNA gene analysis by improving the methods used in previous oral microbiome studies (Sato et al., 2015; Yamagishi et al., 2016). As described in the previous section, we analyzed the microbiota of saliva and plaque obtained from 1,349 TMM cohort participants as the first trial to compare their profiles. To determine whether all the ASVs present in the dataset were recovered in the 16S amplicon sequencing, we carried out rarefaction analysis (**Figure 2A** and **Supplementary Figure S1**). After quality checks and subsampling, we obtained 10,000 high-quality reads in both the saliva and plaque samples of the 1,289 participants (519 males and 770 females, mean age 60.16 ± 6.39 years). The clinical characteristics of 834 participants from the TMM CommCohort Study (discovery cohort) and 455 participants from the TMM BirThree Cohort Study (validation cohort) are described in **Tables 2** and **3**, respectively.

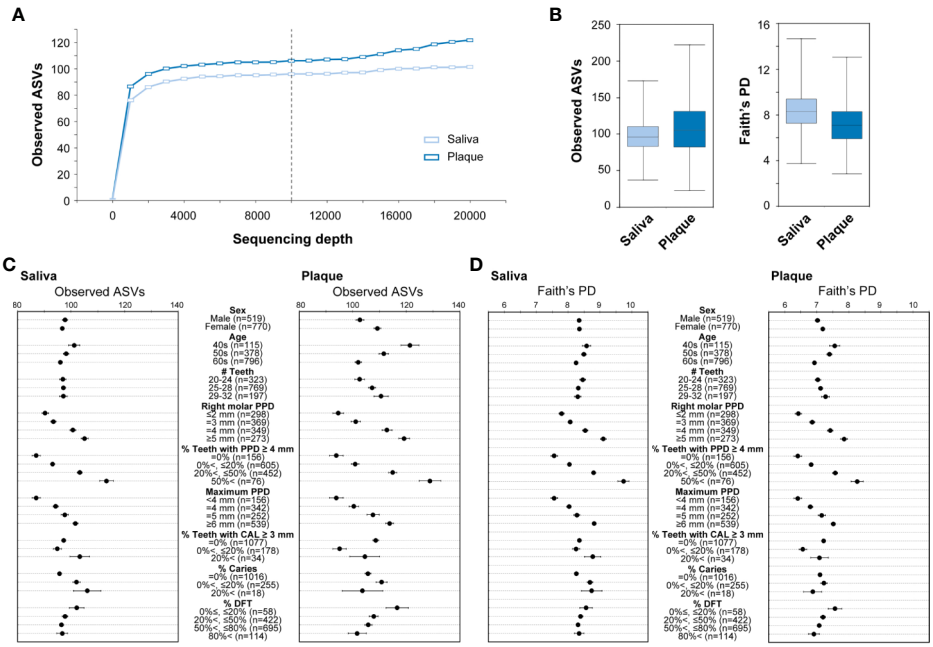

FIGURE 2 | The α-diversity of the microbiota in saliva and plaque. **(A)** Rarefaction curves based on the observed ASVs. The colors indicate sample type: saliva (light blue) and plaque (blue). The vertical black dashed line indicates the 10,000-read rarefaction threshold. **(B)** The α-diversity in saliva and plaque. The box plots show two different indices: the number of observed ASVs (left) and Faith's phylogenetic diversity (right). Data obtained from 1,289 participants in the TMM CommCohort Study and the TMM BirThree Cohort Study were analyzed and used for discovery and validation, respectively. **(C, D)** Number of observed ASVs **(C)** and Faith's phylogenetic diversity **(D)** compared under the indicated conditions. The dots indicate the means; the error bars indicate the standard errors (SEs). PD, phylogenetic diversity; PPD, periodontal pocket depth; CAL, clinical attachment level; DFT, decayed and filled teeth.

TABLE 2 | Dental characteristics of the study population in the TMM CommCohort Study.

Periodontal Disease Severity	Healthy	Mild	Moderate	Severe
# Participants	110	399	287	38
Age (Years)				
Mean ± S.D.	53.3 ± 7.1	60.1 ± 6.8	59.9 ± 6.6	59.9 ± 6.1
Sex				
Female	72	262	179	22
Male	38	137	108	16
# Teeth				
Mean ± S.D.	26.3 ± 2.7	26.3 ± 2.5	26.1 ± 2.7	25.1 ± 3.1
# Teeth with PPD ≥ 4 mm				
Mean ± S.D.	0	2.7 ± 1.4	7.8 ± 2.1	16.0 ± 3.4
# DFT				
Mean ± S.D.	14.1 ± 5.2	14.4 ± 4.9	14.5 ± 4.6	12.7 ± 5.1

S.D., standard deviation; PPD, periodontal pocket depth; DFT, decayed and filled teeth.

We analyzed the species richness, which is often referred to as α-diversity, in the oral microbial communities by comparing the number of ASVs among the individuals. The α-diversity was calculated using combined data from the TMM CommCohort Study and the TMM BirThree Cohort Study. Each 10,000 high-quality reads from the saliva and plaque were employed to assign ASVs. There was considerably more intra-member variability in the ASV numbers in the plaque samples than in the saliva samples (**Figure 2B**). The influence of the ratio of teeth with deep pockets (PPD ≥ 4 mm), PPD of right molar and maximum PPD on the number of ASVs was statistically significant in both saliva and plaque samples, suggesting that the richness of oral bacterial communities was relevant to dental characteristics (**Figure 2C**).

To calculate the α-diversity, we employed Faith's phylogenetic diversity, which is one of the indices for α-diversity (Faith, 1992). We confirmed that the α-diversity was increased stepwise and that the increase was markedly correlated with the ratio of teeth with deep pockets in both saliva and plaque samples (**Figure 2D**). Our data also indicated that the phylogenetic diversity values were higher in younger individuals. The results were consistent with the results calculated by the

TABLE 3 | Dental characteristics of the study population in the TMM BirThree Cohort Study.

Periodontal Disease Severity	Healthy	Mild	Moderate	Severe
# Participants	46	206	165	38
Age (Years)				
Mean ± S.D.	59.4 ± 5.9	61.1 ± 5.5	60.4 ± 5.7	60.2 ± 6.2
Sex				
Female	30	101	90	14
Male	16	105	75	24
# Teeth				
Mean ± S.D.	26.4 ± 2.6	26.4 ± 2.7	25.9 ± 2.8	25.7 ± 2.9
# Teeth with PPD ≥ 4 mm				
Mean ± S.D.	0	2.7 ± 1.6	8.5 ± 2.2	16.5 ± 3.7
# DFT				
Mean ± S.D.	13.7 ± 4.8	13.8 ± 5.0	14.0 ± 5.3	12.7 ± 6.4

S.D., standard deviation; PPD, periodontal pocket depth; DFT, decayed and filled teeth.

Shannon diversity index and Pielou's evenness index for α-diversity metrics (**Supplementary Figure S2**). These results demonstrate that the increase in species diversity is a distinctive feature of oral microbiota accompanying periodontitis. This conclusion is consistent with that reported by Curtis et al., 2020.

According to the α-diversity analysis results, we decided to focus on the association of periodontal disease severity with microbial communities in the saliva and plaque. In this study, we defined the severity of periodontal disease based on the ratio of teeth with deep pockets (PPD ≥ 4 mm) as four classes: healthy (0%), mild (20% or less), moderate (higher than 20% and 50% or less), and severe (higher than 50%).

Significant Differences in Salivary and Plaque Microbiome Structures (β-Diversity)

We then analyzed the phylogenetic diversity among the oral microbiota structures, which is often referred to as β-diversity, in participants of the TMM CommCohort Study (discovery cohort; n = 834) using PCoA. We conducted PCoA by categorizing the discovery cohort participants into four severity categories (*i.e.*, healthy, mild, moderate, and severe) of periodontal disease depending on the scores shown in **Figure 2C**. As shown in **Figure 3**, the PCoA plot based on the weighted UniFrac distance displayed apparent differences between the saliva (middle panels) and plaque (lower panels) samples, while variations in the PCoA plot among the four severity categories were not found. We also analyzed the β-diversity of saliva and plaque microbiomes in participants of the TMM BirThree Cohort Study (validation cohort; n = 455) independently and found that the findings discovered in the TMM CommCohort Study were reproducible in the TMM BirThree Cohort Study (**Supplementary Figure S3**). These results indicate that the microbial community compositions differed notably between saliva and plaque samples, regardless of periodontal disease status.

Relative Microbial Abundance Differs in Saliva and Plaque

Comparison of relative microbial abundance at the phylum level indicates that the abundance ratios of the phylum *Firmicutes* (**Figure 4A**, blue) and the phylum *Actinobacteria* (green) were higher and lower, respectively, in saliva than in plaque, regardless of oral disease condition. This observation in saliva and plaque microbiomes was reproducible in participants of the TMM BirThree Cohort Study (**Figure 4B**).

Similarly, when we examined the relative microbial abundance at the family level, we found that the families *Neisseriaceae* (**Figure 4C**, pink) and *Fusobacteriaceae* (dark navy), both of which are known as resident bacteria in the oral cavity, were dominant in both saliva and plaque samples. The former was more abundant in saliva than in plaque, while the latter was more abundant in plaque than in saliva. Similarly, the relative abundances of the family *Prevotellaceae* (orange) and the family *Veillonellaceae* (light blue) were higher in saliva than in plaque. In addition, these two families in plaque samples showed a tendency to increase in participants with periodontal disease. Our results are consistent with the finding that periodontal disease was found frequently in a group with a higher ratio of the *Prevotellaceae* and *Veillonellaceae* families (Takeshita et al., 2009).

The dataset also showed that the relative abundances of the families *Leptotrichiaceae* (navy) and *Corynebacteriaceae* (green) were higher in plaque than in saliva. It has been reported that *Corynebacterium matruchotii* comprises the central filament of corn-cob formations in mature dental plaque and is involved in tartar formation (Paster et al., 2001). We also analyzed the β-diversity of saliva and plaque microbiomes in participants of the validation cohort, and these findings in the discovery cohort were substantially validated in the validation cohort (**Figure 4D**).

Changes in Microbial Abundance According to Periodontal Disease Severity

To address details of the dysbiotic nature of oral microbiota in periodontal disease severity, we then searched bacterial genera whose relative abundance was featured in one of the four categories of periodontal disease in either saliva or plaque samples. In the discovery cohort (the TMM CommCohort Study), a significant increase in the genera *Treponema* and *Selenomonas* was identified in our dataset (**Figures 5A, B**), and both of these genera are well known as periodontal disease-causing bacteria. The genus *Treponema* was significantly increased in saliva of the severe periodontal disease category

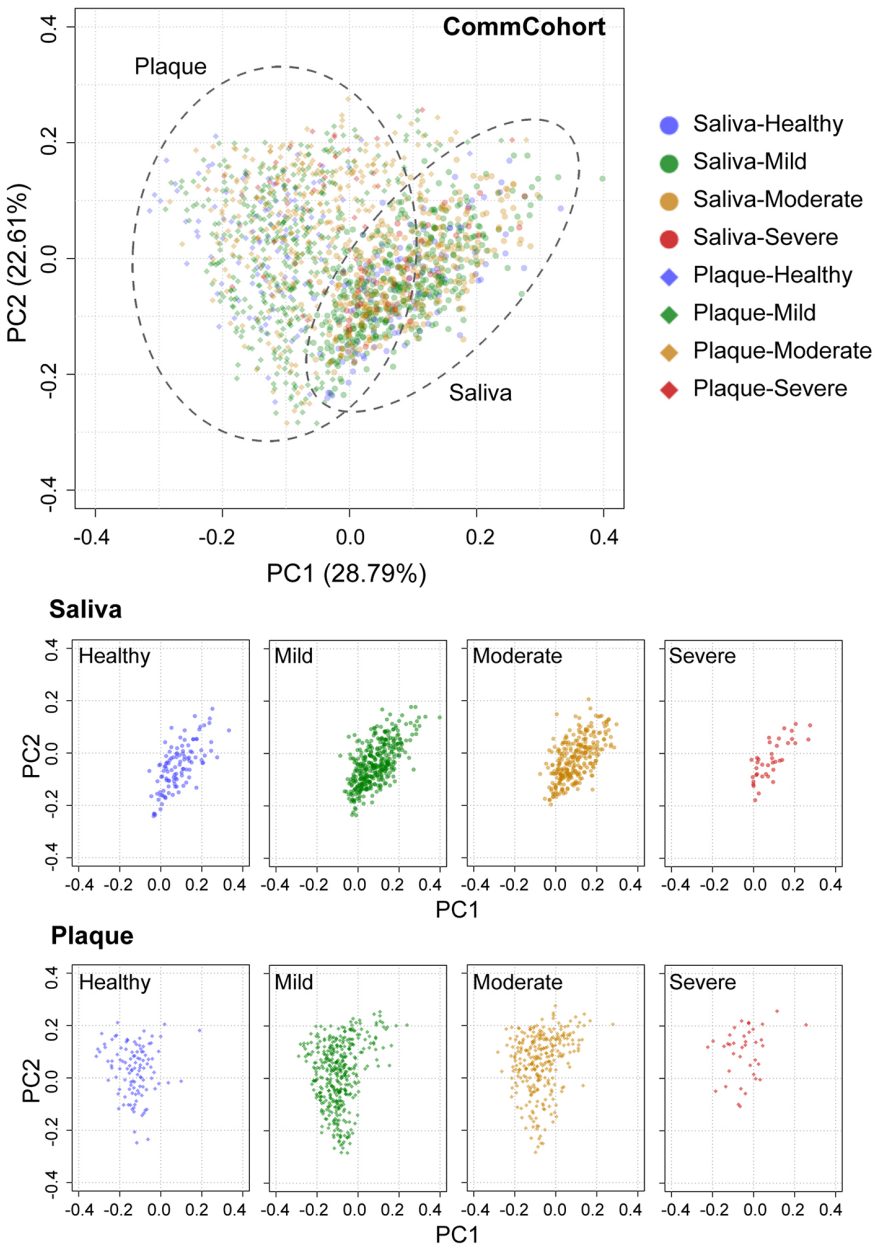

FIGURE 3 | PCoA plots of oral microbial communities in the TMM CommCohort Study based on weighted UniFrac distance. Each dot represents the microbial community in the saliva (circles, n = 834) and plaque (diamonds, n = 834) of one individual. The dots in the top panel were separated into eight groups by sample type, which are shown at the bottom. The severity of periodontal disease was classified into four categories based on the ratio of teeth with deep pockets: healthy (0%, blue), mild (> 0% and ≤ 20%, green), moderate (> 20% and ≤ 50%, yellow), and severe (> 50%, red).

and in plaque (**Figure 5A**). Of note, the genus *Treponema* contains *Treponema denticola*, which has been implicated as a key pathogen in periodontal disease (Holt and Ebersole, 2005). In contrast, the genus *Selenomonas* was significantly increased in plaque of the severe periodontal disease category (**Figure 5B**). In addition, the genera *Tannerella* and *Prevotella* also showed significant differences in relative abundance among the four severity categories in saliva and plaque, respectively (**Supplementary Figure S4**).

These results clearly demonstrate that relative microbiome abundance changes according to the severity of periodontal disease. Substantial changes can be observed at the family and genus levels. Of note, in certain cases, the directions of these changes are distinct in saliva and plaque; most significantly, at the genus level, the increase occurs preferentially in saliva (*Treponema*) or in plaque (*Selenomonas*). The results were reproducible in the microbiome data of the validation cohort (TMM BirThree Cohort Study) (**Figures 5C, D**).

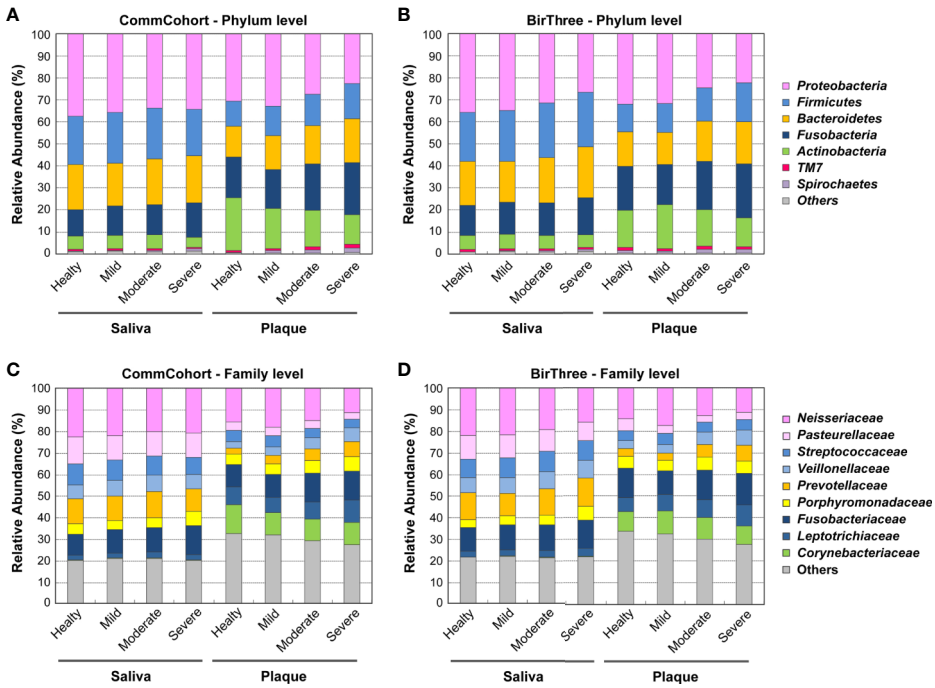

FIGURE 4 | Comparison of microbial composition in saliva and plaque. **(A, B)** Stacked bar plots showing the relative abundance of microbial taxa at the phylum level in the TMM CommCohort Study **(A)** and the TMM BirThree Cohort Study **(B)**. Data from these cohorts were used for discovery and validation, respectively. The labels indicate the phyla with mean relative abundances ≥ 2% in at least one group. The remaining phyla were binned together. **(C, D)** Stacked bar plots showing the mean relative abundances of microbial taxa at the family level in the TMM CommCohort Study **(C)** and the TMM BirThree Cohort Study **(D)**. The labels indicate the top 9 taxa at the family level, and the remaining families were binned together.

PCoA Plots of the Oral Microbial Community Based on Unweighted UniFrac Distance

The PCoA plot based on unweighted UniFrac distance, which emphasizes the abundance change in minor lineages, showed differences in the microbial community structure by sample type in the discovery cohort (TMM CommCohort Study) (**Figure 6**). The results show very good agreement with those based on the weighted UniFrac distance (**Figure 3**), but it should be noted that PCoA based on unweighted UniFrac distance revealed a distinct separation of the saliva samples that fall into two clusters according to the PC1 axis (**Figure 6**). We referred to the left and right clusters in saliva as clusters A and B, respectively. In contrast, only one component appeared in the PC1 axis of plaque samples. Similar results were obtained in saliva and plaque microbiotas in the validation cohort (TMM BirThree Cohort Study) (**Supplementary Figure S5**). Thus, the PCoA plot based on the unweighted UniFrac distance revealed abundance differences in minor lineages.

Association Between Severe Periodontal Disease and Minor Taxa in Saliva

When we filtered out the low frequency ASVs detected once or more in less than 500 samples to exclude minor taxa, PCoA dots concentrated on one cluster in saliva samples of the discovery and validation cohorts (**Supplementary Figures S6A** and **S6B**). However, as the PCoA plot based on the unweighted UniFrac distance revealed the abundance changes in minor lineages, we decided to examine whether there are unclassified bacteria in clusters A and B (**Figure 7**). While we found that the distribution of major bacterial classes was almost comparable in clusters A and B (**Supplementary Figure S7**), unclassified bacteria were detected almost exclusively in cluster A in saliva samples of nearly all participants. Unclassified bacteria were rarely found in cluster B. Thus, the existence of susceptible minor ASVs appears to contribute to the creation of an unusual cluster.

Since there are two clusters in the unweighted UniFrac distance matrix, we next focused on the differences in the two clusters of the saliva microbiome. Therefore, we evaluated the dental condition of participants in each cluster and found that the percentages of participants belonging to the severe periodontal disease categories were higher in cluster A (7.02% and 11.72%, respectively) than in cluster B (2.18% and 4.85%, respectively) both in the discovery cohort (TMM CommCohort Study) and the validation cohort (TMM BirThree Cohort Study) (**Figure 8A**). In the discovery cohort (TMM CommCohort Study), the odds ratio for the risk of having severe periodontal disease was adjusted as 5.26 (95% confidence interval (Cl) 2.15 to 12.86; $p = 0.0003$) in participants in cluster B compared to those in cluster A (**Figure 8B**). Similarly, the relative number of deep pockets was significantly higher in cluster A (0.18, median) than in cluster B (0.12, median) (**Figure 8C**). These results were

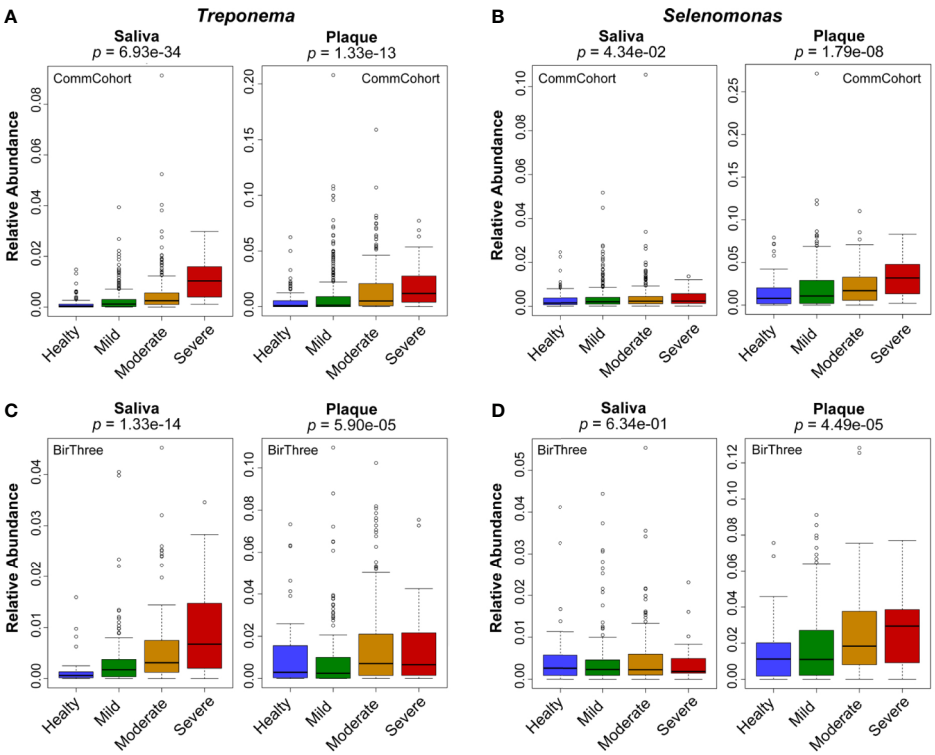

FIGURE 5 | Changes in relative microbial abundance at the genus level according to periodontal disease severity. Box plots showing the relative abundance of the genera *Treponema* **(A, C)** and *Selenomonas* **(B, D)** in saliva and plaque among the four severity categories of periodontal disease. Data from two independent cohorts, the TMM CommCohort Study **(A, B)** and the TMM BirThree Cohort Study **(C, D)**, were used for discovery and validation, respectively. The significance of the differences was estimated by using logistic regression analysis.

consistent in the validation cohort (TMM BirThree Cohort Study) (**Figures 8B, C**).

These results revealed that unknown bacteria are more enriched in cluster A than in cluster B in saliva and that participants with severe periodontal disease are more enriched in cluster A than in cluster B. Taken together, these results suggest the contribution of certain unknown bacteria in the unclassified fraction to the severity of periodontal disease, supporting the notion that novel microbes associated with oral diseases may reside in the unclassified fraction.

Microbiome Network and Community Structure

To examine the oral microbial ecology in saliva and plaque, we performed co-occurrence network analyses at the class level based on the relative abundance of ASVs. As shown in **Figures 9A, B**, we identified 18 microbial taxa that have correlative relationships in either or both saliva and plaque. In this figure, the direction and strength of correlations between two taxa are shown by the thickness of red (positive) or blue (negative) lines. The correlative relationships of the plaque microbiome are stronger than those of salivary microbiome.

In plaque, six microbial taxa, *i.e.*, the classes *Bacteroidia*, *Clostridia*, *Erysipelotrichi, Fusobacteriia*, *Spirochaetes*, and *Synergistia* were found to positively correlate with each other (**Figure 9A**). In particular, the classes *Bacteroidia* and *Spirochaetes*, showed the strongest positive correlation. The class *Bacteroidia* contains *Porphyromonas gingivalis* and *Tannerella forsythia*, which are very strong periodontal pathogen species together with *Treponema denticola* in the class *Spirochaetes* (Holt and Ebersole, 2005). When we analyzed the correlation of the relative abundance of the microbiome with the relative number of deep pockets, we found that these 6 microbial taxa were listed in the top 6 with a positive correlation (**Figure 9C**), indicating that these taxa proliferate concomitantly in periodontal disease conditions. In contrast, there were only weak correlations among microbial taxa in saliva (**Figure 9B**). We surmise that this is probably due to the composited microbiome structure derived from various oral surfaces.

The class *Synergistia* had a positive correlation with *Spirochaetes* in saliva and plaque and *Bacteroidia* in plaque. *Synergistia* is known to be anaerobic gram-negative bacteria that resides in sites of human disease, such as periodontal disease (Horz et al., 2006). It has been reported that *Synergistia* contains the species *Fretibacterium fastidiosum* and *Fretibacterium* sp. in human oral taxon 360, and both species have been isolated as common periodontitis-associated species

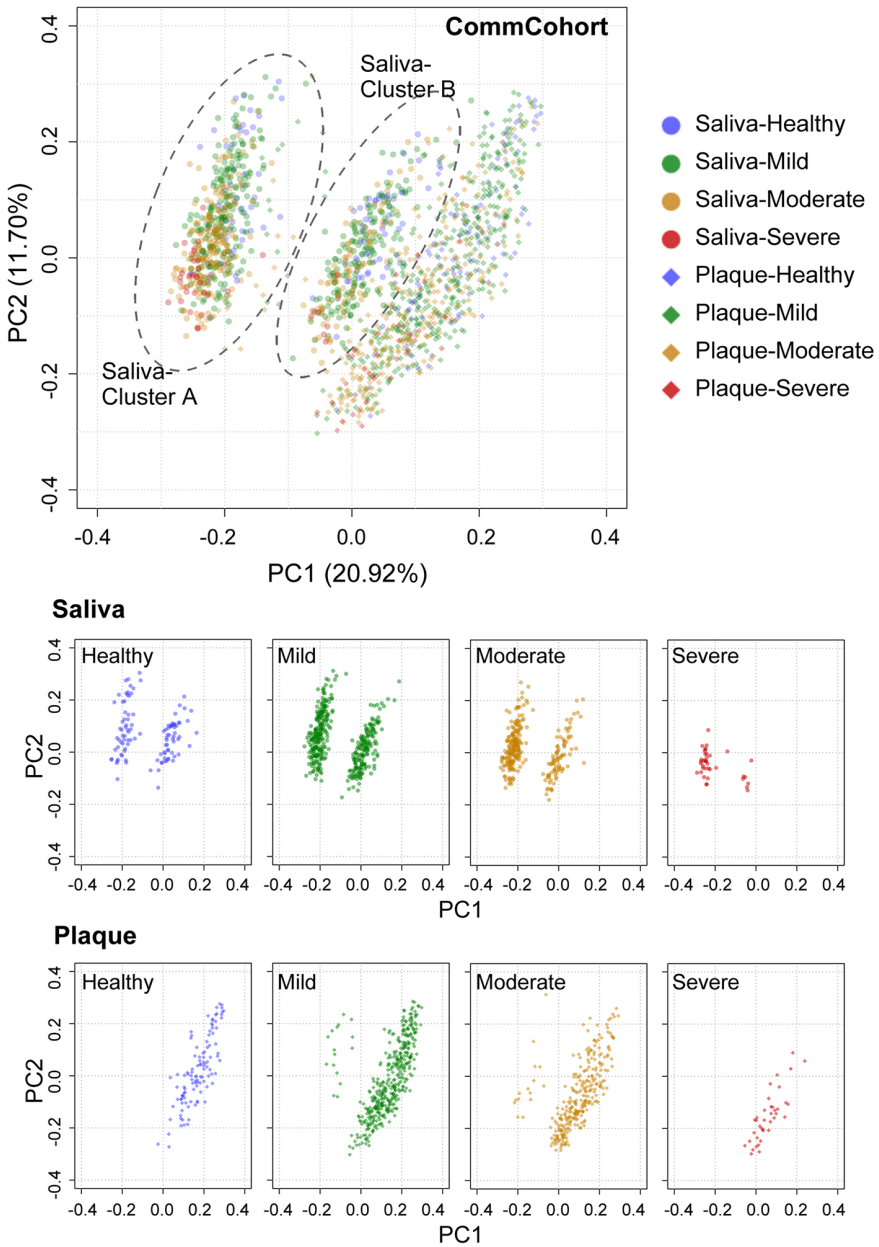

FIGURE 6 | PCoA plots of oral microbial communities in the TMM CommCohort Study based on unweighted UniFrac distance. Each dot represents the microbial community in the saliva (circles, n = 834) and plaque (diamonds, n = 834) of one individual. The dots in the top panel were separated into eight groups by sample type, which are shown at the bottom. A distinct separation of the saliva samples that fall into two clusters (cluster A and cluster B) according to the PC1 axis is shown. The severity of periodontal disease was classified into four categories based on the ratio of teeth with deep pockets: healthy (0%, blue), mild (> 0% and ≤ 20%, green), moderate (> 20% and ≤ 50%, yellow), and severe (> 50%, red).

by 16S rRNA gene sequencing in microbiome studies (Curtis et al., 2020). Indeed, correlation analysis of the relative abundance of *Synergistia* and the relative number of deep periodontal pockets showed a high correlation both in saliva and plaque (**Figures 9C, D**). The relative abundance of the other 7 taxa (*Deltaproteobacteria, Epsilonproteobacteria, TM7-3, Anaerolineae*, *Coriobacteriia*, *Methanobacteria*, and *RF3*) also showed a positive correlation with the relative number of deep pockets in plaque (**Figure 9C**), indicating that microbial species that were currently not identified as periodontal pathogens may also be present in these taxa. Current data showed that *Desulfomicrobium orale* in the class *Deltaproteobacteria* had a positive correlation with the ratio of deep pockets in plaque (**Supplementary Figure S8**).

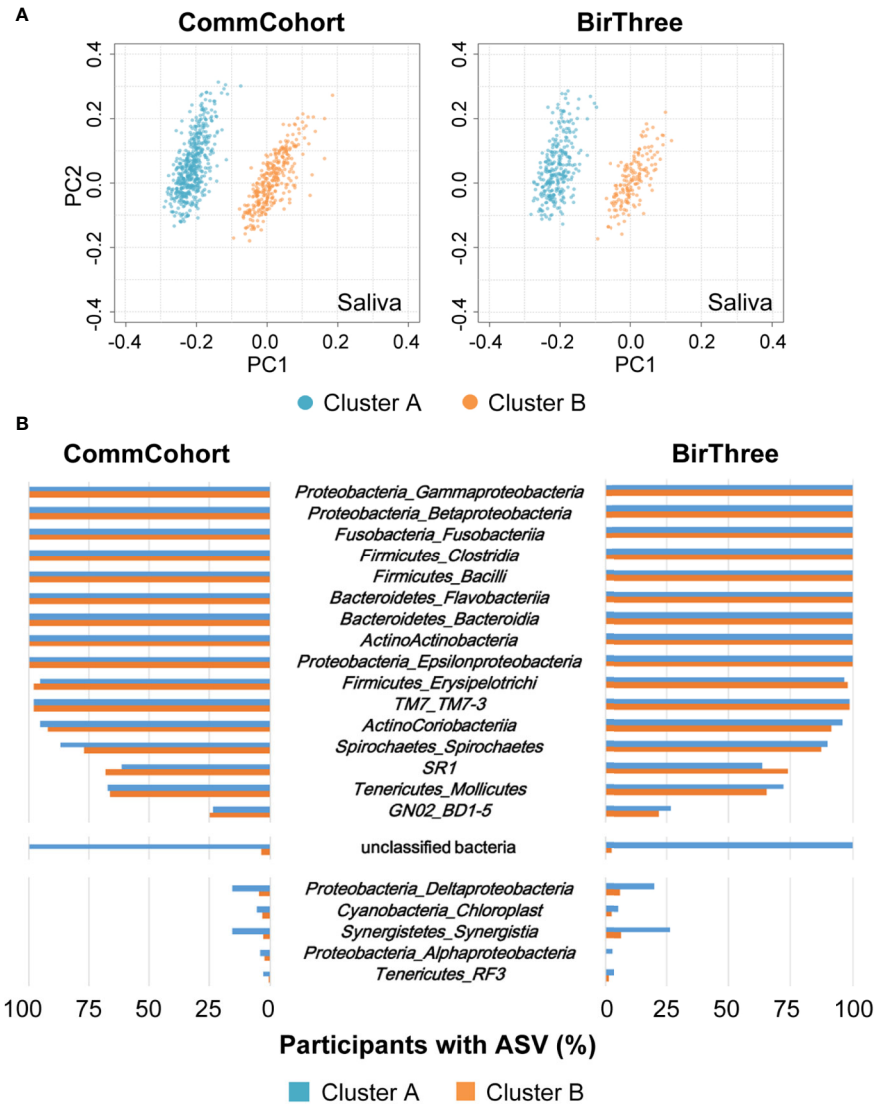

FIGURE 7 | Association between salivary microbiome clusters and minor taxa. **(A)** PCoA plots of the saliva microbial communities based on unweighted UniFrac distances in the TMM CommCohort Study (left) and the TMM BirThree Cohort Study (right). Two distinct clusters of the microbial community, one on the left (cluster A, light blue) and another on the right (cluster B, orange), are shown. **(B)** The bar graph shows the frequency at which the indicated microbial taxa were detected at the class level in the saliva samples from participants of the TMM CommCohort Study (left) and the TMM BirThree Cohort Study (right). Note that several unclassified bacteria were found in the participants in cluster A.

The class *Betaproteobacteria* exhibited a strong negative correlation with *Clostridia* in plaque and saliva and *Fusobacteriia* in plaque. In plaque, *Actinobacteria* and *Betaproteobacteria* showed a moderate negative correlation with *Bacteroidia* (**Figure 9A**). Stepwise plaque formation has been shown to be achieved by sequential colonization from early colonizers to late colonizers and red complex bacteria species, which consist of keystone periodontal pathogens involved in the onset of periodontal diseases (Socransky et al., 1998; Kolenbrander et al., 2010; Kirst et al., 2015). The relative abundance of the classes *Betaproteobacteria* and *Actinobacteria* showed a negative correlation with the relative number of deep pockets in plaque (**Figure 9C**), supporting the notion that this sort of taxa balance is associated with the progression of periodontal diseases.

DISCUSSION

As the oral cavity is the initial entry point of the gastrointestinal tract, the oral microbiome may be involved in the pathogenesis or progression of systemic diseases. In this study, we approached the oral microbiome study by using independent discovery (TMM CommCohort Study) and validation (TMM BirThree Cohort Study) cohorts and selected microbial taxa of interest for oral

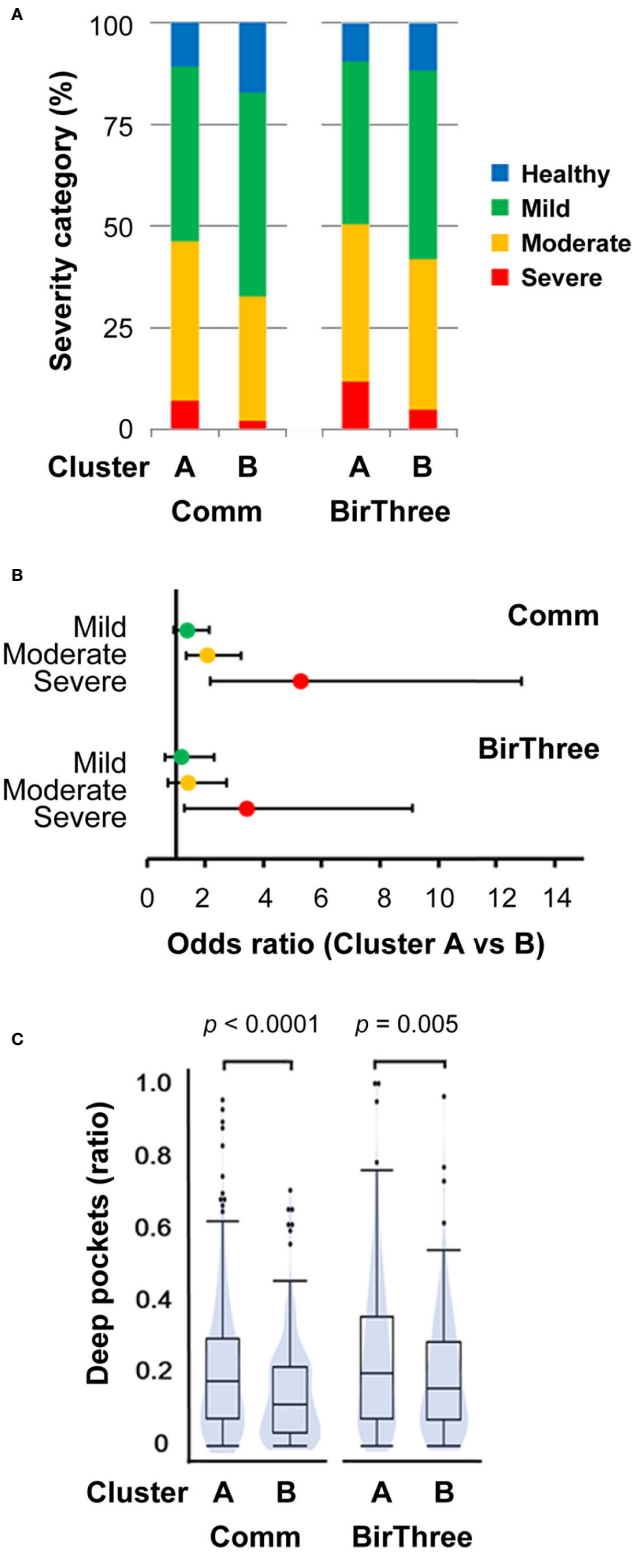

FIGURE 8 | Association between salivary microbiome cluster and periodontal disease severity. **(A)** Distribution of the four periodontal disease severity categories among participants in clusters A and B. **(B)** The odds ratios adjusted for age and the number of teeth with periodontal disease falling into each severity category (with 95% confidence intervals) for participants in cluster B compared to those in cluster A. **(C)** Violin plots of the relative number of deep pockets (≥ 4 mm). The significance of the differences was estimated by using unpaired Student's t-tests. Comm, TMM CommCohort Study; BirThree, TMM BirThree Cohort Study.

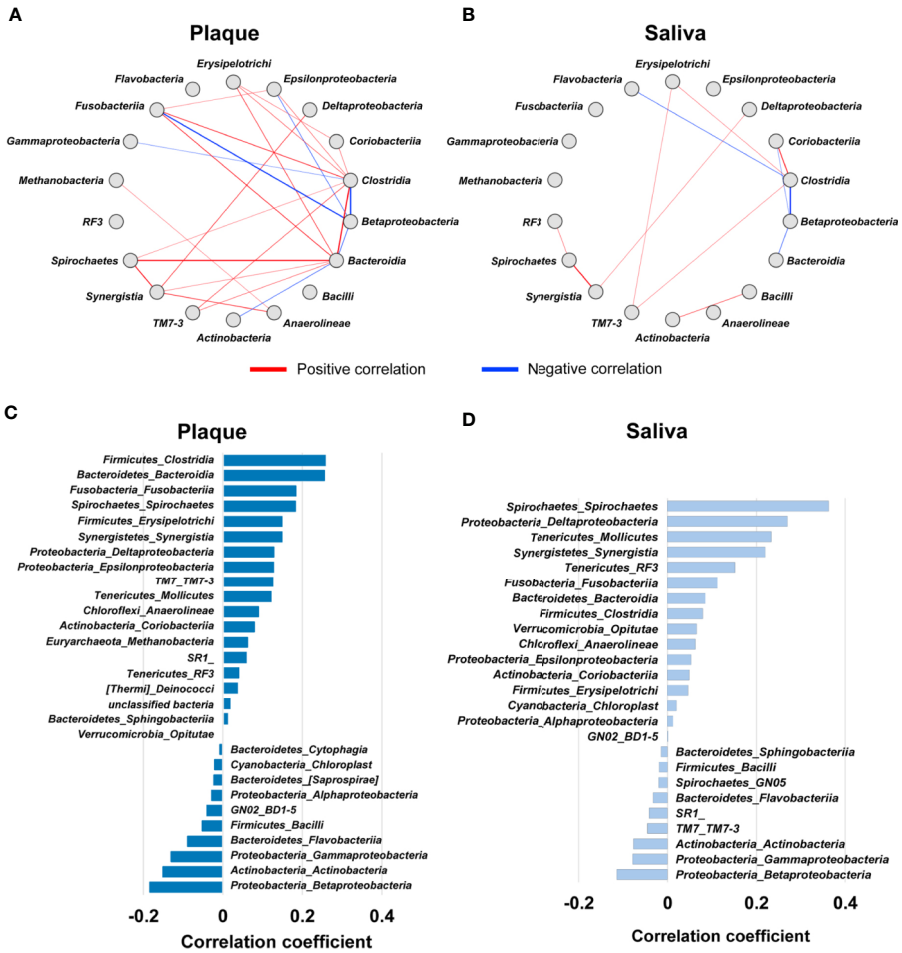

FIGURE 9 | Co-occurrence network of oral microbial communities. **(A, B)** Significant correlations of microbial taxa (Spearman's correlation coefficient ≥ 0.4 or ≤ -0.4, $p < 0.05$) in plaque **(A)** and saliva **(B)**. Each node represents a microbial taxon at the class level. The direction and strength of the correlations between two taxa is represented by the thickness of the red (positive) or blue (negative) lines. **(C, D)** Bar plot indicating Pearson's correlation coefficients between the ratio of deep pockets (≥ 4 mm) and the relative microbial abundance in plaque **(C)** and saliva **(D)**. The microbial taxa at the class level with $p \leq 0.05$ are arranged in descending order by correlation coefficient.

disease. We found through 16S rRNA gene sequencing analysis of 1,289 participants, in which 834 participants in the discovery cohort and 455 participants in the validation cohort, significant differences in the microbial composition and community structure between saliva and plaque. We also found that the species diversities in both saliva and plaque were increased in correlation with the severity of periodontal disease. By means of co-occurrence network analysis, a strong association of microbial taxa in plaque with periodontitis-associated biofilm formation was detected. These results thus revealed unique features of the oral microbiome in plaque and saliva, which were associated with the severity of periodontal diseases.

As a biobank, the TMM biobank wishes to share data from various genome studies with the research community to advance diverse scientific fields. The microbiome dataset of the ToMMo baseline oral microbiome study has been released to public through the dbTMM and jMorp databases. The latter contains and has already been sharing large-scale cohort data in the TMM project, covering genomics, transcriptomics, and metabolomics along with clinical information. The integrative approach by using microbiome and multiomics is expected to serve for the discovery of novel targets for the treatment and prevention of oral diseases.

In this study, we analyzed the microbiota of whole saliva and supragingival plaque from adult TMM cohort participants by means of 16S rRNA gene amplicon sequencing and measured the composition and relative abundance of the oral microbial population. Showing very good agreement with a previous report by the Human Microbiome Project (HMP; Segata et al., 2012), the frequency of the phylum *Firmicutes* in plaque is reduced compared with that in saliva, while the relative abundance of the phylum *Actinobacteria*, especially the genus *Corynebacterium*, is increased in plaque compared with that in saliva. The relative abundances of the phyla *Proteobacteria* and *TM7* tended to be lower in the TMM cohort than in the HMP cohort in both saliva and plaque. This may be due to variations caused by differences in the experimental protocol, at least in part. Accumulating lines of evidence imply

that the comparison of microbiome datasets from different research programs requires careful attention for variations. In this regard, large-scale microbiome analyses performed by a single facility would further improve the usability of genome/omics data supplemented with medical information in understanding human health.

Since saliva and supragingival plaque collection are less invasive, oral microbial studies employing saliva and plaque are commonly carried out. However, the relationship between salivary and plaque microbiota remains elusive. In this study, we clarified that the microbial ecology in saliva is different from that in plaque through co-occurrence network analysis of salivary and plaque microbiomes. The symbiotic relationship of the plaque microbiome is stronger than that of salivary microbiome, and the plaque microbiome at the class level has a strong correlation with periodontitis conditions. We plan to conduct a whole genome metagenomics analysis, which will provide sufficient taxonomic resolution to perform species-level association study with oral microbiome and oral diseases. Of note, in addition to the positive correlations of pathogenic microorganisms in plaque, we also identified negative correlations of the classes *Betaproteobacteria* and *Actinobacteria* with pathogenic microbial taxa in plaque. This result evokes an intriguing issue, *i.e.*, the microbiome switches from beneficial bacteria to pathogenic bacteria. However, considering the finding that the absolute amount of total oral bacteria is increased in the presence of periodontitis (Abusleme et al., 2013), quantitative analysis of the microbiome seems to be a prerequisite to fully understand the positive-negative relationships between oral microbiomes in disease conditions.

In addition, the mutual relationship in the salivary microbiome was much weaker than that in the plaque microbiome. Nonetheless, intriguingly, a positive correlation between the classes *Actinobacteria* and *Bacilli* was observed only in saliva. Previous 16S rRNA gene sequencing studies of the subgingival microbiome consistently identified the species *Actinomyces naeslundii*, *Actinomyces* sp. human oral taxon 171, *Rothia aeria*, *Rothia dentocariosa*, and *Streptococcus sanguinis* as health-associated taxa, since these taxa were replaced by pathogenic microbiota under periodontitis conditions (Abusleme et al., 2013; Hong et al., 2015; Curtis et al., 2020). Of note, these health-associated species are classified as the *Actinobacteria* or *Bacilli* class. Based on these results, we envisage that saliva may play an important role in maintaining the healthy oral microbiome. We also envisage that the salivary microbiome composition may be valuable to evaluate oral health status.

We examined the oral microbiome by using two independent cohorts of the TMM and found important microbial taxa for oral diseases. Our current results further suggest that in addition to its importance as a probe for oral diseases, oral microbiome analysis will emerge as a new approach for searching for therapeutic and preventive targets of systemic diseases.

DATA AVAILABILITY STATEMENT

The data presented in the study are deposited in jMorp (https://jmorp.megabank.tohoku.ac.jp/) and dbTMM (http://www.dist.megabank.tohoku.ac.jp/) release version 2.0.2.

ETHICS STATEMENT

The studies involving human participants were reviewed and approved by the Ethics Committees of Tohoku University Graduate School of Medicine and by the Ethics Committees of Iwate Medical University. Written informed consent was provided by all of the participants. For participants with insufficient ability to understand the study protocol, we obtained informed consent from their guardians with approval by the ethics committees.

AUTHOR CONTRIBUTIONS

SS, RY, OT, AT, RS, and MY developed the concepts and designed the study. TT, MG, HM, JK, AH, SKuri, YS, NF, SKure, and AT conducted the cohort studies and collected the biospecimens and clinical information. RY and NM conducted biospecimen banking. SS, ID, and RY designed and performed the experiments. YA, TT, and KK performed the bioinformatics analysis. SS, YA, TT, MG, AT, and RS interpreted the results and prepared draft manuscript. All authors contributed to the article and approved the submitted version.

FUNDING

This work was supported by Tohoku Medical Megabank Project from the Ministry of Education, Culture, Sports, Science and Technology (MEXT) and the Japan Agency for Medical Research and Development (AMED) under the grant numbers JP20km0105001 and JP20km0105002. It was also supported by the Advanced Genome Research and Bioinformatics Study to Facilitate Medical Innovation (GRIFIN) grant number JP20km0405203 and Facilitation of R&D Platform for AMED Genome Medicine Support conducted by AMED grant number JP20km0405001.

ACKNOWLEDGMENTS

We would like to thank all the volunteers who took part in this study. We also thank Ayako Okumoto for technical assistance with the experiments. We would like to acknowledge the members who contributed in the early phases of this study, and all members of the ToMMo for the assistance with the study. The member list is available at the following website: https://www.megabank.tohoku.ac.jp/english/a200601/.

SUPPLEMENTARY MATERIAL

The Supplementary Material for this article can be found online at: https://www.frontiersin.org/articles/10.3389/fcimb.2020.604596/full#supplementary-material

REFERENCES

Abusleme, L., Dupuy, A. K., Dutzan, N., Silva, N., Burleson, J. A., Strausbaugh, L. D., et al. (2013). The subgingival microbiome in health and periodontitis and its relationship with community biomass and inflammation. *ISME J.* 7 (5), 1016–1025. doi: 10.1038/ismej.2012.174

Bokulich, N. A., Kaehler, B. D., Rideout, J. R., Dillon, M., Bolyen, E., Knight, R., et al. (2018). Optimizing taxonomic classification of marker-gene amplicon sequences with QIIME 2's q2-feature-classifier plugin. *Microbiome* 6 (1), 90. doi: 10.1186/s40168-018-0470-z

Bolyen, E., Rideout, J. R., Dillon, M. R., Bokulich, N. A., Abnet, C. C., Al-Ghalith, G. A., et al. (2019). Reproducible, interactive, scalable and extensible microbiome data science using QIIME 2. *Nat. Biotechnol.* 37 (8), 852–857. doi: 10.1038/s41587-019-0209-9

Bryan, N. S., Tribble, G., and Angelov, N. (2017). Oral microbiome and nitric oxide: the missing link in the management of blood pressure. *Curr. Hypertens. Rep.* 19 (4), 33. doi: 10.1007/s11906-017-0725-2

Callahan, B. J., McMurdie, P. J., Rosen, M. J., Han, A. W., Johnson, A. J., and Holmes, S. P. (2016). DADA2: High-resolution sample inference from Illumina amplicon data. *Nat. Methods* 13 (7), 581–583. doi: 10.1038/nmeth.3869

Chen, B., Zhao, Y., Li, S., Yang, L., Wang, H., Wang, T., et al. (2018). Variations in oral microbiome profiles in rheumatoid arthritis and osteoarthritis with potential biomarkers for arthritis screening. *Sci. Rep.* 8 (1), 17126. doi: 10.1038/s41598-018-35473-6

Cobb, C. M., Kelly, P. J., Williams, K. B., Babbar, S., Angolkar, M., and Derman, R. J. (2017). The oral microbiome and adverse pregnancy outcomes. *Int. J. Womens Health* 9, 551–559. doi: 10.2147/IJWH.S142730

Curtis, M. A., Diaz, P. I., and Van Dyke, T. E. (2020). The role of the microbiota in periodontal disease. *Periodontol 2000* 83 (1), 14–25. doi: 10.1111/prd.12296

Donnelly, P. (2008). Progress and challenges in genome-wide association studies in humans. *Nature* 456 (7223), 728–731. doi: 10.1038/nature07631

Faith, D. P. (1992). Conservation evaluation and phylogenetic diversity. *Biol. Conserv.* 61, 1–10. doi: 10.1016/0006-3207(92)91201-3

Fettweis, J. M., Serrano, M. G., Brooks, J. P., Edwards, D. J., Girerd, P. H., Parikh, H. I., et al. (2019). The vaginal microbiome and preterm birth. *Nat. Med.* 25 (6), 1012–1021. doi: 10.1038/s41591-019-0450-2

Fuse, N., Sakurai-Yageta, M., Katsuoka, F., Danjoh, I., Shimizu, R., Tamiya, G., et al. (2019). Establishment of Integrated Biobank for Precision Medicine and Personalized Healthcare: The Tohoku Medical Megabank Project. *JMA J.* 2, 113–122. doi: 10.31662/jmaj.2019-0014

Graves, D. T., Corrêa, J. D., and Silva, T. A. (2019). The Oral Microbiota Is Modified by Systemic Diseases. *J. Dent. Res.* 98 (2), 148–156. doi: 10.1177/0022034518805739

Gupta, V. K., Paul, S., and Dutta, C. (2017). Geography, Ethnicity or Subsistence-Specific Variations in Human Microbiome Composition and Diversity. *Front. Microbiol.* 8, 1162. doi: 10.3389/fmicb.2017.01162

Holt, S. C., and Ebersole, J. L. (2005). Porphyromonas gingivalis, Treponema denticola, and Tannerella forsythia: the "red complex", a prototype polybacterial pathogenic consortium in periodontitis. *Periodontol* 2000. 38, 72–122. doi: 10.1111/j.1600-0757.2005.00113.x

Hong, B. Y., Furtado Araujo, M. V., Strausbaug, L. D., Terzi, E., Ioannidou, E., and Diaz, P. I. (2015). Microbiome profiles in periodontitis in relation to host and disease characteristics. *PloS One* 10 (5), e0127077. doi: 10.1371/journal.pone.0127077

Horz, H. P., Citron, D. M., Warren, Y. A., Goldstein, E. J., and Conrads, G. (2006). Synergistes group organisms of human origin. *J. Clin. Microbiol.* 44 (8), 2914–2920. doi: 10.1128/JCM.00568-06

Hozawa, A., Tanno, K., Nakaya, N., Nakamura, T., Tsuchiya, N., Hirata, T., et al. (2020). Study profile of The Tohoku Medical Megabank Community-Based Cohort Study. *J. Epidemiol.* 31 (1), 65–76. doi: 10.2188/jea.JE20190271

Katoh, K., and Standley, D. M. (2013). MAFFT multiple sequence alignment software version 7: improvements in performance and usability. *Mol. Biol. Evol.* 30 (4), 772–780. doi: 10.1093/molbev/mst010

Kilian, M. (2018). The oral microbiome - friend or foe? *Eur. J. Oral. Sci.* 126 Suppl 1, 5–12. doi: 10.1111/eos.12527

Kirst, M. E., Li, E. C., Alfant, B., Chi, Y. Y., Walker, C., Magnusson, I., et al. (2015). Dysbiosis and alterations in predicted functions of the subgingival microbiome in chronic periodontitis. *Appl. Environ. Microbiol.* 81 (2), 783–793. doi: 10.1128/AEM.02712-14

Kolenbrander, P. E., Palmer, R. J.Jr, Periasamy, S., and Jakubovics, N. S. (2010). Oral multispecies biofilm development and the key role of cell-cell distance. *Nat. Rev. Microbiol.* 8 (7), 471–480. doi: 10.1038/nrmicro2381

Koshiba, S., Motoike, I. N., Saigusa, D., Inoue, J., Shirota, M., Katoh, Y., et al. (2018). Omics research project on prospective cohort studies from the Tohoku Medical Megabank Project. *Genes Cells* 23 (6), 406–417. doi: 10.1111/gtc.12588

Kuriyama, S., Yaegashi, N., Nagami, F., Arai, T., Kawaguchi, Y., Osumi, N., et al. (2016). The Tohoku Medical Megabank Project: Design and mission. *J. Epidemiol.* 26, 493–511. doi: 10.2188/jea.JE20150268

Kuriyama, S., Metoki, H., Kikuya, M., Obara, T., Ishikuro, M., Yamanaka, C., et al. (2019). Cohort Profile: Tohoku Medical Megabank Project Birth and Three-Generation Cohort Study (TMM BirThree Cohort Study): Rationale, progress and perspective. *Int. J. Epidemiol.* 49 (1), 18–19m. doi: 10.1093/ije/dyz169

Leishman, S. J., Ford, P. J., Do, H. L., Palmer, J. E., Heng, N. C. K., West, M. J., et al. (2012). Periodontal pathogen load and increased antibody response to heat shock protein 60 in patients with cardiovascular disease. *J. Clin. Periodontol.* 39 (10), 923–930. doi: 10.1111/j.1600-051X.2012.01934.x

Lloyd-Price, J., Arze, C., Ananthakrishnan, A. N., Schirmer, M., Avila-Pacheco, J., Poon, T. W., et al. (2019). Multi-omics of the gut microbial ecosystem in inflammatory bowel diseases. *Nature* 569 (7758), 655–662. doi: 10.1038/s41586-019-1237-9

McCarthy, M. I., Abecasis, G. R., Cardon, L. R., Goldstein, D. B., Little, J., Ioannidis, J. P., et al. (2008). Genome-wide association studies for complex traits: consensus, uncertainty and challenges. *Nat. Rev. Genet.* 9 (5), 356–369. doi: 10.1038/nrg2344

Minegishi, N., Nishijima, I., Nobukuni, T., Kudo, H., Ishida, N., Terakawa, T., et al. (2019). Biobank establishment and sample management in the Tohoku Medical Megabank Project. *Tohoku J. Exp. Med.* 248 (1), 45–55. doi: 10.1620/tjem.248.45

Paster, B. J., Boches, S. K., Galvin, J. L., Ericson, R. E., Lau, C. N., Levanos, V. A., et al. (2001). Bacterial diversity in human subgingival plaque. *J. Bacteriol.* 183 (12), 3770–3783. doi: 10.1128/JB.183.12.3770-3783.2001

Plomin, R., Haworth, C. M. A., and Davis, O. S. P. (2009). Common disorders are quantitative traits. *Nat. Rev. Genet.* 10 (12), 872–878. doi: 10.1038/nrg2670

Price, M. N., Dehal, P. S., and Arkin, A. P. (2010). FastTree 2 –approximately maximum-likelihood trees for large alignments. *PloS One* 5 (3), e9490. doi: 10.1371/journal.pone.0009490

Sato, Y., Yamagishi, J., Yamashita, R., Shinozaki, N., Ye, B., Yamada, T., et al. (2015). Inter-individual differences in the oral bacteriome are greater than intra-day fluctuations in individuals. *PloS One* 10 (6), e0131607. doi: 10.1371/journal.pone.0131607

Segata, N., Haake, S. K., Mannon, P., Lemon, K. P., Waldron, L., Gevers, D., et al. (2012). Composition of the adult digestive tract bacterial microbiome based on seven mouth surfaces, tonsils, throat and stool samples. *Genome Biol.* 13 (6), R42. doi: 10.1186/gb-2012-13-6-r42

Socransky, S. S., Haffajee, A. D., Cugini, M. A., Smith, C., and Kent, R. (1998). Microbial complexes in subgingival plaque. *J. Clin. Periodontol.* 25 (2), 134–144. doi: 10.1111/j.1600-051x.1998.tb02419.x

Tadaka, S., Saigusa, D., Motoike, I. N., Inoue, J., Aoki, Y., Shirota, M., et al. (2018). jMorp: Japanese Multi Omics Reference Panel. *Nucleic Acids Res.* 46 (D1), D551–D557. doi: 10.1093/nar/gkx978

Takai-Igarashi, T., Kinoshita, K., Nagasaki, M., Ogishima, S., Nakamura, N., Nagase, S., et al. (2017). Security controls in an integrated Biobank to protect privacy in data sharing: rationale and study design. *BMC Med. Inf. Decis Making* 17 (1), 100. doi: 10.1186/s12911-017-0494-5

Takeshita, T., Nakano, Y., Kumagai, T., Yasui, M., Kamio, N., Shibata, Y., et al. (2009). The ecological proportion of indigenous bacterial populations in saliva is correlated with oral health status. *ISME J.* 3 (1), 65–78. doi: 10.1038/ismej.2008.91

Tsuboi, A., Matsui, H., Shiraishi, N., Murakami, T., Otsuki, A., Kawashima, J., et al. (2020). Design and progress of oral health examinations in the Tohoku Medical Megabank project. *Tohoku J. Exp. Med.* 251 (2), 97–115. doi: 10.1620/tjem.251.97

Willis, J. R., and Gabaldón, T. (2020). The human oral microbiome in health and disease: From sequences to ecosystems. *Microorganisms* 8 (2), 308. doi: 10.3390/microorganisms8020308

Yamagishi, J., Sato, Y., Shinozaki, N., Ye, B., Tsuboi, A., Nagasaki, M., et al. (2016). Comparison of boiling and robotics automation method in DNA extraction for

metagenomic sequencing of human oral microbes. *PloS One* 11 (4), e0154389. doi: 10.1371/journal.pone.0154389

Yasuda, J., Kinoshita, K., Katsuoka, F., Danjoh, I., Sakurai-Yageta, M., Motoike, I. N., et al. (2019). Genome analyses for the Tohoku Medical Megabank Project towards establishment of personalized healthcare. *J. Biochem.* 165 (2), 139–158. doi: 10.1093/jb/mvy096

Zheng, W., Zhang, Z., Liu, C., Qiao, Y., Zhou, D., Qu, J., et al. (2015). Metagenomic sequencing reveals altered metabolic pathways in the oral microbiota of sailors during a long sea voyage. *Sci. Rep.* 5, 9131. doi: 10.1038/srep09131

Zhou, W., Sailani, M. R., Contrepois, K., Zhou, Y., Ahadi, S., Leopold, S. R., et al. (2019). Longitudinal multi-omics of host-microbe dynamics in prediabetes. *Nature* 569 (7758), 663–671. doi: 10.1038/s41586-019-1236-x

Conflict of Interest: The authors declare that the research was conducted in the absence of any commercial or financial relationships that could be construed as a potential conflict of interest.

frontiers in Cellular and Infection Microbiology

ORIGINAL RESEARCH
published: 10 March 2021
doi: 10.3389/fcimb.2021.640309

Salivary Microbiota for Gastric Cancer Prediction: An Exploratory Study

Kun Huang[1,2†], Xuefeng Gao[3†], Lili Wu[4†], Bin Yan[1], Zikai Wang[1], Xiaomei Zhang[1], Lihua Peng[1], Jiufei Yu[2], Gang Sun[1] and Yunsheng Yang[1]*

[1] Department of Gastroenterology and Hepatology, The First Medical Center, Chinese PLA General Hospital, Medical School of Chinese PLA, Beijing, China, [2] Department of Gastroenterology, Civil Aviation General Hospital, Beijing, China, [3] Central Laboratory, Shenzhen Key Laboratory of Precision Medicine for Hematological Malignancies, Shenzhen University General Hospital, Shenzhen, China, [4] Department of Gastroenterology, The Second Medical Center, Chinese PLA General Hospital, Beijing, China

OPEN ACCESS

Edited by:
Tomomi Hashizume-Takizawa, Nihon University, Japan

Reviewed by:
Junfeng Zhang, Nanjing University of Chinese Medicine, China
William K. K. Wu, Chinese University of Hong Kong, China
Javier Torres, Mexican Social Security Institute (IMSS), Mexico

***Correspondence:**
Yunsheng Yang
sunnyddc@plagh.org

†These authors have contributed equally to this work and share first authorship

Specialty section:
This article was submitted to Microbiome in Health and Disease, a section of the journal Frontiers in Cellular and Infection Microbiology

Received: *11 December 2020*
Accepted: *03 February 2021*
Published: *10 March 2021*

Citation:
Huang K, Gao X, Wu L, Yan B, Wang Z, Zhang X, Peng L, Yu J, Sun G and Yang Y (2021) Salivary Microbiota for Gastric Cancer Prediction: An Exploratory Study. Front. Cell. Infect. Microbiol. 11:640309. doi: 10.3389/fcimb.2021.640309

To characterize the salivary microbiota in patients at different progressive histological stages of gastric carcinogenesis and identify microbial markers for detecting gastric cancer, two hundred and ninety-three patients were grouped into superficial gastritis (SG; n = 101), atrophic gastritis (AG; n = 93), and gastric cancer (GC; n = 99) according to their histology. 16S rRNA gene sequencing was used to access the salivary microbiota profile. A random forest model was constructed to classify gastric histological types based on the salivary microbiota compositions. A distinct salivary microbiota was observed in patients with GC when comparing with SG and AG, which was featured by an enrichment of putative proinflammatory taxa including *Corynebacterium* and *Streptococcus*. Among the significantly decreased oral bacteria in GC patients including *Haemophilus*, *Neisseria*, *Parvimonas*, *Peptostreptococcus*, *Porphyromonas*, and *Prevotella*, *Haemophilus*, and *Neisseria* are known to reduce nitrite, which may consequently result in an accumulation of carcinogenic N-nitroso compounds. We found that GC can be distinguished accurately from patients with AG and SG (AUC = 0.91) by the random forest model based on the salivary microbiota profiles, and taxa belonging to *unclassified Streptophyta* and *Streptococcus* have potential as diagnostic biomarkers for GC. Remarkable changes in the salivary microbiota functions were also detected across three histological types, and the upregulation in the isoleucine and valine is in line with a higher level of these amino acids in the gastric tumor tissues that reported by other independent studies. Conclusively, bacteria in the oral cavity may contribute gastric cancer and become new diagnostic biomarkers for GC, but further evaluation against independent clinical cohorts is required. The potential mechanisms of salivary microbiota in participating the pathogenesis of GC may include an accumulation of proinflammatory bacteria and a decline in those reducing carcinogenic N-nitroso compounds.

Keywords: gastric cancer, precancerous lesions, salivary microbiota, 16S rRNA, high-throughput sequencing

INTRODUCTION

Gastric cancer (GC) constitutes the third highest cause of cancer mortality worldwide (Bray et al., 2018), and the 5-year survival rates are 27.4 and 32% in China and the USA, respectively. The occurrence and development of gastric carcinogenesis is a complex pathogenic process involving multiple factors, multi-stage changes and polygenic alterations (Massarrat and Stolte, 2014; Goral, 2016). A late-stage presentation is common in most GC cases, because symptoms in early stages of the disease are usually vague and non-specific. As early detection leads to better outcomes, there is a critical need for new avenues of prevention, risk stratification, and early detection for GC.

Microbes in the upper digestive tract have been shown to facilitate carcinogenesis by contributing inflammatory processes *via* activation of Toll-like receptors pathway (Kauppila and Selander, 2014), or protect against carcinogenesis by providing barriers to pathogen invasion (Yang et al., 2014). Chronic infection with *Helicobacter pylori* is a well-established risk factor for gastric carcinogenesis. Lines of evidence demonstrated that the process of Correa's cascade of gastric carcinogenesis initiated by *H. pylori* involves multiple virulence factors, host genetic make-up, and nutritional factors (Warren and Marshall, 1983; Polk and Peek, 2010; Engstrand and Lindberg, 2013; Plummer et al., 2015). Nevertheless, only about 3% of those infected with *H. pylori* will eventually develop into gastric cancer, and the eradication of *H. pylori* does not completely prevent the occurrence of GC (Peek and Crabtree, 2006). These lines of evidence suggest that non-*H. pylori* microorganisms colonizing the stomach may represent an additional modifier of gastric cancer risk (Sung et al., 2020). The enrichment of some bacteria in the gastric mucosa has been associated with the progression of gastric cancer, including *Peptostreptococcus stomatis*, *Streptococcus anginosus*, *Parvimonas micra*, *Slackia exigua*, and *Dialister pneumosintes* (Coker et al., 2018). Our recent study suggested that a reduction of nitrite-oxidizing Nitrospirae taxa in the gastric mucosa may contribute to gastric neoplastic progression *via* nitrate accumulation (Wang et al., 2020).

Most of the microbial sources in the stomach are believed from the external environment. The oral cavity contains a large number of microorganisms, including bacteria, viruses, fungi, mycoplasma, and chlamydia (Aas et al., 2005; Wade, 2013; He et al., 2015). The oral microbiota can enter the downstream digestive tract from the oral cavity through saliva and can also migrate to various parts of the body to cause infections and local inflammatory reactions in corresponding sites (Han and Wang, 2013), oral microbes are closely correlated with several systemic diseases such as the oral tumors, type 2 diabetes, cardiovascular disease, urinary systemic diseases and rheumatoid arthritis (Seymour, 2010; Ahn et al., 2012; Salazar et al., 2012; Whitmore and Lamont, 2014; Gao et al., 2018). Recently, oral microbiota has been suggested to play a role in the etiology of esophageal cancer, colorectal cancer (CRC), and pancreatic cancer (Michaud and Izard, 2014; Peters et al., 2017; Flemer et al., 2018). Interestingly, a higher incidence of GC was found among people with worse oral hygiene (Watabe et al.), indicating a potential link between the oral microbiota and the occurrence/development of gastric cancer. In this study, we characterized the microbial compositional and ecological changes in salivary microbiota of patients with GC and non-malignant gastric lesions including superficial gastritis (SG) and atrophic gastritis (AG). We demonstrated the possibility of using salivary microbes as biomarkers GC detection, and explored the potential mechanisms of oral microbiota in the pathogenesis of GC.

MATERIALS AND METHODS

Participants

Two hundred and ninety-three patients who received an endoscopic examination in the Chinese PLA General Hospital and Civil Aviation General Hospital were enrolled in this study. The study cohort was recruited from October 2017 to October 2019. The inclusion criteria were: (1) adult male or female; (2) Han nationality from northern China; (3) able and willing to provide signed and dated informed consent; (4) able and willing to provide salivary samples. The exclusion criteria were: (1) taking antibiotics, proton pump inhibitors (PPIs), probiotics, prebiotics, chemotherapeutic drugs, and any other drugs affecting oral microbiota within the last month; (2) diagnosed with acute or chronic pulmonary, cardiovascular, hepatic, or renal disorders; (3) positive test for human immunodeficiency virus, hepatitis B or C virus; (4) a history of major surgery; and (5) women who were pregnant or lactating.

Data collection was conducted for all subjects, including demographics, medical history, drugs, and hematology tests.

Endoscopic and Histologic Examination

Patients' diagnostic evaluation was based on the endoscopic and histological examination. SG was confirmed according to the infiltrating depth and density of chronic inflammatory cells in the mucosa, without the reduction of proper gastric glands at each biopsy site. If the gastric mucosa in the antrum and the body were atrophied and thinned, the submucosal vessels could be well visualized under the gastroscopy; in the meantime, the proper gastric glands reduced at each biopsy site, it was defined as AG. IM was defined as the replacement of gastric mucosal epithelial cells by intestinal epithelial cells at each biopsy site. GC was confirmed by the histological examination; according to WHO gastric adenocarcinoma grading criteria, it was divided into well differentiated, moderately differentiated, and poorly differentiated (Jean-François, 2011).

Sample Collection

Salivary sample collection and preparation were carried out in accordance with previously published consensus (Shi et al., 2019). All the subjects were fasting and did not brush the teeth in the morning. Thirty minutes before sampling, subjects were asked to rinse the mouth with water, and then 1 ml saliva was collected in a sterilized tube containing 1.0 ml RNAlater (Life Technologies, USA), transferred to the laboratory and stored at room temperature until DNA extraction.

DNA Extraction and 16S rRNA Gene Amplicons

To evaluate the salivary bacterial diversity, high-throughput sequencing of the 16S rRNA was performed. Bacterial genomic DNA of the saliva was isolated using the QIAamp DNA Mini Kit (QIAGEN, Valencia, CA, USA) combined with the bead-beating method. The DNA concentrations of each sample were adjusted to 50 ng/μl and stored at −80°C for sequencing. The hypervariable V3–V4 region of the 16S rRNA gene was amplified using the universal primers (515F, GTGCCAGCMGCCGCGGTAA and 806R, GGACTACHV GGGTWTCTAAT) with a 6-bp barcode. All PCR reactions (including denaturation, annealing and elongation) were carried out with Phusion ® High-Fidelity PCR Master Mix (New England Biolabs). The single amplifications were performed in 25 μl reactions with 50 ng template DNA. Normalized equimolar concentrations of PCR products were pooled and sequenced using the Illumina MiSeq PE300 platform (Illumina, San Diego, CA, United States) at Shenzhen Decipher Biotechnology Laboratory.

We employed the QIIME 2 (Bolyen et al., 2019) *dada2 denoise-paired* method to denoise, dereplicate, and filter chimeras from the sequence data. For taxonomic classification, we trained a Naive Bayes classifier on the 16S rRNA V3–V4 regions with *q2-feature-classifier* method (**Supplementary File S1**). The metagenome functions of the salivary microbiota were predicted through PICRUSt2 on the basis of 16S rRNA gene sequencing profiles (Douglas et al., 2020).

Statistical and Bioinformatic Analyses

The baseline continuous data were presented by mean ± standard deviation (SD) and analyzed by independent *t* test or non-parametric rank test. The categorical data were described in percentages and compared by χ^2 test or Fisher's exact test. All tests for significance were two-sided, and P <0.05 was considered significant.

Calypso (version 8.84) was used to conduct statistical analysis of the microbiota compositional data. The read counts were normalized with total sum normalization, and taxa having less than 0.02% relative abundance across all samples were excluded from the following analysis. The Amplicon sequence variant (ASV) counts were normalized with total-sum scaling (TSS) followed by cumulative-sum scaling (CSS). The alpha diversity of the salivary microbiota was measured by Shannon's index and Chao1 index. The relative abundances of taxa were log2 transformed to account for the non-normality. Principal coordinate analysis (PCoA) based on unweighted and weighted UniFrac distance matrices were employed to stratify samples and identify group level clusters, and the corresponding statistical significance was assessed using Permutational multivariate analysis of variance (PERMANOVA). Anosim was applied to compare the intra-group distances with between-group distances. Kruskal–Wallis test was used to detect significant differences in the alpha diversity, abundances of taxa, and metabolic pathways across the histological stages, which was followed by Wilcoxon rank-sum test confirming the significant differences between each two groups. Benjamini–Hochberg (BH) procedure was applied to control the false discovery rate. The Linear discriminant analysis Effect Size (LEfSe) (Segata et al., 2011) was applied to identify the features (ASV or functions) most likely to explain differences in the salivary microbiota between histological types. Spearman correlation networks were constructed based on the top 30 most abundant genera and edges of correlations with Holm-corrected P <0.05 were shown.

The random forest (RF) model was built through the caret R package. Five-fold cross-validation and area under the receiver operating characteristic (ROC) curve (AUC) were used to evaluate the prediction performance of the model and was implemented using pROC R package. The RF disease classifier using oral bacterial abundances at the genus level was constructed with 60% randomly selected samples as the training set and tuneLength = 4. The R code and taxa abundance table used for constructing the random forest model are provided in the **Supplementary Code 1**.

RESULTS

Demographic Characteristics of the Patient Cohort

After a standardized endoscopic procedure and histopathological evaluation, a total of 101 SG, 93 AG (21 without IM, 72 with IM), and 99 GC subjects were enrolled. The gender and age were matched among the four groups (P = 0.9152 and P = 0.3582, respectively). There were also no significant differences in body mass index (BMI), socioeconomic, medical history (including periodontosis), or lifestyle characteristics (smoking and drinking status) among the four groups (**Table 1**).

Salivary Microbiota Changes Are Associated With Gastric Neoplastic Progression

This study assessed the salivary microbiota by sequence analysis of the 16S ribosomal RNA gene. A total of 14,989,371 raw reads were obtained after quality filtering, with an average of 51,158 for each sample. The refined reads were clustered into 1,275 ASVs. The salivary microbiota alpha diversity was significantly lower in

TABLE 1 | Distribution of demographic characteristics among SG, AG, and GC.

Histological types	SG	AG		GC	P-value
		Without IM	With IM		
n	101	21	72	99	
Gender (male, female)	(51, 50)	(10, 11)	(39, 33)	(64, 35)	0.9152
Age	48.2 ± 10.2	49.9 ± 12.5	48.5 ± 11.7	49.6 ± 8.8	0.3582
BMI	23.5 ± 2.4	22.7 ± 3.4	22.8 ± 4.5	21.4 ± 2.2	0.8062
Periodontosis	15	13	21	42	0.0951
Smoking	34	10	29	40	0.2482
Drinking	42	14	38	51	0.8502

GC than that of SG and AG (**Figures 1A, B**). Beta analysis with PCoA showed that the cluster of GC samples could be separated from SG and AG (**Figures 1C, D**). Regarding AG, the alpha and beta diversities in the salivary microbiota in patients with and without intestinal metaplasia were not distinguishable (**Figure S1**). For GC patients with different histological grades (well differentiated, moderately differentiated, and poorly differentiated), there was no significant difference in the biodiversity among in the salivary microbiota (**Figure S2**).

Compositionally, the most abundant phyla in the salivary microbiota are *Bacteroidetes, Protobacteria, Firmicutes, Fusobacteria*, and *Acinobacteria*, which account for more than 94% of the bacterial community for each histological stage of GC (**Figure S3A**). Patients with GC had a higher relative abundance of Cyanobacteria (**Table S1**). At the genus level, *Prevotella*, *Neisseria*, *Veillonella*, *Haemophilus*, *Porphyromonas*, *Streptococcus*, *Fusobacterium*, and *Rothia* constitute more than 70% of the salivary microbiota for each histological stage of GC (**Figure S3B**). The levels of *Anaerovorax, Bulleidia, unclassified F16*, and *Peptostreptococcus* gradually decreased from SG through AG to GC (**Figure 2; Table S1**), indicating a negative association of these bacteria with GC development. The genera *Streptococcus* and *unclassified Streptophyta* were significantly higher in GC, whereas *Fusobacterium*, *Haemophilus*, *Neisseria*, *Parvimonas*, *Peptostreptococcus*, *Porphyromonas*, and *Prevotella* were less abundant in GC. In addition, *Bacteroides* genus was found particularly more abundant in the patients with AG.

It has been shown that the composition and function of the oral microbiota are affected by lifestyle factors such as alcohol and tobacco use and health characteristics such as periodontitis, tooth status, and HP infection (Bornigen et al., 2017; Zhao et al., 2019). We used MaAsLin2 to access the multivariable association between metadata and salivary microbiota. Analysis result indicated that only *Faecalibacterium* had a significant negative correlation with tabaco usage (**Figure 3**), while no taxa were found to be significantly associated with alcohol usage, periodontosis, or HP-infection. There were 13 genera that had significant correlationships with GC, including five positive correlations (enriched in GC) and eight negative correlations (reduced in GC). Six genera were found to be negatively correlated with both AG and GC, and *Bacteroidetes* had a significant positive correlation with AG. Taken together, the results of multivariate analysis are in accordance with the results of univariate analysis.

Salivary Microbiota Is Predictive of Stages of Gastric Carcinogenesis

To identify the most relevant taxa responsible for the differences among the disease stages, we performed LEfSe analysis based on the genus (**Figure 4A**; **Figure S4A**). The representative bacterial

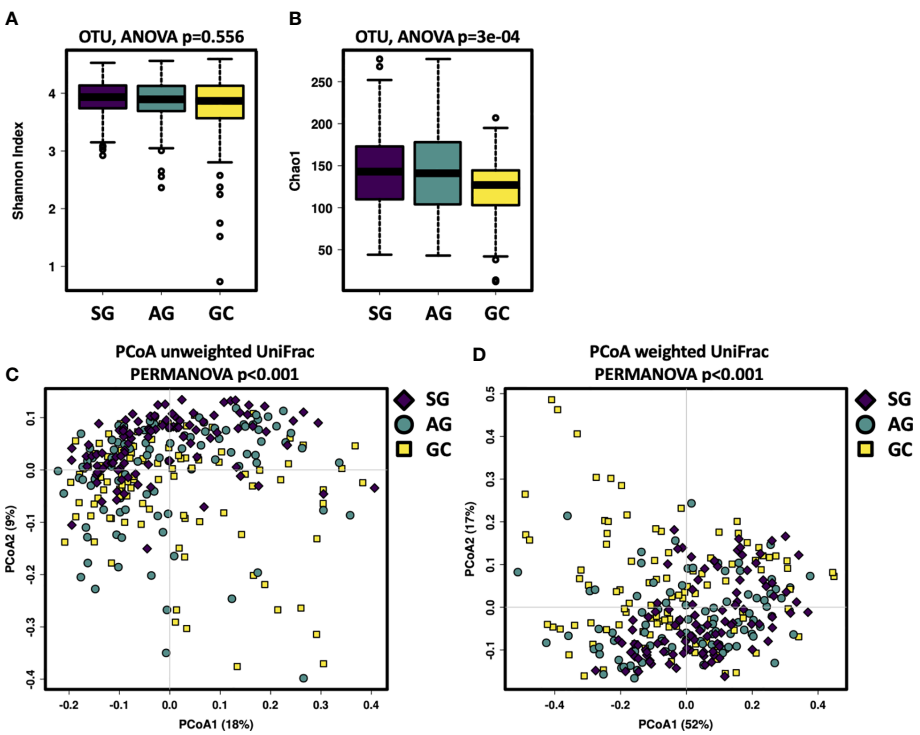

FIGURE 1 | The salivary microbiota biodiversity in patients with malignant and non-malignant gastric lesions. The alpha diversity of salivary microbiota was measured at the ASV level by using **(A)** Shannon index, **(B)** Chao1. Significance was determined by using Kruskal–Wallis rank sum test, and Wilcoxon rank-sum tests for each of the two groups. PCoA based on **(C)** unweighted UniFrac distance matrix, and **(D)** weighted UniFrac distance matrix revealed distinct clustering of GC samples.

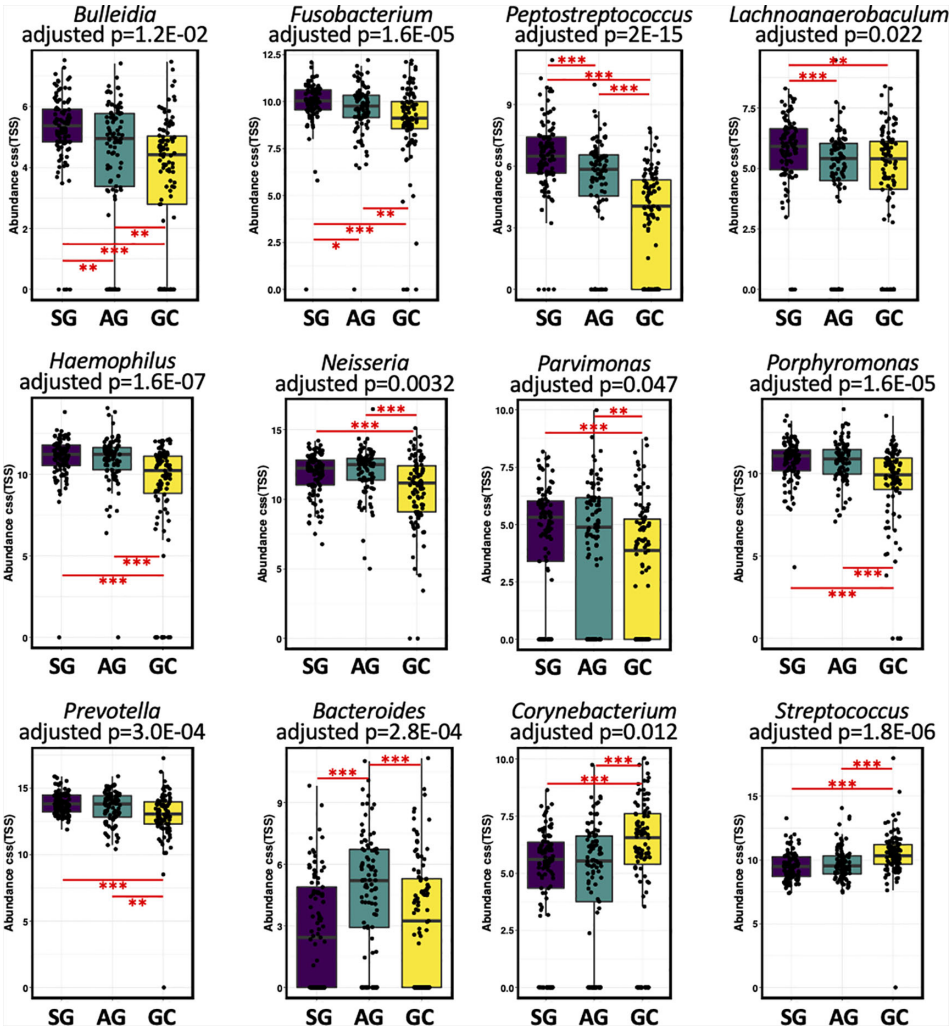

FIGURE 2 | The salivary microbiota composition in patients with malignant and non-malignant gastric lesions. The salivary microbiota composition in patients with malignant and non-malignant gastric lesions. Relative abundance of salivary taxa of the three groups were compared at the genus level. Significance was determined by using Kruskal-Wallis rank sum test with BH-adjusted $P < 0.001$, and Wilcoxon rank-sum tests for each of the two groups with *BH-adjusted $P < 0.05$, **BH-adjusted $P < 0.01$, and ***BH-adjusted $P < 0.001$.

genera in the salivary microbiota of GC patients were *unclassified Streptophyta*, *Streptococcus*, and *Bifidobacterium*; patients with AG showed increased levels of *Bacteroides* and *Haemophilus* genera; the salivary microbiota in SG patients was featured by an enrichment of *Peptostreptococcus*, *unclassified Mogibacteriaceae*, and *unclassified SR1* genera.

To further explore the potential of the salivary microbiota as diagnostic biomarkers for GC, we constructed a random forest model for identifying malignancy based on the salivary microbiota at the genus level. This model showed a high accuracy in distinguishing GC from non-malignant lesions, yielding an AUC of 0.91 (95% confidence interval 0.778–0.99) (**Figure 4B**). Moreover, the random forest modeling approach was also able to distinguish SG, AG, and GC subjects, resulting in an AUC of 0.84, 0.76, and 0.877 for SG, AG, and GC, respectively (**Supplementary Figure S4B**). Among the top 10 genera with highest contributions to the model classification performance (**Figure 4C**; **Figure S4C**), *unclassified Streptophyta* and *Streptococcus* were also identified as GC-associated microbial features by LEfSe (**Figure 4A**; **Figure S4A**), enhancing their potential in becoming biomarkers for GC diagnosis.

In addition, we performed a network analysis to visualize the commensal relationships among the salivary microbiota of the three histological types (**Figure S5**). Interestingly, we found that the correlations between *Prevotella* and other taxa dominated the negative relationships for all the three histological types, with their number reduced in AG and GC.

Salivary Microbiome Functional Capacity in SG, AG, and GC

Analysis of PICRUSt2 revealed differentially abundant metabolic functions in the bacterial communities across the histological

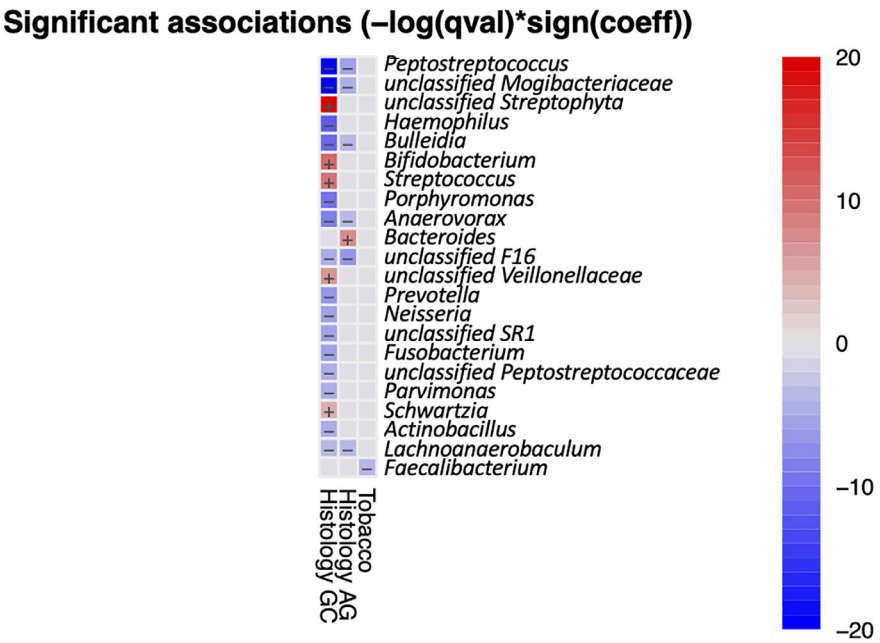

FIGURE 3 | Heatmap summarizing the significant associations between oral bacteria and metadata. Color key: -log(q-value)*sign(coefficient). Cells that denote significant associations are colored (red or blue) and overlaid with a plus (+) or minus (–) sign that indicates the direction of association.

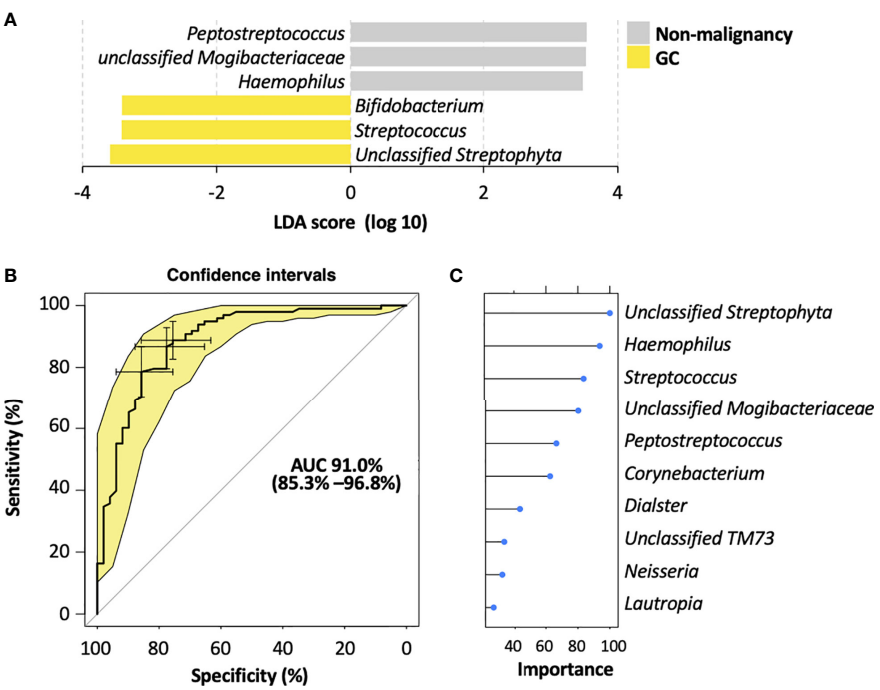

FIGURE 4 | Salivary bacterial biomarkers for classifying different stages of gastric carcinogenesis. **(A)** Microbiological features of the salivary microbiota associated with different histological stages of gastric tumorigenesis. Bacteria taxa that enriched in each histological stage were determined by LEfSe with Kruskal–Wallis test P <0.05 and log 10 LDA score >3.4. **(B)** ROC curves analysis to evaluate the discriminatory potential of salivary bacteria in identifying GC out of pre-malignant lesions. **(C)** The top 10 bacterial genera that are most important for discriminating GC with non-malignant types. Each genus is ranked according to an importance score (mean decrease accuracy).

stages of gastric carcinogenesis (**Figure S6**). The expression of thiamin salvage II (PWY-6897), lipid IVA biosynthesis (NAGLIPASYN-PWY): CMP-3-deoxy-D-manno-octulosonate biosynthesis I (PWY-1269), Kdo transfer to lipid IVA III (PWY-6467), preQ0 biosynthesis (PWY6703), and superpathway of thiamin diphosphate biosynthesis I (THISYN-PWY) were found to be decreased from SG, through AG to GC. In contrast, pathways involved in L-isoleucine biosynthesis II (PWY-5101 and PWY-5103), L-valine biosynthesis (VALSYN-PWY), L-isoleucine biosynthesis I from threonine (ILEUSYN-PWY), superpathway of branched amino acid (BRANCHED-CHAIN-AA-SYN-PWY), pyruvate fermentation to isobutanol (PWY-7111), and UDP-N-acetyl-D-glucosamine biosynthesis I (UDPNAGSYN-PWY) were upregulated from SG through AG to GC. It is worth noting that the increased expression of biosynthesis of amino acids such as isoleucine and valine was also previously detected in the gastric cancer tissues (Jung et al., 2014; Wang et al., 2016).

DISCUSSION

Previous studies have shown that periodontal disease and poor oral health status were associated with increased incidence of malignant diseases (Dizdar et al., 2017; Michaud et al., 2018), pointing to a potentially oncogenic role of oral microorganisms in the development of cancer. Some species have been identified that correlate strongly with oral squamous cell carcinoma (OSCC), such as *Capnocytophaga gingivalis*, *Prevotella melaninogenica*, and *Streptococcus mitis* (Mager et al., 2005), which were suggested as diagnostic markers since they predicted 80% of cancer cases. Oral microbes are also detected in tumors distant to the oral cavity. For example, many works have shown that the oral periopathogens *Fusobacterium nucleatum* and *Porphyromonas gingivalis* are essential in the development of colorectal and pancreatic cancer, respectively (Rubinstein et al., 2013; Fan et al., 2018a). The oral microbiota was shown to reflect an inflammatory status of the stomach in patients with *H. pylori* infection (Zhao et al., 2019), and could detect GC with a high accuracy (Coker et al., 2018; Wu et al., 2018). In this study, we demonstrated that the salivary microbiota could identify GC among patients with non-malignant gastric diseases including SG and AG, yielding a high accuracy (AUC of 91%). With a cohort consisting of 37 GC patients and 13 healthy individuals, a previous study also showed a high sensitivity rate (AUC of 97%) of using oral microbiota screening gastric cancer (Sun et al., 2018), further enhancing the diagnostic potential of the oral bacteria for gastric malignancy. The microbiome is exclusive to the individual and influenced by lifestyle and phenotypic and genotypic determinants. For example, alcohol consumption and tobacco usage have been shown to influence the oral microbiome composition (Wu et al., 2016; Fan et al., 2018b). Therefore, lifestyle should be considered as confounding factors when identifying diagnostic microbial markers from the oral microbiome. Multivariate analysis method revealed that enrichment of Faecalibacterium was negatively associated with smoking, and no significant correlation was found between salivary bacteria and alcohol or HP-infection. Thus, the potential biomarkers identified based on our data seemed not affected by the recorded lifestyle and HP infection.

Our data showed that alpha diversity of the salivary microbiota was similar among patients with different gastric histological types, which was consistent with another study (Kageyama et al., 2019). One previous study found that the microbial diversity of saliva and dental plaque significantly increased in GC patients (Sun et al., 2018), whereas another one suggested that the microbiota diversity significantly reduced in the tongue coating of GC patients (Cui et al., 2019). Taken together, the microbial diversity of oral microbiota seems not strongly associated with the development of GC.

Data from our recent study (Wang et al., 2020) as well as others (Dicksved et al., 2009; Castano-Rodriguez et al., 2017; Chen et al., 2019) showed that commensals of the oral cavity including *Fusobacterium*, *Peptostreptococcus*, *Prevotella*, *Streptococcus*, and *Veillonella* were found to have higher relative abundances in the gastric mucosa of GC patients. Notably, these genera are also commensals of oral cavity, but their translocation and expansion may be involved in the onset and development of multiple diseases including cancers. One possible mechanism of oral microbiota participating carcinogenesis is enrichment of pro-inflammatory oral bacterial species. For example, *Streptococcus bovis* has been shown to promote the development of colon cancer by enhancing the inflammation (Abdulamir et al., 2011). We observed that *Streptococcus* genus was enriched in the saliva microbiota of GC patients, which agrees with the findings in a recent study (Sun et al., 2018). Interestingly, an enrichment of *Streptococcus* spp. was also reported across several types of cancer such as colorectal adenocarcinomas (Abdulamir et al., 2011). Taken together, these results indicate a potential of some strains of *Streptococcus* being involved in gastric carcinogenesis. In addition, *Corynebacterium* genus was also found to be enriched in the saliva of GC patients, which was in line with (Wu et al., 2018) a higher level *Corynebacterium;* this genus was found higher in the tongue coating microbiota community of GC patients than that of the healthy controls. Species of *Corynebacterium* are widely distributed in the microbiota of human skin, and most of them are innocuous while some species are known to cause infection such as *C. diphtheria*. In recent years, they have been increasingly reported as emerging opportunistic pathogens in immunocompromised patients with cancer, hematologic malignancy, and critical condition (Chen et al., 2012). Thus, a higher level of *Corynebacterium* spp., which appeared in the oral cavity, may reflect immune deficiency in cancer patients. Altogether, an enrichment of proinflammatory bacteria in the oral cavity is likely an import factor contributing to the development and progression of GC.

Several bacterial taxa were found reduced in the salivary microbiota of GC patients, including *Bulleidia*, *Fusobacterium*, *Haemophilus*, *Lachnoanaerobaculum*, *Neisseria, Parvimonas, Peptostreptococcus*, *Porphyromonas*, and *Prevotella*. Intriguingly, a decreased carriage of *Bulleidia* was also

captured in the oral cavity of patients with esophageal squamous cell carcinoma (Chen et al., 2015). Moreover, some taxa of these genera were found to be enriched in tumor and stool samples of colorectal cancer patients, such as *Fusobacterium nucleatum, Parvimonas* micra, *Porphyromonas asaccharolytica*, and *Peptostreptococcus stomatis*, *Prevotella intermedia* (Ternes et al., 2020). And we recently found a higher load of *Fusobacterium* in the gastric mucosa of GC patients compared to SG (Wang et al., 2020). In the present study, a low level of these genera was observed in the oral cavity of GC patients as compared with SG and/or AG. In fact, bacterial abundance is majorly regulated by nutrient availability and antimicrobial signals specific to their environmental conditions. Thus, albeit these bacteria colonize and expanded in the tumor site (such as gut of patients with colorectal cancer), they may not overgrow in their original localization such as the oral cavity.

Network analysis revealed that *Prevotella* was negatively correlated with a variety of oral bacteria in the oral cavity of all three histological stages, and the number of its negative relationships decreased in AG and GC groups. In the GC patients, the abundance of *Prevotella* in the salivary cavity was lower than that of SG and AG groups, which is opposite to the findings in Sun et al.'s study (Sun et al., 2018). This discrepancy at the genus level may be explained by increasing the phylogenetic resolution *via* metagenomic sequencing and identifying the specific species/strains that related to gastric cancer.

We previously found that patients with intraepithelial neoplasia had higher relative abundances of *Haemophilus parainfluenzae* and *Nitrospirae* family in the gastric mucosa, which decreased in that of GC patients (Wang et al., 2020). Both *Haemophilus* and *Nitrospirae* are nitrate-reducing bacteria, which convert nitrate to nitrite, and also to nitric oxide (NO), which can be absorbed through the blood vessels in the oral cavity or through being swallowed into the gastrointestinal system. Accumulation of N-nitroso compounds in the gastrointestinal tract is likely to increase the risk of carcinogenesis (Forsythe and Cole, 1987; Bryan et al., 2012). Thus, the decreased abundances of *Haemophilus* in the salivary microbiota may contribute to the formation of gastric tumor.

Functional analysis based on the PICRUSt2-predicted pathways suggested that metabolic functions of salivary microbiota changed along with the disease progression in the stomach. In particular, pathways involved in isoleucine and valine biosynthesis were highly expressed by the salivary microbiota in GC patients compared to the non-malignant stages. Interestingly, an upregulation of amino acids including isoleucine and valine was also detected in human gastric tumor tissues (Jung et al., 2014; Wang et al., 2016). Higher levels of most amino acids and their primary derivatives in gastric tumor tissues were thought to be related to two main sources: the degradation of extracellular matrix by matrix metalloproteinases and the autophagic degradation of intracellular proteins (Hirayama et al., 2009). The production of amino acid from microbes in the oral cavity and gastrointestinal tract has not been quantified and deserves further investigation in terms of proliferation and survival of gastric cancer cells.

There were several limitations in this study. Firstly, we didn't collect samples from healthy individuals as control. Secondly, amplicon sequencing of 16S rRNA has limited resolution in determining the bacterial species or strains, and it is therefore difficult to access the functions of specific bacteria involved in gastric cancer development and progression. In addition, the 16S rRNA gene V1–V3 region has been shown to provide superior taxonomic resolution for the bacterial microbiota of the human oral and respiratory tracts compared to the V3–V4 region (Zheng et al., 2015; Escapa et al., 2018). Thus, some other oral taxa with diagnostic potential for gastric cancer might not have been detected in the present data. Finally, independent clinical cohorts from multiple centers are required to evaluate the diagnostic value of the identified GC-associated saliva bacteria.

CONCLUSIONS

We demonstrated, with a large cohort, that the salivary microbiota can be used to predict GC as well as its non-malignant stages. The contributions of the oral microbiota in the pathogenesis of GC include an accumulation of proinflammatory bacteria and a decline in those reducing carcinogenic N-nitroso compounds.

DATA AVAILABILITY STATEMENT

The data presented in the study are deposited in European Nucleotide Archive (https://www.ebi.ac.uk/ena/submit/sra/#studies), accession number PRJEB42657.

ETHICS STATEMENT

The studies involving human participants were reviewed and approved by the ethics committee of the Chinese PLA General Hospital (No. S2016-057-02). The patients/participants provided their written informed consent to participate in this study.

AUTHOR CONTRIBUTIONS

YY conceived the study and revised the manuscript. KH, LW, BY, ZW, XZ, LP, JY, and GS performed the subject's enrolment and sample collection. XG and KH analyzed clinical and sequencing data. KH and XG wrote this manuscript. All authors contributed to the article and approved the submitted version.

ACKNOWLEDGMENTS

We would like to extend our sincere gratitude to Dr. Xiaolin Zhao for her invaluable contributions to the development of this manuscript.

SUPPLEMENTARY MATERIAL

The Supplementary Material for this article can be found online at: https://www.frontiersin.org/articles/10.3389/fcimb.2021.640309/full#supplementary-material

Supplementary Table 1 | Differences in the salivary microbiota compositions among patients at different progressive histological stages of gastric tumorigenesis.

Supplementary Figure 1 | The salivary microbiota biodiversity in AG patients with and without intestinal metaplasia. The alpha diversity of salivary microbiota was measure at the ASV level by using **(A)** Shannon index, **(B)** Chao1. Comparison between intra-group and inter-group community distances by **(C)** unweighted UniFrac distance matrix and **(D)** weighted UniFrac distance matrix revealed no significant difference between the microbiota compositions between AG patients with and without intestinal metaplasia. *P* value was calculated by Anosim comparing the intra-group distances with between-group distances.

Supplementary Figure 2 | The salivary microbiota biodiversity in GC patients with different histological grades. The alpha diversity of salivary microbiota was measure at the ASV level by using **(A)** Shannon index, and **(B)** Chao1 index. Comparison between intra-group and inter-group community distances by **(C)** unweighted UniFrac distance matrix and **(D)** weighted UniFrac distance matrix revealed no significant difference between the microbiota compositions among patients with well differentiated (W), moderately differentiated (M), and poorly differentiated(P) gastric tumor. *P* value was calculated by Anosim comparing the intra-group distances with between-group distances.

Supplementary Figure 3 | The salivary microbiota compositions in patients at different histological stages of gastric tumorigenesis. The relative abundances of most abundant **(A)** phyla and **(B)** genera detected in the salivary microbiota in SG, AG, and GC patients.

Supplementary Figure 4 | Microbiological features of the salivary microbiota associated with different histological stages of gastric tumorigenesis. **(A)** Bacteria taxa that enriched in each histological stage were determined by LEfSe with Kruskal–Wallis test $P<0.05$ and log 10 LDA score>3.4. **(B)** ROC curves analysis to evaluate the discriminatory potential of salivary bacteria in identifying GC out of pre-malignant lesions. **(C)**The top 10 bacterial genera that are most important for discriminating between SG, AG, and GC. Each genus is ranked according to an importance score (mean decrease accuracy).

Supplementary Figure 5 | Network analyses reveal commensal relationships among the salivary bacteria. Spearman correlation network analyses showing the commensal relationships among the top 30 most abundant genera in the salivary microbiota of **(A)** superficial gastritis, **(B)** atrophic gastritis, and **(C)** gastric cancer. Taxa are represented as nodes, taxa abundance as node size, and are colored based on their belonging phylum. Edges represent significant correlations (Holm-corrected $P < 0.05$) among these taxa. Red and blue edges represent positive and negative correlations, respectively.

Supplementary Figure 6 | Functional changes in the salivary microbiota are associated with the progression of gastric carcinoma. PICRUSt2 predicted metabolic pathways that significantly different in the salivary microbiota of patients at different progressive histological stages of gastric tumorigenesis. Significance was determined by using Kruskal–Wallis rank sum test with BH-adjusted $P < 0.05$.

Supplementary File 1 | ASVs obtained from Naive Bayes classifier on the 16S rRNA sequencing of V3–V4 hypervariable regions.

Supplementary Code 1 | R code and taxa abundance table used for constructing the random forest model and generating the AUC ROC curve.

REFERENCES

Aas, J. A., Paster, B. J., Stokes, L. N., Olsen, I., and Dewhirst, F. E. (2005). Defining the normal bacterial flora of the oral cavity. *J. Clin. Microbiol.* 43 (11), 5721–5732. doi: 10.1128/JCM.43.11.5721-5732.2005

Abdulamir, A. S., Hafidh, R. R., and Abu Bakar, F. (2011). The association of Streptococcus bovis/gallolyticus with colorectal tumors: the nature and the underlying mechanisms of its etiological role. *J. Exp. Clin. Cancer Res.* 30, 11. doi: 10.1186/1756-9966-30-11

Ahn, J., Chen, C. Y., and Hayes, R. B. (2012). Oral microbiome and oral and gastrointestinal cancer risk. *Cancer Causes Control* 23 (3), 399–404. doi: 10.1007/s10552-011-9892-7

Bolyen, E., Rideout, J. R., Dillon, M. R., Bokulich, N. A., Abnet, C. C., Al-Ghalith, G. A., et al. (2019). Reproducible, interactive, scalable and extensible microbiome data science using QIIME 2. *Nat. Biotechnol.* 37 (8), 852–857. doi: 10.1038/s41587-019-0209-9

Bornigen, D., Ren, B., Pickard, R., Li, J., Ozer, E., Hartmann, E. M., et al. (2017). Alterations in oral bacterial communities are associated with risk factors for oral and oropharyngeal cancer. *Sci. Rep.* 7 (1), 17686. doi: 10.1038/s41598-017-17795-z

Bray, F., Ferlay, J., Soerjomataram, I., Siegel, R. L., Torre, L. A., and Jemal, A. (2018). Global cancer statistics 2018: GLOBOCAN estimates of incidence and mortality worldwide for 36 cancers in 185 countries. *CA Cancer J. Clin.* 68 (6), 394–424. doi: 10.3322/caac.21492

Bryan, N. S., Alexander, D. D., Coughlin, J. R., Milkowski, A. L., and Boffetta, P. (2012). Ingested nitrate and nitrite and stomach cancer risk: an updated review. *Food Chem. Toxicol.* 50 (10), 3646–3665. doi: 10.1016/j.fct.2012.07.062

Castano-Rodriguez, N., Goh, K. L., Fock, K. M., Mitchell, H. M., and Kaakoush, N. O. (2017). Dysbiosis of the microbiome in gastric carcinogenesis. *Sci. Rep.* 7 (1), 15957. doi: 10.1038/s41598-017-16289-2

Chen, F. L., Hsueh, P. R., Teng, S. O., Ou, T. Y., and Lee, W. S. (2012). Corynebacterium striatum bacteremia associated with central venous catheter infection. *J. Microbiol. Immunol. Infect.* 45 (3), 255–258. doi: 10.1016/j.jmii.2011.09.016

Chen, X., Winckler, B., Lu, M., Cheng, H., Yuan, Z., Yang, Y., et al. (2015). Oral Microbiota and Risk for Esophageal Squamous Cell Carcinoma in a High-Risk Area of China. *PloS One* 10 (12), e0143603. doi: 10.1371/journal.pone.0143603

Chen, X. H., Wang, A., Chu, A. N., Gong, Y. H., and Yuan, Y. (2019). Mucosa-Associated Microbiota in Gastric Cancer Tissues Compared With Non-cancer Tissues. *Front. Microbiol.* 10, 1261. doi: 10.3389/fmicb.2019.01261

Coker, O. O., Dai, Z., Nie, Y., Zhao, G., Cao, L., Nakatsu, G., et al. (2018). Mucosal microbiome dysbiosis in gastric carcinogenesis. *Gut* 67 (6), 1024–1032. doi: 10.1136/gutjnl-2017-314281

Cui, J., Cui, H., Yang, M., Du, S., Li, J., Li, Y., et al. (2019). Tongue coating microbiome as a potential biomarker for gastritis including precancerous cascade. *Protein Cell* 10 (7), 496–509. doi: 10.1007/s13238-018-0596-6

Dicksved, J., Lindberg, M., Rosenquist, M., Enroth, H., Jansson, J. K., and Engstrand, L. (2009). Molecular characterization of the stomach microbiota in patients with gastric cancer and in controls. *J. Med. Microbiol.* 58 (Pt 4), 509–516. doi: 10.1099/jmm.0.007302-0

Dizdar, O., Hayran, M., Guven, D. C., Yılmaz, T. B., Taheri, S., Akman, A. C., et al. (2017). Increased cancer risk in patients with periodontitis. *Curr. Med. Res. Opin.* 33 (12), 2195–2200. doi: 10.1080/03007995.2017.1354829

Douglas, G. M., Maffei, V. J., Zaneveld, J. R., Yurgel, S. N., Brown, J. R., Taylor, C. M., et al. (2020). PICRUSt2 for prediction of metagenome functions. *Nat. Biotechnol.* 38 (6), 685–688. doi: 10.1038/s41587-020-0548-6

Engstrand, L., and Lindberg, M. (2013). Helicobacter pylori and the gastric microbiota. *Best Pract. Res. Clin. Gastroenterol.* 27 (1), 39–45. doi: 10.1016/j.bpg.2013.03.016

Escapa, I. F., Chen, T., Huang, Y., Gajare, P., Dewhirst, F. E., and Lemon, K. P. (2018). New Insights into Human Nostril Microbiome from the Expanded Human Oral Microbiome Database (eHOMD): a Resource for the Microbiome of the Human Aerodigestive Tract. *mSystems* 3 (6), e00187-18. doi: 10.1128/mSystems.00187-18

Fan, X., Alekseyenko, A. V., Wu, J., Peters, B. A., Jacobs, E. J., Gapstur, S. M., et al. (2018a). Human oral microbiome and prospective risk for pancreatic cancer: a population-based nested case-control study. *Gut* 67 (1), 120–127. doi: 10.1136/gutjnl-2016-312580

Fan, X., Peters, B. A., Jacobs, E. J., Gapstur, S. M., Purdue, M. P., Freedman, N. D., et al. (2018b). Drinking alcohol is associated with variation in the human oral microbiome in a large study of American adults. *Microbiome* 6 (1), 59. doi: 10.1186/s40168-018-0448-x

Flemer, B., Warren, R. D., Barrett, M. P., Cisek, K., Das, A., Jeffery, I. B., et al. (2018). The oral microbiota in colorectal cancer is distinctive and predictive. *Gut* 67 (8), 1454–1463. doi: 10.1136/gutjnl-2017-314814

Forsythe, S. J., and Cole, J. A. (1987). Nitrite accumulation during anaerobic nitrate reduction by binary suspensions of bacteria isolated from the achlorhydric stomach. *J. Gen. Microbiol.* 133 (7), 1845–1849. doi: 10.1099/00221287-133-7-1845

Gao, L., Xu, T., Huang, G., Jiang, S., Gu, Y., and Chen, F. (2018). Oral microbiomes: more and more importance in oral cavity and whole body. *Protein Cell* 9 (5), 488–500. doi: 10.1007/s13238-018-0548-1

Goral, V. (2016). Etiopathogenesis of Gastric Cancer. *Asian Pac. J. Cancer Prev.* 17 (6), 2745–2750.

Han, Y. W., and Wang, X. (2013). Mobile microbiome: oral bacteria in extra-oral infections and inflammation. *J. Dental Res.* 92 (6), 485–491. doi: 10.1177/0022034513487559

He, J., Li, Y., Cao, Y., Xue, J., and Zhou, X. (2015). The oral microbiome diversity and its relation to human diseases. *Folia Microbiol.* 60 (1), 69–80. doi: 10.1007/s12223-014-0342-2

Hirayama, A., Kami, K., Sugimoto, M., Sugawara, M., Toki, N., Onozuka, H., et al. (2009). Quantitative metabolome profiling of colon and stomach cancer microenvironment by capillary electrophoresis time-of-flight mass spectrometry. *Cancer Res.* 69 (11), 4918–4925. doi: 10.1158/0008-5472.CAN-08-4806

Jean-François, F. (2011). [WHO Classification of digestive tumors: the fourth edition]. *Ann. Pathol.* 31 (5 Suppl), S27–S31. doi: 10.1016/j.annpat.2011.1008.1001-1031

Jung, J., Jung, Y., Bang, E. J., Cho, S. I., Jang, Y. J., Kwak, J. M., et al. (2014). Noninvasive diagnosis and evaluation of curative surgery for gastric cancer by using NMR-based metabolomic profiling. *Ann. Surg. Oncol.* 21 (Suppl 4), S736–S742. doi: 10.1245/s10434-014-3886-0

Kageyama, S., Takeshita, T., Takeuchi, K., Asakawa, M., Matsumi, R., Furuta, M., et al. (2019). Characteristics of the Salivary Microbiota in Patients With Various Digestive Tract Cancers. *Front. Microbiol.* 10, 1780. doi: 10.3389/fmicb.2019.01780

Kauppila, J. H., and Selander, K. S. (2014). Toll-like receptors in esophageal cancer. *Front. Immunol.* 5, 200. doi: 10.3389/fimmu.2014.00200

Mager, D. L., Haffajee, A. D., Devlin, P. M., Norris, C. M., Posner, M. R., and Goodson, J. M. (2005). The salivary microbiota as a diagnostic indicator of oral cancer: a descriptive, non-randomized study of cancer-free and oral squamous cell carcinoma subjects. *J. Transl. Med.* 3, 27. doi: 10.1186/1479-5876-3-27

Massarrat, S., and Stolte, M. (2014). Development of gastric cancer and its prevention. *Arch. Iran. Med.* 17 (7), 514–520.

Michaud, D. S., and Izard, J. (2014). Microbiota, oral microbiome, and pancreatic cancer. *Cancer J.* 20 (3), 203–206. doi: 10.1097/PPO.0000000000000046

Michaud, D. S., Lu, J., Peacock-Villada, A. Y., Barber, J. R., Joshu, C. E., Prizment, A. E., et al. (2018). Periodontal Disease Assessed Using Clinical Dental Measurements and Cancer Risk in the ARIC Study. *J. Natl. Cancer Inst.* 110 (8), 843–854. doi: 10.1093/jnci/djx278

Peek, R.M.Jr., and Crabtree, J. E. (2006). Helicobacter infection and gastric neoplasia. *J. Pathol.* 208 (2), 233–248. doi: 10.1002/path.1868

Peters, B. A., Wu, J., Pei, Z., Yang, L., Purdue, M. P., Freedman, N. D., et al. (2017). Oral Microbiome Composition Reflects Prospective Risk for Esophageal Cancers. *Cancer Res.* 77 (23), 6777–6787. doi: 10.1158/0008-5472.CAN-17-1296

Plummer, M., Franceschi, S., Vignat, J., Forman, D., and de Martel, C. (2015). Global burden of gastric cancer attributable to Helicobacter pylori. *Int. J. Cancer* 136 (2), 487–490. doi: 10.1002/ijc.28999

Polk, D. B., and Peek, R. M.Jr (2010). Helicobacter pylori: gastric cancer and beyond. *Nat. Rev. Cancer* 10 (6), 403–414. doi: 10.1038/nrc2857

Rubinstein, M. R., Wang, X., Liu, W., Hao, Y., Cai, G., and Han, Y. W. (2013). Fusobacterium nucleatum promotes colorectal carcinogenesis by modulating E-cadherin/beta-catenin signaling via its FadA adhesin. *Cell Host Microbe* 14 (2), 195–206. doi: 10.1016/j.chom.2013.07.012

Salazar, C. R., Francois, F., Li, Y., Corby, P., Hays, R., Leung, C., et al. (2012). Association between oral health and gastric precancerous lesions. *Carcinogenesis* 33 (2), 399–403. doi: 10.1093/carcin/bgr284

Segata, N., Izard, J., Waldron, L., Gevers, D., Miropolsky, L., Garrett, W. S., et al. (2011). Metagenomic biomarker discovery and explanation. *Genome Biol.* 12 (6), R60. doi: 10.1186/gb-2011-12-6-r60

Shi, Y. C., Wang, Z. K., and Yang, Y. S. (2019). Biobank Branch China Medicinal Biotech Association, the Digestive Biobanking Committee China Association of Medical Equipment, the Gut Microbiome Committee China Society of Gastroenterology. (2019). Consensus on standard biobanking of gut microbiota. *J. Dig. Dis.* 20 (3), 114–121. doi: 10.1111/1751-2980.12705

Seymour, R. A. (2010). Is oral health a risk for malignant disease? *Dental Update* 37 (5), 279–283. doi: 10.12968/denu.2010.37.5.279

Sun, J.-H., Li, X.-L., Yin, J., Li, Y.-H., Hou, B.-X., and Zhang, Z. (2018). A screening method for gastric cancer by oral microbiome detection. *Oncol. Rep.* 39 (5), 2217–2224. doi: 10.3892/or.2018.6286

Sung, J. J. Y., Coker, O. O., Chu, E., Szeto, C. H., Luk, S. T. Y., Lau, H. C. H., et al. (2020). Gastric microbes associated with gastric inflammation, atrophy and intestinal metaplasia 1 year after Helicobacter pylori eradication. *Gut* 69 (9), 1572–1580. doi: 10.1136/gutjnl-2019-319826

Ternes, D., Karta, J., Tsenkova, M., Wilmes, P., Haan, S., and Letellier, E. (2020). Microbiome in Colorectal Cancer: How to Get from Meta-omics to Mechanism? *Trends Microbiol.* 28 (5), 401–423. doi: 10.1016/j.tim.2020.01.001

Wade, W. G. (2013). The oral microbiome in health and disease. *Pharmacol. Res.* 69 (1), 137–143. doi: 10.1016/j.phrs.2012.11.006

Wang, H., Zhang, H., Deng, P., Liu, C., Li, D., Jie, H., et al. (2016). Tissue metabolic profiling of human gastric cancer assessed by (1)H NMR. *BMC Cancer* 16, 371. doi: 10.1186/s12885-016-2356-4

Wang, Z., Gao, X., Zeng, R., Wu, Q., Sun, H., Wu, W., et al. (2020). Changes of the Gastric Mucosal Microbiome Associated With Histological Stages of Gastric Carcinogenesis. *Front. Microbiol.* 11, 997. doi: 10.3389/fmicb.2020.00997

Warren, J. R., and Marshall, B. (1983). Unidentified curved bacilli on gastric epithelium in active chronic gastritis. *Lancet (London England)* 1 (8336), 1273–1275.

Watabe, K., Nishi, M., Miyake, H., and Hirata, K. (1998). Lifestyle and gastric cancer: a case-control study. *Oncol. Rep.* 5 (5), 1191–1194. doi: 10.3892/or.5.5.1191

Whitmore, S. E., and Lamont, R. J. (2014). Oral bacteria and cancer. *PloS Pathog.* 10 (3), e1003933–e1003933. doi: 10.1371/journal.ppat.1003933

Wu, J., Peters, B. A., Dominianni, C., Zhang, Y., Pei, Z., Yang, L., et al. (2016). Cigarette smoking and the oral microbiome in a large study of American adults. *ISME J.* 10 (10), 2435–2446. doi: 10.1038/ismej.2016.37

Wu, J., Xu, S., Xiang, C., Cao, Q., Li, Q., Huang, J., et al. (2018). Tongue Coating Microbiota Community and Risk Effect on Gastric Cancer. *J. Cancer* 9 (21), 4039–4048. doi: 10.7150/jca.25280

Yang, L., Chaudhary, N., Baghdadi, J., and Pei, Z. (2014). Microbiome in reflux disorders and esophageal adenocarcinoma. *Cancer J.* 20 (3), 207–210. doi: 10.1097/PPO.0000000000000044

Zhao, Y., Gao, X., Guo, J., Yu, D., Xiao, Y., Wang, H., et al. (2019). Helicobacter pylori infection alters gastric and tongue coating microbial communities. *Helicobacter* 24 (2), e12567. doi: 10.1111/hel.12567

Zheng, W., Tsompana, M., Ruscitto, A., Sharma, A., Genco, R., Sun, Y., et al. (2015). An accurate and efficient experimental approach for characterization of the complex oral microbiota. *Microbiome* 3, 48. doi: 10.1186/s40168-015-0110-9

Conflict of Interest: The authors declare that the research was conducted in the absence of any commercial or financial relationships that could be construed as a potential conflict of interest.

frontiers in Cellular and Infection Microbiology

ORIGINAL RESEARCH
published: 19 March 2021
doi: 10.3389/fcimb.2021.643913

Oral Pathogen *Fusobacterium nucleatum* Coaggregates With *Pseudomonas aeruginosa* to Modulate the Inflammatory Cytotoxicity of Pulmonary Epithelial Cells

Qian Li[1], *Hongyan Wang*[2], *Lisi Tan*[2], *Shuwei Zhang*[2], *Li Lin*[2], *Xiaolin Tang*[2] *and Yaping Pan*[1,2*]

[1] Liaoning Provincial Key Laboratory of Oral Diseases, Department of Oral Biology, School and Hospital of Stomatology, China Medical University, Shenyang, China, [2] Liaoning Provincial Key Laboratory of Oral Diseases, Department of Periodontics, School and Hospital of Stomatology, China Medical University, Shenyang, China

OPEN ACCESS

Edited by:
Loreto Abusleme,
University of Chile, Chile

Reviewed by:
Denisse Bravo,
University of Chile, Chile
Anilei Hoare,
University of Chile, Chile

***Correspondence:**
Yaping Pan
yppan@cmu.edu.cn

Specialty section:
This article was submitted to Bacteria and Host, a section of the journal Frontiers in Cellular and Infection Microbiology

Received: 19 December 2020
Accepted: 02 March 2021
Published: 19 March 2021

Citation:
Li Q, Wang H, Tan L, Zhang S, Lin L, Tang X and Pan Y (2021) Oral Pathogen Fusobacterium nucleatum Coaggregates With Pseudomonas aeruginosa to Modulate the Inflammatory Cytotoxicity of Pulmonary Epithelial Cells. Front. Cell. Infect. Microbiol. 11:643913. doi: 10.3389/fcimb.2021.643913

Chronic obstructive pulmonary disease (COPD) is the third leading cause of mortality worldwide, and inflammatory damage induced by bacterial infections is an important contributor to the etiology of COPD. *Fusobacterium nucleatum*, a recognized periodontal pathogen, is considered as a biomarker of lung function deterioration of COPD patients coinfected with *Pseudomonas aerugionsa*, but the underlying mechanism is still unclear. This study established single- and dual-species infection models, bacterial simultaneous and sequential infection models, and found that *F. nucleatum* could coaggregate with *P. aeruginosa* to synergistically invade into pulmonary epithelial cells and transiently resist *P. aeruginosa*-induced cytotoxic damage to amplify IL-6 and TNF-α associated inflammation in pulmonary epithelial cells simultaneously infected with *P. aeruginosa* and *F. nucleatum*. Furthermore, *F. nucleatum* pretreatment or subsequential infection could maintain or even aggravate *P. aeruginosa*-induced inflammatory cytotoxicity of pulmonary epithelial cells. These results indicate that oral pathogen *F. nucleatum* coaggregates with *P. aeruginosa* to facilitate bacterial invasion and modulates the inflammatory cytotoxicity of pulmonary epithelial cells, which may contribute to lung function deterioration of COPD patients accompanied with *P. aeruginosa* and *F. nucleatum* coinfection.

Keywords: ***Pseudomonas aeruginosa*, *Fusobacterium nucleatum*, chronic obstructive pulmonary disease, bacterial coaggregation, pulmonary epithelial cells, inflammatory cytotoxicity**

INTRODUCTION

Chronic obstructive pulmonary disease (COPD) is the third leading cause of mortality worldwide, characterized by persistent airflow limitation and respiratory symptoms including dyspnea, cough and/or sputum production (Singh et al., 2019). 54.7% of patients with COPD exacerbations admitted to the hospital are associated with respiratory bacterial infection, (Papi et al., 2006). *Pseudomonas*

aeruginosa, a ubiquitous opportunistic pathogen, is one of the most prevalent bacteria responsible for respiratory infection in COPD patients (Choi et al., 2019). *P. aeruginosa* is associated with prolonged hospitalization, increased exacerbation rate and poor lone-term prognosis in COPD patients (Garcia-Vidal et al., 2009; Almagro et al., 2012; Eklof et al., 2020).

In 1999, Dr. Scannapieco first proposed that oral microbiota is closely related to respiratory infections (Scannapieco, 1999). The dynamic and polymicrobial dental plaque biofilm has been proved as a reservoir of respiratory pathogens, direct inhalation of the shedding of dental plaque colonized by respiratory pathogens into lung is one of the most possible mechanisms involved in the association between oral microbiota and respiratory diseases (Tan et al., 2014; Sands et al., 2017). *Fusobacterium nucleatum*, an oral commensal and periodontal pathogen, is ubiquitous in the oral cavity of healthy and diseased individuals. *F. nucleatum* acts as a coaggregation bridge between early and late colonizing bacteria in the polymicrobial dental plaque biofilm, and affects the composition and architecture of supra- and subgingival biofilm (Thurnheer et al., 2019). Recent studies demonstrate that *F. nucleatum* colonizes in the respiratory tract, not only leads to respiratory infection in patients with chronic diseases such as tumors and diabetes (Yang et al., 2011; Bailhache et al., 2013; Shamriz et al., 2015), but also causes endobronchial lesion in healthy children (Gedik et al., 2014). Meanwhile, our previous study finds that *F. nucleatum* and *P. aeruginosa* frequently coexisted in the respiratory tract of patients with COPD exacerbation, and as the number of *F. nucleatum* in the respiratory tract microbiota increases, their lung function declines (Li et al., 2020). These results suggest that *F. nucleatum* and *P. aeruginosa* may play a synergistic role in respiratory infection of COPD patients, but the mechanism underlying this is still unclear.

The ability to adhere and invade host cells is a virulence property of certain bacteria. Although *P. aeruginosa* is usually considered an extracellular pathogen, some studies have demonstrated that *P. aeruginosa* can invade a variety of epithelial cells *via* an endocytic process dependent on actin microfilaments (Fleiszig et al., 1994; Fleiszig et al., 1995). The invasive *P. aeruginosa* induces membrane blebs in epithelial cells, which are utilized as a niche for bacterial intracellular replication and motility (Angus et al., 2008). In contrast, *F. nucleatum* adheres to and invades epithelial cells *via* a zipping mechanism relying on its outer membrane proteins to bind to the cell-surface receptors (Han et al., 2000). At the same time, *F. nucleatum* can coaggregate with almost all of the oral bacteria dependent on its outer membrane proteins (Kaplan et al., 2009; Loozen et al., 2014; Coppenhagen-Glazer et al., 2015). *F. nucleatum* not only enhances the adhesion and invasion of invasive bacteria such as *Porphyromonas gingivalis* and *Aggregatibacter actinomycetemcomitans* to tissue cells (Li et al., 2015), but also transports noninvasive bacteria such as *Streptococcus cristatus* and *Streptococcus sanguis* into epithelial cells (Edwards et al., 2006). It is still unclear whether *F. nucleatum* will affect the infection of *P. aeruginosa* to pulmonary epithelial cells due to interspecies coaggregation in COPD patients accompanied with coinfection of *F. nucleatum* and *P. aeruginosa*.

Mucosal epithelium is not only the first physical barrier between host and bacteria, but also an active participant in natural immunity and inflammation (Proud and Leigh, 2011). IL-1β is considered a biomarker of bacteria-associated exacerbation of COPD, and TNF-α and IL-6 are the potential markers of IL-1β-associated exacerbation of COPD (Bafadhel et al., 2011; Damera et al., 2016). Vos et al. found that *P. aeruginosa* infection of human bronchial epithelial cells can significantly induce the expression of IL-1 family members IL-1β and IL-1F9 (Vos et al., 2005). *P. aeruginosa*-derived flagellin induces IL-6 and IL-8 production in bronchial epithelial cells through the phosphorylation of p38, ERK and JNK, which partially explains the underlying mechanism of *P. aeruginosa* causing acute exacerbation of COPD (Nakamoto et al., 2019). Hayata et al. report that *F. nucleatum* induces the productions of proinflammatory cytokines IL-6 and IL-8 by the bronchial and pharyngeal epithelial cells, which may trigger exacerbation of COPD (Hayata et al., 2019). Therefore, we speculate that coinfection of *P. aeruginosa* and *F. nucleatum* may induce cytokine release dysregulation in pulmonary epithelial cells, we plan to establish bacterial simultaneous and sequential infection models to simulate three types of clinical mixed-infection modes in order to fully confirm our scientific hypothesis, and to further reveal the possible mechanism of *P. aeruginosa* and *F. nucleatum* coinfection causing lung function decline in COPD patients.

On the basis of the above thinking and hypothesis, the aim of this study was to explore the potential mechanism by which *F. nucleatum* cooperated with *P. aeruginosa* to exacerbate COPD. First, we investigated the effect of bacterial coinfection on bacterial adhesion and invasion ability, and the role of bacterial coaggregation in this process. Second, we established bacterial simultaneous and sequential infection models to simulate three types of clinical mixed-infection modes, and detected the effect of the combined infection with *P. aeruginosa* and *F. nucleatum* on inflammation and damage of pulmonary epithelial cells.

MATERIALS AND METHODS

Bacteria Culture

F. nucleatum (ATCC 25586) and *P. aeruginosa* PAO1 strain (ATCC BAA-47) were obtained from American Type Culture Collection (ATCC). *F. nucleatum* was grown in tryptic soy broth (TSB. Becton, Dickinson and Company, Sparks, MD, USA) supplemented with 5% defibrinated sheep blood, 10mg/ml hemin and 5mg/ml menadione in anaerobic atmosphere (10% H_2, 10% CO_2, 80% N_2) at 37 °C (Yu et al., 2017; Wu et al., 2018). *P. aeruginosa* was cultured in TSB under aerobic conditions at 37°C.

Bacterial Aggregation Assay

P. aeruginosa and *F. nucleatum* were standardized in sterile coaggregation buffer (150 mM NaCl, 1 mM Tris, 0.1 mM $CaCl_2$ and 0.1 mM $MgCl_2$) to give a final cell density of 1×10^9 colony-forming units per mL (CFUs/mL). Equal numbers of

single- or dual-species bacterial cells were suspended and vortexed for 30 s in a reaction tube (T=0 h). The tubes were incubated at room temperature for 1 h to allow aggregation (T=1 h). A visual rating scale of 0-4 was used to grade the reaction. "0" indicates an evenly turbid suspension with no visible aggregates, meaning no coaggregation; "1+" indicates turbid supernatant with finely dispersed coaggregates; "2+" indicates definite coaggregates that do not precipitate immediately; "3+" indicates slightly turbid supernatant with formation of large precipitating coaggregates; and "4+" indicates complete sedimentation with a clear supernatant (Cisar et al., 1979; Shimazu et al., 2016). In addition, a spectrophotometric assay was employed to determine the percentage of bacterial auto- and coaggregation (Cisar et al., 1979; Kaplan et al., 2009). The optical density of bacterial suspensions at 600 nm wavelength (OD600) were measured at the time points of 0 and 1 h. Percentage aggregation was calculated using the following equation: % autoaggregation or coaggregation $=(OD600_{(T0)}\text{-}OD600_{(T1)})/OD600_{(T0)} \times 100$. Percentage aggregation were classified as high (more than 40%), intermediate (30-40%) and low aggregation (less than 30%).

Phase Contrast Microscopy

Auto- and coaggregation of the test bacterial species were also studied by phase contrast microscopy. After preparing bacterial suspensions with or without partner species in coaggregation buffer for 1 h as described above, 10 μL from each preparation was mounted on a microscopic glass slide with a coverslip and photographed by phase contrast microscope (Olympus, Japan).

Cell Culture

Human pulmonary epithelial cell line A549 was obtained from ATCC and cultured in Dulbecco's modified Eagle's medium (DMEM. HyClone Laboratories, Logan, UT, USA) supplemented with 10% fetal bovine serum (FBS. HyClone Laboratories, Logan, UT, USA), 100 U/mL penicillin and 100 mg/mL streptomycin in a humidified 37°C incubator with 5% CO_2.

Bacterial Infection of Pulmonary Epithelial Cells

The *in vitro* bacterial infection model used in this study was performed as described previously (Pan et al., 2009; Li et al., 2019). Briefly, A549 cells were seeded into 24-well tissue culture plates at a density of 10^5 cells/well. Cells were inoculated and grown for 24 h to allow the cells to reach confluence. Logarithmic growth phase bacteria were harvested and resuspended to 10^7 CFUs/mL in DMEM without antibiotics. A549 cells were incubated with *F. nucleatum* and *P. aeruginosa* alone or together at multiplicity of infection (MOI, bacteria: epithelial cells) of 10, 50 or 100 in DMEM without antibiotics. For bacterial simultaneous infection model, A549 cells were incubated with both *F. nucleatum* (MOI 100) and *P. aeruginosa* (MOI 100) at the same times in DMEM without antibiotics. For bacterial sequential infection model, A549 cells were treated with *F. nucleatum* (MOI 100) or *P. aeruginosa* (MOI 100) in DMEM without antibiotics for 12 h, and then added the other bacteria (MOI 100) to continue infection for 12 h. In order to exclude the effect of the increased bacterial load, the single *P. aeruginosa* or *F. nucleatum* infection groups at a MOI of 200 were used as controls in the bacterial simultaneous infection assay, and the sequential inoculation of the same bacteria were used as controls in the bacterial sequential infection assay.

Antibiotic Protection Adhesion and Invasion Assay

Assays of bacterial adherence and invasion were performed using methods previously described (Pan et al., 2009). Briefly, bacteria were harvested, washed, and resuspended in DMEM without antibiotics. A549 cells were infected with bacteria in DMEM without antibiotics in the humidified 37°C incubator with 5% CO_2 for 3 h, and washed with phosphate-buffered saline (PBS). For determining total adhesion and invasion levels (attachment levels), cells were lysed with sterile distilled water for 30 min, then dilutions of the lysate were plated and cultured anaerobically on TSB agar supplemented with 5% defibrinated sheep blood, 10mg/ml hemin and 5mg/ml menadione to determine CFUs for *F. nucleatum*, or cultured aerobically on TSB agar to determine CFUs for *P. aeruginosa*. For invasion assay, extracellular bacteria were killed with 200 μg/mL gentamicin (Sigma, St. Louis, MO, USA) and 300 μg/mL metronidazole (Sigma, St. Louis, MO, USA) for 1 h. Cellular lysate were diluted and cultured to determine CFUs. The number of bacterial attachment or invasion is equal to CFUs divided by the number of cells.

Scanning Electron Microscopy (SEM)

A549 cells were infected with *P. aeruginosa* (MOI 100) and *F. nucleatum* (MOI 100) alone or together in DMEM without antibiotics for 3 h, washed with PBS, and fixed with 2.5% glutaraldehyde (BioChemika, Fluka, Switzerland). A549 cells were gradually dehydrated with ethanol and smeared onto copper plates followed by gold sputtering, and images were acquired using SEM (Inspect F50, FEI Company, USA) to observe the bacterial adhesion and cell morphology.

CCK-8 Cell Viability Assay

Cell counting kit (Dojindo Molecular Technologies, Inc., Kumamoto, Japan) was used to assess cell proliferation according to the manufacturer's manual. Briefly, A549 cells were infected with *P. aeruginosa* and *F. nucleatum* alone (MOI 10, 50 or 100) or together (MOI 100) in DMEM without antibiotics for 4, 8, 16 and 24 h. 10 μL of CCK-8 solution was added to 100 μL of medium solution and incubated for 1 h at 37°C. OD450 was measured with a microplate reader (Infinite M200, Tecan, Austria) to reflect the cell proliferation.

Cytotoxicity Assessment by Lactate Dehydrogenase (LDH) Leakage Assay

LDH activity was monitored by the Pierce™ LDH cytotoxicity assay kit (Thermo Scientific, USA) in accordance with the manufacturer's recommendations. A549 cells were exposed to *P. aeruginosa* and *F. nucleatum* alone (MOI 10, 50 or 100) or

together (MOI 100) in DMEM without antibiotics for the desired time, the culture supernatant was harvested and centrifuged at 12000 g for 5 min, and 50 μL supernatant was mixed with 50 μL Reaction mixture and incubated at room temperature in the dark for 30 min. 50 μL stop solution was added to stop reaction. OD490 and OD680 were measured with a microplate reader (Infinite M200, Tecan, Austria). LDH activity = OD490-OD680.

Live/Dead Assay by Calcein Acetoxymethyl Ester/Propidium Iodide (Calcein-AM/PI) Staining

The effects of *P. aeruginosa* and *F. nucleatum* on the viability or cytotoxicity of pulmonary epithelial cells were evaluated using the Calcein-AM/PI Double Stain Kit (Molecular Probes, Eugene, OR, USA). In brief, A549 cells were exposed to *P. aeruginosa* and *F. nucleatum* alone or together in DMEM without antibiotics for the desired time, washed with PBS. Cells were stained with 200 μL Calcein-AM/PI stain working solution at 37°C for 15 min. Living cells (green cytoplasmic fluorescence) and dead cells (red nucleus fluorescence) were immediately observed by fluorescence microscope.

Enzyme-Linked Immunosorbent Assay (ELISA)

A549 cells were exposed to *P. aeruginosa* and *F. nucleatum* alone or together in DMEM without antibiotics for the desired time, the culture supernatant was harvested and centrifuged at 12000 g for 5 min. IL-1β, IL-6 and TNF-α levels in the culture supernatant were determined *via* ELISA kits (Invitrogen, Cambrillo, USA) according to the manufacturer's protocol. After the procedure, plates were read on the spectrometer at 450 nm wavelength. The results were converted to numeric values using standard curves.

Statistical Analysis

All experiments were performed in triplicate and repeated three times. All values were presented as mean ± standard deviation (SD) and analyzed by analysis of variance followed by multiple comparisons test using GraphPad Prism version 7.00 (GraphPad Software, La Jolla, CA, USA). Differences were considered statistically significant at $P<0.05$.

RESULTS

The Interaction Between *F. nucleatum* and *P. aeruginosa*: *F. nucleatum* Coaggregates With *P. aeruginosa* and Adheres to Pulmonary Epithelial Cells

To detect the relationship between *P. aeruginosa* and *F. nucleatum*, bacterial aggregation assay was performed. The profiles of microbial aggregation of *P. aeruginosa* and *F. nucleatum* were showed in **Figures 1A–C**. *P. aeruginosa* displayed a poor autoaggregation with an autoaggregation score of "0" and a low percentage autoaggregation (8.1 ± 3.66%) (**Figures 1A–C**). *F. nucleatum* showed a strong autoaggregation with an autoaggregation score of "4+" and a high percentage autoaggregation (72.99 ± 9.43%) (**Figures 1A–C**). Moreover, *F. nucleatum* and *P. aeruginosa* were intermediate coaggregators with an autoaggregation score of "2+" and a percentage autoaggregation of 30.52 ± 7.28% (**Figures 1A–C**).

To explore whether bacterial coaggregation affect the form of bacterial adherence to host cells, bacterial adhesion assay and SEM were performed. **Figure 1D** demonstrated that *P. aeruginosa* mainly attached to the cellular junction of pulmonary epithelial cells, which shrunk and became round (**Figure 1D**). *F. nucleatum* auto-aggregated to form a bacterial network and attached to the cellular surface of pulmonary epithelial cells, which remained stretched (**Figure 1D**). When *P. aeruginosa* and *F. nucleatum* coinfected pulmonary epithelial cells, *F. nucleatum* coaggregated with *P. aeruginosa* and adhered to the cellular junction and surface of pulmonary epithelial cells, which shrunk and became round (**Figure 1D**).

The Model of Pulmonary Epithelial Cells Simultaneously Infected With *P. aeruginosa* and *F. nucleatum*

Coinfection with *P. aeruginosa* and *F. nucleatum* Promotes Each Bacterial Invasion of Pulmonary Epithelial Cells

To explore the effect of *P. aeruginosa* and *F. nucleatum* coinfection on bacterial attachment and invasion, pulmonary epithelial cells were infected with *P. aeruginosa* and/or *F. nucleatum* at different MOI (10, 50, 100). **Figures 2A, B** demonstrated that both *P. aeruginosa* and *F. nucleatum* could adhere to and invade the pulmonary epithelial cells, and as the bacterial MOI value increased, the number of *P. aeruginosa* and *F. nucleatum* attaching to and invading pulmonary epithelial cells increased. When the pulmonary epithelial cells were simultaneously infected with *P. aeruginosa* and *F. nucleatum* at different MOI (10, 50, 100), *F. nucleatum* did not affect the attachment number of *P. aeruginosa* to pulmonary epithelial cells, but *F. nucleatum* (MOI=100) significantly enhanced the invasion number of *P. aeruginosa* into pulmonary epithelial cells (**Figure 2C**). Meanwhile, *P. aeruginosa* did not affect the attachment number of *F. nucleatum* to pulmonary epithelial cells, but *P. aeruginosa* (MOI=100) significantly enhanced the invasion number of *F. nucleatum* into pulmonary epithelial cells (**Figure 2D**). In order to prove that interaction between these two bacterial species promotes each bacterial invasion of pulmonary epithelial cells, the single *P. aeruginosa* or *F. nucleatum* infection groups at a MOI of 200 were used as controls. **Figures 2C, D** demonstrated that there was not significantly difference in the number of bacterial attachment and invasion between Pa100 and Pa200 groups, and between Fn100 and Fn200 groups.

F. nucleatum Coinfection Transiently Resists *P. aeruginosa*-Induced Cytotoxicity of Pulmonary Epithelial Cells

To exploit the effect of *P. aeruginosa* and *F. nucleatum* coinfection on the biological activity of pulmonary epithelial cells, cell proliferation and cytotoxicity were examined by CCK8 assay and LDH activity assay, respectively. Compared with the control

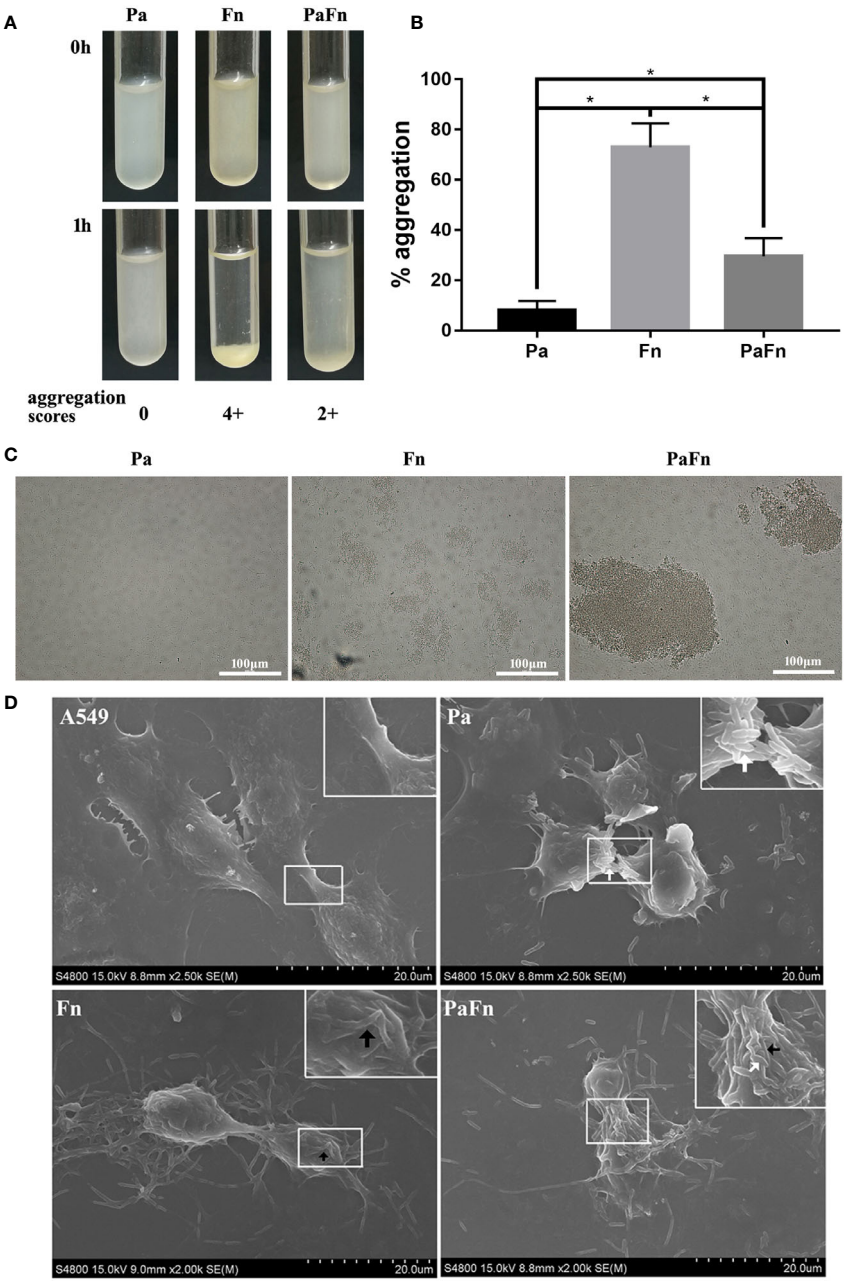

FIGURE 1 | *F. nucleatum* coaggregates with *P. aeruginosa* and adheres to pulmonary epithelial cells. **(A)** Photographs of autoaggregation and coaggregation of *P. aeruginosa* and *F. nucleatum*. The aggregation score of each bacterial group was indicated below the photograph. **(B)** Percentage aggregation of *P. aeruginosa* and *F. nucleatum*. *$P < 0.05$, statistics were achieved by analysis of variance followed by Tukey's multiple comparisons test. **(C)** Representative images of auto- and coaggregation of *P. aeruginosa* and *F. nucleatum* observed by phase contrast microscope. **(D)** Representative SEM images of pulmonary epithelial cells infected with *P. aeruginosa* and *F. nucleatum* alone or together. A549 cells were infected with *P. aeruginosa* (MOI 100) and *F. nucleatum* (MOI 100) alone or together for 3 h. White arrow indicates *P. aeruginosa*, and black arrow indicates *F. nucleatum*. Pa, *P. aeruginosa*; Fn, *F. nucleatum*.

(A549), *P. aeruginosa* (MOI 10, 50, 100) significantly inhibited the proliferation of pulmonary epithelial cells (**Figure 3A**). When the MOI of *P. aeruginosa* were 50 and 100, *P. aeruginosa* significantly induced cytotoxicity of pulmonary epithelial cells, and the cytotoxicity increased with the extension of infection time (**Figure 3A**). In contrast, *F. nucleatum* had no effect on the cytotoxicity of pulmonary epithelial cells, but enhanced the proliferation of pulmonary epithelial cells, which were infected by *F. nucleatum* at MOI of 100 at 8 h (**Figure 3B**). However, when pulmonary epithelial cells were simultaneously infected with *P. aeruginosa* and *F. nucleatum*, cell proliferation activity was lower than the single *F. nucleatum*-infected groups but higher than the

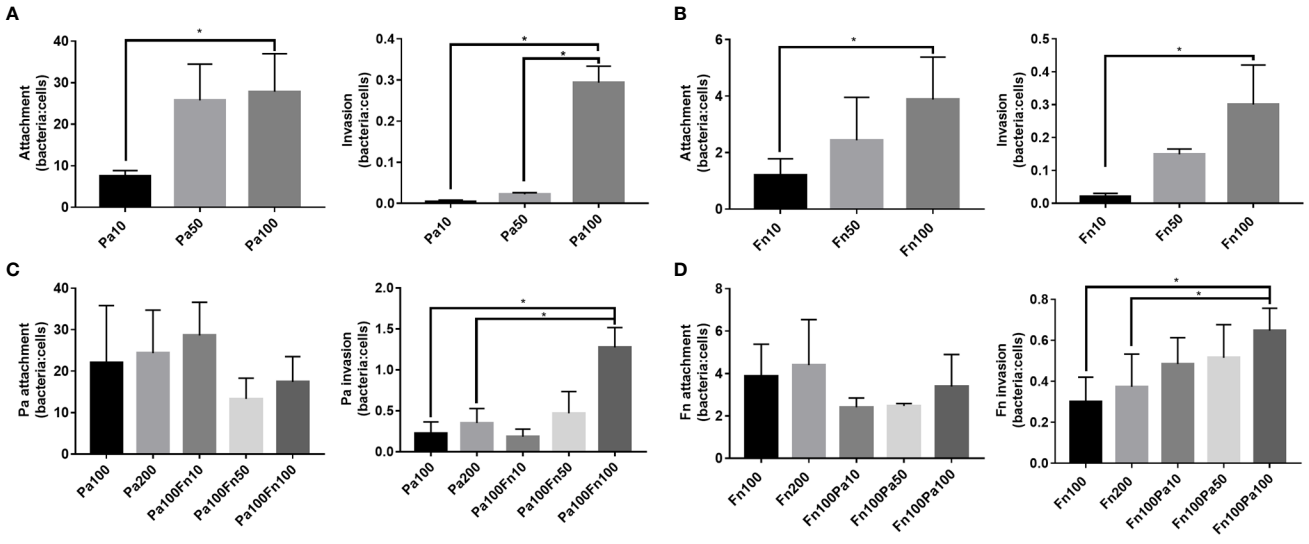

FIGURE 2 | The adherence and invasion of *P. aeruginosa* and *F. nucleatum* to pulmonary epithelial cells. **(A)** The attachment and invasion of *P. aeruginosa* to pulmonary epithelial cells. A549 cells were infected with different MOI (10, 50, 100) of *P. aeruginosa*. **(B)** The attachment and invasion of *F. nucleatum* to pulmonary epithelial cells. A549 cells were infected with different MOI (10, 50, 100) of *F. nucleatum*. **(C)** The effect of *F. nucleatum* on the attachment and invasion of *P. aeruginosa*. A549 cells were simultaneously infected with *P. aeruginosa* (MOI 100) and *F. nucleatum* (MOI 10, 50, 100), and the single *P. aeruginosa* infection groups (MOI 100, 200) were used as control. **(D)** The effect of *P. aeruginosa* on the attachment and invasion of *F. nucleatum*. A549 cells were simultaneously infected with *F. nucleatum* (MOI 100) and *P. aeruginosa* (MOI 10, 50, 100), and the single *F. nucleatum* infection groups (MOI 100, 200) were used as control. *$P < 0.05$, statistics were achieved by analysis of variance followed by Sidak's multiple comparisons test. Pa, *P. aeruginosa*; Fn, *F. nucleatum*.

single *P. aeruginosa*-infected groups after 12 h (**Figure 3C**). Meanwhile, the combined infection of *P. aeruginosa* and *F. nucleatum* significantly enhanced the cytotoxic response compared to A549 and single *F. nucleatum*-infected groups, but the cytotoxicity level of the combined infection group was lower than that of the single *P. aeruginosa* groups after 12 h (**Figure 3C**). In order to eliminate the effect of the increased bacterial load on cell proliferation and cytotoxicity, the single *P. aeruginosa* or *F. nucleatum* infection groups at a MOI of 200 were used as controls. **Figure 3C** demonstrated there was not significantly difference in cell proliferation and cytotoxicity of pulmonary epithelial cells between Pa100 and Pa200 groups, and between Fn100 and Fn200 groups.

In order to observe the cell viability or cytotoxicity intuitively, pulmonary epithelial cells were labeled with Calcein-AM and PI dyes. **Figure 3D** demonstrated that pulmonary epithelial cells infected with *F. nucleatum* were mainly live, but the *P. aeruginosa* alone or combination with *F. nucleatum* groups were mainly dead cells at 24 h.

P. aeruginosa and *F. nucleatum* Coinfection Enhances IL-6 and TNF-α Expression in Pulmonary Epithelial Cells Compared With Single *P. aeruginosa* Infection

To detect the effect of *P. aeruginosa* and *F. nucleatum* coinfection on inflammatory response of pulmonary epithelial cells, the expressions of IL-1β, IL-6 and TNF-α were examined by ELISA. Compared with the control group (A549), *P. aeruginosa* significantly increased the secretion of IL-1β and IL-6 in pulmonary epithelial cells, but there was not significant difference in IL-1β and IL-6 secretion levels between different MOI groups (**Figure 4A**). *P. aeruginosa* had no significant effect on TNF-α secretion of pulmonary epithelial cells (**Figure 4A**). **Figure 4B** showed that compared with the control group (A549), *F. nucleatum* (MOI 100) significantly enhanced the secretion of IL-1β, IL-6 and TNF-α, and the secretion levels of IL-1β, IL-6 and TNF-α in *F. nucleatum* MOI 100 group were higher than those of *F. nucleatum* MOI 10 and/or MOI 50 groups. Moreover, *P. aeruginosa* and *F. nucleatum* coinfection significantly enhanced the secretion of IL-1β, IL-6 and TNF-α in pulmonary epithelial cells compared to A549 group, and the secretion levels of IL-6 and TNF-α in the combined infection group were significantly higher than those of *P. aeruginosa* alone groups (**Figure 4C**). In addition, the single *P. aeruginosa* or *F. nucleatum* infection groups at a MOI of 200 were also used as controls. **Figure 4C** demonstrated that there was not significantly difference in the expressions of IL-1β, IL-6 and TNF-α in pulmonary epithelial cells between Pa100 and Pa200 groups, and between Fn100 and Fn200 groups.

The Model of Pulmonary Epithelial Cells Pretreated With *P. aeruginosa*: *F. nucleatum* Subsequential Infection Maintains *P. aeruginosa*-Induced Inflammatory Cytotoxicity of Pulmonary Epithelial Cells

To determine the role of *F. nucleatum* in the case where respiratory *P. aeruginosa* infection has already occurred,

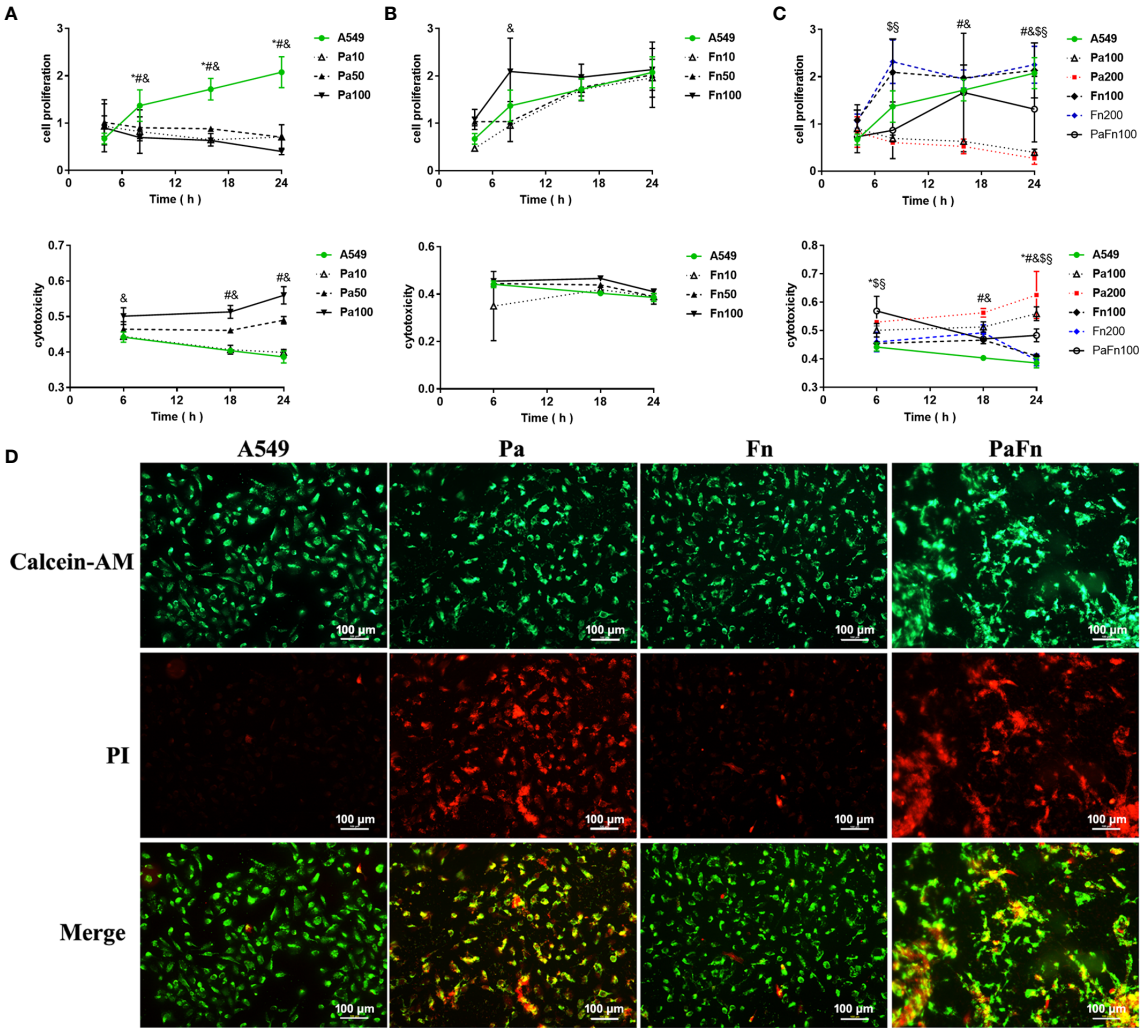

FIGURE 3 | The effect of *P. aeruginosa* and *F. nucleatum* on cellular proliferation and cytotoxicity. **(A)** The effect of *P. aeruginosa* on cell proliferation and cytotoxicity of pulmonary epithelial cells. A549 cells were infected with different MOI (10, 50, 100) of *P. aeruginosa*. * Pa10 compared with A549, # Pa50 compared with A549, & Pa100 compared with A549. **(B)** The effect of *F. nucleatum* on cell proliferation and cytotoxicity of pulmonary epithelial cells. A549 cells were infected with different MOI (10, 50, 100) of *F. nucleatum*. * Fn10 compared with A549, # Fn50 compared with A549, & Fn100 compared with A549. **(C)** The effect of the simultaneous infection of *P. aeruginosa* and *F. nucleatum* on cell proliferation and cytotoxicity of pulmonary epithelial cells. A549 cells were simultaneously infected with *P. aeruginosa* (MOI 100) and *F. nucleatum* (MOI 100), and the single *P. aeruginosa* or *F. nucleatum* infection groups (MOI 100, 200) were used as control. * A549 compared with PaFn100, # Pa100 compared with PaFn100, & Pa200 compared with PaFn100, $ Fn100 compared with PaFn100, § Fn200 compared with PaFn100. */#/&/$/§ $P<0.05$, statistics were achieved by analysis of variance followed by Dunnett's multiple comparisons test. **(D)** Representative fluorescence images of pulmonary epithelial cells infected with *P. aeruginosa* and *F. nucleatum* alone or together. A549 cells were infected with *P. aeruginosa* (MOI 100) and *F. nucleatum* (MOI 100) alone or together for 24 h. Pa, *P. aeruginosa*; Fn, *F. nucleatum*.

pulmonary epithelial cells were pretreated with *P. aeruginosa* followed with *F. nucleatum* infection (**Figure 5A**). **Figures 5B, C** demonstrated that single *F. nucleatum* infection did not affect the proliferation and cytotoxicity of pulmonary epithelial cell (Fn versus A549), while *P. aeruginosa* significantly inhibited the proliferation and induced cytotoxicity of pulmonary epithelial cells no matter with or without bacterial subsequential infection (Pa/Pa-Pa/Pa-Fn versus A549, **Figures 5B, C**). But, either *F. nucleatum* or *P. aeruginosa* subsequential infection just maintained the inhibition of cell proliferation and the induction of cytotoxicity caused by *P. aeruginosa* (Pa-Fn/Pa-Pa versus Pa, **Figures 5B, C**). In addition, although single *F. nucleatum* infection significantly induced the secretions of IL-1β, IL-6 and TNF-α in pulmonary epithelial cells (Fn versus A549), *P. aeruginosa* just upregulated the expressions of IL-1β and IL-6 no matter with or without bacterial subsequential infection (Pa/Pa-Pa/Pa-Fn versus A549, **Figure 5D**). The expression levels of IL-1β and IL-6 in *P. aeruginosa* and *F. nucleatum* sequential infection group were consistent with those of single *P. aeruginosa* infection group and *P. aeruginosa*

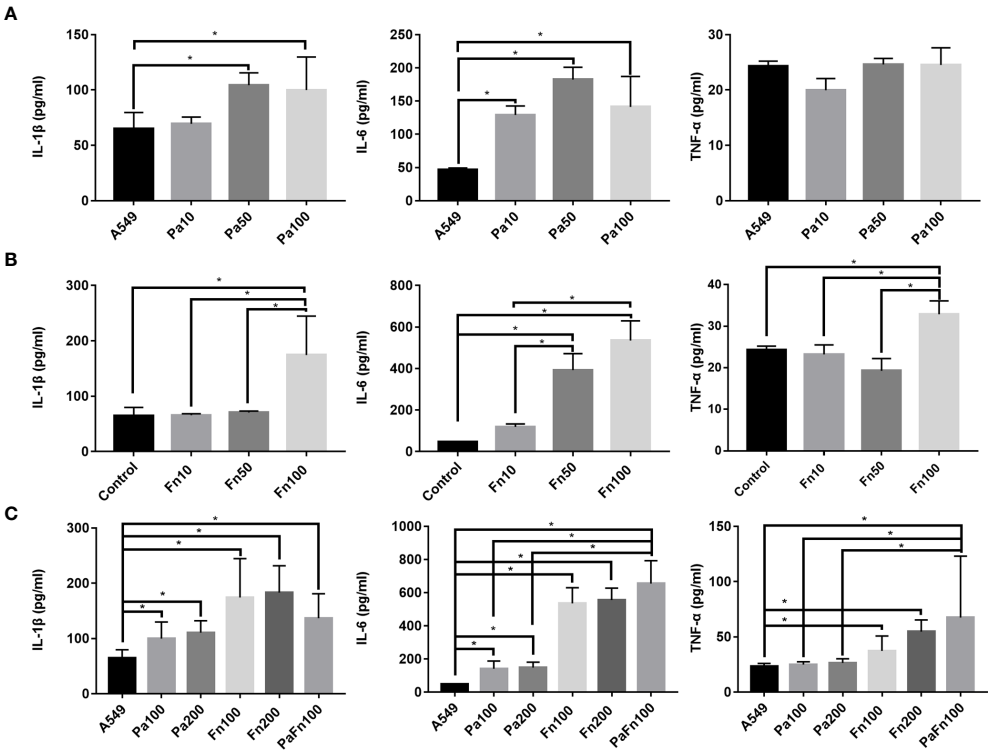

FIGURE 4 | The effect of *P. aeruginosa* and *F. nucleatum* on IL-1β, IL-6 and TNF-α productions. **(A)** The effect of *P. aeruginosa* on IL-1β, IL-6 and TNF-α productions of pulmonary epithelial cells. A549 cells were infected with different MOI (10, 50, 100) of *P. aeruginosa* for 24 h. **(B)** The effect of *F. nucleatum* on IL-1β, IL-6 and TNF-α productions of pulmonary epithelial cells. A549 cells were infected with different MOI (10, 50, 100) of *F. nucleatum* for 24 h. **(C)** The effect of the simultaneous infection of *P. aeruginosa* and *F. nucleatum* on IL-1β, IL-6 and TNF-α productions of pulmonary epithelial cells. A549 cells were simultaneously infected with *P. aeruginosa* (MOI 100) and *F. nucleatum* (MOI 100) for 24 h, and the single *P. aeruginosa* or *F. nucleatum* infection groups (MOI 100, 200) were used as control. *$P < 0.05$, statistics were achieved by analysis of variance followed by Sidak's multiple comparisons test. Pa, *P. aeruginosa*; Fn, *F. nucleatum*.

subsequential infection group (Pa-Fn versus Pa, Pa-Fn versus Pa-Pa), but higher than those of single *F. nucleatum* infection group (Pa-Fn versus Fn, **Figure 5D**).

The Model of Pulmonary Epithelial Cells Pretreated With *F. nucleatum*: *F. nucleatum* Pretreatment Enlarged TNF-α Associated Cytotoxicity of Pulmonary Epithelial Cells Subsequentially Infected With *P. aeruginosa*

In order to explore whether the presence of *F. nucleatum* would affect the progress of respiratory *P. aeruginosa* infection, pulmonary epithelial cells were pretreated with *F. nucleatum* followed with *P. aeruginosa* infection (**Figure 6A**). **Figures 6B, C** demonstrated that single *F. nucleatum* infection did not affect the proliferation and cytotoxicity of pulmonary epithelial cell (Fn versus A549), but *P. aeruginosa* subsequential infection significantly inhibited the proliferation and induced cytotoxicity of pulmonary epithelial cells, no matter which were pretreated with *F. nucleatum* or not (Pa versus A549, Fn-Pa versus A549/Fn). In addition, *F. nucleatum* alone significantly upregulated the secretions of IL-1β, IL-6 and TNF-α (Fn versus A549), while *P. aeruginosa* alone significantly upregulated the secretions of IL-1β and IL-6 without affecting TNF-α expression (Pa versus A549, **Figure 6D**). However, *P. aeruginosa* subsequential infection significantly enhanced the secretions of IL-1β, IL-6 and TNF-α in pulmonary epithelial cells pretreated with *F. nucleatum* compared with A549 and single *P. aeruginosa* group (Fn-Pa versus A549/Pa), but only TNF-α secretion in *F. nucleatum* and *P. aeruginosa* sequential infection group was also higher than that of *F. nucleatum* alone group (Fn-Pa versus Fn, **Figure 6D**). In order to eliminate the effect of the increment in bacterial loads on the sequential infection assay, *F. nucleatum* subsequential infection group (Fn-Fn) was included. **Figures 6B–D** demonstrated that there was not significantly difference in cell proliferation, cytotoxicity and the secretions of IL-1β, IL-6 and TNF-α in pulmonary epithelial cell between Fn group and Fn-Fn group.

DISCUSSION

Several studies have analyzed oral microbiome and lung microbiome of patients with respiratory infection, and

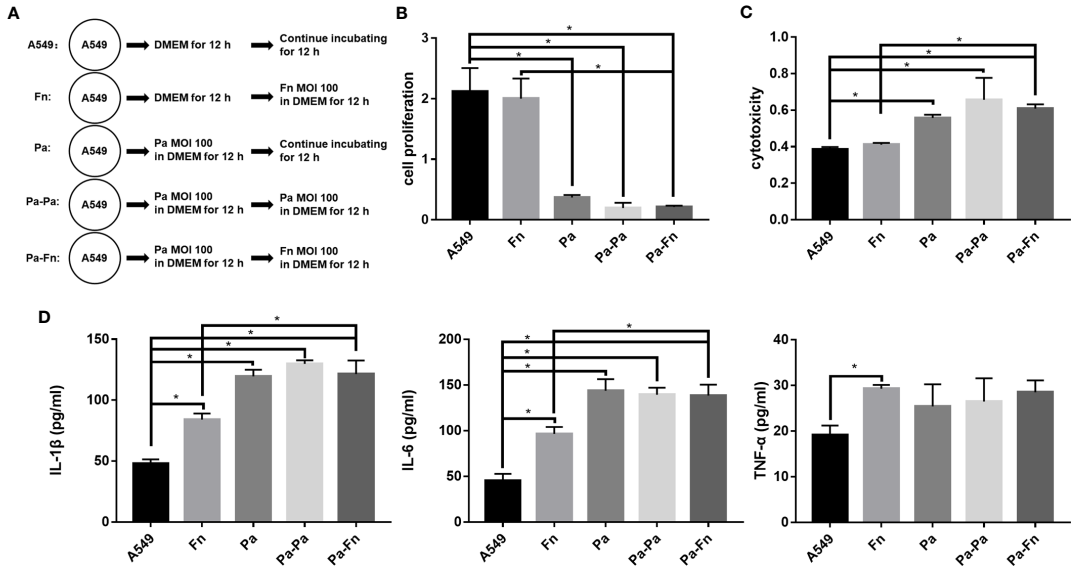

FIGURE 5 | The effect of *F. nucleatum* subsequential infection on cellular proliferation, cytotoxicity and inflammation. **(A)** Schematic representation of cell assay. A549 cells cultured in DMEM for 24 h were the blank control. Fn represented A549 cells precultured in DMEM for 12 h followed by *F. nucleatum* (MOI 100) infection for other 12 h. Pa represented A549 cells treated with *P. aeruginosa* (MOI 100) for 24 h. Pa-Pa means that A549 cells pretreated with *P. aeruginosa* (MOI 100) for 12 h continue to be infected with another *P. aeruginosa* (MOI 100) for 12 h. Pa-Fn means that A549 cells pretreated with *P. aeruginosa* (MOI 100) for 12 h continue to be infected with *F. nucleatum* (MOI 100) for 12 h. **(B)** The effect of *F. nucleatum* subsequential infection on cellular proliferation of pulmonary epithelial cells. **(C)** The effect of *F. nucleatum* subsequential infection on cytotoxicity of pulmonary epithelial cells. **(D)** The effect of *F. nucleatum* subsequential infection on IL-1β, IL-6 and TNF-α productions of pulmonary epithelial cells. $^*P < 0.05$, statistics were achieved by analysis of variance followed by Sidak's multiple comparisons test.

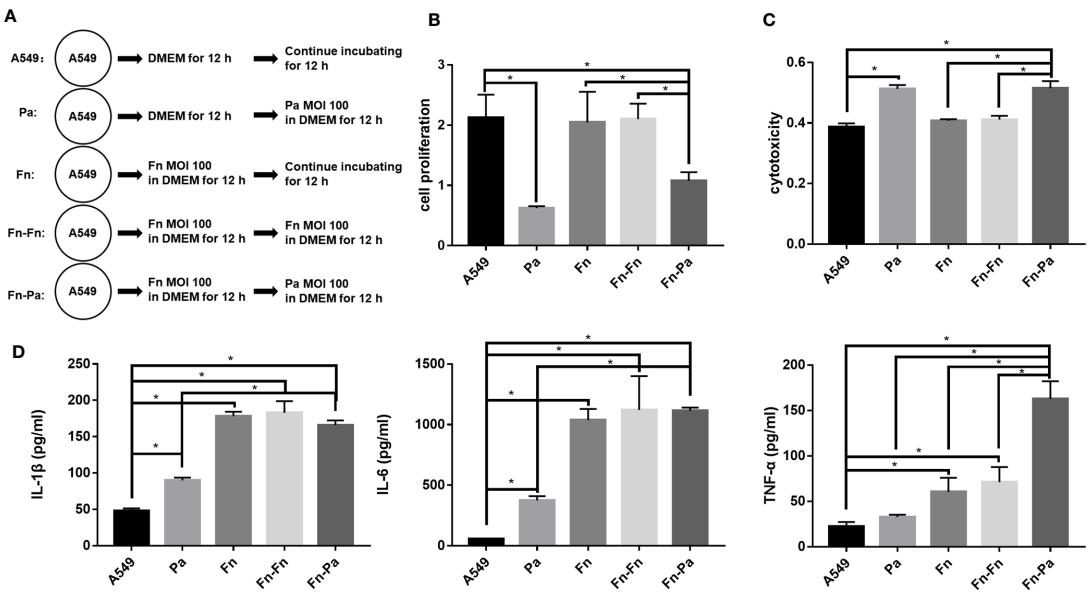

FIGURE 6 | The effect of *F. nucleatum* pretreatment on cellular proliferation, cytotoxicity and inflammation. **(A)** Schematic representation of cell assay. A549 cells cultured in DMEM for 24 h were the blank control. Pa represented A549 cells precultured in DMEM for 12 h followed by *P. aeruginosa* (MOI 100) infection for other 12 h. Fn represented A549 cells treated with *F. nucleatum* (MOI 100) for 24 h. Fn-Fn means that A549 cells pretreated with *F. nucleatum* (MOI 100) for 12 h continue to be infected with another *F. nucleatum* (MOI 100) for 12 h. Fn-Pa means that A549 cells pretreated with *F. nucleatum* (MOI 100) for 12 h continue to be infected with *P. aeruginosa* (MOI 100) for 12 h. **(B)** The effect of *F. nucleatum* pretreatment on cellular proliferation of pulmonary epithelial cells. **(C)** The effect of *F. nucleatum* pretreatment on cytotoxicity of pulmonary epithelial cells. **(D)** The effect of *F. nucleatum* pretreatment on IL-1β, IL-6 and TNF-α productions of pulmonary epithelial cells. $^*P < 0.05$, statistics were achieved by analysis of variance followed by Sidak's multiple comparisons test.

demonstrate that the bacterial composition of dental plaque and lung samples is highly similar, and pathogens isolated from the lung are genetically indistinguishable from strains of the same species isolated from the oral cavity (Heo et al., 2008; Tan et al., 2014). In addition, some studies analyzing the microbiome associated with respiratory infection indicate that *F. nucleatum* widely exists in the respiratory tract of patients with respiratory diseases such as COPD, empyema and lung abscess (Nagaoka et al., 2017; Dyrhovden et al., 2019; Li et al., 2020), and *F. nucleatum* is considered as a biomarker of lung function deterioration in COPD patients coinfected with *P. aeruginosa* (Li et al., 2020). In polymicrobial diseases, there are complex interactions among different species, leading to synergisms in creating clinical symptoms and pathologies. Therefore, this study plans to explore the potential mechanism of *F. nucleatum* cooperating with *P. aeruginosa* to weaken lung function of COPD patients from two aspects: interspecies interaction between *P. aeruginosa* and *F. nucleatum*, and the interaction of *P. aeruginosa* and *F. nucleatum* with pulmonary epithelial cells.

Bacterial autoaggregation and coaggregation were defined as the adherence of bacteria belonging to the same strain and different bacterial strains, respectively, which are essential for the development of multispecies biofilm communities and the infection of host cell (Polak et al., 2012; Karched et al., 2015). This study demonstrated that *F. nucleatum*, a Gram-negative obligate anaerobe in the oral cavity, was a strong autoaggregator, which is consistent with Karched's study (Karched et al., 2015). *F. nucleatum* expresses a variety of surface adhesins, allowing coaggregation with most oral bacteria (Kinder and Holt, 1993; Kaplan et al., 2009; Coppenhagen-Glazer et al., 2015). That may be the reason that *P. aeruginosa* coaggregates with *F. nucleatum* moderately, although *P. aeruginosa* is a poor autoaggregator. On the other hand, the adhesion and invasion of bacteria to host cells is a prerequisite for their virulence and infection. This study found that both *P. aeruginosa* and *F. nucleatum* were able to adhere to and invade into pulmonary epithelial cells, which was consistent with the previous studies (Fleiszig et al., 1994; Fleiszig et al., 1995; Han et al., 2000), and their infection number increased as the MOI of bacteria increased. Interestingly, the number of *P. aerugionosa* attaching to pulmonary epithelial cells at a MOI of 50 was similar to that at a MOI of 100, but the number of *P. aerugionosa* invading pulmonary epithelial cells at a MOI of 50 was significantly lower than that at a MOI of 100. Pan et al. have explained this phenomenon as "adhesion may not be the sole prerequisite for invasion" (Pan et al., 2009), which may also be the reason why coinfection with *P. aeruginosa* and *F. nucleatum* did not affect the adhesion of each other to pulmonary epithelial cells but enhanced each bacterial invasion. In addition, when pulmonary epithelial cells were coinfected with *P. aeruginosa* and *F. nucleatum*, the number of *P. aeruginosa* or *F. nucleatum* adhering to pulmonary epithelial cells is equal to that of the single *P. aeruginosa* or *F. nucleatum* group, respectively. That means that the total number of bacteria attached to the cell surface in the combined infection group is equivalent to the sum of the number of the single species infection groups, which is also the reason that more bacteria to coaggregate and adhere to the cell surface in the combined infection group compared with the single species groups. It has been reported that *F. nucleatum* not only enhances the adhesion and invasion of invasive bacteria such as *P. gingivalis* and *A. actinomycetemcomitans* (Saito et al., 2012; Li et al., 2015), but also transports bacteria with limited adhesion abilities such as *S. cristatus* and *S. sanguis* into the oral epithelium *via* its coaggregation function (Edwards et al., 2006). This study also demonstrated that when the MOI of bacteria was increased from 100 to 200, it did not significantly change the number of bacterial attachment and invasion. Therefore, these results suggest that coinfection with *P. aeruginosa* and *F. nucleatum* promotes each bacterial invasion into pulmonary epithelial cells due to coaggregation between two bacterial species, which may allow bacteria to evade host immune defenses, but also make host cells suffer huge damage.

After bacteria entry into host cells, some bacteria can inhibit the apoptosis of host cells to replicate and survive within the cells in order to avoid host immune defense, but certain bacteria directly induce cell death to aggravate tissue damage. Previous studies show that *P. aeruginosa* can directly act on tissue cells through its type III secretion system or toxic factors such as pyocyanin to induce apoptosis (Broquet and Asehnoune, 2015; Ranjani et al., 2015). This study demonstrated that *P. aeruginosa* attached to and destroyed the cell junction of pulmonary epithelial cells, significantly inhibited cell proliferation, and induced cytotoxic death of pulmonary epithelial cells. As distinct from *P. aeruginosa*, *F. nucleatum* promoted the proliferation of pulmonary epithelial cells without inducing cytotoxicity in the initial stage of infection (8 h). However, the presence of *F. nucleatum* transiently alleviated the inhibitory effect of *P. aeruginosa* on cell proliferation and weaken *P. aeruginosa*-induced cytotoxicity of pulmonary epithelial cells that simultaneously infected with *P. aeruginosa* and *F. nucleatum*, but simply increasing the MOI of the same bacteria could not change the effects of this bacteria on cell proliferation and cytotoxicity of pulmonary epithelial cells. Our previous study also demonstrated that periodontal pathogen *P. gingivalis* could transiently inhibit *P. aeruginosa*-induced apoptosis of pulmonary epithelial cells though the STAT3 signaling pathway (Li et al., 2014). These results indicate that *F. nucleatum* promotes *P. aeruginosa* invasion and transiently resists *P. aeruginosa*-induced damage of pulmonary epithelial cells, which may be a common characteristic of periodontal anaerobic pathogen to cause chronic persistent infection of *P. aeruginosa* in the lung of COPD patients.

It is well-known that the acute exacerbation of COPD is closely related to the persistent airway inflammation induced by bacterial infection. The expression of IL-1β in patients with COPD is upregulated, and IL-1β level is correlated with the increase of airway neutrophils and the decline of lung function (Sapey et al., 2009). Airway (sputum) IL-1β is considered to be a biomarker for acute exacerbation of COPD associated with bacteria (Bafadhel et al., 2011). Demera et al. found that the content of *P. aeruginosa* in the sputum was positively corelated with IL-1β level, and TNF-α and IL-6 are IL-1β signature and

associated with IL-1β-mediated COPD exacerbation (Damera et al., 2016). This study showed that both *P. aeruginosa* and *F. nucleatum* could significantly induce IL-1β and IL-6 secretion, *F. nucleatum* also induce TNF-α secretion in pulmonary epithelial cells. In addition, the simultaneous infection with *P. aeruginosa* and *F. nucleatum* significantly enhance IL-6 and TNF-α expressions in pulmonary epithelial cells compared with single *P. aeruginosa* infection group, which were similar to respiratory syncytial virus that enhanced the release of inflammatory factors IL-6 and IL-8 in bronchial epithelial cells coinfected with *P. aeruginosa* (Bellinghausen et al., 2016). However, there was no statistical difference in the expressions of IL-1β, IL-6 and TNF-α between *F. nucleatum* group and the combined infection group, which may be due to the fact that coinfection with *P. aeruginosa* and *F. nucleatum* significantly induced cytotoxicity death of pulmonary epithelial cells at 24 h. In addition, this study also demonstrated that simply increasing the MOI of the same bacteria could not change the effects of this bacteria on the secretions of IL-1β, IL-6 and TNF-α in pulmonary epithelial cells. Fu et al. pointed out that sputum IL-1β and serum IL-6 were higher in the frequent exacerbators with COPD, which activated the IL-1β-system inflammation axis to increase the risk of frequent exacerbations of COPD patients (Fu et al., 2015). Therefore, these results suggest that the simultaneous infection with *F. nucleatum* and *P. aeruginosa* induces over-release of pro-inflammatory cytokines IL-6 and TNF-α in pulmonary epithelial cells, which may contribute to increase the susceptibility of COPD exacerbation.

It is a widely recognized clinical phenomenon that patients with more severe COPD are more likely to have severe periodontal disease (Si et al., 2012; Tan et al., 2019), and a significantly increased risk of COPD occurs among severe periodontitis subjects (Takeuchi et al., 2019). Our previous study finds that 45.3% patients with COPD exacerbation are associated with respiratory coinfection with *F. nucleatum* and *P. aeruginosa* (Li et al., 2020), two types of sequential infection model with *P. aeruginosa* and *F. nucleatum* are established to fully elaborate the role of mixed infection in COPD. The current study demonstrated that no matter with *F. nucleatum* pretreatment or subsequential infection, *P. aeruginosa* significantly induced cytotoxic damage of pulmonary epithelial cells. *F. nucleatum* pretreatment or subsequential infection kept or even amplified *P. aeruginosa*-induced cytotoxicity of pulmonary epithelial cells, which may explain why *F. nucleatum* reduced lung function of COPD patients accompanied with *P. aeruginosa* infection (Li et al., 2020). On the other hand, *F. nucleatum* subsequential infection maintained the secretion levels of IL-1β, IL-6 and TNF-α in pulmonary epithelial cells compared to the single *P. aeruginosa* group, which may be due to the low cellular viability caused by *P. aeruginosa* pretreatment. Nevertheless, *F. nucleatum* pretreatment amplified the secretions of IL-1β, IL-6 and TNF-α of pulmonary epithelial cells induced by *P. aeruginosa*, and only TNF-α secretion of *F. nucleatum* and *P. aeruginosa* sequential infection group showed a significant synergistic increase effect compared with the single species groups. In addition, sequential inoculation of

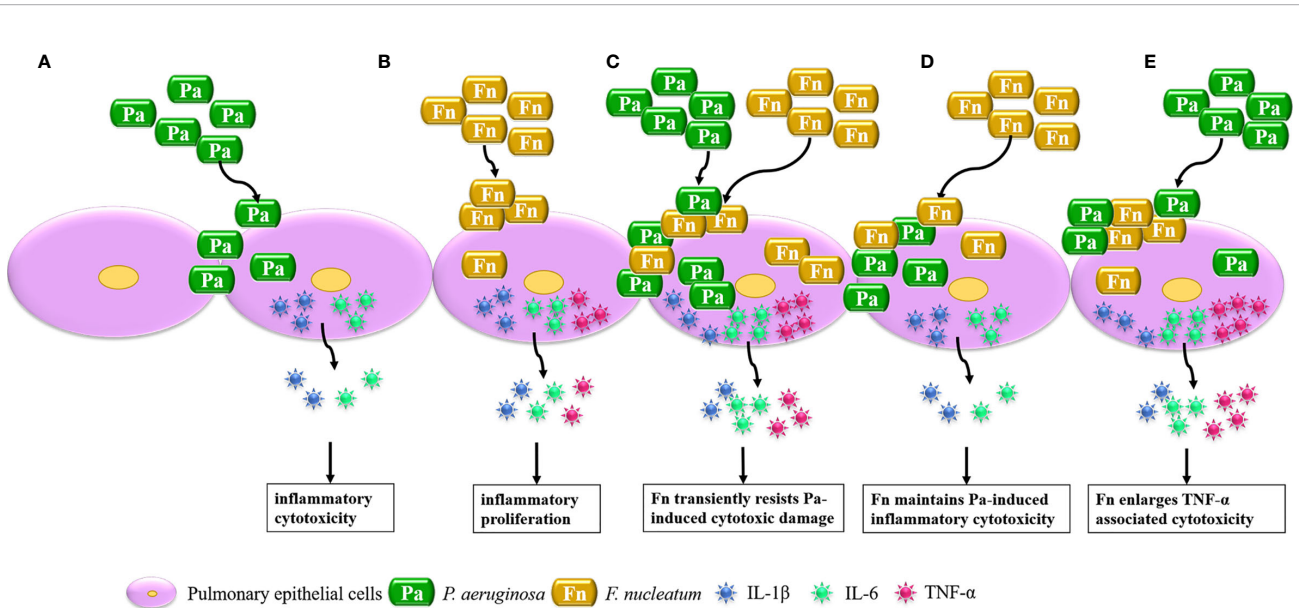

FIGURE 7 | Schematic diagram of the effect of mixed infection with *P. aeruginosa* and *F. nucleatum* on pulmonary epithelial cells based on the present model. **(A)** When pulmonary epithelial cells are infected with *P. aeruginosa* alone, *P. aeruginosa* induces IL-1β and IL-6 associated inflammatory cytotoxicity of pulmonary epithelial cells. **(B)** When pulmonary epithelial cells are infected with *F. nucleatum* alone, *F. nucleatum* initiates high inflammatory proliferation of pulmonary epithelial cells. **(C)** When pulmonary epithelial cells are simultaneously infected with *P. aeruginosa* and *F. nucleatum*, *F. nucleatum* coaggregates with *P. aeruginosa* to synergistically invade into pulmonary epithelial cells and transiently resists *P. aeruginosa*-induced cytotoxic damage to induce over-release of IL-6 and TNF-α. **(D)** When pulmonary epithelial cells are pretreated with *P. aeruginosa*, *F. nucleatum* subsequential infection maintains *P. aeruginosa*-induced inflammatory cytotoxicity. **(E)** When pulmonary epithelial cells are pretreated with *F. nucleatum*, *F. nucleatum* pretreatment enlarged TNF-α associated cytotoxicity of pulmonary epithelial cells subsequentially infected with *P. aeruginosa*.

the same bacteria did not significant affect the effects of this bacteria on cell proliferation, cytotoxicity and inflammation of pulmonary epithelial cells. These results suggest that *F. nucleatum* can maintain or even aggravate *P. aeruginosa*-induced inflammatory cytotoxicity of pulmonary epithelial cells in the sequential infection models, which may be the reason for *F. nucleatum* cooperating with *P. aeruginosa* to exacerbate lung injury and induce acute exacerbation of COPD.

In conclusion, considerable research has focused on the interaction between single bacterium and host cells, while this study highlights the effect of bacterial mixed infection on cellular biological function through establishing bacterial simultaneous and sequential infection models, which is summarized in **Figure 7**. It demonstrated that *P. aeruginosa* mainly induces IL-1β and IL-6 associated inflammatory cytotoxicity of pulmonary epithelial cells, *F. nucleatum* mainly initiates high inflammatory proliferation of pulmonary epithelial cells. When pulmonary epithelial cells are simultaneously infected with *P. aeruginosa* and *F. nucleatum*, *F. nucleatum* coaggregates with *P. aeruginosa* to synergistically invade into pulmonary epithelial cells and transiently resists *P. aeruginosa*-induced cytotoxic damage, and induces over-release of IL-6 and TNF-α, which may cause a chronic persistent pulmonary infection and increase the susceptibility of COPD exacerbation. In addition, the presence of *F. nucleatum* maintains or even aggravates *P. aeruginosa*-induced inflammatory cytotoxicity of pulmonary epithelial cells in the sequential infection models, which may be the reason for *F. nucleatum* reducing lung function of COPD patients accompanied with *P. aeruginosa* infection and may contribute to persistent and/or frequent exacerbation of COPD patients accompanied with *P. aeruginosa* and *F. nucleatum* coinfection. Therefore, oral anaerobic pathogens, especially *F. nucleatum*, should never be neglected in the treatment of COPD.

DATA AVAILABILITY STATEMENT

The original contributions presented in the study are included in the article/supplementary material. Further inquiries can be directed to the corresponding author.

AUTHOR CONTRIBUTIONS

All authors contributed to the article and approved the submitted version. QL designed and performed the experiments, analyzed the data, wrote and revised the draft of the paper. HW, LT, SZ, LL and XT participated in the experiments, analyzed the data and revised the article. YP developed the idea for this study and revised the manuscript.

FUNDING

This work was supported by the National Natural Science Foundation of China (NO. 81670997 to YP), the Plan of the talents for Liaoning Development (NO. XLYC1802129 to YP) and the Higher Education Fundamental Research Project of Liaoning Province (NO. LQNK201724 to QL).

REFERENCES

Almagro, P., Salvado, M., Garcia-Vidal, C., Rodriguez-Carballeira, M., Cuchi, E., Torres, J., et al. (2012). Pseudomonas aeruginosa and mortality after hospital admission for chronic obstructive pulmonary disease. *Respiration* 84 (1), 36–43. doi: 10.1159/000331224

Angus, A. A., Lee, A. A., Augustin, D. K., Lee, E. J., Evans, D. J., and Fleiszig, S. M. (2008). Pseudomonas aeruginosa induces membrane blebs in epithelial cells, which are utilized as a niche for intracellular replication and motility. *Infect. Immun.* 76 (5), 1992–2001. doi: 10.1128/IAI.01221-07

Bafadhel, M., McKenna, S., Terry, S., Mistry, V., Reid, C., Haldar, P., et al. (2011). Acute exacerbations of chronic obstructive pulmonary disease: identification of biologic clusters and their biomarkers. *Am. J. Respir. Crit. Care Med.* 184 (6), 662–671. doi: 10.1164/rccm.201104-0597OC

Bailhache, M., Mariani-Kurkdjian, P., Lehours, P., Sarlangue, J., Pillet, P., Bingen, E., et al. (2013). Fusobacterium invasive infections in children: a retrospective study in two French tertiary care centres. *Eur. J. Clin. Microbiol. Infect. Dis.* 32 (8), 1041–1047. doi: 10.1007/s10096-013-1848-2

Bellinghausen, C., Gulraiz, F., Heinzmann, A. C., Dentener, M. A., Savelkoul, P. H., Wouters, E. F., et al. (2016). Exposure to common respiratory bacteria alters the airway epithelial response to subsequent viral infection. *Respir. Res.* 17 (1), 68. doi: 10.1186/s12931-016-0382-z

Broquet, A., and Asehnoune, K. (2015). Apoptosis induced by Pseudomonas aeruginosa: a lonely killer? *Microb. Biotechnol.* 8 (1), 49–51. doi: 10.1111/1751-7915.12144

Choi, J., Oh, J. Y., Lee, Y. S., Hur, G. Y., Lee, S. Y., Shim, J. J., et al. (2019). Bacterial and viral identification rate in acute exacerbation of chronic obstructive pulmonary disease in Korea. *Yonsei Med. J.* 60 (2), 216–222. doi: 10.3349/ymj.2019.60.2.216

Cisar, J. O., Kolenbrander, P. E., and McIntire, F. C. (1979). Specificity of coaggregation reactions between human oral streptococci and strains of Actinomyces viscosus or Actinomyces naeslundii. *Infect. Immun.* 24 (3), 742–752. doi: 10.1128/IAI.24.3.742-752.1979

Coppenhagen-Glazer, S., Sol, A., Abed, J., Naor, R., Zhang, X., Han, Y. W., et al. (2015). Fap2 of Fusobacterium nucleatum is a galactose-inhibitable adhesin involved in coaggregation, cell adhesion, and preterm birth. *Infect. Immun.* 83 (3), 1104–1113. doi: 10.1128/IAI.02838-14

Damera, G., Pham, T. H., Zhang, J., Ward, C. K., Newbold, P., Ranade, K., et al. (2016). A sputum proteomic signature that associates with increased IL-1beta levels and bacterial exacerbations of COPD. *Lung* 194 (3), 363–369. doi: 10.1007/s00408-016-9877-0

Dyrhovden, R., Nygaard, R. M., Patel, R., Ulvestad, E., and Kommedal, O. (2019). The bacterial aetiology of pleural empyema. A descriptive and comparative metagenomic study. *Clin. Microbiol. Infect.* 25 (8), 981–986. doi: 10.1016/j.cmi.2018.11.030

Edwards, A. M., Grossman, T. J., and Rudney, J. D. (2006). Fusobacterium nucleatum transports noninvasive Streptococcus cristatus into human epithelial cells. *Infect. Immun.* 74 (1), 654–662. doi: 10.1128/IAI.74.1.654-662.2006

Eklof, J., Sorensen, R., Ingebrigtsen, T. S., Sivapalan, P., Achir, I., Boel, J. B., et al. (2020). Pseudomonas aeruginosa and risk of death and exacerbations in patients with chronic obstructive pulmonary disease: an observational cohort study of 22 053 patients. *Clin. Microbiol. Infect.* 26 (2), 227–234. doi: 10.1016/j.cmi.2019.06.011

Fleiszig, S. M., Zaidi, T. S., Fletcher, E. L., Preston, M. J., and Pier, G. B. (1994). Pseudomonas aeruginosa invades corneal epithelial cells during experimental infection. *Infect. Immun.* 62 (8), 3485–3493. doi: 10.1128/IAI.62.8.3485-3493.1994

Fleiszig, S. M., Zaidi, T. S., and Pier, G. B. (1995). Pseudomonas aeruginosa invasion of and multiplication within corneal epithelial cells in vitro. *Infect. Immun.* 63 (10), 4072–4077. doi: 10.1128/IAI.63.10.4072-4077.1995

Fu, J. J., McDonald, V. M., Baines, K. J., and Gibson, P. G. (2015). Airway IL-1beta and systemic inflammation as predictors of future exacerbation risk in asthma and COPD. *Chest* 148 (3), 618–629. doi: 10.1378/chest.14-2337

Garcia-Vidal, C., Almagro, P., Romani, V., Rodriguez-Carballeira, M., Cuchi, E., Canales, L., et al. (2009). Pseudomonas aeruginosa in patients hospitalised for COPD exacerbation: a prospective study. *Eur. Respir. J.* 34 (5), 1072–1078. doi: 10.1183/09031936.00003309

Gedik, A. H., Cakir, E., Soysal, O., and Umutoglu, T. (2014). Endobronchial lesion due to pulmonary Fusobacterium nucleatum infection in a child. *Pediatr. Pulmonol.* 49 (3), E63–E65. doi: 10.1002/ppul.22834

Han, Y. W., Shi, W., Huang, G. T., Kinder Haake, S., Park, N. H., Kuramitsu, H., et al. (2000). Interactions between periodontal bacteria and human oral epithelial cells: Fusobacterium nucleatum adheres to and invades epithelial cells. *Infect. Immun.* 68 (6), 3140–3146. doi: 10.1128/iai.68.6.3140-3146.2000

Hayata, M., Watanabe, N., Tamura, M., Kamio, N., Tanaka, H., Nodomi, K., et al. (2019). The periodontopathic bacterium Fusobacterium nucleatum induced proinflammatory cytokine production by human respiratory epithelial cell lines and in the lower respiratory organs in mice. *Cell Physiol. Biochem.* 53 (1), 49–61. doi: 10.33594/000000120

Heo, S. M., Haase, E. M., Lesse, A. J., Gill, S. R., and Scannapieco, F. A. (2008). Genetic relationships between respiratory pathogens isolated from dental plaque and bronchoalveolar lavage fluid from patients in the intensive care unit undergoing mechanical ventilation. *Clin. Infect. Dis.* 47 (12), 1562–1570. doi: 10.1086/593193

Kaplan, C. W., Lux, R., Haake, S. K., and Shi, W. (2009). The Fusobacterium nucleatum outer membrane protein RadD is an arginine-inhibitable adhesin required for inter-species adherence and the structured architecture of multispecies biofilm. *Mol. Microbiol.* 71 (1), 35–47. doi: 10.1111/j.1365-2958.2008.06503.x

Karched, M., Bhardwaj, R. G., and Asikainen, S. E. (2015). Coaggregation and biofilm growth of Granulicatella spp. with Fusobacterium nucleatum and Aggregatibacter actinomycetemcomitans. *BMC Microbiol.* 15, 114. doi: 10.1186/s12866-015-0439-z

Kinder, S. A., and Holt, S. C. (1993). Localization of the Fusobacterium nucleatum T18 adhesin activity mediating coaggregation with Porphyromonas gingivalis T22. *J. Bacteriol.* 175 (3), 840–850. doi: 10.1128/JB.175.3.840-850.1993

Li, Q., Pan, C., Teng, D., Lin, L., Kou, Y., Haase, E. M., et al. (2014). Porphyromonas gingivalis modulates Pseudomonas aeruginosa-induced apoptosis of respiratory epithelial cells through the STAT3 signaling pathway. *Microbes Infect.* 16 (1), 17–27. doi: 10.1016/j.micinf.2013.10.006

Li, Y., Guo, H., Wang, X., Lu, Y., Yang, C., and Yang, P. (2015). Coinfection with Fusobacterium nucleatum can enhance the attachment and invasion of Porphyromonas gingivalis or Aggregatibacter actinomycetemcomitans to human gingival epithelial cells. *Arch. Oral. Biol.* 60 (9), 1387–1393. doi: 10.1016/j.archoralbio.2015.06.017

Li, Q., Zhou, J., Lin, L., Zhao, H., Miao, L., and Pan, Y. (2019). Porphyromonas gingivalis degrades integrin beta1 and induces AIF-mediated apoptosis of epithelial cells. *Infect. Dis. (Lond)* 51 (11-12), 793–801. doi: 10.1080/23744235.2019.1653490

Li, Q., Tan, L., Wang, H., Kou, Y., Shi, X., Zhang, S., et al. (2020). Fusobacterium nucleatum interaction with Pseudomonas aeruginosa induces biofilm-associated antibiotic tolerance via Fusobacterium adhesin A. *ACS Infect. Dis.* 6 (7), 1686–1696. doi: 10.1021/acsinfecdis.9b00402

Loozen, G., Ozcelik, O., Boon, N., De Mol, A., Schoen, C., Quirynen, M., et al. (2014). Inter-bacterial correlations in subgingival biofilms: a large-scale survey. *J. Clin. Periodontol.* 41 (1), 1–10. doi: 10.1111/jcpe.12167

Nagaoka, K., Yanagihara, K., Morinaga, Y., and Kohno, S. (2017). Detection of Fusobacterium nucleatum in two cases of empyema and lung abscess using paromomycin-vancomycin supplemented Brucella HK agar. *Anaerobe* 43, 99–101. doi: 10.1016/j.anaerobe.2016.12.011

Nakamoto, K., Watanabe, M., Sada, M., Inui, T., Nakamura, M., Honda, K., et al. (2019). Pseudomonas aeruginosa-derived flagellin stimulates IL-6 and IL-8 production in human bronchial epithelial cells: A potential mechanism for progression and exacerbation of COPD. *Exp. Lung Res.* 45 (8), 255–266. doi: 10.1080/01902148.2019.1665147

Pan, Y., Teng, D., Burke, A. C., Haase, E. M., and Scannapieco, F. A. (2009). Oral bacteria modulate invasion and induction of apoptosis in HEp-2 cells by Pseudomonas aeruginosa. *Microb. Pathog.* 46 (2), 73–79. doi: 10.1016/j.micpath.2008.10.012

Papi, A., Bellettato, C. M., Braccioni, F., Romagnoli, M., Casolari, P., Caramori, G., et al. (2006). Infections and airway inflammation in chronic obstructive pulmonary disease severe exacerbations. *Am. J. Respir. Crit. Care Med.* 173 (10), 1114–1121. doi: 10.1164/rccm.200506-859OC

Polak, D., Shapira, L., Weiss, E. I., and Houri-Haddad, Y. (2012). The role of coaggregation between Porphyromonas gingivalis and Fusobacterium nucleatum on the host response to mixed infection. *J. Clin. Periodontol.* 39 (7), 617–625. doi: 10.1111/j.1600-051X.2012.01889.x

Proud, D., and Leigh, R. (2011). Epithelial cells and airway diseases. *Immunol. Rev.* 242 (1), 186–204. doi: 10.1111/j.1600-065X.2011.01033.x

Ranjani, J., Pushpanathan, M., Mahesh, A., Niraimathi, M., Gunasekaran, P., and Rajendhran, J. (2015). Pseudomonas aeruginosa PAO1 induces distinct cell death mechanisms in H9C2 cells and its differentiated form. *J. Basic Microbiol.* 55 (10), 1191–1202. doi: 10.1002/jobm.201500037

Saito, A., Kokubu, E., Inagaki, S., Imamura, K., Kita, D., Lamont, R. J., et al. (2012). Porphyromonas gingivalis entry into gingival epithelial cells modulated by Fusobacterium nucleatum is dependent on lipid rafts. *Microb. Pathog.* 53 (5-6), 234–242. doi: 10.1016/j.micpath.2012.08.005

Sands, K. M., Wilson, M. J., Lewis, M. A. O., Wise, M. P., Palmer, N., Hayes, A. J., et al. (2017). Respiratory pathogen colonization of dental plaque, the lower airways, and endotracheal tube biofilms during mechanical ventilation. *J. Crit. Care* 37, 30–37. doi: 10.1016/j.jcrc.2016.07.019

Sapey, E., Ahmad, A., Bayley, D., Newbold, P., Snell, N., Rugman, P., et al. (2009). Imbalances between interleukin-1 and tumor necrosis factor agonists and antagonists in stable COPD. *J. Clin. Immunol.* 29 (4), 508–516. doi: 10.1007/s10875-009-9286-8

Scannapieco, F. A. (1999). Role of oral bacteria in respiratory infection. *J. Periodontol.* 70 (7), 793–802. doi: 10.1902/jop.1999.70.7.793

Shamriz, O., Engelhard, D., Temper, V., Revel-Vilk, S., Benenson, S., Brooks, R., et al. (2015). Infections caused by Fusobacterium in children: a 14-year single-center experience. *Infection* 43 (6), 663–670. doi: 10.1007/s15010-015-0782-x

Shimazu, K., Oguchi, R., Takahashi, Y., Konishi, K., and Karibe, H. (2016). Effects of surface reaction-type pre-reacted glass ionomer on oral biofilm formation of Streptococcus gordonii. *Odontology* 104 (3), 310–317. doi: 10.1007/s10266-015-0217-2

Si, Y., Fan, H., Song, Y., Zhou, X., Zhang, J., and Wang, Z. (2012). Association between periodontitis and chronic obstructive pulmonary disease in a Chinese population. *J. Periodontol.* 83 (10), 1288–1296. doi: 10.1902/jop.2012.110472

Singh, D., Agusti, A., Anzueto, A., Barnes, P. J., Bourbeau, J., Celli, B. R., et al. (2019). Global Strategy for the diagnosis, management, and prevention of chronic obstructive lung disease: the GOLD science committee report 2019. *Eur. Respir. J.* 53 (5), 1900164. doi: 10.1183/13993003.00164-2019

Takeuchi, K., Matsumoto, K., Furuta, M., Fukuyama, S., Takeshita, T., Ogata, H., et al. (2019). Periodontitis is associated with chronic obstructive pulmonary disease. *J. Dent. Res.* 98 (5), 534–540. doi: 10.1177/0022034519833630

Tan, L., Wang, H., Li, C., and Pan, Y. (2014). 16S rDNA-based metagenomic analysis of dental plaque and lung bacteria in patients with severe acute exacerbations of chronic obstructive pulmonary disease. *J. Periodontal Res.* 49 (6), 760–769. doi: 10.1111/jre.12159

Tan, L., Tang, X., Pan, C., Wang, H., and Pan, Y. (2019). Relationship among clinical periodontal, microbiologic parameters and lung function in participants with chronic obstructive pulmonary disease. *J. Periodontol.* 90 (2), 134–140. doi: 10.1002/JPER.17-0705

Thurnheer, T., Karygianni, L., Flury, M., and Belibasakis, G. N. (2019). Fusobacterium Species and Subspecies Differentially Affect the Composition and Architecture of Supra- and Subgingival Biofilms Models. *Front. Microbiol.* 10:1716:1716. doi: 10.3389/fmicb.2019.01716

Vos, J. B., van Sterkenburg, M. A., Rabe, K. F., Schalkwijk, J., Hiemstra, P. S., and Datson, N. A. (2005). Transcriptional response of bronchial epithelial cells to Pseudomonas aeruginosa: identification of early mediators of host defense. *Physiol. Genomics* 21 (3), 324–336. doi: 10.1152/physiolgenomics.00289.2004

Wu, C., Al Mamun, A. A. M., Luong, T. T., Hu, B., Gu, J., Lee, J. H., et al. (2018). Forward Genetic Dissection of Biofilm Development by Fusobacterium

nucleatum: Novel Functions of Cell Division Proteins FtsX and EnvC. *MBio* 9 (2), e00360–18. doi: 10.1128/mBio.00360-18

Yang, C. C., Ye, J. J., Hsu, P. C., Chang, H. J., Cheng, C. W., Leu, H. S., et al. (2011). Characteristics and outcomes of Fusobacterium nucleatum bacteremia–a 6-year experience at a tertiary care hospital in northern Taiwan. *Diagn. Microbiol. Infect. Dis.* 70 (2), 167–174. doi: 10.1016/j.diagmicrobio.2010.12.017

Yu, T., Guo, F., Yu, Y., Sun, T., Ma, D., Han, J., et al. (2017). Fusobacterium nucleatum Promotes Chemoresistance to Colorectal Cancer by Modulating Autophagy. *Cell* 170 (3), 548–563 e516. doi: 10.1016/j.cell.2017.07.008

Conflict of Interest: The authors declare that the research was conducted in the absence of any commercial or financial relationships that could be construed as a potential conflict of interest.

frontiers in Cellular and Infection Microbiology

ORIGINAL RESEARCH
published: 19 March 2021
doi: 10.3389/fcimb.2021.649925

Systemic and Extraradicular Bacterial Translocation in Apical Periodontitis

María José Bordagaray[1,2], Alejandra Fernández[1,3], Mauricio Garrido[1,2], Jessica Astorga[1], Anilei Hoare[4,5] and Marcela Hernández[1,4]**

[1] Laboratory of Periodontal Biology, Faculty of Dentistry, Universidad de Chile, Santiago, Chile, [2] Department of Conservative Dentistry, Faculty of Dentistry, Universidad de Chile, Santiago, Chile, [3] Faculty of Dentistry, Universidad Andres Bello, Santiago, Chile, [4] Department of Pathology and Oral Medicine, Faculty of Dentistry, Universidad de Chile, Santiago, Chile, [5] Laboratory of Oral Microbiology, Faculty of Dentistry, Universidad de Chile, Santiago, Chile

Apical periodontitis is an inflammatory disease of microbial etiology. It has been suggested that endodontic bacterial DNA might translocate to distant organs *via* blood vessels, but no studies have been conducted. We aimed first to explore overall extraradicular infection, as well as specifically by *Porphyromonas* spp; and their potential to translocate from infected root canals to blood through peripheral blood mononuclear cells. In this cross-sectional study, healthy individuals with and without a diagnosis of apical periodontitis with an associated apical lesion of endodontic origin (both, symptomatic and asymptomatic) were included. Apical lesions (N=64) were collected from volunteers with an indication of tooth extraction. Intracanal samples (N=39) and respective peripheral blood mononuclear cells from apical periodontitis (n=14) individuals with an indication of endodontic treatment, as well as from healthy individuals (n=14) were collected. The detection frequencies and loads (DNA copies/mg or DNA copies/μL) of total bacteria, *Porphyromonas endodontalis* and *Porphyromonas gingivalis* were measured by qPCR. In apical lesions, the detection frequencies (%) and median bacterial loads (DNA copies/mg) respectively were 70.8% and 4521.6 for total bacteria; 21.5% and 1789.7 for *Porphyromonas endodontalis;* and 18.4% and 1493.9 for *Porphyromonas gingivalis*. In intracanal exudates, the detection frequencies and median bacterial loads respectively were 100% and 21089.2 (DNA copies/μL) for total bacteria, 41% and 8263.9 for *Porphyromonas endodontalis*; and 20.5%, median 12538.9 for *Porphyromonas gingivalis*. Finally, bacteria were detected in all samples of peripheral blood mononuclear cells including apical periodontitis and healthy groups, though total bacterial loads (median DNA copies/μL) were significantly higher in apical periodontitis (953.6) compared to controls (300.7), $p<0.05$. *Porphyromonas endodontalis* was equally detected in both groups (50%), but its bacterial load tended to be higher in apical periodontitis (262.3) than controls (158.8), $p>0.05$; *Porphyromonas gingivalis* was not detected. Bacteria and specifically *Porphyromonas* spp. were frequently detected in endodontic canals and apical lesions. Also, total bacteria and *Porphyromonas*

OPEN ACCESS

Edited by:
Tomomi Hashizume-Takizawa, Nihon University, Japan

Reviewed by:
Brenda P. Gomes, Campinas State University, Brazil
Tomoki Maekawa, Niigata University, Japan

***Correspondence:**
Anilei Hoare
a.hoare@odontologia.uchile.cl
Marcela Hernández
mhernandezrios@gmail.com

Specialty section:
This article was submitted to Bacteria and Host, a section of the journal Frontiers in Cellular and Infection Microbiology

Received: *05 January 2021*
Accepted: *01 March 2021*
Published: *19 March 2021*

Citation:
Bordagaray MJ, Fernández A, Garrido M, Astorga J, Hoare A and Hernández M (2021) Systemic and Extraradicular Bacterial Translocation in Apical Periodontitis. Front. Cell. Infect. Microbiol. 11:649925. doi: 10.3389/fcimb.2021.649925

endodontalis DNA were detected in peripheral blood mononuclear cells, supporting their plausible role in bacterial systemic translocation.

Keywords: periapical periodontitis, periapical lesion, *Porphyromonas*, bacterial translocation, peripheral blood mononuclear cells (PBMC)

INTRODUCTION

Apical periodontitis (AP) is the inflammatory destruction of the apical periodontium as the result of endodontic infection. The hallmark of AP is the development of an osteolytic apical lesion of endodontic origin (ALEO). From an epidemiological point of view, AP represents a highly frequent cause of tooth loss and a non-classic risk factor for several non-communicable diseases (NCD), in part, by inducing low-grade systemic inflammation (Garrido et al., 2019). AP can vary over time between two clinical entities, symptomatic and asymptomatic apical periodontitis (SAP and AAP, respectively), depending on the dynamic balance between bacterial consortia and the host's response (Hsiao et al., 2012). Among them, the former is considered an immunologically exacerbated stage (Veloso et al., 2020).

ALEOs result from the direct communication between the former sterile pulp tissue and the oral microbiota, often caused by dental caries. The endodontic pathogens organize in multispecies biofilm communities within the root canal, favoring the selection of Gram-negative anaerobic bacteria (Sakko et al., 2016). Though a substantial heterogeneity can be found among geographically diverse populations the black-pigmented anaerobes, *Porphyromonas endodontalis* and *Porphyromonas gingivalis*, are key pathogens in light of their high prevalence within the root canals, prominent virulence factors and/or significance in the bacterial community's stability and virulence (Rôças and Siqueira, 2018).

Bacterial translocation involves the circulation of bacteria and/or their immunogenic products, such as DNA, even without overt infection or clinical signs (Kane et al., 1998; Martinez-Martinez et al., 2009; Ibrahiem et al., 2011). ALEOs might provide a direct pathogenic pathway toward general circulation provoking low-grade systemic inflammation and associated NCD risk. In fact, extraradicular infections have been increasingly identified during the last years, suggesting an initial step in bacterial dissemination beyond the tooth structure, in which they can reach the blood vessels from the apical granuloma (Sunde et al., 2000; Buonavoglia et al., 2013). Furthermore, evidence of endodontic bacterial translocation is indirectly supported by the well-documented enrichment of oral bacterial DNA in diseased peripheral tissues (i.e. atheroma plaques, arthritic joints) (Reichert et al., 2013; Chhibber-Goel et al., 2016; Berthelot and Wendling, 2020). It has been proposed that periodontal bacteria can be transported to distant tissues internalized in immune cells in arthritis (Martinez-Martinez et al., 2009; Ibrahiem et al., 2011), involving mononuclear cell activation, production of pro-inflammatory cytokines, and risk for future NCD complications (Sahingur et al., 2010; Rodriguez-Laiz et al., 2019). Up to now, reports of extraradicular endodontic infection are limited, whereas further bacterial outreach to blood remains unknown. We aimed first to explore overall extraradicular infection, as well as specifically by *Porphyromonas* spp; and their potential to translocate from infected root canals to the blood through peripheral blood mononuclear cells (PBMCs).

MATERIAL AND METHODS

Study Design

Cross-sectional. The study was approved by the Ethics-Scientific Committee of the Central Metropolitan Health Service (N 2017/70) and from the Faculty of Dentistry, Universidad de Chile (N 2016/08). The objectives and procedures of the study were informed to the participants and all of them signed the informed consent or its corresponding forms in the case of underage participants. All procedures followed the ethical standards of the institutional and/or national research committee and with the 1964 Helsinki declaration and its later amendments or comparable ethical standards.

Patient Recruitment

Patients aged between 15 and 40 years old consulting at the dental clinic, School of Dentistry, Universidad de Chile and the Clinic of Surgery, Faculty of Dentistry, Universidad Andrés Bello, Santiago, Chile, were enrolled between 2016 and 2019 if they were otherwise healthy and had a clinical diagnosis of AP in the presence of a radiographic apical radiolucency due to extensive caries in a tooth with negative sensitivity pulpal test with no previous endodontic intervention. SAP and AAP were diagnosed when clinical symptoms in response to percussion were present or absent, respectively, according to previously defined diagnostic terminology (Gutmann et al., 2009). Controls met the same criteria and the absence of any tooth with ALEOs. Exclusion criteria were obesity (body mass index $\geq$30 kg/m^2), pregnancy, moderate to severe periodontitis, and antibiotic and/or anti-inflammatory drug consumption 3 months before the study (Garrido et al., 2019).

Sample Collection

Periapical tissue samples were collected from individuals having indication of tooth extraction. Tissue samples from ALEOs (n=64), including AAP (n=29) and SAP (n=35), or healthy periodontal ligaments (HPL) as negative controls (n=9), were obtained by surgical separation of the tissue from the root surface with sterile curettes. Then the samples were washed with 3 mL of sterile NaCl solution before their storage in 100 µL of RNAlater (Qiagen, Valencia, CA, USA) at -80°C until processed for tissue homogenization.

Root canal exudates and the respective blood samples were collected from AP patients having indication of endodontic treatment. For intracanal exudate sampling (N=39; AAP=29 and SAP=10), the involved tooth was isolated with a rubber dam and disinfected with 70% ethanol solution. After coronal access, sterile paper points (Maillefer®) were inserted into the infected root canal for 1 minute, transported in a vial containing 1 mL of cold sterilized reduced transport fluid (RTF), and stored at -80°C for posterior analysis. Blood samples were collected from a subset of AP patients (n=14) and also from healthy control volunteers (n=14) by venipuncture of the antecubital vein (Fouad et al., 2002; Rocas and Siqueira, 2011). PBMCs were isolated using Ficoll-Paque Premium 1.073 (GE Healthcare®), following the manufacturer's instructions.

DNA Extraction

Apical tissue samples were homogenized in a lysis buffer with lysozyme 20 mg/mL at 37°C for 1 h. DNA was extracted using a commercial kit to obtain bacterial DNA (NucleoSpin® TriPrep, Macherey-Nagel), according to the recommendations of the manufacturer. Intracanal exudate DNA was extracted by the boiling modified method (Queipo-Ortuño et al., 2008); the Eppendorf tubes containing the paper points and the RTF medium were boiled in a water bath for 10 minutes, followed by cooling down to -20°C for 10 minutes and were finally centrifuged for five minutes at 1000 rpm. PBMC bacterial DNA was extracted in a lysis buffer using lysozyme followed by the TE buffer and DNEasy isolation kit (QIAGEN Inc., Valencia, CA, USA), according to the manufacturer. The concentration and quality of DNA were confirmed by the 260:280 ratio in a spectrophotometer (Bio-Tek, Winooski, VT).

qPCR Assay

Quantitative PCR (SteponePlus®; Applied Biosystems, Singapore) was carried out to determine bacterial loads and frequencies of detection of total bacteria, *P. gingivalis* and *P. endodontalis*. Primer sets are shown in **Table 1**. Briefly, total bacteria were quantified using specific primers targeting 16S ribosomal RNA (rRNA) gene previously published (Nadkarni et al., 2002); as well as *P. gingivalis*, which was identified by using previously validated 16S rRNA gene primers (Byrne et al., 2009). The primer set for targeting *P. gingivalis* included 16S rRNA from base 729 to 1192 (GenBank: L16492.1). For *P. endodontalis* identification, specific primers targeting the heat shock protein 60 were used (Hsp60 gene) (Sakamoto and Ohkuma, 2010). The Hsp60 gene sequence was obtained from GeneBank NIH genetic sequence database (GenBank: AB547580.1). Primer pairs were designed and assessed manually in the Primer Blast tool, considering the real-time PCR guide (BIO RAD). Which included having a melting temperature (Tm) between 50°C and 65°C, a GC content of 50–60%, to be limited to obtain an amplicon ranging from 75 to 200 bp. The selected primer pairs, targeting from base 84 to 201, were checked for specificity and cross-reactivity using Primer Blast and UniProt databases. Experimental validation included: firstly, the analysis of the molecular weight of the DNA fragments of three positive samples for *P. endodontalis* in agarose gel electrophoresis. Secondly, positive samples in step 1 were confirmed by Sanger sequencing (Macrogen, Seoul, Korea), showing 100% alignment with *P. endodontalis* (Hsp60 gene). Also, to determine the primer specificity, a dissociation curve analysis was performed, using temperatures between 60°C and 95°C for the recognition of non-specific product formation or contamination.

Each qPCR was performed using KAPA SYBR ® Fast qPCR Kits (KAPA Biosystems, Woburn, MA, USA). Positive controls consisting of *P. gingivalis* ATCC 33277 and *P. endodontalis* ATCC 35406 DNA, and negative control (no DNA) were included in each experiment. Cycling conditions consisted of the following steps: 95°C for 3 min, 40 cycles: total bacteria 95°C for 15 sec and 60°C for 1 min; *P. gingivalis* 95°C for 3 sec and 58°C for 1 min; *P. endodontalis* 95°C for 30 seconds and 58°C for 1 min. As it was stated above, both *in silico* and experimental approaches were used for primers validation.

Absolute quantifications of total bacterial and individual species loads were carried out by comparing the threshold cycle (Dorn et al., 2002) values of the test samples to standard curves of known DNA copy numbers of *P. gingivalis* and *P. endodontalis* (**Supplementary Figure 1**). The lower and higher detection limits were 10^2 and the 10^8 DNA copy numbers, respectively. All experiments were performed with a linear quantitative detection range, **Supplementary Figure 1**. Bacterial loads were expressed as DNA copies/mg in the case of ALEOs, and DNA copies/μL in the case of intracanal exudates and PBMCs.

Statistical Analysis

The sample size was calculated during a pilot study based on the positive detection of *P. endodontalis* in AAP versus SAP in ALEOs. Considering an 80% statistical power and 5% alpha error, a minimum of 23 samples in each group (SAP and AAP) were required.

Data distribution was evaluated by the Shapiro-Wilk test. Fisher's exact Chi-square tests were used to compare the frequency of bacterial detection between two groups; Mann-Whitney test was used to compare bacterial loads between two groups; and McNemar's and Spearman's correlation tests were conducted to compare the associations in the frequencies of detection and bacterial loads, respectively between intracanal

TABLE 1 | Primers used to determine the bacterial loads and frequency of target bacteria.

Target bacteria	Target gene	Forward primer (5'-3')	Reverse primer (5'-3')
Total Bacteria	16S rRNA	TCCTACGGGAGGCAGCAGT	GGACTACCAGGGTATCTAATCCTGTT
P. endodontalis	Hsp 60	TATTGACAAGGCTGTGGCTACC	TTCTTCGTCCCCATTAGCCGA
P. gingivalis	16S rRNA	AGGCAGCTTGCCATACTGCG	ACTGTTAGTAACTACCGATGT

exudates and PBMCs within AP individuals. Analyses were performed using STATA 12® (StataCorp LP, TX, USA). The level of statistical significance was $p<0.05$.

RESULTS

This study included a total of 126 individuals. Demographics and smoking habits are shown in **Table 2**. **Figures 1A, B** shows extraradicular infection rates for total bacteria, *P. endodontalis*, and *P. gingivalis*. The detection frequency, expressed as n (%), and bacterial loads expressed as medians (interquartile range) in ALEOs were 46 (70.8%) and 4521.6 (7789.1) DNA copy number/mg, respectively for total bacteria; 14 (21.5%) and 1789.7(1338.8) DNA copy number/mg for *P. endodontalis*; 12 (18.4%) and 1493.9 (26919.9) DNA copy number/mg for *P. gingivalis*. A higher frequency of detection was identified for *P. endodontalis* in symptomatic ALEOs compared to asymptomatic ALEOs ($p = 0.003$), while no significant differences were found in the detection frequencies of total bacteria and *P. gingivalis* or bacterial loads ($p > 0.05$). Healthy periodontal ligaments confirmed no bacterial detection.

The frequency of detection and loads of total bacteria and *Porphyromonas* spp. in intracanal exudates are shown in **Figures 2A, B**. The frequencies of detection expressed as n (%) and bacterial loads expressed as median (interquartile range) DNA copy number/µL, respectively in AP were n=39 (100%) and 21089.2 (263450.7) for total bacteria; n=16 (41%) and 8263.9 (85001.8) for *P. endodontalis;* and n=8 (20.5%), 12538.9 (72957.3) for *P. gingivalis*. The frequency of detection and bacterial loads for *P. endodontalis* were 48.3% and 6127.9 (121214.7) in AAP, and 20%, and 9331.2 (6437.1) in SAP exudates, ($p > 0.05$). *P. gingivalis* was only identified in intracanal exudates from AAP with positive detection of n=8 (27.6%) and a bacterial load of 12538.9 (107919.3) DNA copy number/µL.

The frequency of bacterial DNA detection and loads in PBMCs are presented in **Figures 3A, B**. Bacteria were detected in 100% of the PBMC samples from AP and control groups. The total bacterial load was significantly higher in AP individuals compared to healthy controls (953.6 vs 300.6 median DNA copy number/µL respectively; $p = 0.0002$). On the other hand, *P. endodontalis* was detected in 50% of the samples of both, AP individuals and controls, showing an even higher frequency of detection than in intracanal exudates and apical lesions, though its bacterial loads were low, and no statistically significant differences were found between AP and healthy groups ($p > 0.05$). *P. gingivalis* was not detected in any of the evaluated PBMC samples (data not shown).

To explore the potential endodontic origin of the bacteria detected in PBMCs, the frequencies and loads of total bacteria, *P. endodontalis*, and *P. gingivalis* were associated between the intracanal samples and PBMCs within each AP individual (**Table 3**). Detection of total bacteria was positive in all intracanal exudates and PBMCs samples (14/14). *P. endodontalis* was identified in only two intracanal exudate samples (2/14) and seven PBMC samples (7/14) in AP individuals. From them, only one patient was positive for *P.*

TABLE 2 | Demographic data and smoking habits of study groups.

Parameters	Tissue Samples		Intracanal (n = 39)	PBMCs	
	ALEOs (n = 64)	HPL (n = 9)		AP (n = 14)	Control (n = 14)
Age [years, median (IQR)]	38 (22.5)	22 (5)	25 (5)	24 (9.25)	22 (6.5)
Females (n, %)	27 (42.2%)	6 (66.7%)	18 (46.2%)	5 (35.7%)	4 (28.6%)
Smokers (n, %)	28 (44.4%)	2 (22%)	14 (35%)	9 (64.3%)	1 (7.1%)
Educational level (median)	Full high school	Full high school	Full high school	Full high school	Full high school

ALEOs, Apical lesions of endodontic origin; HPL, healthy periodontal ligament; PBMCs, Peripheral blood mononuclear cells; IQR, interquartile range.

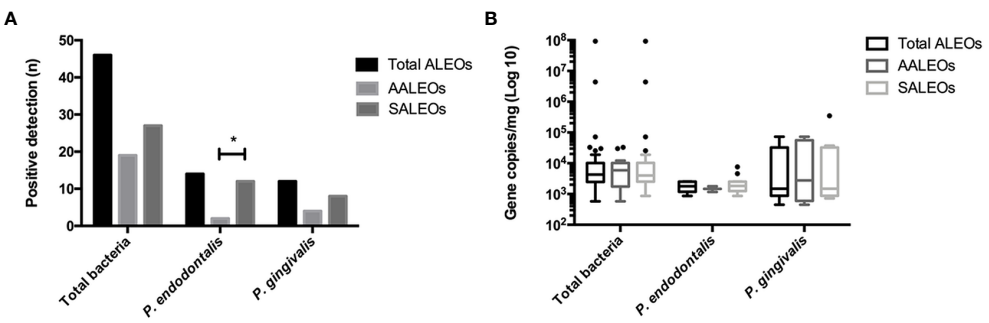

FIGURE 1 | **(A)** Frequency of detection and **(B)** copy numbers of 16S rRNA gene of total bacteria and *P. gingivalis*, and Hsp60 gene of *P. endodontalis* in total ALEOs (n = 64) including AALEOs (n = 29) and SALEOs (n = 35). ALEOs Apical lesions of endodontic origin; AALEO asymptomatic apical lesions of endodontic origin; SALEOs symptomatic apical lesions of endodontic origin. *$p < 0.05$.

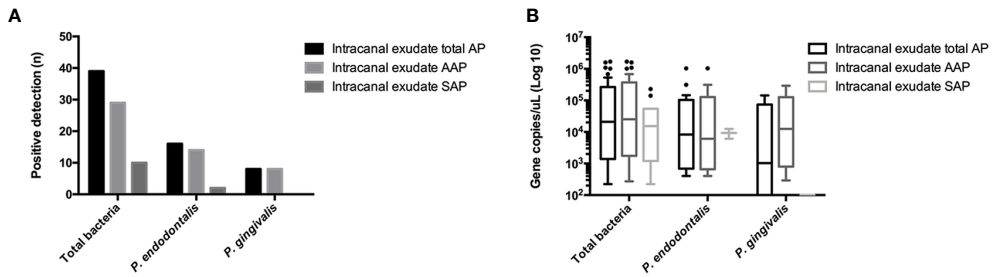

FIGURE 2 | **(A)** Frequency of detection and **(B)** copy numbers of 16S rRNA gene of total bacteria and *P. gingivalis*, and Hsp60 gene of *P. endodontalis* in the root canal system exudates in AP (n = 39) including AAP (n = 29) and SAP (n = 10). AP Apical periodontitis; AAP asymptomatic apical periodontitis; SAP symptomatic apical periodontitis.

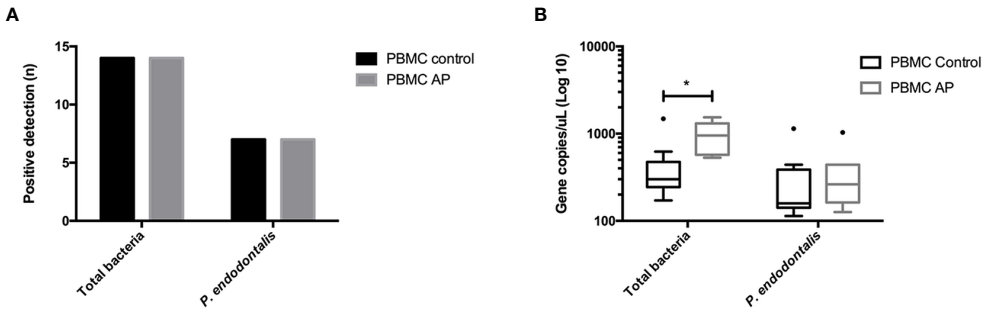

FIGURE 3 | **(A)** Frequency of detection and **(B)** copy numbers of 16S rRNA gene of total bacteria and *P. gingivalis*, and Hsp60 gene of *P. endodontalis* in PMBCs from patients with AP (n = 14) and healthy subjects (n = 14). PBMCs Peripheral blood mononuclear cells; AP Apical periodontitis. *p < 0.05.

TABLE 3 | Endodontic/oral bacterial detection in intracanal exudates and respective PBMCs samples in AP individuals.

Intracanal exudates (n = 14)	PBMC (n = 14) Total Bacteria		*P. endodontalis*		*P. gingivalis*	
Detection	**Positive**	**Negative**	**Positive**	**Negative**	**Positive**	**Negative**
Positive	14	0	1	1	0	3
Negative	0	0	6	6	0	11

PBMC, Peripheral blood mononuclear cells; AP, apical periodontitis; P. Porphyromonas. Detection expressed like positive and negative detection in intracanal exudates and PBMCs. p > 0.05.

endodontalis at both, the intracanal exudate and the respective PBMCs. On the other hand, *P. gingivalis* was detected in three intracanal samples, though it was not detected in PBMCs. Regarding bacterial loads, no correlation was found between intracanal exudates and PBMCs (Spearman's rho = 0.28, p = 0.33; data now shown).

DISCUSSION

ALEO is the result of a polymicrobial infection of the root canal system that causes local inflammation and destruction of the periapical tissues. Though bacteria have been largely assumed to be confined within the necrotic tooth canal, emerging evidence suggests that they can disseminate beyond the tooth structures (Liljestrand et al., 2016). Based on bacterial DNA detection, in the current study, we show a high frequency of extraradicular infection. Specifically, *P. endodontalis* was detected with a higher frequency in symptomatic compared to asymptomatic ALEO. Moreover, endodontic bacteria were detected in circulating mononuclear cells, whereas total bacterial loads were higher in PBMCs from AP compared to healthy individuals.

The presence of bacteria in the root canal system of teeth with AP has long been documented (Ricucci and Siqueira, 2010), but the concept of extraradicular infection is rather recent with only a few studies available. Given their high sensitivity, molecular techniques are widely being used to characterize the microbial communities (Rôças and Siqueira, 2008; Zhang et al., 2010; Rôças et al., 2011). Herein, we seek for unspecific oral bacteria and specific *Porphyromonas* spp. in ALEOs by qPCR. Identification

of viable *Porphyromonas* spp. was formerly demonstrated through bacterial culture techniques in periapical abscesses (Van Winkelhoff et al., 1985). As part of the endodontic microbiome, Gram-negative species, such as *P. endodontalis* and *P. gingivalis*, are likely to have a clinical significance due to their wide repertoire of virulence factors (Sundqvist et al., 1989). Our results revealed high detection frequencies of total bacteria (70.8%), *P. gingivalis* (18.4%), and *P. endodontalis* (21.5%) in ALEOs. Specific identification of *P. endodontalis* and *P. gingivalis* with frequencies of 45% and 27% respectively, was also reported in ALEOs from persistent apical periodontitis based on qPCR (Zhang et al., 2010). The current study also explored the association between extraradicular infection and clinical symptoms, reporting a significantly higher detection frequency of *P. endodontalis* in ALEOs from SAP compared to AAP, while the detection frequencies and bacterial loads of *P. gingivalis* and total bacteria did not show differences. Though experimental mono-infection by *P. endodontalis* generates low pathogenicity compared to *P. gingivalis*, anaerobic mixed communities containing both species can trigger severe infective responses (Van Winkelhoff et al., 1985). Presumably, *P. endodontalis* might contribute to the bacterial mixed community to become more virulent, recruiting an enhanced immune response and giving rise to clinical symptoms. Therefore, it seems plausible that extraradicular translocation of *P. endodontalis* plays a relevant role in active forms of ALEOs.

The infection of the root canal system has been extensively characterized in AP (Gharbia et al., 1994; Fouad et al., 2002; Siqueira, 2002; Ricucci and Siqueira, 2010). Bacteria have been detected up to 100% within root canals from primary endodontic infection by molecular techniques (Conrads et al., 1997; Rôças and Siqueira, 2010). In line with this, intracanal samples of AP were all positive for bacterial DNA in our study. In earlier studies, the intracanal detection of *Porphyromonas* spp. revealed low recovery rates (9-23.9%) by culture methods (Hashioka et al., 1992; Baumgartner et al., 1999; Jacinto et al., 2003), though recent data based on molecular techniques report higher prevalence in primary endodontic infections (between 23.3-50% and 33-44%, respectively) (Tomazinho and Avila-Campos, 2007; Cao et al., 2012). Similarly, our results show detection frequencies of 41.0% for *P. endodontalis* and 20.5% for *P. gingivalis* in intracanal samples, confirming the relevant etiologic role of these black-pigmented anaerobic rods in AP (Dougherty et al., 1998; Baumgartner et al., 1999; de Oliveira et al., 2000).

Though the etiologic role of the intracanal bacterial infection is a matter of fact, its association with clinical symptoms remains unclear. Our results show that the detection frequencies and loads of total bacteria and *Porphyromonas* spp. in endodontic canals remained similar among AAP and SAP. Previous studies have reported comparable detection rates in root canals, especially for *P. endodontalis*, varying between 56% to 62% in AAP; and 40% to 69% in SAP (Van Winkelhoff et al., 1985; Rôças et al., 2002; Rôças and Siqueira, 2008; Rôças et al., 2011; Cardoso et al., 2016); while the available evidence of the detection of *P. gingivalis* ranges between 8-38% in SAP and 4-29% in AAP (Wang et al., 2010; Buonavoglia et al., 2013). The frequent intracanal detection of *Porphyromonas* spp. in association with AAP might be related to the confinement of the infection to the root canal. Importantly, in this condition bacteria gain no access to blood vessels as pulpal tissue is necrotic (Rôças and Siqueira, 2010). Moreover, our results showed that the relative detection of both, *P. endodontalis* and *P. gingivalis*, was higher in ALEOs than intracanal exudates from SAP; and conversely, they were higher in intracanal exudates than ALEOs in AAP; even though a direct comparison cannot be performed because ALEOs and intracanal exudates were obtained from different individuals based on their treatment indications, altogether these antecedents suggest that the transit to an acute periapical process and the consecutive onset of clinical symptoms might rely on the host's inability to confine the endodontic pathogens -such as *P. endodontalis*- within the root canals and extraradicular infection might represent the first step for bacterial dissemination.

Given the anatomic relation of ALEOs with the bloodstream, it is plausible that inflammatory mediators, bacteria, and/or their products translocate from their endodontic sites to the systemic circulation (Garrido et al., 2019). Oral bacteria can be transported to distant tissues as free circulating DNA and/or internalized in immune cells (Martinez-Martinez et al., 2009; Ibrahiem et al., 2011), though the former is less probable because circulating oral bacteria are cleared within few minutes (Minasyan, 2019). Accordingly, we screened for bacterial DNA within PBMCs from AP and healthy individuals and found significantly higher total bacterial loads in the former, suggesting that ALEOs create a favorable environment for the overgrowth of microorganisms and their systemic dissemination. Moreover, *P. endodontalis* DNA was also detected in PBMCs from individuals in both groups (50%). In fact, a previous study reported the carriage of bacterial DNA (16S rDNA) in PBMCs from arthritis and control individuals (Ibrahiem et al., 2011). Despite no studies are available in AP, a pathophysiological role for blood dendritic cells in systemic dissemination of periodontal pathobionts to atherosclerotic plaques was proposed, particularly of *P. gingivalis* (Carrion et al., 2012). Herein we failed to detect *P. gingivalis* in PBMCs, probably because our study individuals were free from periodontitis. Instead, *P. endodontalis* might analogously translocate to distant sites from oral/endodontic sites *via* PBMCs and has also the ability to invade endothelial cells *in vitro* (Dorn et al., 2002). Additionally, bacterial carriage has been associated with mononuclear cell activation, production of pro-inflammatory cytokines, prolonged survival of circulating monocytes, and further risk of future complications of systemic non-communicable diseases, including cirrhosis and hemodialysis (Hazzah et al., 2015; Rodriguez-Laiz et al., 2019). These results are in line with the higher inflammatory burden of serum markers reported in patients with ALEOs (Garrido et al., 2019). Altogether, these preliminary studies support that oral/endodontic microorganisms can translocate from their habitats to systemic circulation and reach distant organs using mononuclear cells as Trojan horses. The capacity for intracellular survival of bacteria within phagocytes is likely a critical factor facilitating the dissemination. Some bacteria can hide within autophagosomes, where they protected themselves from phagocytic killing (Berthelot and Wendling, 2020).

Despite the abovementioned bacterial translocation in AP, no association was found between the presence and loads of bacteria between endodontic canals and PBMCs within the study individuals. Oral bacteria and specifically *P. endodontalis* might coexist in various oral habitat, including subgingival sites and periodontal pockets, as well as oral mucosa (*i.e.* tonsils and tongue), where they can also be phagocytosed by mononuclear cells and reach the general circulation (Lombardo Bedran et al., 2012; Scapoli et al., 2015).

Although bacterial cultures are considered the reference method to determine the presence of microorganisms (Zweitzig et al., 2013), molecular analysis is more sensitive, especially in anaerobic conditions, such as necrotized root canals (Baumgartner, 2004). Particularly, *Porphyromonas* is considered fastidious genera and culture methods may underestimate their frequency (Gomes and Herrera, 2018). Also, no viable oral bacteria can be recovered from peripheral lesions in most studies (Martinez-Martinez et al., 2009; Chhibber-Goel et al., 2016), whereas PCR has proven to be highly sensitive to detect bacterial translocation (Kane et al., 1998). Instead, bacterial DNA is much more likely to disseminate from oral niches through blood and can trigger and perpetuate inflammation after bacterial clearance.

Summarizing, total bacteria and specific *Porphyromonas* spp. were frequently found in endodontic canals and extra-radicular infection in AP patients. Extraradicular bacteria and specifically, detection of *P. endodontalis*, associated with symptomatic forms of the disease and might represent a first step in the dissemination process. Also, *P. endodontalis* was frequently detected in PBMCs from study individuals and higher total bacterial loads were found in AP, supporting a role for these cells in the bacterial carriage during AP.

DATA AVAILABILITY STATEMENT

The raw data supporting the conclusions of this article will be made available by the authors, without undue reservation.

ETHICS STATEMENT

The studies involving human participants were reviewed and approved by Ethics-Scientific Committee of the Central Metropolitan Health Service (N 2017/70) and from the Faculty of Dentistry, Universidad de Chile (N 2016/08). Written informed consent to participate in this study was provided by the participants' legal guardian/next of kin.

AUTHOR CONTRIBUTIONS

MH, MG, AH: Conceptualization and design. MG, MB: Data curation. MH: Funding acquisition. MH, AF, MB, AH: Formal analysis. MB, JA, AH: Laboratory experiments. MH: Project administration. AH: Design the figures. MH: Resources. MH: Software. MG, MH: Supervision. MB, AF, MH: Writing manuscript. All authors contributed to the article and approved the submitted version.

FUNDING

This study was funded by FONDECYT 1160741 and 1200098. AF is a recipient of scholarship CONICYT 21181377, from Chilean Government.

ACKNOWLEDGMENTS

We want to thank Bernardita Parada for her contribution in patient recruitment and sample collection procedures.

SUPPLEMENTARY MATERIAL

The Supplementary Material for this article can be found online at: https://www.frontiersin.org/articles/10.3389/fcimb.2021.649925/full#supplementary-material

Supplementary Figure 1 | Quantitative PCR standard curves obtained for total bacteria **(A)**, P. gingivalis **(B)** and P. endodontalis **(C)** quantification. The regression line from the 10-fold dilutions curve was used to determine the copy number of all samples. All reactions were performed in duplicate.

REFERENCES

Baumgartner, J. C., Watkins, B. J., Bae, K.-S., and Xia, T. (1999). Association of black-pigmented bacteria with endodontic infections. *J. Endodontics* 25, 413–415. doi: 10.1016/S0099-2399(99)80268-4

Baumgartner, J. C. (2004). Microbiological and molecular analysis of endodontic infections. *Endodontic Topics* 7, 35–51. doi: 10.1111/j.1601-1546.2004.00061.x

Berthelot, J. M., and Wendling, D. (2020). Translocation of dead or alive bacteria from mucosa to joints and epiphyseal bone-marrow: facts and hypotheses. *Joint Bone Spine* 87, 31–36. doi: 10.1016/j.jbspin.2019.01.004

Buonavoglia, A., Latronico, F., Pirani, C., Greco, M. F., Corrente, M., and Prati, C. (2013). Symptomatic and asymptomatic apical periodontitis associated with red complex bacteria: clinical and microbiological evaluation. *Odontology* 101, 84–88. doi: 10.1007/s10266-011-0053-y

Byrne, S. J., Dashper, S. G., Darby, I. B., Adams, G. G., Hoffmann, B., and Reynolds, E. C. (2009). Progression of chronic periodontitis can be predicted by the levels of Porphyromonas gingivalis and Treponema denticola in subgingival plaque. *Oral. Microbiol. Immunol.* 24, 469–477. doi: 10.1111/j.1399-302X.2009.00544.x

Cao, H., Qi, Z., Jiang, H., Zhao, J., Liu, Z., and Tang, Z. (2012). Detection of Porphyromonas endodontalis, Porphyromonas gingivalis and Prevotella intermedia in primary endodontic infections in a Chinese population. *Int. Endodontic J.* 45, 773–781. doi: 10.1111/j.1365-2591.2012.02035.x

Cardoso, F. G. D. R., Chung, A., Martinho, F. C., Camargo, C. H. R., Carvalho, C. A. T., Gomes, B. P. F. D. A., et al. (2016). Investigation of Bacterial Contents From Persistent Endodontic Infection and Evaluation of Their Inflammatory Potential. *Braz. Dental J.* 27, 412–418. doi: 10.1590/0103-6440201600520

Carrion, J., Scisci, E., Miles, B., Sabino, G. J., Zeituni, A. E., Gu, Y., et al. (2012). Microbial carriage state of peripheral blood dendritic cells (DCs) in chronic

periodontitis influences DC differentiation, atherogenic potential. *J. Immunol. (Baltimore Md. 1950)* 189, 3178–3187. doi: 10.4049/jimmunol.1201053

Chhibber-Goel, J., Singhal, V., Bhowmik, D., Vivek, R., Parakh, N., Bhargava, B., et al. (2016). Linkages between oral commensal bacteria and atherosclerotic plaques in coronary artery disease patients. *NPJ Biofilms Microbiomes* 2, 7. doi: 10.1038/s41522-016-0009-7

Conrads, G., Gharbia, S. E., Gulabivala, K., Lampert, F., and Shah, H. N. (1997). The use of a 16S rDNA directed PCR for the detection of endodontopathogenic bacteria. *J. Endodontics* 23, 433–438. doi: 10.1016/S0099-2399(97)80297-X

de Oliveira, J. C. M., Siqueira, J. F. Jr, Alves, G. B., Hirata, R. Jr, and Andrade, A. F. (2000). Detection of Porphyromonas endodontalis in infected root canals by 16S rRNA gene-directed polymerase chain reaction. *J. Endodontics* 26, 729–732. doi: 10.1097/00004770-200012000-00016

Dorn, B., Harris, L., Wujick, C., Vertucci, F., and Progulske-Fox, A. (2002). Invasion of vascular cells in vitro by Porphyromonas endodontalis. *Int. Endodontic J.* 35, 366–371. doi: 10.1046/j.0143-2885.2001.00489.x

Dougherty, W., Bae, K., Watkins, B., and Baumgartner, J. (1998). Black-pigmented bacteria in coronal and apical segments of infected root canals. *J. Endodontics* 24, 356–358. doi: 10.1016/S0099-2399(98)80134-9

Fouad, A. F., Barry, J., Caimano, M., Clawson, M., Zhu, Q., Carver, R., et al. (2002). PCR-based identification of bacteria associated with endodontic infections. *J. Clin. Microbiol.* 40, 3223–3231. doi: 10.1128/JCM.40.9.3223-3231.2002

Garrido, M., Cardenas, A. M., Astorga, J., Quinlan, F., Valdes, M., Chaparro, A., et al. (2019). Elevated Systemic Inflammatory Burden and Cardiovascular Risk in Young Adults with Endodontic Apical Lesions. *J. Endodontics* 45, 111–115. doi: 10.1016/j.joen.2018.11.014

Gharbia, S. E., Haapasalo, M., Shah, H. N., Kotiranta, A., Lounatmaa, K., Pearce, M. A., et al. (1994). Characterization of Prevotella intermedia and Prevotella nigrescens isolates from periodontic and endodontic infections. *J. Periodontol.* 65, 56–61. doi: 10.1902/jop.1994.65.1.56

Gomes, B., and Herrera, D. (2018). Etiologic role of root canal infection in apical periodontitis and its relationship with clinical symptomatology. *Braz. Oral. Res.* 32, 82–110. doi: 10.1590/1807-3107bor-2018.vol32.0069

Gutmann, J. L., Baumgartner, J. C., Gluskin, A. H., Hartwell, G. R., and Walton, R. E. (2009). Identify and define all diagnostic terms for periapical/periradicular health and disease states. *J. Endodontics* 35, 1658–1674. doi: 10.1016/j.joen.2009.09.028

Hashioka, K., Yamasaki, M., Nakane, A., Horiba, N., and Nakamura, H. (1992). The relationship between clinical symptoms and anaerobic bacteria from infected root canals. *J. Endodontics* 18, 558–561. doi: 10.1016/S0099-2399(06)81214-8

Hazzah, W. A., Hashish, M. H., El-Koraie, A. F., Ashour, M. S., and Abbass, A. A. (2015). Circulating bacterial DNA fragments in chronic hemodialysis patients. *Saudi J. Kidney Dis. Transpl.* 26, 1300–1304. doi: 10.4103/1319-2442.168689

Hsiao, W. W., Li, K. L., Liu, Z., Jones, C., Fraser-Liggett, C. M., and Fouad, A. F. (2012). Microbial transformation from normal oral microbiota to acute endodontic infections. *BMC Genomics* 13, 345. doi: 10.1186/1471-2164-13-345

Ibrahiem, B. E., El Haliem, N. F., El-Khouly, N., El-Bazz, W. F., Al-Raoof, M. A., and Said, Z. N. (2011). Detection of bacterial DNA in peripheral blood mononuclear cells of patients with reactive arthritis. *Egyptian J. Immunol.* 2, 67–76.

Jacinto, R., Gomes, B., Ferraz, C., Zaia, A., and Filho, F. S. (2003). Microbiological analysis of infected root canals from symptomatic and asymptomatic teeth with periapical periodontitis and the antimicrobial susceptibility of some isolated anaerobic bacteria. *Oral. Microbiol. Immunol.* 18, 285–292. doi: 10.1034/j.1399-302X.2003.00078.x

Kane, T. D., Alexander, J. W., and Johannigman, J. A. (1998). The detection of microbial DNA in the blood: a sensitive method for diagnosing bacteremia and/or bacterial translocation in surgical patients. *Ann. Surg.* 227, 1–9. doi: 10.1097/00000658-199801000-00001

Liljestrand, J. M., Mantyla, P., Paju, S., Buhlin, K., Kopra, K. A., Persson, G. R., et al. (2016). Association of Endodontic Lesions with Coronary Artery Disease. *J. Dental Res.* 95, 1358–1365. doi: 10.1177/0022034516660509

Lombardo Bedran, T. B., Marcantonio, R. A. C., Spin Neto, R., Alves Mayer, M. P., Grenier, D., Spolidorio, L. C., et al. (2012). Porphyromonas endodontalis in chronic periodontitis: a clinical and microbiological cross-sectional study. *J. Oral. Microbiol.* 4, 10123. doi: 10.3402/jom.v4i0.10123

Martinez-Martinez, R. E., Abud-Mendoza, C., Patino-Marin, N., Rizo-Rodriguez, J. C., Little, J. W., and Loyola-Rodriguez, J. P. (2009). Detection of periodontal bacterial DNA in serum and synovial fluid in refractory rheumatoid arthritis patients. *J. Clin. Periodontol.* 36, 1004–1010. doi: 10.1111/j.1600-051X.2009.01496.x

Minasyan, H. (2019). Sepsis: mechanisms of bacterial injury to the patient. *Scandinavian J. Trauma Resuscitation Emergency Med.* 27, 19–19. doi: 10.1186/s13049-019-0596-4

Nadkarni, M. A., Martin, F. E., Jacques, N. A., and Hunter, N. (2002). Determination of bacterial load by real-time PCR using a broad-range (universal) probe and primers set. *Microbiology* 148, 257–266. doi: 10.1099/00221287-148-1-257

Queipo-Ortuño, M. I., De Dios Colmenero, J., Macias, M., Bravo, M. J., and Morata, P. (2008). Preparation of bacterial DNA template by boiling and effect of immunoglobulin G as an inhibitor in real-time PCR for serum samples from patients with brucellosis. *Clin. Vaccine Immunol.* 15, 293–296. doi: 10.1128/CVI.00270-07

Reichert, S., Haffner, M., Keysser, G., Schafer, C., Stein, J. M., Schaller, H. G., et al. (2013). Detection of oral bacterial DNA in synovial fluid. *J. Clin. Periodontol.* 40, 591–598. doi: 10.1111/jcpe.12102

Ricucci,, and Siqueira, (2010). Biofilms and apical periodontitis: study of prevalence and association with clinical and histopathologic findings. *J. Endodontics* 36, 1277–1288. doi: 10.1016/j.joen.2010.04.007

Rôças,, and Siqueira, (2008). Root Canal Microbiota of Teeth with Chronic Apical Periodontitis. *J. Clin. Microbiol.* 46, 3599. doi: 10.1128/JCM.00431-08

Rôças,, and Siqueira, (2010). Identification of bacteria enduring endodontic treatment procedures by a combined Reverse Transcriptase–Polymerase Chain reaction and Reverse-Capture Checkerboard approach. *J. Endodontics* 36, 45–52.

Rocas, I. N., and Siqueira, J. F. Jr. (2011). In vivo antimicrobial effects of endodontic treatment procedures as assessed by molecular microbiologic techniques. *J. Endod.* 37, 304–310. doi: 10.1016/j.joen.2010.11.003

Rôças,, and Siqueira, (2018). Frequency and levels of candidate endodontic pathogens in acute apical abscesses as compared to asymptomatic apical periodontitis. *PloS One* 13, e0190469.

Rôças,, Siqueira,, Andrade,, and Uzeda, D. (2002). Identification of selected putative oral pathogens in primary root canal infections associated with symptoms. *Anaerobe* 8, 200–208. doi: 10.1006/anae.2002.0431

Rôças,, Siqueira,, and Debelian, (2011). Analysis of Symptomatic and Asymptomatic Primary Root Canal Infections in Adult Norwegian Patients. *J. Endodontics* 37, 1206–1212.

Rodriguez-Laiz, G. P., Zapater, P., Melgar, P., Alcazar, C., Franco, M., Gimenez, P., et al. (2019). Bacterial DNA translocation contributes to systemic inflammation and to minor changes in the clinical outcome of liver transplantation. *Sci. Rep.* 9, 835. doi: 10.1038/s41598-018-36904-0

Sahingur, S. E., Xia, X. J., Alamgir, S., Honma, K., Sharma, A., and Schenkein, H. A. (2010). DNA from Porphyromonas gingivalis and Tannerella forsythia induce cytokine production in human monocytic cell lines. *Mol. Oral. Microbiol.* 25, 123–135. doi: 10.1111/j.2041-1014.2009.00551.x

Sakamoto, M., and Ohkuma, M. (2010). Usefulness of the hsp60 gene for the identification and classification of Gram-negative anaerobic rods. *J. Med. Microbiol.* 59, 1293–1302. doi: 10.1099/jmm.0.020420-0

Sakko, M., Tjaderhane, L., and Rautemaa-Richardson, R. (2016). Microbiology of Root Canal Infections. *Primary Dental J.* 5, 84–89. doi: 10.1308/205016816819304231

Scapoli, L., Girardi, A., Palmieri, A., Martinelli, M., Cura, F., Lauritano, D., et al. (2015). Quantitative analysis of periodontal pathogens in periodontitis and gingivitis. *J. Biol. Regulators Homeostatic Agents* 29, 101–110.

Siqueira, (2002). Endodontic infections: Concepts, paradigms, and perspectives. *Oral. Surg. Oral. Med. Oral. Pathol. Oral. Radiol. Endodontol.* 94, 281–293. doi: 10.1067/moe.2002.126163

Sunde, P. T., Tronstad, L., Eribe, E. R., Lind, P. O., and Olsen, I. (2000). Assessment of periradicular microbiota by DNA-DNA hybridization. *Endodontics Dental Traumatol.* 16, 191–196. doi: 10.1034/j.1600-9657.2000.016005191.x

Sundqvist, G., Johansson, E., and Sjögren, U. (1989). Prevalence of black-pigmented bacteroides species in root canal infections. *J. Endodontics* 15, 13–19. doi: 10.1016/S0099-2399(89)80092-5

Tomazinho, L. F., and Avila-Campos, M. J. (2007). Detection of Porphyromonas gingivalis, Porphyromonas endodontalis, Prevotella intermedia, and Prevotella

nigrescens in chronic endodontic infection. *Oral. Surg. Oral. Med. Oral. Pathol. Oral. Radiol. Endodontol.* 103, 285–288. doi: 10.1016/j.tripleo.2006.05.010

Van Winkelhoff, A., Carlee, A., and De Graaff, J. (1985). Bacteroides endodontalis and other black-pigmented Bacteroides species in odontogenic abscesses. *Infection Immun.* 49, 494–497. doi: 10.1128/IAI.49.3.494-497.1985

Veloso, P., Fernandez, A., Terraza-Aguirre, C., Alvarez, C., Vernal, R., Escobar, A., et al. (2020). Macrophages skew towards M1 profile through reduced CD163 expression in symptomatic apical periodontitis. *Clin. Oral. Investig.* 24, 4571–4581. doi: 10.1007/s00784-020-03324-2

Wang, Q., Zhou, X.-D., Zheng, Q.-H., Wang, Y., Tang, L., and Huang, D.-M. (2010). Distribution of Porphyromonas gingivalis fimA Genotypes in Chronic Apical Periodontitis Associated with Symptoms. *J. Endodontics* 36, 1790–1795. doi: 10.1016/j.joen.2010.08.018

Zhang, S., Wang, Q. Q., Zhang, C. F., and Soo, I. (2010). Identification of dominant pathogens in periapical lesions associated with persistent apical periodontitis. *Chin. J. Dental Res.* 13, 115–121.

Zweitzig, D. R., Riccardello, N. M., Morrison, J., Rubino, J., Axelband, J., Jeanmonod, R., et al. (2013). Measurement of microbial DNA polymerase activity enables detection and growth monitoring of microbes from clinical blood cultures. *PloS One* 8, e78488. doi: 10.1371/journal.pone.0078488

Conflict of Interest: The authors declare that the research was conducted in the absence of any commercial or financial relationships that could be construed as a potential conflict of interest.

frontiers in Cellular and Infection Microbiology

ORIGINAL RESEARCH
published: 02 April 2021
doi: 10.3389/fcimb.2021.652837

Potential Roles of Oral Microbiota in the Pathogenesis of Immunoglobin A Nephropathy

Jia-Wei He, Xu-Jie Zhou, Ping Hou, Yan-Na Wang, Ting Gan, Yang Li, Yang Liu, Li-Jun Liu, Su-Fang Shi, Li Zhu, Ji-Cheng Lv and Hong Zhang*

Renal Division, Peking University First Hospital, Peking University Institute of Nephrology, Key Laboratory of Renal Disease, Ministry of Health of China, Key Laboratory of Chronic Kidney Disease Prevention and Treatment (Peking University), Ministry of Education, Beijing, China

Disturbance in microbiota affects the mucosal immune response, and it is gradually recognized to be associated with the Immunoglobin A nephropathy (IgAN). This study aims to explore the potential roles of oral microbiota in disease pathogenesis. Saliva samples were collected from 31 patients with IgAN and 30 controls for 16S rRNA gene sequencing. The evenness, diversity, and composition of oral microbiota were analyzed. Moreover, sub-phenotype association analysis was conducted. Phylogenetic Investigation of Communities by Reconstruction of Unobserved States (PICRUSt) based on the Kyoto Encyclopedia of Genes and Genomes (KEGG) database was used to investigate microbiota functions. Compared to healthy controls, microbial diversity tended to decrease in IgAN, and the microbial profiles were remarkably distinguished. The relative abundance of *Capnocytophaga* and *SR1_genera_incertae_sedis* were enriched, whereas 17 genera, such as *Rothia*, were significantly reduced in IgAN. Variable importance in projection scores showed that 12 genera, including *Capnocytophaga*, *Rothia*, and *Haemophilus*, could discriminate between the two groups. In the sub-phenotype correlation analysis, the relative abundance of *Capnocytophaga* and *Haemophilus* was positively associated with levels of proteinuria and serum IgA, respectively. Further metabolic pathway analysis showed 7 predictive functional profiles, including glycosphingolipid biosynthesis, oxidative phosphorylation, and N-glycan biosynthesis were enriched in IgAN. In conclusion, disturbance in oral microbiota was observed to be associated with IgAN and its sub-phenotypes, which may shed novel insights into disease pathogenesis from a microbiome perspective.

Keywords: IgA nephropathy, oral microbiota, pathogenesis, *Capnocytophaga*, *Rothia*, *Haemophilus*

OPEN ACCESS

Edited by:
Ana Carolina Morandini, University of the Pacific, United States

Reviewed by:
Jonathan Barratt, University of Leicester, United Kingdom
Na Liu, Tongji University, China

****Correspondence:***
Xu-Jie Zhou
zhouxujie@bjmu.edu.cn

Specialty section:
This article was submitted to Microbiome in Health and Disease, a section of the journal Frontiers in Cellular and Infection Microbiology

Received: *13 January 2021*
Accepted: *16 March 2021*
Published: *02 April 2021*

Citation:
He J-W, Zhou X-J, Hou P, Wang Y-N, Gan T, Li Y, Liu Y, Liu L-J, Shi S-F, Zhu L, Lv J-C and Zhang H (2021) Potential Roles of Oral Microbiota in the Pathogenesis of Immunoglobin A Nephropathy. Front. Cell. Infect. Microbiol. 11:652837. doi: 10.3389/fcimb.2021.652837

INTRODUCTION

Microbial dysbiosis has been shown to be associated with several autoimmune disorders, such as systemic lupus erythematosus, inflammatory bowel disease, rheumatoid arthritis, and multiple sclerosis (Zhang et al., 2015; Cosorich et al., 2017; Vich Vila et al., 2018; Chen et al., 2020). Disturbance in microbiota can affect host immune response, involving maturation and balance of

immune cells, the release of various cytokines and chemokines, protection against pathogens, and absorption and metabolism of medicine and nutrients (Belkaid and Hand, 2014).

IgAN is the most common glomerulonephritis in the world, but its pathogenesis is poorly understood. Recent studies highlight the potential roles of microbial dysbiosis in the pathogenesis of IgAN (McCarthy et al., 2011; Kiryluk et al., 2014; Chemouny et al., 2018; He et al., 2020). To date, much of the work focuses on gut-microbiota-associated analysis. However, nasopharynx-associated lymphoid tissue is also an essential component of the host mucosal immune system. Tonsils have been considered one of the primary sources of the poorly O-glycosylated IgA1, which may play a key role in the pathogenesis of IgAN (Horie et al., 2003). Disturbance in microbiota in oral mucosa affects local as well as systematic immune responses. For instance, the dysbiotic microbiome in the local oral cavity determines the periodontitis-associated expansion of Th17 cells (Dutzan et al., 2018). It is also observed that oral pathobionts can translocate to the gut, inducing the migration of Th17 cells, inflammation, and the exacerbation of colitis (Kitamoto et al., 2020). For IgAN, emerging studies begin to investigate the role of oral microbiome profiles (Piccolo et al., 2015; Cao et al., 2018; Luan et al., 2019; Yamaguchi et al., 2021). Changes in the oral microbiome may participate in disease onset and progression. However, there is still a lack of sufficient studies demonstrating the relationship between oral microbiota and the pathogenesis of IgAN.

A better understanding of oral microbiota-immune response dialog may provide novel insights into disease pathogenesis. Thus, in this study, we aim to explore the potential roles of oral microbiota in the pathogenesis of IgAN.

MATERIALS AND METHODS

Study Population

For microbial analysis, we enrolled participants whose age was >18 y, with Chinese Han ancestry. A total of 61 participants, comprising 31 cases with IgAN and 30 healthy controls (HC), were initially recruited from Peking University First Hospital. The diagnosis of IgAN was confirmed by kidney biopsy with immunofluorescence studies for IgA deposits. Typical pathology images of IgAN were shown in **Figure 1**. Patients with any oral diseases, renal replacement therapies (hemodialysis, peritoneal dialysis, or renal transplantation), secondary IgAN (systematic lupus erythematosus, rheumatic disease, or IgA vasculitis), or type 2 diabetes mellitus were excluded. Ethnically and geographically matched healthy controls were voluntarily recruited. Healthy controls had no oral diseases either. Age, gender, and body mass index were matched between cases and healthy controls.

Those who reported the use of antibiotics, microbial agents, traditional Chinese medicine, glucocorticoid, or other kinds of immunosuppressants within 8 weeks before entry were excluded to minimize the confounding factors. Some supportive medications, such as renin-angiotensin system inhibitors and diuretics, were not controlled.

16S rRNA Gene Sequencing

Blood, urine, and saliva samples were collected the day after they were confirmed with IgAN (within one week of kidney biopsy). Patients with fever, cough, or shivers on the day of sample collection were also excluded. All the samples were collected in the hospital and were immediately stored at −80°C until 16S rRNA gene sequencing.

Saliva genomic DNA was extracted using the QIAamp DNA Mini Kit (#51304, QIAGEN). The targeted V3-V4 hypervariable region of the bacterial 16S rRNA genes was amplified by PCR using the primers 341F (5'-CCTACGGGRSGCAGCAG-3') and 806R (5'-GGACTACVVGGGTATCTAATC-3'). Amplicons were extracted from 2% agarose gels and purified using the AxyPrep DNA Gel Extraction Kit (#AP-GX-50, Axygen Biosciences) and quantified using Qubit2.0 (Invitrogen, MA, USA). After preparing the library, sequencing was performed on a HiSeq platform to generate paired-end reads of 250 bp (Illumina, CA, USA).

Data Preprocessing

The 16S rRNA gene sequences were processed using USEARCH v.10 and in-house scripts (Edgar, 2010; Zhang et al., 2018). The quality of the paired-end Illumina reads was checked by FastQC v.0.11.5 (Perez-Rubio et al., 2019), and processed in the following steps by VSEARCH: joining of paired-end reads and relabeling of sequencing names; removal of barcodes and primers and filtering of low-quality reads (Q<20); and finding non-redundant reads. Unique reads were denoised into amplicon sequence variants (ASVs)/operational taxonomic units (OTUs). The representative sequences were picked by UPARSEH (Edgar, 2013). The OTU table was generated by USEARCH. The taxonomy of the representative sequences was classified with the RDP classifier (Wang et al., 2007). Analysis of the differential OTU abundance and taxa was performed using the edgeR v3.26.8 package in R v.3.6.1. We subsample ("rarefy") an OTU table to a fixed number of reads per sample (n=23848) using random subsampling without replacement. Besides, the abnormal observations were filtered if the connectivity was <2.5, using the Weighted Correlation Network Analysis (WGCNA) package (Langfelder and Horvath, 2008).

Diversity analysis was carried out using R (LSD.test function in "agricolae" package) and USEARCH. Alpha diversity was evaluated by the Chao1 diversity index. The significance of differences between the two groups was assessed by permutational multivariate analysis of variance with the Bray–Curtis distance. The number of permutations was 9,999 (vegan package in R). Partial least-squares discriminant analysis (PLS-DA), a supervised learning method, was used to reveal taxonomic changes in different groups. The variable importance in projection (VIP) scores were used to rank the abilities of different taxa to discriminate groups (Rohart et al., 2017). A taxon with a VIP score ≥1 was considered necessary in the group's discrimination. The comparison of any two groups

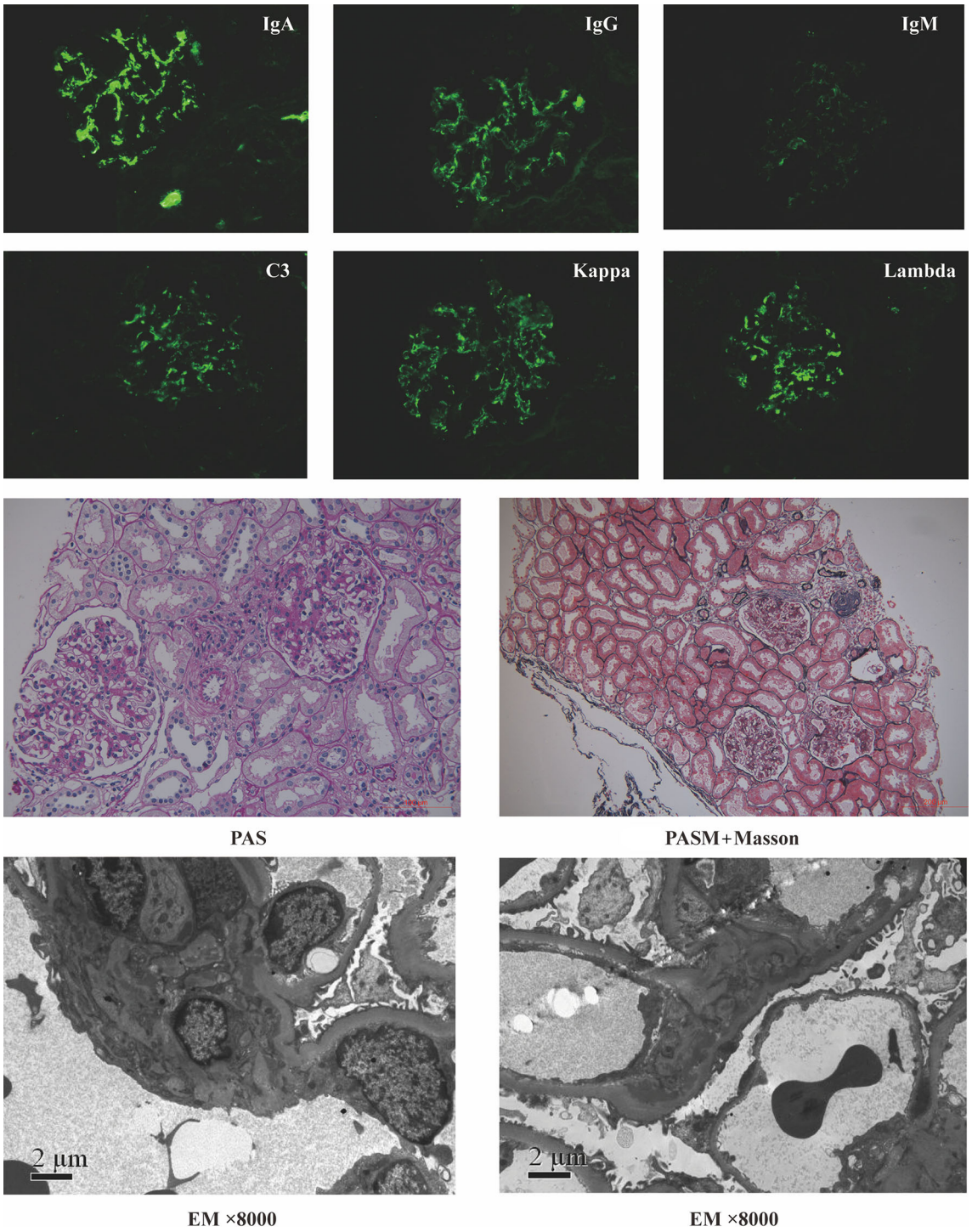

FIGURE 1 | Representative pathology images of patients with IgA nephropathy. PAS, Periodic Acid-Schiff stain; PASM+Masson, periodic acid-silver metheramine+ Masson's trichrome stain; EM, electron microscope.

was conducted by the Wilcoxon rank sum test (two-tailed). The q value represented the False discovery rate-adjusted P-value.

Moreover, we predicted metagenome functional contents from marker gene surveys using the Phylogenetic Investigation of Communities by Reconstruction of Unobserved States (PICRUSt) (Langille et al., 2013). Functional predictions of KEGG Ortholog (KOs) predictions would use the corrected OTU table as input (edge package in R).

Clinical Variables

Details about the demographics and clinical data, such as age, gender, BMI, blood pressure, urinary sediment microscopy, 24-hour urine protein excretion, serum immunoglobin, complement component 3, and creatinine, were recorded. The estimated glomerular filtration rate (eGFR) was calculated by the modification of diet in renal disease equation. Other serological markers also included levels of serum leukocytes, neutrophils, lymphocytes, monocytes, and high-sensitivity C-reactive protein. All renal biopsies were processed for microscopy (light, electron, immunofluorescence). We scored the renal biopsies according to the Oxford Classification in patients with IgAN (Trimarchi et al., 2017).

Statistical Analysis

Continuous variables in this study were compared using an unpaired *t* test between groups if the variables were normally distributed; otherwise, a Mann–Whitney U test was performed. Categorical variables were compared using the chi-square test or Fisher's exact test. Spearman rank correlation coefficient was used for correlation analysis. A two-tailed *P* value of <0.05 was considered statistically significant. The statistical analysis was performed with SPSS 26.0 software (SPSS Inc., USA).

RESULTS

General Information of All the Participants

After quality control, we had a total of 60 saliva samples (IgAN=30; HC=30). The age/gender/BMI were matched between cases and controls. Likewise, the proportion of smokers did not differ between the two groups. All the details were shown in **Table 1**.

TABLE 1 | Clinical characteristics of all the participants in this study.

Characteristic	IgAN (n=30)	healthy controls (n=30)	*P*-values
Age (years)	38.00 (30.00, 47.00)	34.00 (28.00, 40.00)	0.14
Female (%)	14 (46.67%)	17 (56.67%)	0.44
BMI (kg/m^2)	23.17 (21.08, 25.43)	22.42 (21.08, 24.03)	0.49
Smoker (%)	5 (16.67%)	4 (13.33%)	1.00
Hypertension (%)	15 (50.00%)		
Hematuria (counts/HPF)	95.40 (32.50, 168.20)		
Proteinuria (g/24h)	2.15 (1.53)		
Serum creatinine (μmol/L)	143.22 (101.90, 186.94)		
Estimated glomerular filtration rate (ml/min/1.73m^2)	55.32 (32.63)		
Serum IgA (g/L)	3.20 (1.10)		
lEukocytes (10^9/L)	7.21 (1.66)		
Neutrophils (10^9/L)	4.78 (1.37)		
Lymphocytes (10^9/L)	1.60 (1.40, 2.00)		
Monocytes (10^9/L)	0.50 (0.40, 0.60)		
High-sensitivity C-reactive protein (mg/L)	1.29 (0.59, 2.06)		
Complement C3 (g/L)	0.81 (0.72, 0.93)		
Pathological Oxford classification			
M1	23 (76.67%)		
E1	17 (56.67%)		
S1	21 (70.00%)		
T0	14 (46.67%)		
T1	13 (43.33%)		
T2	3 (10.00%)		
C0	7 (23.33%)		
C1	20 (66.67%)		
C2	3 (10.00%)		

Profiling of the Oral Microbiota in Individuals With IgAN and Controls

A total of 75 bacterial genera was identified from the salivary 16S rRNA gene sequencing (**Supplementary Table 1**). The ten most abundant bacterial genera based on the 16S sequencing data were displayed in **Figure 2A**. After excluding those unassigned genera, the 10 most predominant genera were *Fusobacterium*/*Haemophilus*/*Leptotrichia*/*Neisseria*/*Porphyromonas*/*Prevotella*/*Saccharibacteria_genera_incertae_sedis*/*SR1_genera_incertae_sedis*/*Streptococcus* and *Veillonella*. The Venn diagram displayed the shared and specific OTUs for the abundant taxa with the mean relative abundance >5×10^{-4}. Among 302 OTUs identified using 16S rRNA gene sequencing, 167 OTUs constituted the shared OTUs between cases and controls. Besides, 80 and 55 OTUs belonged to the specific OTUs for controls and patients with IgAN, respectively (**Figure 2B**).

Rarefaction analysis showed that the number of OTUs richness nearly approached saturation in both groups as the percentage of samples increased (**Figure 2C**). Microbial diversity tended to decrease in patients with IgAN. However, at the genus level, no difference in alpha-diversity (richness index) was observed between the two groups (**Figure 2D**). PLS-DA showed a distinct clustering pattern between samples from cases with IgAN and healthy controls (*P*<0.05; **Figure 2E**). We listed the specific genera with a significant difference between the two groups. Two genera, including *Capnocytophaga* and *SR1_genera_incertae_sedis*, were enriched in patients with IgAN, whereas 17 genera including Actinomyces, *Rothia*, and *Dialister* were significantly reduced in patients with IgAN (all *q* values<0.05, **Figure 2F** and **Supplementary Table 2**). Last, the VIP scores were used to reveal which genera contributed significantly to differentiate cases from controls. As shown in **Figure 2G**, 12 genera contributed to the differentiation of the two groups. The top 5 microbes included *Neisseria*/*Veillonella*/*Streptococcus*/*SR1_genera_incertae_sedis* and *Prevotella*.

Subgroup Analysis of the Oral Microbiota in Individuals With the Same Gender

In this study, we enrolled the participants age >18 y. Previous studies indicated that different gender might affect the composition of the microbiota. Thus, a subgroup analysis was performed to study whether the microbial profiles were different between cases and controls with the same gender. Age and BMI were also matched between cases and healthy controls (**Supplementary Table 3**). As shown in **Figure 3**, we didn't observe that gender significantly affecting oral microbiota composition between IgAN patients and controls. There was

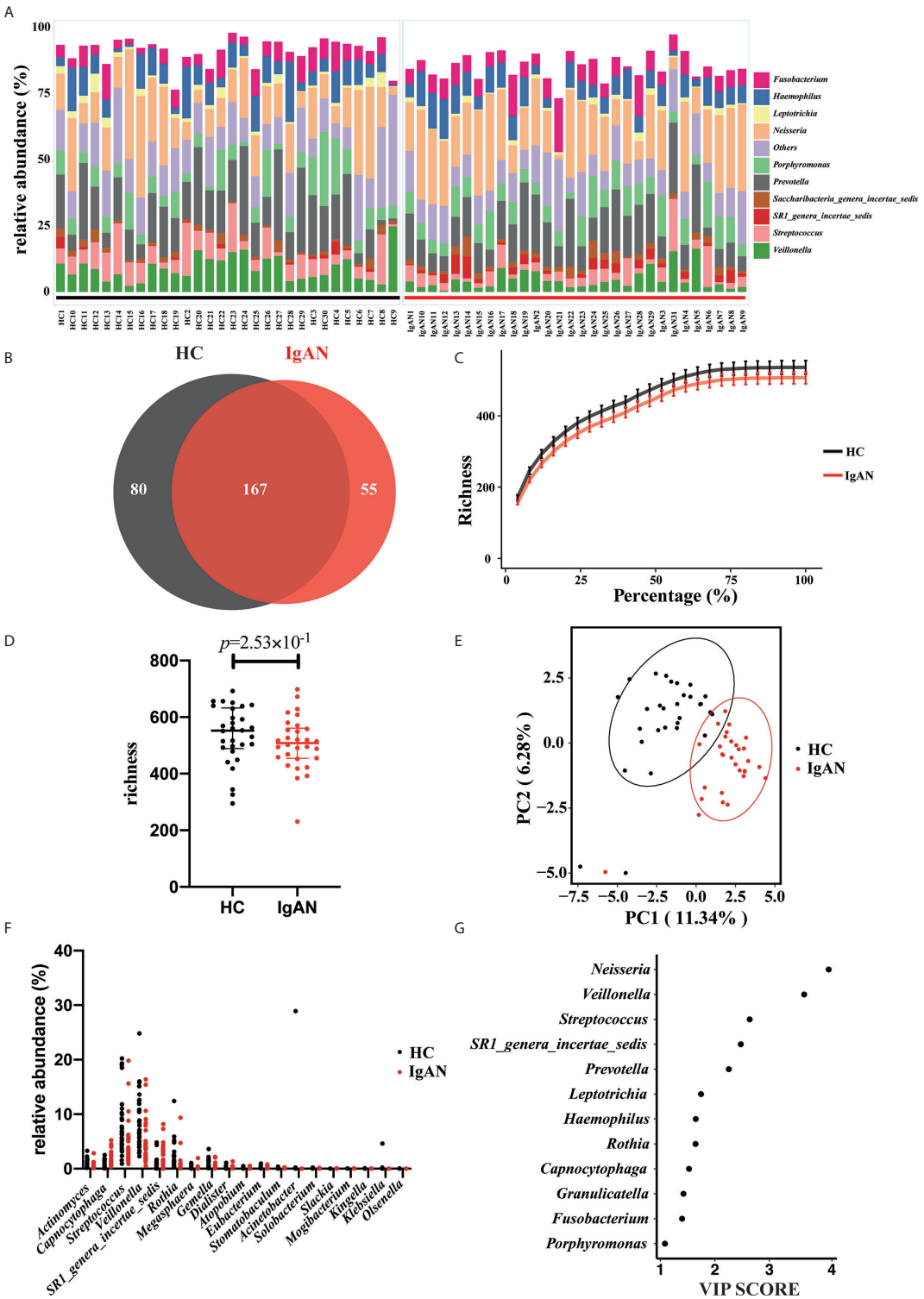

FIGURE 2 | Profiling of the oral microbiota in the present study. **(A)** The bar plot showed the 10 most abundant bacterial genera in patients with IgAN and controls. **(B)** The Venn plot showed the shared and specific OTUs between cases and controls. **(C)** Rarefaction curves were a representation of the species richness for a given number of individual samples. **(D)** As estimated by the richness index, oral microbial diversity tended to reduce in patients with IgAN but without significant difference. **(E)** PLS-DA plot showed a distinct clustering pattern between groups. **(F)** The relative abundance of specific genera with a significant difference among groups (q<0.05). **(G)** A taxon with a VIP score ≥1 was considered necessary in the group's discrimination.

no statistical difference in alpha diversity (richness index) between cases and controls with the same gender (male: **Figure 3A**; female **Figure 3B**). Moreover, PLS-DA showed a distinct clustering pattern between patients and healthy controls, regardless of gender (male: **Figure 3C**; female **Figure 3D**). The top four genera that contributed significantly to differentiate cases from controls were the same, including *Neisseria*, *Streptococcus*, *Prevotella*, and *Veillonella*. Moreover, *SR1_genera_incertae_sedis*, *Rothia*, and *Capnocytophaga* also contributed to the group's differentiation (male: **Figure 3E**; female **Figure 3F**).

Correlation Analysis Between the Oral Microbiota and Clinical Sub-Phenotypes

We further analyzed the correlations between the oral microbiota and some essential sub-phenotypes (**Figure 4** and **Supplementary Table 4**). It was observed that levels of IgA, hs-CRP, lymphocytes, and proteinuria were associated with the specific microbe. Among all, *Haemophilus* was positively associated with the level of serum IgA (r=0.36, $P<0.05$). *Granulicatella* and *Capnocytophaga* were positively associated with the levels of lymphocytes and proteinuria, respectively (r=0.37, $P<0.05$; r=0.39, $P<0.05$). Instead, *Rothia* was negatively associated with hs-CRP (r=-0.43, $P<0.05$).

Predictive Functional Profiles That May Be Associated With IgAN

The volcano plot showed statistical significance versus the magnitude of change (fold change). As shown in **Figure 5**, only those KEGG Orthologs with P value<0.05, FDR<0.1, and logFC thresholds >0 or <0 were colored. In total, 53 KOs with a significant difference were filtered, including 7 KOs (Glycosphingolipid biosynthesis- lacto and neolacto series/ peroxisome/oxidative phosphorylation/various types of N-glycan bio-synthesis/streptomycin biosynthesis/MAPK signaling pathway and polyketide sugar unit biosynthesis) were enriched in patients with IgAN. The rest 46 KOs, which were enriched in healthy controls, were shown in **Supplementary Table 5**.

DISCUSSION

Microbiota interacts with the innate and adaptive immune response. The perturbed microbiota affects the balance of the host immune response (Honda and Littman, 2016; Thaiss et al., 2016). Aberrations in the communication between the host immune system and microbiota may contribute to IgAN.

Our current results showed that perturbations in the oral microbiota might be implicated in IgAN. We conducted the 16S rRNA gene sequencing among age/gender/BMI matched patients and healthy controls. Comparative and association analyses were used to reveal the crucial microbiota and their potential roles in IgAN. Predictive functional profiles provided additional insights into disease etiology and mechanisms. We found that microbial diversity tended to decrease in patients with IgAN but without significant difference. Intriguingly, there was a distinct clustering pattern between cases and controls. Based on the VIP scores, a total of 12 genera were considered necessary to distinguish between cases and controls, including *Capnocytophaga*, *Rothia*, and *Haemophilus*. A subgroup analysis was performed to understand the role of gender on oral microbial profiles. It was observed that gender was not a significant factor impacting oral microbiota between IgAN patients and controls. Results from the alpha diversity analysis, PLS-DA, and VIP index supported the above inference. Moreover, sub-phenotypes association analysis showed that *Capnocytophaga* and *Haemophilus* are positively associated with the levels of proteinuria and serum IgA, respectively. Instead, *Rothia* was negatively associated with the level of hs-CRP. Predictive functional profiles showed that glycosphingolipid biosynthesis, oxidative phosphorylation, polyketide sugar unit biosynthesis, and N-glycan biosynthesis pathways were enriched in IgAN. Analyzing the potential roles of these crucial microbes and those predictive functional profiles can help in further understanding disease pathogenesis.

The decreased *Rothia* and its negative association with hs-CRP might reflect the inflammatory state of the body, which was associated with the production of IgA (Meng et al., 2012). Another study revealed that IgA recognition of the microbiota would be altered during mucosal inflammation status (Palm et al., 2014). In a study about stunted children, several of the highly targeted genera included *Haemophilus* (Huus et al., 2020). *Haemophilus* inhabit the mucous membranes of the upper respiratory tract and mouth. Multiple species of *Haemophilus*, such as *H. influenzae* and *H. ducreyi*, can counter the host immune system and cause human disease. A previous study represented that patients with IgAN had significantly more IgA antibodies against *H. parainfluenzae* than did patients with other glomerular diseases (Suzuki et al., 1994). IgA is a critical mediator of mucosal immune homeostasis. However, excess and poorly O-glycosylated IgA1 seems to play important roles in the pathogenesis of IgAN. Last, *Capnocytophaga* is a commensal genus in the oropharyngeal tract of mammals, which is considered an opportunistic pathogen. In immunocompetent patients, these bacteria are responsible for common kinds of periodontitis (Nonnenmacher et al., 2001). Periodontal-related bacteria affect the host immune response, contributing to IgAN and colitis (Nagasawa et al., 2014; Kitamoto et al., 2020). Consistent with our results, another study confirmed that the relative abundance of *Capnocytophaga* was also increased in chronic periodontitis patients with IgAN (Cao et al., 2018).

Although IgAN is the most common glomerulonephritis globally, the lack of precise therapeutic strategies limits clinical outcomes. Thus, the above results may have significant clinical implications. First, interventions against the specific microbe may relieve the excessive immune responses, reduce the production of poorly O-glycosylated IgA1, and improve clinical outcomes. Some preliminary studies targeting the microbiome in IgAN show promising results (Chemouny et al., 2018). Second, using high-throughput sequencing technologies

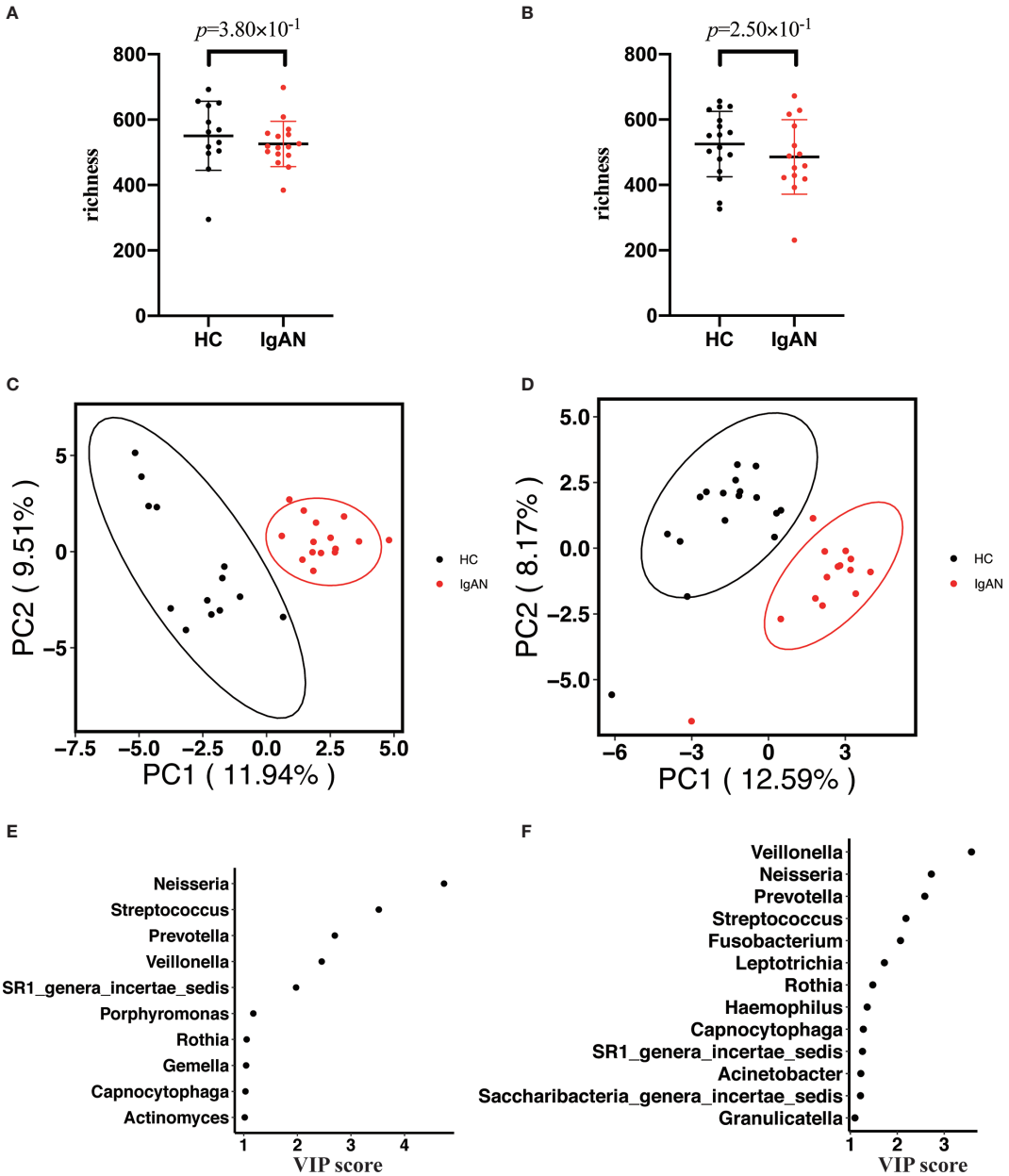

FIGURE 3 | Subgroup analysis of the oral microbiota between cases and controls with the same gender. **(A, B)** The alpha diversity (richness index) between cases and controls in male or female participants (**A** for male participants; **B** for female participants). **(C, D)** PLS-DA plot showed a distinct clustering pattern between groups, regardless of their gender (**C** for male participants; **D** for female participants). **(E, F)** A taxon with a VIP score ≥1 was considered necessary in the group's discrimination among male and female participants **(E)** for male participants; **(F)** for female participants).

may contribute to risk stratification. Since the microbial profiles are in a dynamic state, the total relative abundance of some critical microbes (such as *Capnocytophaga*, *Rothia*, and *Haemophilus*) may reflect disease activity. Third, as larger-scale studies continue, using supervised machine learning techniques to analyze the phenotype of microbiota may predict the occurrence of IgAN and assist disease diagnosis. Thus, future studies focusing on the microbiome may shed more light on precision medicine studies.

Through this preliminary study, we shall note some limitations. First, the small sample size precluded analyzing for potential confounders. Microbial profiles will be affected by many factors, such as BMI, gender, alcohol or cigarette consumptions, place of residence, and diet (Vujkovic-Cvijin et al., 2020). Moreover, various kinds of medications have significant impacts on the host microbiome. Except for the antibiotics and glucocorticoid, other drugs, such as metformin, proton pump inhibitors, nonsteroidal anti-inflammatory drugs,

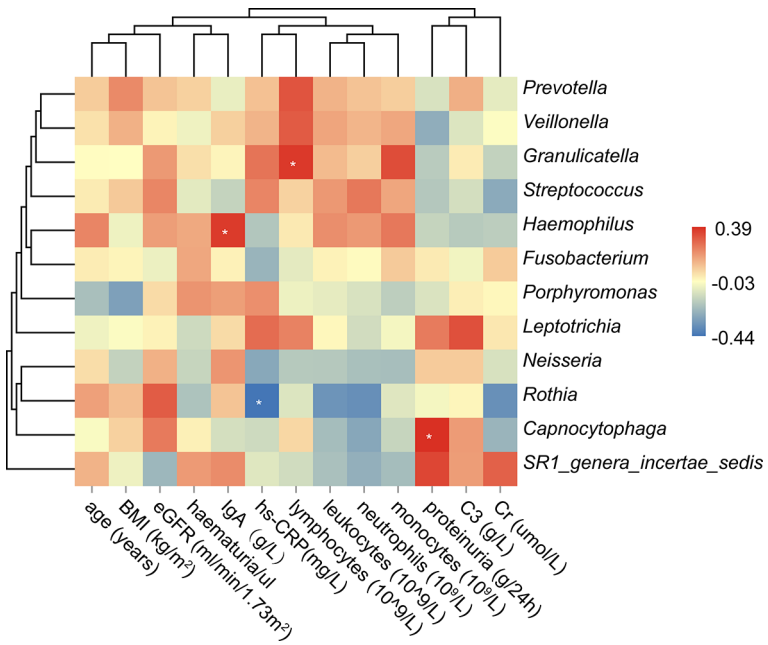

FIGURE 4 | Correlation analysis between the oral microbiota and the clinical sub-phenotypes. The asterisk meant the *P* value<0.05.

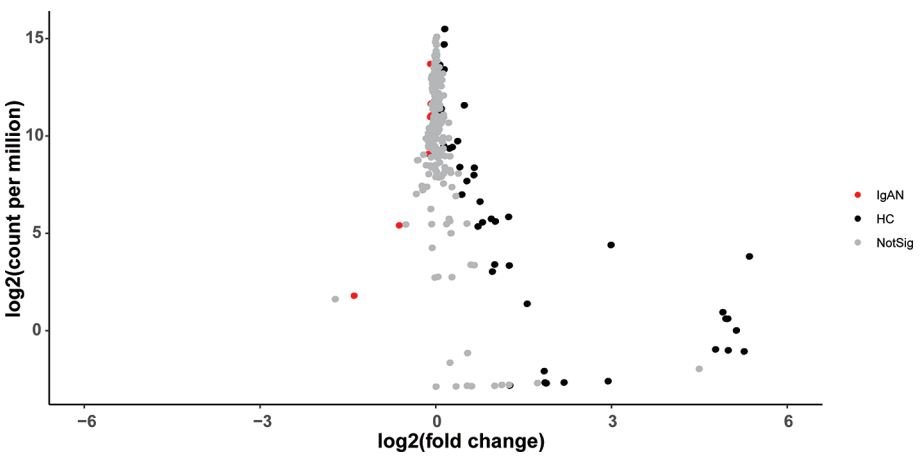

FIGURE 5 | The volcano plot showed distinct KOs between the two groups. Gray points represented those KOs with no significant difference between groups.

atypical antipsychotics, and traditional Chinese medicine, will also affect the composition and the function of our host-microbiome (Forslund et al., 2015; Imhann et al., 2016; Rogers and Aronoff, 2016; Suez et al., 2018; Guo et al., 2020). To avoid host variables confounders and medication impacts, a larger-scale study with IgAN patients and matched healthy controls will be required to clarify the comprehensive microbiome analysis in IgAN. Second, the accuracy observed for reference-based mapping of 16S was much lower. Metagenomic sequencing strategies are recommended for microbiota research. Besides, a multi-omics study, such as blood glycomics, saliva metabolomics, and host genetics in understanding the pathogenic role of oral microbiota in IgAN is warranted. Third, the primary results in our study are based on association analysis. Thus, the validation of the potential roles of these critical microbes in IgAN model animals is required. Understanding how these microbes modulate host immune responses may provide important insights in future intervention studies. Fourth, this study did not enroll patients with other glomerulonephritis in the original study. Thus, we could not know whether these microbial changes were IgAN-specific or shared with chronic kidney disease. More widespread

replications and functional studies are still needed in the future. Lastly, the association analyses may not bear multiple corrections. With 12 independent microbial species and 13 clinical variables, a conservative Bonferroni threshold to declare significant association would be $3.21x10^{-4}$ (0.05/12/13). The indirect effect of oral microbiota in mediating pathogenesis, low statistical power, or sample heterogeneity might account for the marginal significance.

In conclusion, disturbance in oral microbiota was associated with immune response and IgAN. This evidence might provide preliminary clues for future pathogenesis and intervention studies.

DATA AVAILABILITY STATEMENT

The data presented in the study are deposited in the Genome Sequence Archive (Wang et al., 2017) in National Genomics Data Center (CNCB-NGDC Members and Partners, 2021), China National Center for Bioinformation / Beijing Institute of Genomics, Chinese Academy of Sciences, accession number CRA003794.

ETHICS STATEMENT

The studies involving human participants were reviewed and approved by the Ethics Committee of Peking University First Hospital (Institutional Review Board numbers: 2013 [548] and 2019 [76]). The patients/participants provided their written informed consent to participate in this study.

AUTHOR CONTRIBUTIONS

Conceptualization, X-JZ, J-CL, and HZ; methodology, X-JZ, J-WH, PH, and Y-NW; software, J-WH and Y-NW; validation, X-JZ and J-WH; formal analysis, X-JZ and J-WH; investigation, L-JL, S-FS, TG, and YL.; resources, L-JL and S-FS; data curation, X-JZ, J-WH, TG, and YL; writing—original draft preparation, X-JZ and J-WH; writing—review and editing, X-JZ, J-WH, J-CL, and HZ; visualization, X-JZ, J-WH, Y-NW, and TG; supervision, J-CL and HZ; project administration, J-CL and HZ; funding acquisition, X-JZ and J-CL. All authors contributed to the article and approved the submitted version.

FUNDING

This research was funded by Beijing Natural Science Foundation, grant number Z190023; National Science Foundation of China, grant numbers 82131430172, 82022010, 81970613, 81925006, 81670649, 82070733; King's College London-Peking University Health Science Center Joint Institute for Medical Research, grant number 2021; Fok Ying Tung Education Foundation, grant number 171030; Beijing Nova Program Interdisciplinary Cooperation Project, grant number Z191100001119004; Beijing Youth Top-notch Talent Support Program, grant number 2017000021223ZK31; Clinical Medicine Plus X-Young Scholars Project of Peking University, grant number PKU2020LCXQ003; the University of Michigan Health System–Peking University Health Science Center Joint Institute for Translational and Clinical Research, grant number BMU2017JI007; Chinese Academy of Medical Sciences Research Unit, grant number 2019RU023.

ACKNOWLEDGMENTS

We are grateful to all patients and healthy control subjects for their participation in this study.

SUPPLEMENTARY MATERIAL

The Supplementary Material for this article can be found online at: https://www.frontiersin.org/articles/10.3389/fcimb.2021.652837/full#supplementary-material

Supplementary Table 1 | 16S rRNA gene data on bacterial taxonomy and relative abundance.

Supplementary Table 2 | Specific microbiota with a significant difference between cases and controls.

Supplementary Table 3 | Clinical characteristics between cases and controls with the same gender.

Supplementary Table 4 | Spearman correlation coefficients and *P* values in the association analysis between oral microbiota and clinical sub-phenotypes.

Supplementary Table 5 | Specific KEGG Orthologs with a significant difference between cases and controls.

REFERENCES

Belkaid, Y., and Hand, T. W. (2014). Role of the microbiota in immunity and inflammation. *Cell* 157 (1), 121–141. doi: 10.1016/j.cell.2014.03.011

Cao, Y., Qiao, M., Tian, Z., Yu, Y., Xu, B., Lao, W., et al. (2018). Comparative Analyses of Subgingival Microbiome in Chronic Periodontitis Patients with and Without IgA Nephropathy by High Throughput 16S rRNA Sequencing. *Cell Physiol. Biochem.* 47 (2), 774–783. doi: 10.1159/000490029

Chemouny, J. M., Gleeson, P. J., Abbad, L., Lauriero, G., Boedec, E., Le Roux, K., et al. (2018). Modulation of the microbiota by oral antibiotics treats immunoglobulin A nephropathy in humanized mice. *Nephrol. Dial. Transplant.* 34 (7), 1135–1144. doi: 10.1093/ndt/gfy323

Chen, B. D., Jia, X. M., Xu, J. Y., Zhao, L. D., Ji, J. Y., Wu, B. X., et al. (2020). The gut microbiota of non-treated patients with SLE defines an autoimmunogenic and proinflammatory profile. *Arthritis Rheumatol.* 73 (2), 232–243. doi: 10.1002/art.41511

CNCB-NGDC Members and Partners. (2021). Database Resources of the National Genomics Data Center, China National Center for Bioinformation in 2021. *Nucleic Acids Res.* 49 (D1), D18–D28. doi: 10.1093/nar/gkaa1022

Cosorich, I., Dalla-Costa, G., Sorini, C., Ferrarese, R., Messina, M. J., Dolpady, J., et al. (2017). High frequency of intestinal TH17 cells correlates with microbiota alterations and disease activity in multiple sclerosis. *Sci. Adv.* 3 (7), e1700492. doi: 10.1126/sciadv.1700492

Dutzan, N., Kajikawa, T., Abusleme, L., Greenwell-Wild, T., Zuazo, C. E., Ikeuchi, T., et al. (2018). A dysbiotic microbiome triggers TH17 cells to mediate oral mucosal

immunopathology in mice and humans. *Sci. Transl. Med.* 10 (463), eaat0797. doi: 10.1126/scitranslmed.aat0797

Edgar, R. C. (2010). Search and clustering orders of magnitude faster than BLAST. *Bioinformatics* 26 (19), 2460–2461. doi: 10.1093/bioinformatics/btq461

Edgar, R. C. (2013). UPARSE: highly accurate OTU sequences from microbial amplicon reads. *Nat. Methods* 10 (10), 996–998. doi: 10.1038/nmeth.2604

Forslund, K., Hildebrand, F., Nielsen, T., Falony, G., Le Chatelier, E., Sunagawa, S., et al. (2015). Disentangling type 2 diabetes and metformin treatment signatures in the human gut microbiota. *Nature* 528 (7581), 262–266. doi: 10.1038/nature15766

Guo, M., Wang, H., Xu, S., Zhuang, Y., An, J., Su, C., et al. (2020). Alteration in gut microbiota is associated with dysregulation of cytokines and glucocorticoid therapy in systemic lupus erythematosus. *Gut Microbes* 11 (6), 1758–1773. doi: 10.1080/19490976.2020.1768644

He, J. W., Zhou, X. J., Lv, J. C., and Zhang, H. (2020). Perspectives on how mucosal immune responses, infections and gut microbiome shape IgA nephropathy and future therapies. *Theranostics* 10 (25), 11462–11478. doi: 10.7150/thno.49778

Honda, K., and Littman, D. R. (2016). The microbiota in adaptive immune homeostasis and disease. *Nature* 535 (7610), 75–84. doi: 10.1038/nature18848

Horie, A., Hiki, Y., Odani, H., Yasuda, Y., Takahashi, M., Kato, M., et al. (2003). IgA1 molecules produced by tonsillar lymphocytes are under-O-glycosylated in IgA nephropathy. *Am. J. Kidney Dis.* 42 (3), 486–496. doi: 10.1016/s0272-6386(03)00743-1

Huus, K. E., Rodriguez-Pozo, A., Kapel, N., Nestoret, A., Habib, A., Dede, M., et al. (2020). Immunoglobulin recognition of fecal bacteria in stunted and non-stunted children: findings from the Afribiota study. *Microbiome* 8 (1), 113. doi: 10.1186/s40168-020-00890-1

Imhann, F., Bonder, M. J., Vich Vila, A., Fu, J., Mujagic, Z., Vork, L., et al. (2016). Proton pump inhibitors affect the gut microbiome. *Gut* 65 (5), 740–748. doi: 10.1136/gutjnl-2015-310376

Kiryluk, K., Li, Y., Scolari, F., Sanna-Cherchi, S., Choi, M., Verbitsky, M., et al. (2014). Discovery of new risk loci for IgA nephropathy implicates genes involved in immunity against intestinal pathogens. *Nat. Genet.* 46 (11), 1187–1196. doi: 10.1038/ng.3118

Kitamoto, S., Nagao-Kitamoto, H., Jiao, Y., Gillilland, M. G., Hayashi, A., Imai, J., et al. (2020). The Intermucosal Connection between the Mouth and Gut in Commensal Pathobiont-Driven Colitis. *Cell* 182 (2), 447–462.e14. doi: 10.1016/j.cell.2020.05.048

Langfelder, P., and Horvath, S. (2008). WGCNA: an R package for weighted correlation network analysis. *BMC Bioinf.* 9 (1), 559. doi: 10.1186/1471-2105-9-559

Langille, M. G., Zaneveld, J., Caporaso, J. G., McDonald, D., Knights, D., Reyes, J. A., et al. (2013). Predictive functional profiling of microbial communities using 16S rRNA marker gene sequences. *Nat. Biotechnol.* 31 (9), 814–821. doi: 10.1038/nbt.2676

Luan, S., Zhang, S., Zhong, H., Zhang, Y., Wei, X., Lin, R., et al. (2019). Salivary microbial analysis of Chinese patients with immunoglobulin A nephropathy. *Mol. Med. Rep.* 20 (3), 2219–2226. doi: 10.3892/mmr.2019.10480

McCarthy, D. D., Kujawa, J., Wilson, C., Papandile, A., Poreci, U., Porfilio, E. A., et al. (2011). Mice overexpressing BAFF develop a commensal flora-dependent, IgA-associated nephropathy. *J. Clin. Invest.* 121 (10), 3991–4002. doi: 10.1172/JCI45563

Meng, H., Ohtake, H., Ishida, A., Ohta, N., Kakehata, S., and Yamakawa, M. (2012). IgA production and tonsillar focal infection in IgA nephropathy. *J. Clin. Exp. Hematop.* 52 (3), 161–170. doi: 10.3960/jslrt.52.161

Nagasawa, Y., Iio, K., Fukuda, S., Date, Y., Iwatani, H., Yamamoto, R., et al. (2014). Periodontal disease bacteria specific to tonsil in IgA nephropathy patients predicts the remission by the treatment. *PloS One* 9 (1), e81636. doi: 10.1371/journal.pone.0081636

Nonnenmacher, C., Mutters, R., and de Jacoby, L. F. (2001). Microbiological characteristics of subgingival microbiota in adult periodontitis, localized juvenile periodontitis and rapidly progressive periodontitis subjects. *Clin. Microbiol. Infect.* 7 (4), 213–217. doi: 10.1046/j.1469-0691.2001.00210.x

Palm, N. W., de Zoete, M. R., Cullen, T. W., Barry, N. A., Stefanowski, J., Hao, L., et al. (2014). Immunoglobulin A coating identifies colitogenic bacteria in inflammatory bowel disease. *Cell* 158 (5), 1000–1010. doi: 10.1016/j.cell.2014.08.006

Perez-Rubio, P., Lottaz, C., and Engelmann, J. C. (2019). FastqPuri: high-performance preprocessing of RNA-seq data. *BMC Bioinf.* 20 (1), 226. doi: 10.1186/s12859-019-2799-0

Piccolo, M., De Angelis, M., Lauriero, G., Montemurno, E., Di Cagno, R., Gesualdo, L., et al. (2015). Salivary Microbiota Associated with Immunoglobulin A Nephropathy. *Microb. Ecol.* 70 (2), 557–565. doi: 10.1007/s00248-015-0592-9

Rogers, M. A. M., and Aronoff, D. M. (2016). The influence of non-steroidal anti-inflammatory drugs on the gut microbiome. *Clin. Microbiol. Infect.* 22 (2), 178 e1–178 e9. doi: 10.1016/j.cmi.2015.10.003

Rohart, F., Gautier, B., Singh, A., and Le Cao, K. A. (2017). mixOmics: An R package for 'omics feature selection and multiple data integration. *PloS Comput. Biol.* 13 (11), e1005752. doi: 10.1371/journal.pcbi.1005752

Suez, J., Zmora, N., Zilberman-Schapira, G., Mor, U., Dori-Bachash, M., Bashiardes, S., et al. (2018). Post-Antibiotic Gut Mucosal Microbiome Reconstitution Is Impaired by Probiotics and Improved by Autologous FMT. *Cell* 174 (6), 1406–1423.e16. doi: 10.1016/j.cell.2018.08.047

Suzuki, S., Nakatomi, Y., Sato, H., Tsukada, H., and Arakawa, M. (1994). Haemophilus parainfluenzae antigen and antibody in renal biopsy samples and serum of patients with IgA nephropathy. *Lancet* 343 (8888), 12–16. doi: 10.1016/s0140-6736(94)90875-3

Thaiss, C. A., Zmora, N., Levy, M., and Elinav, E. (2016). The microbiome and innate immunity. *Nature* 535 (7610), 65–74. doi: 10.1038/nature18847

Trimarchi, H., Barratt, J., Cattran, D. C., Cook, H. T., Coppo, R., Haas, M., et al. (2017). Oxford Classification of IgA nephropathy 2016: an update from the IgA Nephropathy Classification Working Group. *Kidney Int.* 91 (5), 1014–1021. doi: 10.1016/j.kint.2017.02.003

Vich Vila, A., Imhann, F., Collij, V., Jankipersadsing, S. A., Gurry, T., Mujagic, Z., et al. (2018). Gut microbiota composition and functional changes in inflammatory bowel disease and irritable bowel syndrome. *Sci. Transl. Med.* 10 (472), eaap8914. doi: 10.1126/scitranslmed.aap8914

Vujkovic-Cvijin, I., Sklar, J., Jiang, L., Natarajan, L., Knight, R., and Belkaid, Y. (2020). Host variables confound gut microbiota studies of human disease. *Nature* 5870 (7834), 448–454. doi: 10.1038/s41586-020-2881-9

Wang, Q., Garrity, G. M., Tiedje, J. M., and Cole, J. R. (2007). Naive Bayesian classifier for rapid assignment of rRNA sequences into the new bacterial taxonomy. *Appl. Environ. Microbiol.* 73 (16), 5261–5267. doi: 10.1128/AEM.00062-07

Wang, Y., Song, F., Zhu, J., Zhang, S., Yang, Y., Chen, Y., et al (2017). GSA: Genome Sequence Archive. *Genomics Proteomics Bioinformatics* 15 (1), 14–18. doi: 10.1016/j.gpb.2017.01.001

Yamaguchi, H., Goto, S., Takahashi, N., Tsuchida, M., Watanabe, H., Yamamoto, S., et al. (2021). Aberrant mucosal immunoreaction to tonsillar microbiota in immunoglobulin A nephropathy. *Nephrol. Dial. Transplant.* 36 (1), 75–86. doi: 10.1093/ndt/gfaa223

Zhang, X., Zhang, D., Jia, H., Feng, Q., Wang, D., Liang, D., et al. (2015). The oral and gut microbiomes are perturbed in rheumatoid arthritis and partly normalized after treatment. *Nat. Med.* 21 (8), 895–905. doi: 10.1038/nm.3914

Zhang, J., Zhang, N., Liu, Y. X., Zhang, X., Hu, B., Qin, Y., et al. (2018). Root microbiota shift in rice correlates with resident time in the field and developmental stage. *Sci. China Life Sci.* 61 (6), 613–621. doi: 10.1007/s11427-018-9284-4

Conflict of Interest: The authors declare that the research was conducted in the absence of any commercial or financial relationships that could be construed as a potential conflict of interest.

frontiers in Cellular and Infection Microbiology

ORIGINAL RESEARCH
published: 19 May 2021
doi: 10.3389/fcimb.2021.671968

Treponema denticola-Induced RASA4 Upregulation Mediates Cytoskeletal Dysfunction and MMP-2 Activity in Periodontal Fibroblasts

*Erin Trent Malone[1], Sean Ganther[1], Nevina Mena[1], Allan Radaic[1], Keemia Shariati[1], Abigail Kindberg[2], Christian Tafolla[1], Pachiyappan Kamarajan[1], J. Christopher Fenno[3], Ling Zhan[4] and Yvonne L. Kapila[1]**

[1] Kapila Laboratory, Department of Orofacial Sciences, School of Dentistry San Francisco, University of California San Francisco, San Francisco, CA, United States, [2] Bush Laboratory, Department of Cell and Tissue Biology, Biomedical Sciences Graduate, University of California San Francisco, San Francisco, CA, United States, [3] Fenno Laboratory, Department of Biological and Material Sciences & Prosthodontics, School of Dentistry, University of Michigan, Ann Arbor, MI, United States, [4] Zhan Laboratory, Department of Orofacial Sciences, School of Dentistry San Francisco, University of California San Francisco, San Francisco, CA, United States

OPEN ACCESS

Edited by:
Ana Carolina Morandini, University of the Pacific, United States

Reviewed by:
Rodrigo Oliveira, University of São Paulo, Brazil
Michelle B. Visser, University at Buffalo, United States

***Correspondence:**
Yvonne L. Kapila
Yvonne.Kapila@ucsf.edu

Specialty section:
This article was submitted to Bacteria and Host, a section of the journal Frontiers in Cellular and Infection Microbiology

Received: *24 February 2021*
Accepted: *26 April 2021*
Published: *19 May 2021*

Citation:
Malone ET, Ganther S, Mena N, Radaic A, Shariati K, Kindberg A, Tafolla C, Kamarajan P, Fenno JC, Zhan L and Kapila YL (2021) Treponema denticola-Induced RASA4 Upregulation Mediates Cytoskeletal Dysfunction and MMP-2 Activity in Periodontal Fibroblasts. Front. Cell. Infect. Microbiol. 11:671968. doi: 10.3389/fcimb.2021.671968

The periodontal complex consists of the periodontal ligament (PDL), alveolar bone, and cementum, which work together to turn mechanical load into biological responses that are responsible for maintaining a homeostatic environment. However oral microbes, under conditions of dysbiosis, may challenge the actin dynamic properties of the PDL in the context of periodontal disease. To study this process, we examined host-microbial interactions in the context of the periodontium *via* molecular and functional cell assays and showed that human PDL cell interactions with *Treponema denticola* induce actin depolymerization through a novel actin reorganization signaling mechanism. This actin reorganization mechanism and loss of cell adhesion is a pathological response characterized by an initial upregulation of RASA4 mRNA expression resulting in an increase in matrix metalloproteinase-2 activity. This mechanism is specific to the *T. denticola* effector protein, dentilisin, thereby uncovering a novel effect for *Treponema denticola*-mediated RASA4 transcriptional activation and actin depolymerization in primary human PDL cells.

Keywords: actin reorganization, matrix mettaloproteinase-2, RASA4, *Treponema denticola*, periodontal ligament (PDL)

INTRODUCTION

Periodontal disease is characterized by an altered periodontal ligament space, chronic inflammation, and destruction of the periodontal tissues, including a breakdown of the extracellular matrix (ECM) (Armitage, 2004). The periodontal complex consists of the periodontal ligament (PDL), alveolar bone, and cementum, which work together to turn mechanical load into biological responses that are responsible for maintaining a homeostatic environment (Jang et al., 2018). Cytopathic mechanisms in mechanotransduction are facilitated by cytoskeletal interaction with the ECM (Humphrey et al., 2014) and include ECM degradation and remodeling (Tsuji et al., 2004; Manokawinchoke et al., 2015),

altered cellular differentiation (Kanzaki et al., 2002), altered cellular migration, and altered cellular adhesion or de-adhesion processes (Kang et al., 2010; Wang et al., 2019). A failure of mechanotransduction and actin organization within the periodontium results in loss of regeneration of periodontal tissues, remodeling of the ECM, and progression of disease; processes highly regulated within the PDL (Chukkapalli and Lele, 2018). The disease process is initiated by pathogenic microbes under conditions of microbial dysbiosis. *Treponema denticola*, an oral spirochete identified as a periodontal pathogen, is implicated in this dysbiosis leading to chronic inflammation, ECM remodeling, including enhanced MMP-2 activation, and periodontal tissue destruction (Takeuchi et al., 2001; Miao et al., 2011; Miao et al., 2014; Ruby et al., 2018).

Actin monomer and filament dynamics are necessary for mechanotransduction and are capable of regulating epigenetic enzymes (Sadhukhan et al., 2014; Serebryannyy et al., 2016), chromatin reprogramming (Zhao et al., 1998; Kapoor and Shen, 2014), transcriptional machinery (Visa and Percipalle, 2010), and gene expression (Misu et al., 2017). Mechanotransduction and actin dynamics can also influence homeostatic conditions towards disease through extracellular process and tissue destructive mechanisms (Humphrey et al., 2014). Actin dynamics are also involved in the regulation of tissue destructive genes, like matrix metalloproteinases (MMP) (Bildyug, 2016). MMP-2 is overexpressed in periodontal tissues compromised by apical periodontitis (Fernández et al., 2019), chronic apical abscesses (Letra et al., 2013), and chronic periodontitis (Ateia et al., 2018); implicating MMP-2 regulation in periodontitis. Major periodontopathogens, like *Porphyromonas gingivalis*, *Fusobacterium nucleatum*, and *Actinobacillus actinomycetemcomitans* can induce actin reorganization, thereby providing a possible mechanism through which microbial infection can facilitate periodontitis (Hassell et al., 1997; Yilmaz et al., 2003; Gutiérrez-Venegas et al., 2007; Hasegawa et al., 2008; Kinane et al., 2012; Zhang et al., 2013). *T. denticola* is also capable of affecting filamentous actin abundance in human gingival fibroblasts and epithelial cells (Baehni et al., 1992; Yang et al., 1998). Previous literature suggests that *T. denticola* induces subcortical actin polymerization through its effector protein, major surface protein (Wang et al., 2001; Amin et al., 2004; Visser et al., 2011). However, little is known regarding *T. denticola's ability to* affect the actin dynamic function of human PDL cells (PDL) and the signaling components involved in the host response to *T. denticola* and effector protein dentilisin. In the present study, we characterize a novel mechanism demonstrating *T. denticola*-induced actin remodeling through stimulation of the Ca (2+)-dependent Ras GTPase-activating protein, RASA4 that further regulates MMP-2 activity. The overall objective of this study was to determine *T. denticola's* influence on PDL cellular actin dynamics and the mechanism of action that may contribute to tissue destruction, including activation of MMP-2.

MATERIALS AND METHODS

Human Subjects and IRB Approval

Institutional review board (IRB) approval for human subjects research was obtained *via* the University of California San Francisco institutional review board (# 16-20204; reference #227030).

Periodontal Ligament Cell Harvesting and Cell Culture

Human primary periodontal ligament (PDL) cells were grown as explants from periodontal ligament tissues that were harvested from extracted teeth as previously described (Kapila et al., 1996). All cells were cultured in alpha minimal essential medium (αMEM) supplemented with 10% fetal bovine serum (Gibco, USA), 1% penicillin-streptomycin, and 1% amphotericin B (Gibco, USA). All cells were used between passages 3 and 7. Use of PDL cells for these studies was approved by the University of California San Francisco IRB. Two donor samples were pooled together per independent sample to eliminate variation for all experiments except shRNA experiments (only one donor per independent sample was used for these experiments).

Microbial Culturing of *T. denticola*

T. denticola ATCC 35405 (American Type Culture Collection; Manassas, VA) and *T. denticola* mutants (CF522, isogenic dentilisin-deficient strain) (Godovikova et al., 2010), MHE (isogenic Msp-deficient strain) (Fenno et al., 1997), were cultured at 37°C under anaerobic conditions in oral treponeme enrichment broth (OTEB; Anaerobe Systems, Morgan Hill, CA). Culture purity was monitored using Syto 9 bacterial DNA dye and visualized in a fluorescent microscope for spirochete morphology. *T. denticola* was washed with αMEM cultured media, centrifuged, aspirated thrice, and finally resuspended in αMEM to be used for experiments. Bacteria used for all experiments never exceeded 6 passages.

Purified Dentilisin

The dentilisin protease complex was purified from the detergent phase of the Triton X-114 extracts of *T. denticola* MHE by preparative sodium dodecyl sulfate-polyacrylamide gel electrophoresis (SDS-PAGE) using a model 491 Prep Cell (Bio-Rad Laboratories, Richmond, CA) as described previously (Fenno et al., 1998; Miao et al., 2011). Dentilisin purity was assayed in silver stained SDS-PAGE (Miao et al., 2011). Purified dentilisin migrated as a 100 kDa complex that upon heating resolves to its individual protein components: PrtP, PrcA1 and PrcA2, as documented previously (Miao et al., 2011).

MOI Optimization

Multiplicity of infection (MOI) was optimized by performing a PDL cell viability assay with *T. denticola* at different MOIs (10, 50, and 100). This viability assay (Calcein AM; Thermo Fisher Scientific) was used according to manufacturer's instructions. Cytotoxicity was encountered at an MOI of 500 (data not shown). In previous publications (Miao et al., 2014; Ateia et al., 2018), a *T. denticola* MOI of 50 rendered a strong cellular response in PDL cells without inducing cytotoxicity. Based on these observations, an MOI of 50 was considered optimal for studying the cellular response of PDL cells to *T. denticola* treatment.

Treatment of PDL Cells With *T. denticola*

PDL cells were plated in 4-well chamber slides (Invitrogen), 8-well chamber slides (Invitrogen), or 60mm culture plates (Falcon) overnight at a density of $3x10^4$, $1.5x10^4$ or $1.0x10^6$ cells/well, respectively. Cells were then challenged with *T. denticola* at an optimized MOI of 50 for 2 h or left unchallenged as controls. Post-challenge, cells were washed three times with phosphate buffered saline (PBS, Gibco, USA) and incubated in αMEM media (Gibco, USA) supplemented with 10% fetal bovine serum (FBS; Gibco, USA), 1% amphotericin B (Gibco, USA), and 1% penicillin-streptomycin for 24 h.

General Chemicals

All general chemicals were purchased from Sigma (St. Louis, MO, USA), unless otherwise noted.

Imaging Stress Fibers *via* Immunofluorescence Staining

Human PDL cells were grown to confluency and passaged in sterile 4-well glass bottom plates (627870; Gibco, USA) $1.5x10^{-5}$ cells per well. Cells were initially challenged using the aforementioned protocol. Following incubation, cells were fixed with 4% paraformaldehyde for 15 mins at room temperature, washed with PBS, incubated with 0.2M glycine for 20 mins, washed with PBS, and permeabilized with 0.2% Triton X-100 for 2 mins. Then cells were washed with PBS, incubated with blocking buffer (10% fetal bovine serum in PBS) for 5 mins, washed with PBS, incubated with Hoechst nuclear probe (Sigma 33342; 1:3000) and SiR-Actin (Cytoskeleton Inc; probe for F-actin 1:5000) for 40 mins at 37°C, washed with PBS, and mounted with Faramount mounting media (Dako). All images were captured with a Leica TCS SP8 Confocal Laser Scanning Microscope built on a Leica DMi8 inverted confocal laser scanning microscope (NA 0.95, 506375, Leica). Leica Application Suite X (LASX) imaging software was used for image capture. Images were taken in the xy format at 63x or 20x magnification in oil immersion. LASX software preset fluorescence filters were used for the following: Hoechst (nuclear stain; ThermoFisher Scientific) and SiR-Actin Alexa Fluor 647 (F-actin stain; Cytoskeleton Inc.) The relative optical intensity (ROI) was measured using imaging analysis software (FIJI, Image J, National Institutes of Health).

Live Imaging Immunofluorescence Staining Protocol

Human PDL cells (PDL) were grown to confluency and passaged in sterile 4-well glass bottom plates (627870; Gibco, USA) $1.5x10^{-5}$ cells per well. Before challenge, cells were incubated with SiR-Actin (1:5000 dilution) overnight, and Hoechst nuclear probe (Sigma 33342; 1:3000) for 30 mins. Additionally, wildtype (WT) *T. denticola* cells were incubated 20 mins before challenge with Syto 9 dye (1:500), vortexed and washed with αMEM media twice before challenge. Syto 9 staining has been used previously in bacterial culture assays with *T. denticola* and the stain did not interfere with the functioning or viability of the pathogen (Yamada et al., 2005). PDL cells were challenged using the aforementioned protocol. PDL cells treated with WT *T. denticola* (50 MOI) or control media were imaged at 15-minute intervals from 0 to 24 h at set landmarks. All images were captured with a Zeiss scanning confocal microscope at 20x magnification with fluorescence filters for Hoechst, Alexa Flour 488 filter (Syto 9 dye for DNA; ThermoFisher Scientific) and Alexa Fluor 647 filter (SiR-Actin probe). The relative optical intensity (ROI) was measured using imaging analysis software (FIJI, Image J, National Institutes of Health).

Western Blot Analysis

PDL cells were plated in 60 mm tissue culture plates at $1.5x10^{-6}$ cells/plate overnight. Cells were then challenged with wildtype *T. denticola* at an MOI of 50 for 2 h or left unchallenged as controls. Post-challenge, cells were washed three times with PBS and incubated in αMEM medium for 24hrs. Cells were mechanically harvested with a cell-scraper, pelleted under centrifugation, washed with PBS, and lysed using radioimmunoprecipitation assay (RIPA) buffer. Lysates were then electrophoretically resolved on pre-made 4-12% bis-tris polyacrylamide gels (Invitrogen) and transferred onto immobilon-P PVDF transfer membranes (EMD Millipore) for western blotting analysis to evaluate changes in actin monomers (β-actin and γ-actin). Primary antibodies included: β-actin (Abcam; ab8227; RRID : AB_2305186), γ-actin (Santa Cruz; Cat# sc-65635, RRID : AB_1120816), and glyceraldehye 3-phosphate dehydrogenase (GAPDH) (Santa Cruz; sc-32233, RRID : AB_627679). Supersignal West Pico Plus Chemiluminescent substrate solution (Thermo Scientific) was used to develop protein bands. Densitometry was performed using FIJI imaging analysis software.

RNA Sequencing

Three replicates of primary human periodontal ligament cells (PDL) were derived from three subjects. Cells were challenged with *T. denticola* treatment at a multiplicity of infection of 50 whereas control cells were challenged with αMEM media. At the end of the 24 h incubation period, samples were pelleted, frozen and sent to Novogene Corporation Inc. for RNA extraction, sequencing, and analysis. All samples passed quality control with a Q30 above 80% and sequencing was performed using the Illumina Platform PE150. The RNA-Sequencing data being presented is a subset of genes from the overall analysis. 165 genes were identified from the gene ontology pathways derived from the RNA sequencing data. Biological processes were identified from the top significant differentially regulated processes seen in the 5 h and 24 h gene ontology graphs (**Supporting Information, Figure 2** and **Figure 4**). Pathways identified were titled regulation of actin cytoskeleton organization, positive regulation of cell projection organization, regulation of actin filament organization, ras protein signal transduction, regulation of small GTPase meditated signal transduction, extracellular matrix component, and extracellular matrix organization. Based on these pathways, the top genes were identified and their adjusted p-value and differential expression was plotted as a volcano plot (**Figure 4**). All genes used in the volcano plot came from the 24 h challenge data sets within the pathways specified above. RASA4 was identified as one of the top genes upregulated upon the 24 h *T. denticola* challenge.

Detachment Assay

Cells were challenged using the aforementioned protocol above. Following incubation, cells were vigorously washed with PBS three times. Vigorous washings included full force application of PBS with a 1mL pipette directly on cells and aspiration on high. This is different from normal culture methods; normally, PBS is added slowly on the side of the chamber/plate wall and aspirated on low. Cells were then fixed with 4% paraformaldehyde for 15 mins at room temperature, washed with PBS, incubated with 0.2M Glycine for 20 mins, washed with PBS, permeabilized with 0.2% Triton X-100 for 2 mins, washed with PBS, incubated with blocking buffer (10% fetal bovine serum in PBS; Gibco, USA) for 5 mins, washed with PBS (Gibco, USA), incubated with Hoechst (1:3000) and mounted with fluorescence mounting media (Faramount, Dako). Remaining cells were counted from 5 locations per well and cell number/location were averaged to constitute one experimental group. Mean cell count per experimental group was graphed as a ratio; control samples to wildtype *T. denticola* 50 MOI. Three samples were used per control and wildtype *T. denticola* groups. The images are from one representative experiment. The graph represents results from three separate experiments. Data were compared using a Student's t-test. All images were captured with a Zeiss confocal microscope at 63x and 20x magnification with Hoechst and Alexa 647 (SiR-Actin) fluorescence filters, then cells were counted using imaging analysis software (FIJI).

Gelatin Zymography

Gelatin zymography was conducted as previously described (Miao et al., 2011). Protein concentrations were calculated for each sample using the Pierce BSA Protein Assay kit according to manufacturer's instructions (Cat # 23225, Thermo Scientific). Equal protein for each sample was mixed with 4x sample buffer (0.25 M Tris base, 0.8% SDS, 40% glycerol, and 0.05% bromophenol blue), loaded into each well, and subjected to SDS-PAGE at 4°C on 10% gels containing 2 mg/ml gelatin. After electrophoresis, SDS was removed from the gels by washing them in renaturing buffer (2.5% Triton X-100, 50 mM Tris base) twice for 30 min then gels were placed in developing buffer (50 mM Tris base, pH 8, 10 mM $CaCl_2$, and 0.02% NaN_3) for 30 mins. Developing buffer was changed and gels were incubated at 37°C for 16 h then stained with 0.05% Coomassie blue for 30 mins, and de-stained in 10% acetic acid and 40% methanol until clear bands in a blue background were visible.

Quantitative RT-PCR (qRT-PCR)

RNA was isolated from PDL cells using the RNeasy Mini kit (Qiagen, Valencia, CA), reverse transcribed to cDNA using SuperScript Vilo cDNA Synthesis Kit (Invitrogen; Cat# 11754-050) and amplified by qRT-PCR using gene-specific primers for RASA4 (F: 5′-AGCGCAGCTCGCTGTACATC- 3'; R: 5′-GGCAGGTGCACTTGGTACTC- 3'), β-ACTIN (F: 5′-TGTT AGCGAGGGAGCAGTGG-3′; R: 5′-CCCATCGCCAAA ACTCTTCA-3′), and GAPDH (F: 5′-TTGAGGTCAATG AAGGGGTC-3′; R: 5′-GAAGGTGAAGGTCGGAGTCA-3′) (Jin et al., 2007). Cycle threshold values of the genes of interest and the quantitative gene expression levels normalized to GAPDH for each experimental sample were determined and compared with that of unchallenged control samples.

Transduction of PDL Cultures With RASA4 shRNA

Short hairpin RNA (shRNA) lentiviral particles specific for RASA4 (Santa Cruz Biotechnology; sc-89880-V) was used to inhibit RASA4 expression in PDL cells, according to manufacturer's instructions. Briefly, PDL cells were incubated with polybrene reagent (EMD Millipore, USA) at a final concentration of 5ug/ml and RASA4 shRNA or scrambled shRNA (control) lentiviral particles (sc-108064) for 10 h. After infection, PDL cell media was changed with normal supplemented αMEM media overnight. Lentiviral particles used contain a puromycin resistance gene used for selection. Selection of clones with successfully intake of knockdown constructs were identified by treating infected hPDL cells with puromycin (Calbiochem, USA) at a final concentration of 5 μg/mL until single cell colonies remained. Experiment ended by washing with phosphate buffered saline (PBS, Gibco, USA) and replaced with normal growth medium (αMEM media supplemented with 10% fetal bovine serum (Gibco, USA), 1% amphotericin B (Gibco, USA), and 1% penicillin-streptomycin). Cells were passaged once and validated *via* RT-qPCR before used for experiments.

Actin Dynamics Experiments

Actin polymerization for all experiments was stimulated by Jasplakinolide treatment (Jasp) of PDL cells at a concentration of 500nM for 1 h in αMEM alone media prior to *T. denticola* challenge and throughout *T. denticola* challenge as previously described. Control samples were challenged with αMEM alone media with no bacterial cells. These cells were labelled as Jasplakinolide alone. Actin depolymerization for all experiments was stimulated by Latrunculin B treatment (Lat B) of PDL cells at a concentration of 500nM for 1 h in αMEM alone media prior to *T. denticola* challenge and throughout *T. denticola* challenge as previously described. Control samples were challenged with αMEM alone media with no bacterial cells. These cells were labelled as Latrunculin B alone. Post-challenge, media was removed, washed with PBS thrice, and replaced with αMEM only media. Media was collected after the 24 h incubation for gelatin zymography. Cells were then incubated for 24h, then processed for RNA extraction for qRT-PCR.

Statistical Analysis

All data used in this manuscript was analyzed using the statistical software GraphPad Prism version 8.4.3 (La Jolla California USA). Results were evaluated by The Student's *t* test when comparing two groups. A one-way analysis of variance (ANOVA) was used when comparing three or more groups. ANOVA Turkey's multiple comparison test was used to distinguishing differences of two groups within experiments with three or more groups. The Two-way ANOVA test was used compare more than three groups, while comparing differences between shRNA scrambled and shRNA RASA4 knockdown samples. *P value of* ≤.05 was considered

statistically significant. Annotation within figure legends identify *= p ≤.05, **= p ≤.01, ***= p ≤.001.

RESULTS

PDL Cell Attachment and Contractility Is Impaired by *T. denticola* Challenge

Since little is known about *T. denticola's* effects on the actin filament processes of human PDL cells (PDL), we began this investigation by analyzing *T. denticola's* modulation of cellular adhesion and live actin filament dynamics in PDL cells (**Figure 1** and **Supporting Information, Figure 1** video). *T. denticola* interactions with gingival fibroblasts disrupt cell adhesion (Baehni et al., 1992), therefore we examined *T. denticola's* effects on PDL cell adhesion. *T. denticola* challenged PDL cells exhibited 70% more detachment than unchallenged cells (**Figure 1**). Live imaging of *T. denticola* challenged cells (**Supporting Information, Figure 1** and video) showed an impaired contractility leading to detachment of cells. Together, this indicates that *T. denticola* interaction with PDL cells negatively influences their actin dynamic properties. PDL cell interactions with *T. denticola* at an MOI of 50 were not cytotoxic to PDL cells as assessed with a Calcein AM viability assay (**Supporting Information, Figure 2**).

T. denticola Decreases Stress Fiber and β-Actin Monomer Abundance in PDL Cells

Actin stress fibers are key to the mechanotransducing function of PDL cells (de Araujo et al., 2014). Therefore, we next analyzed *T. denticola's* modulation of actin stress fibers and actin monomers in PDL cells (**Figure 2**). Treatment of PDL cells with *T. denticola* resulted in a significant decrease in stress fiber abundance as evaluated with immunofluorescence staining (**Figure 2A**). A 30% reduction in mean optical density was noted. To further evaluate *T. denticola's* effect on actin fibers, β-actin protein expression was evaluated in this context. Western blotting analyses revealed that *T. denticola* reduced β-actin protein levels by approximately 30% in PDL cells (**Figure 2B**). RNA sequencing analyses further revealed that *T. denticola* also significantly decreased actin RNA levels in PDL cells at 5 and 24 hours by 60 and 76%, respectively (**Figure 2C**). Additionally, gene ontology enrichment analysis revealed a significant differential expression in the biological pathways related to actin and cytoskeletal organization within the 5 h challenge samples compared to the controls (**Supporting Information, Figure 3**).

Gene Pathway and Volcano Plot Analyses Show RASA4 as a Top Upregulated Gene in *T. denticola* Challenged PDL Cells

From the RNA sequencing data referenced previously, gene ontology (GO) enrichment data was derived for 5 h and 24 h challenged samples versus controls (**Supporting Information, Figure 3** and **Figure 3**). Among all biological pathways, actin and cytoskeletal regulatory pathways were significantly and differentially expressed at 5 h after *T. denticola* challenge. Actin cytoskeletal-related pathways were also among the top significantly and differentially expressed biological pathways, including the ras protein signal transduction and regulation of small GTPase mediated signal transduction pathways. In order to identify the top differentially expressed genes that were influenced by actin regulation and that could be upstream of MMP-2 regulation, we plotted genes that were identified within the significantly expressed biological processes from the gene ontology (**Figure 3A**). From these genes, RASA4 was identified as one of the top genes upregulated upon a 24 h *T. denticola* challenge. Since specific tissues are able to regulate MMP-2 activity *via* actin dynamics (Bildyug, 2016), we investigated the role of RASA4, as RASA4 is linked to actin reorganization and stress fiber maintenance. Interestingly, RASA4 was upregulated 1.7-fold in the *T. denticola*-challenged cells compared to controls (**Figure 3B**).

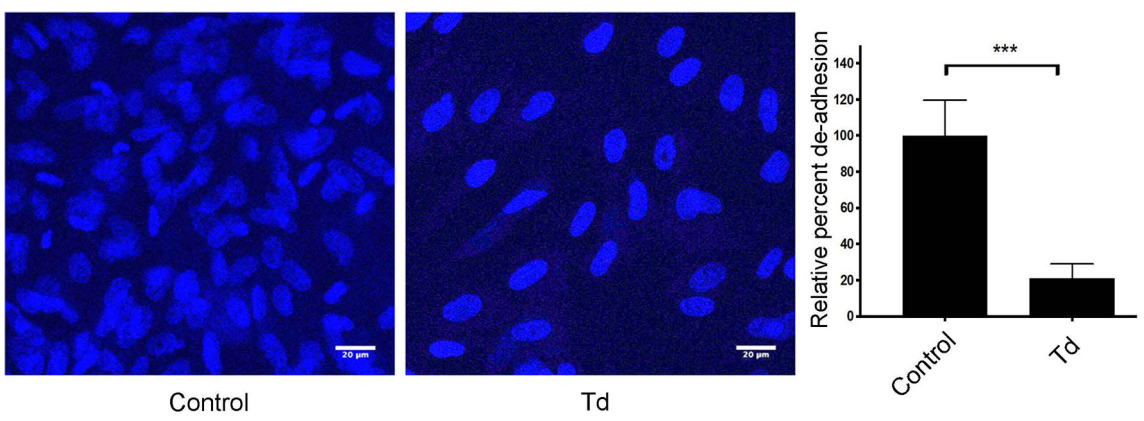

FIGURE 1 | PDL cell attachment and contractility is impaired by *T. denticola* challenge. PDL cells were unchallenged (control) or challenged with *T. denticola* (50 MOI) for 24 h and processed for immunofluorescent staining with Hoechst (nucleus, blue), and imaged with Confocal Microscopy. Representative phase contrast images are shown, and graphs show the percent change in de-adhesion after 24 h. Data represent mean ± SD from three independent experiments. Data were compared using Student's t-test. *** = p<0.001.

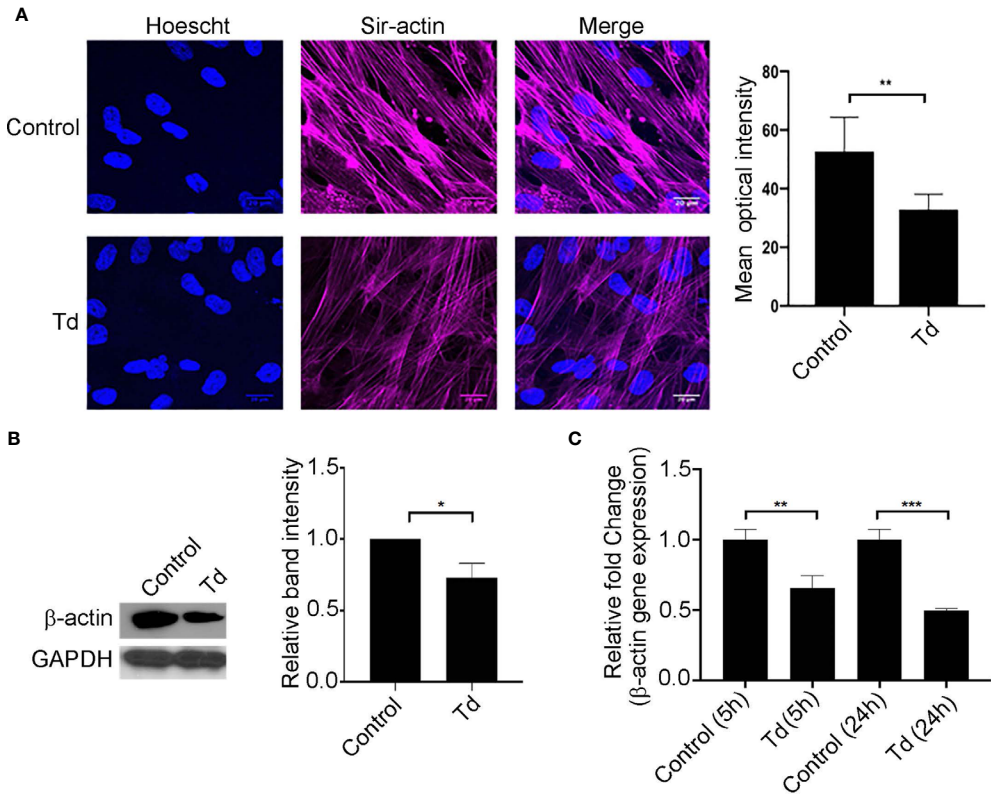

FIGURE 2 | *T. denticola* challenge decreases stress fibers and β-actin protein monomer abundance in PDL cells. **(A)** (*Left*) PDL cells were unchallenged (control) or challenged with *T. denticola* (50 MOI) for 24 h and processed for immunofluorescent staining with Hoechst (nucleus, blue) and SiR-Actin probe, and imaged using confocal microscopy. (*Right*) Relative optical intensities were calculated from three independent experiments. **(B)** (*Left*) Representative immunoblot showing β-actin levels in PDL cells challenged with control medium or media containing *T. denticola* (50 MOI) for 24 h. (*Right*), Densitometry analysis of three independent experiments was performed using ImageJ software, and the ratio of control samples to *T. denticola* was calculated. Data represent mean ± SD from three independent experiments. Data were compared using Student's t-test. * = p<0.05; ** = p<0.01. **(C)** β-actin gene expression in PDL cells challenged with control medium or media containing *T. denticola* (50 MOI) for 5h or 24 h by RNA-Seq. The graph shows the fold changes on a log2 scale. Data were compared using Student's t-test. ** = p<0.01; *** = p<0.001.

Purified Dentilisin and *T. denticola* Upregulate RASA4 Gene Expression in PDL Cells

Previous literature suggests that *T. denticola* induces subcortical actin polymerization through its effector protein, major surface protein (Msp) (Visser et al., 2011; Wang et al., 2019). Purified Msp can induce actin assembly by blocking the calcium influx into fibroblasts (Wang et al., 2001). Since RASA4 is activated by a calcium influx, the *T. denticola*-mediated mechanism of action in our system may be different. Therefore, we investigated the role of another *T. denticola* effector protein, dentilisin. We used purified dentilisin and a *T. denticola* isogenic mutant (CF522-Td; dentilisin null and Msp positive), which lacks the proteolytic PrtP subunit of dentilisin to determine if dentilisin was sufficient to enhance RASA4 upregulation. Additionally, we tested the *T. denticola* MHE strain (an isogenic Msp mutant that is dentilisin-positive) to investigate the role of Msp in this process. *Veillonella parvula* was used as an additional control, since it is a commensal Gram-negative bacterium. Quantitative RT-PCR results indicate that both purified dentilisin and wild type-*T. denticola* induced RASA4 expression (1.7 and 1.67-fold increase, respectively) (**Figure 4**). Neither CF522-Td, MHE-Td nor *V. parvula* had any effect on RASA4 expression compared to untreated PDL cells (**Figure 4**). Thus, our results indicate that while dentilisin contributes to *T. denticola*-mediated RASA4 transcriptional upregulation, Msp activity also contributes, presumably by a different mechanism.

Jasplakinolide Inhibits *T. denticola*-Induced RASA4 Gene Expression, Whereas RASA4 Gene Expression Is Upregulated in Latrunculin B Pretreated and *T. denticola* Challenged PDL Cells

T. denticola causes actin reorganization in fibroblasts (Visser et al., 2011). In this study, we showed that *T. denticola* decreases actin stress fibers in PDL cells (F-actin intensity; **Figure 2**). Previous literature showed that RASA4 can disrupt actin stress fiber organization (Choi and Helfman, 2014) and induce actin

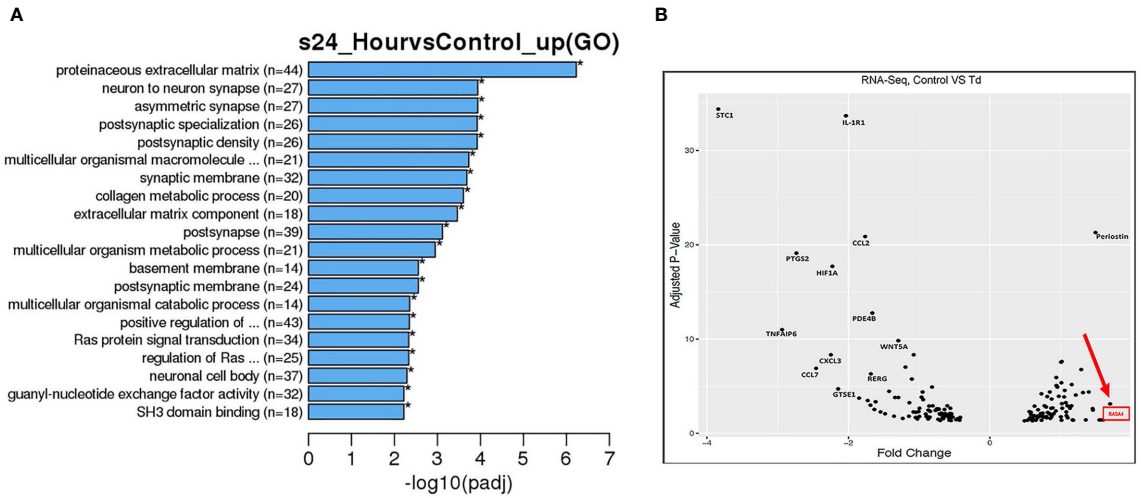

FIGURE 3 | Gene pathways and volcano plot shows RASA4 as a top upregulated gene in *T. denticola* challenged PDL cells. PDL cells were unchallenged or challenged with *T. denticola* (50 MOI) for 24 h and differential gene expression analysis was performed using RNA-Seq. 165 genes were identified from the gene ontology pathways derived from the RNA sequencing data. Biological processes were identified from the top significant processes that were differentially regulated in the gene ontology enrichment analysis from 5 h and 24 h gene ontology graphs (**Supporting Information**, **Figure 3** and **A**). Pathways identified were titled regulation of actin filament organization, positive regulation of cell projection organization, regulation of actin filament organization, *ras* protein signal transduction, regulation of small GTPase meditated signal transduction, extracellular matrix component, and extracellular matrix organization. Based on these pathways, the top genes were identified and their adjusted p-value and differential expression was plotted as a volcano plot **(B)**. All genes used in the volcano plot came from the 24 h challenge data sets within the pathways specified above. RASA4 was identified as one of the top genes upregulated upon 24 h *T. denticola* challenge.

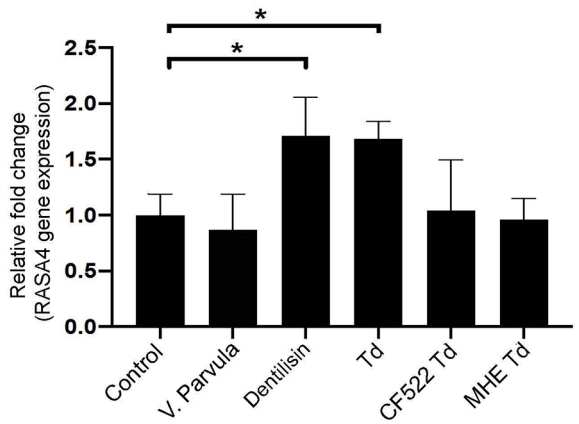

FIGURE 4 | Purified dentilisin and *T. denticola* upregulate RASA4 gene expression in PDL cells. Quantitative RT-PCR analysis of RASA4 relative fold change in PDL cells challenged with *V. parvula*, wild type *T. denticola*, *T. denticola* dentilisin mutant CF522, *T. denticola* MHE or treated with purified dentilisin for 24 h. Data represent mean ± SD from three independent experiments. Data were compared using One-way ANOVA Tukey's Multiple comparisons test. * = p<0.05.

reorganization (Choi and Helfman, 2014; Li et al., 2017). We hypothesized that RASA4 would also be upregulated during actin depolymerization but not during polymerization. Jasplakinolide (Jasp) or Latrunculin B (Lat B) were used to pre-treat PDL cells to induce actin polymerization or depolymerization, respectively. Post-treatment cells were collected for reverse transcriptase-quantitative PCR analysis. Results showed that Jasplakinolide did not have an effect on RASA4 gene expression compared to controls (**Figure 5A**). We next investigated the effect of actin depolymerization (which was induced by Latrunculin B pretreatment) on RASA4 gene expression. RASA4 gene expression was significantly upregulated (1.67 fold) with *T. denticola* and (2.4 fold) with Latrunculin B treatment compared to controls (**Figure 5B**). Combined treatment of Latrunculin B and *T. denticola* further upregulated RASA4 gene expression (4.15 fold). Thus, RASA4 upregulation is associated with *T. denticola*-mediated actin depolymerization and the actin depolymerization agent Latrunculin B.

RASA4 Gene Expression Is Important for *T. denticola*-Mediated Actin Stress Fiber Dysfunction

To further determine the role of RASA4 in *T. denticola*-mediated actin depolymerization, we suppressed RASA4 gene expression in this context. RASA4 expression was reduced by 60% in hPDL cells infected with RASA4 shRNA lentiviral particles compared to control infected cells (**Figure 6A**). These cells were then challenged with or without *T. denticola*. After challenge, cells were stained with actin to visualize cellular stress fiber abundance by confocal microscopy. PDL cells infected with shRNA RASA4 exhibited reduced stress fiber abundance and organization compared to control cells treated with scrambled

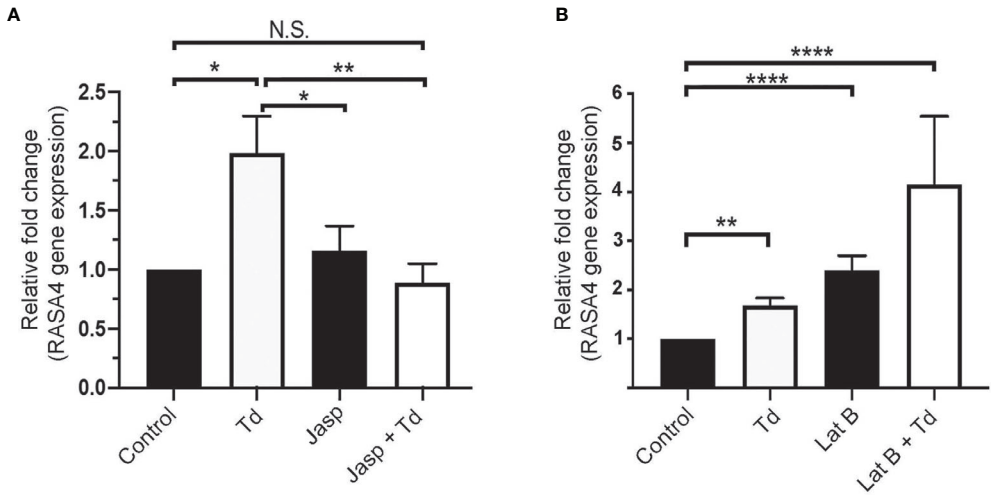

FIGURE 5 | Jasplakinolide inhibited *T. denticola*-induced RASA4 gene expression, whereas RASA4 gene expression is upregulated in Latrunculin B pretreated and *T. denticola* challenged PDL cells. Quantitative RT-PCR analysis of RASA4 relative fold change in the gene expression of PDL cells treated with Jasplakinolide (Jasp; panel **A**) or Latrunculin B (Lat B; panel **B**) and challenged with *T. denticola* (50 MOI). Data represent mean ± SD from three independent experiments. Data were compared using Two-way ANOVA Tukey's Multiple comparisons test. * = p<0.05; ** = p<0.01; **** = p<0.0001; N.S., not significant.

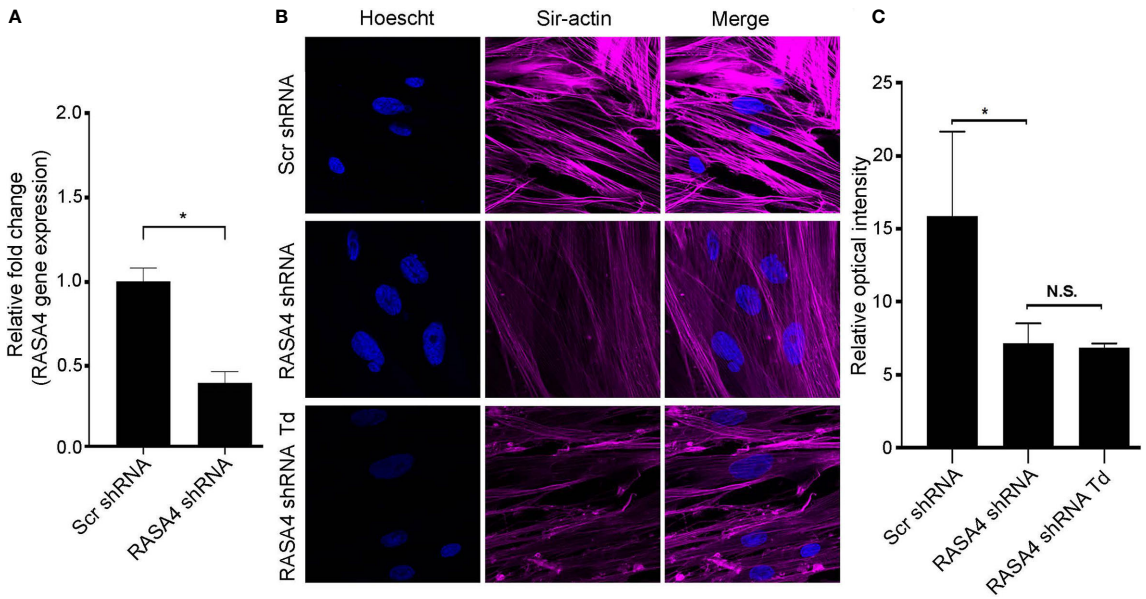

FIGURE 6 | RASA4 gene expression is required for *T. denticola*-mediated actin stress fiber dysfunction. **(A)** Quantitative RT-PCR analysis of RASA4 relative fold change in PDL cells infected with scramble shRNA or RASA4 shRNA. **(B)** Representative confocal images and **(C)** relative optical intensity of stress fiber intensity in scramble shRNA, RASA4 shRNA and RASA4shRNA cells challenged cells with *T. denticola* (50 MOI) for 24 h and stained with SiR-Actin dye (1:5000). Data represent mean ± SD from three independent experiments. Data in panel **(A)** was analyzed using an Unpaired t test. Data in panel **(C)** was analyzed using One-way ANOVA Tukey's Multiple comparisons test. * = p<0.05; N.S., Not significant.

shRNA (Scr shRNA) (**Figure 6B**). Image analysis of actin stress fiber staining intensity showed that shRNA RASA4 infected cells exhibited a 2.4-fold decrease compared to control infected cells (**Figure 6C**). In contrast, *T. denticola* challenge did not change the levels of actin staining intensity any further. These data indicate that RASA4 gene expression is important for homeostatic actin organization and for *T. denticola*-mediated depolymerization of stress fibers in PDL cells.

Actin Depolymerization Through *T. denticola* Challenge and Latrunculin B Pretreatment Increases MMP-2 Enzymatic Activity

Actin dynamics have been shown to regulate MMPs (Bildyug, 2016). Additionally, we previously showed that MMP-2 activation increased upon *T. denticola* challenge (Miao et al., 2014). Thus, we investigated whether *T. denticola*-mediated changes in actin dynamics could modulate MMP-2 activity in PDL cells and if the actin-depolymerizing effect of the chemical inhibitor Latrunculin B (Lat B) would affect MMP expression in this context. As in **Figure 5**, Latrunculin B (Lat B) or Jasplakinolide (Jasp) were used to pre-treat PDL cells to induce actin depolymerization or polymerization, respectively. Following pre-treatment, *T. denticola* challenged PDL cells were collected for gelatin zymography to analyze MMP-2 activity (**Figure 7A**). There were no significant changes in the inactive form of MMP-2 (pro-MMP-2) among any of the samples (**Figure 7B**). Induction of actin polymerization with Jasplakinolide did not result in any difference in MMP-2 activation compared to control (**Figure 7C**). Challenging PDL cells with *T. denticola* alone significantly increased MMP-2 activity 2.8-fold, but pre-treatment with Jasplakinolide before *T. denticola* challenge decreased MMP-2 activity (1.6 fold compared to control), thereby abrogating the effect of *T. denticola* on MMP-2 (**Figure 7C**). In contrast, induction of actin depolymerization in PDL cells with Latrunculin B alone showed a notable increase in active MMP-2 bands (2.8-fold) compared to control (**Figure 7C**). Additionally, samples pretreated with Latrunculin B, then challenged with *T. denticola*, also increased MMP-2 activity (3.2 fold) compared to control. These data indicate that actin dynamics regulate MMP-2 activity, and *T. denticola* mediates these MMP-2 effects through an actin depolymerization mechanism.

RASA4 Gene Expression Is Required for *T. denticola*-Mediated Enhancement of MMP-2 Activity

Since RASA4 is required for *T. denticola*-mediated actin depolymerization and since actin dynamics mediate changes in MMP, we next investigated whether RASA4 is required for *T. denticola*-mediated changes in MMP-2 activity in PDL cells. Using the same experimental set up as in **Figure 6**, we obtained culture media from each group to analyze MMP-2 activation. Gelatin zymography of culture media from these cells showed that *T. denticola* challenge significantly increased active MMP-2 levels (2.5 fold) in controls (Scr shRNA cells plus *T. denticola)* compared to unchallenged (Scr shRNA) cells (**Figures 8A–C**). In contrast, shRNA RASA4 infected cells exhibited decreased MMP-2 activity (1.67-fold) compared to controls (Scr shRNA), and *T. denticola* was unable to increase the levels of MMP-2 activity in the context of RASA4 shRNA (**Figures 8A–C**). This indicates that RASA4 is required for *T. denticola* driven induction of depolymerization and subsequent regulation of MMP-2 activity in PDL cells.

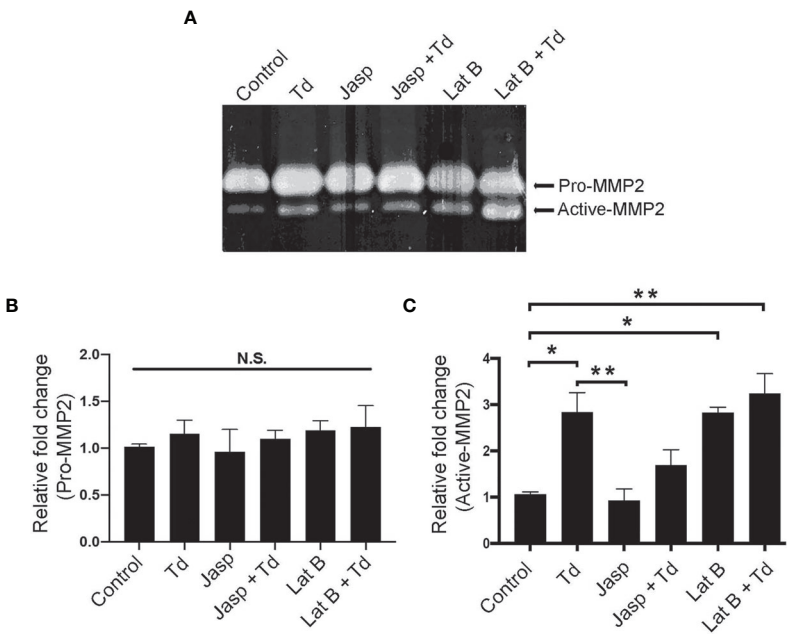

FIGURE 7 | Actin depolymerization through *T. denticola* challenge and Latrunculin B pretreatment increases MMP-2 enzymatic activity. Actin polymerizing agent Jasplakinolide (Jasp) and actin depolymerizing agent Latrunculin B (Lat B) were used to pretreat PDL cells for one h. Cells were then unchallenged or challenged with *T. denticola* (50 MOI) for 24 h. Cultured media was collected and gelatin zymography was used to measure MMP-2 activity. A representative Gelatin zymogram is shown **(A)** and densitometry analysis of pro-MMP-2 **(B)** and active-MMP-2 **(C)**. Data represent mean ± SD from three independent experiments. Data were compared using One-way ANOVA Tukey's Multiple comparisons test. *. = $p<0.05$; ** = $p<0.01$; N.S., not significant.

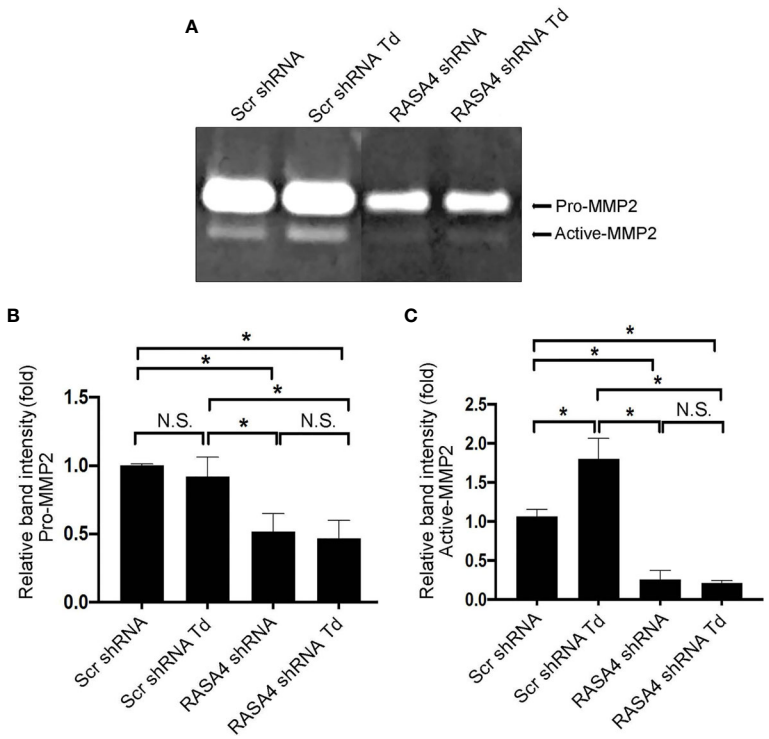

FIGURE 8 | RASA4 gene expression is required for *T. denticola*-mediated enhancement of MMP-2 activity. Pro-MMP-2 and active-MMP-2 in scramble shRNA and RASA4shRNA cells challenged with *T. denticola* (50 MOI) for 24 h. **(A)** a representative zymogram. **(B)** (Pro-Mmp-2) and **(C)** (active Mmp-2) show mean ± SD from three independent experiments. Data was compared using Two-way ANOVA Tukey's Multiple comparisons test. * = $p<0.05$; N.S., not significant.

DISCUSSION

In this study, we show that in *T. denticola*-PDL cell interactions, *T. denticola* drives enhanced MMP-2 activity through a novel actin reorganization signaling mechanism. This reorganization mechanism is a pathological response characterized by upregulation of RASA4, depolymerization of actin filaments, and a subsequent increase in MMP-2 activity. This mechanism is specific to the *T. denticola* effector protein dentilisin (although Msp is also important), thereby uncovering a novel effect for *T. denticola*-mediated actin depolymerization in primary human PDL cells that is distinct from that previously reported for *T. denticola* Msp in human gingival fibroblasts. Although there are different mechanisms reported for *T. denticola*'s contribution to actin reorganization, Jobin et al. found that *T. denticola* purified Msp induces Ca(2+) entry and actin reorganization in cultured fibroblasts (Jobin et al., 2007). This is contrary to other findings by Ko et al. who reported that outer membrane extracts of *T. denticola* inhibited calcium influxes in gingival fibroblasts and disrupted actin-dependent processes (Ko et al., 1998). This suggests that the bacterial source (purified versus bacterial extracts) is important in determining host effects on actin organization and calcium influxes, but knowledge of the overall effects of the whole bacterium is lacking. Furthermore, using *T. denticola* mutant strains carrying defined defects in proteins of interest to assay their biological relevance is important. Earlier literature showed that Latrunculin B treatment induced calcium influxes though that study did not assay effects of a defined Msp mutant strain (Wang et al., 2001). We show here that the calcium influx-triggered gene, RASA4, is upregulated in the presence of Latrunculin B and its expression is further increased in the presence of *T. denticola*. We also show the importance of *T. denticola* dentilisin and the Msp proteins in this process. While neither the dentilisin mutant nor the Msp mutant showed effects on RASA4 expression significantly different from controls, further studies are required to determine whether a double mutant would show a distinguishable difference. Taken in aggregate, these data indicate that dentilisin and Msp are key *T. denticola* proteins important in regulating actin assembly and calcium influx through RASA4 is mechanistically important (Ko et al., 1998; Jobin et al., 2007; Visser et al., 2011).

There are various signaling pathways implicated in actin organization and stress fiber formation. *T. denticola*-mediated actin reorganization is stimulated by PIP-2 dependent signaling leading to activation of the small GTPases RAC1, RhoA, and Ras in fibroblasts (Visser et al., 2011). To further evaluate the global effects of *T. denticola* on the PDL cytoskeleton at the mRNA level, we performed RNA sequencing of PDL challenged cells. RNA sequencing analysis of *T. denticola*-challenged PDL cells compared to non-challenged cells revealed a significant differential expression of genes related to actin cytoskeletal dynamics, including the actin monomer (β-actin), γ-actin, IQGAP3, ACTR3, ACTR2,

ARPC3, ARPC5, RERG, and ARHGEF4. Gene ontology also confirmed that Ras signaling was amongst the top 20 most upregulated pathways. When examining actin organization and *ras* signaling genes, a candidate gene RASA4 was identified as a key upregulated gene (increased 1.7-fold, p-value 7.62E-04) in *T. denticola* challenged cells. Its paralog RASA4B was also upregulated 1.57-fold (p-value 3.82E-02). We confirmed that *T. denticola* and its secreted protease dentilisin are responsible for RASA4 gene upregulation. This is consistent with previous reports identifying RASA4 as important for microbial immune responses to bacterial infection (Zhang et al., 2005). Our study suggests that RASA4 may be a key cellular response to periodontal infection and a possible biomarker for *Treponema denticola* and *Treponema denticola*-associated diseases.

RASA4 can constitutively interact with Rac1 and Cdc42, and it inhibits the RAS/ERK signaling pathway, which is important for maintaining actin organization. Inhibition of the RAS/ERK pathway *via* RASA4 disrupts actin stress fiber organization (Choi and Helfman, 2014) and induces actin reorganization (Choi and Helfman, 2014; Li et al., 2017). This evidence suggests that RASA4 may be a key regulator of actin stress fiber reorganization stimulated by *T. denticola* challenge. By knocking down RASA4 and showing no difference in F-acin abundance with or without *T. denticola*, our results show that RASA4 is required for actin dynamics, specifically, actin depolymerization in the presence of *T. denticola*. Our data is consistent with other reports showing that actin reorganization is induced by *T. denticola.* Other publications suggest that this is facilitated by the effector protein Msp (Visser et al., 2011). Given the current data with the mutant *T. denticola* strains highlighting the role of dentilisin and the importance of the Msp, it is possible that RASA4 is acting through a unique mechanism as a result of both dentilisin and the Msp.

RASA4 has not been previously linked to MMP-2 activity. Our results demonstrate that a periodontal pathogen, *T. denticola* relies on RASA4 genetic expression to induce actin stress fiber disruption and increase MMP-2 activity in PDL cells. In order to confirm that RASA4 was involved in enhanced MMP-2 activity, a suppression strategy was used. Successful suppression of RASA4 expression effectively decreased overall pro-MMP-2 activity and active MMP-2. In the presence of *T. denticola*, MMP-2 activity is normally enhanced in PDL cells (Miao et al., 2011). Our study suggests that this increase is due to actin depolymerization of actin stress fibers, but suppression of RASA4 abrogated the effect of *T. denticola* on these actin components and MMP-2. These results indicate that RASA4 mRNA expression is required for actin-mediated enhanced MMP-2 activity. This study is the first to characterize RASA4 as a key player in *T. denticola*-mediated actin reorganization and MMP-2 activity in PDL cells.

Several periodontal pathogens have been reported to increase MMP-2 expression and activity. Known red and orange complex bacteria (Socransky et al., 1998), *Porphymonas gingivalis*, *Actinobacillus actinomycetemcomitans*, and *Fusobacteria nucleatum* are able to stimulate MMP-2 production and secretion in human epithelial cells and PDL cells (Pattamapun et al., 2003; Tiranathanagul et al., 2004; Gursoy et al., 2008). We have previously shown that *T. denticola* increases both activation of MMP-2 proteolytic activity and transcription through a chronic, epigenetic mechanism (Miao et al., 2011; Ateia et al., 2018), resulting in MMP-2-dependent fibronectin fragmentation (Miao et al., 2011).

Additionally, activators of MMP-2 are affected by *Treponema denticola* interactions. Tissue inhibitors of metalloproteinases, specifically TIMP-1 and -2, are important in the inhibition and activation of MMP-2. Previous studies have shown that *T. denticola* challenge of PDL cells upregulates TIMP-2 and MMP-14 mRNA expression (Miao et al., 2014). Dentilisin is important in the increase in protein levels of TIMP-2 and MMP-14. (Miao et al., 2014) Furthermore, purified dentilisin can breakdown TIMP-1 and TIMP-2 (Nieminen et al., 2018). These conditions would favor a ratio for maximum MMP-2 activation. Together, these studies suggest that bacterial stimulation of MMP-2 and its co-activators/modulators by periodontal pathogens plays a role in tissue destruction; however, the mechanism(s) involved for individual species and host cell types are not well understood. The present study examined RASA4 gene expression as a regulator for *T. denticola*-mediated enhancement of MMP-2 activity. Calcium-dependent signaling can also induce MMP-2 expression in multiple cell types, including human periodontal fibroblasts and oral squamous cell carcinoma cells (Munshi et al., 2002; Osorio et al., 2015). Consistent with this finding, we show that RASA4 (which relies on calcium signaling) is necessary for *T. denticola* interaction to increase MMP-2 activity. Additionally, our results indicate that *T. denticola*-mediated actin reorganization requires RASA4 gene expression. Actin reorganization regulates MMPs in different ways; showing tissue specificity (Bildyug, 2016). MMP-2 expression can increase or decrease due to actin dynamics; polymerization and depolymerization (Sanka et al., 2007; Bildyug, 2016). For example, inhibition of actin polymerization had no effect on MMP-2 expression in HT1080 fibrosarcoma cells, whereas in human trabecular meshwork cells, inhibition of actin polymerization induced the activation of MMP-2 expression (Chintala et al., 1998; Sanka et al., 2007). We examined whether actin dynamics are involved in our system and found that sequestering actin monomers (which depolymerizes actin stress fibers) by treatment with latrunculin B, increased active MMP-2 activity in PDL cells.

MMP-2 and MMP-9 are the major gelatinases amongst MMPs. *T. denticola* is associated with MMP-9 in gingival crevicular fluid from periodontally challenged patients compared to healthy patients (Yakob et al., 2013). PMN interaction with Treponeme components, chiefly the 53-kDa protein and LPS, increased the release of MMP-9 (Ding et al., 1996). The MSP effector protein, enhances the production of MMP-9 in peripheral blood monocytes (Gaibani et al., 2010). In isolation, purified dentilisin does have the ability to convert purified proMMP-9 to active MMP-9 (Nieminen et al., 2018). MMP-9 may play a role in the context of this paper, but PDL cells do not make large amounts of MMP-9. PDL cells are major producers of MMP-2. Clinically, this is relevant because MMP-2 plays a key role in fibronectin cleavage. The presence of 40, 68, and 120kDa fibronectin (FN) fragments in gingival crevicular fluid are markers of periodontal disease

(Huynh et al., 2002). PDL cells create these FN fragments predominately through enhanced production of MMP-2 activity and mRNA expression in response to *T. denticola* and purified dentilisin challenge (Huynh et al., 2002; Miao et al., 2011; Miao et al., 2014). Knockdown of MMP-2 nearly eliminates FN fragments (Gaibani et al., 2010). Therefore MMP-2 was the relevant MMP in this study, but further study may elucidate MMP-9 playing a significant role (Miao et al., 2011; Yakob et al., 2013).

In summary, the current study highlights that *T. denticola* mediates actin reorganization (depolymerization) through RASA4 gene expression, which enhances MMP-2 activity in human PDL cells. RASA4 was identified as a novel contributor to the PDL host response and tissue destruction process. The study also identifies that actin dynamics play a role in the progression of periodontal disease, specifically actin depolymerization as a key contributor to enhance MMP-2 activity. These contributions shed light on new potential targets for *T. denticola*-PDL interactions that influence the progression of periodontitis and the maintenance of a healthy periodontium.

DATA AVAILABILITY STATEMENT

The data presented in the study are deposited in the FigShare repository, ascension number 10.6084/m9.figshare.14336909 (**Supplementary Figure 1** High Resolution Videos) and 10.6084/m9.figshare.13530566 (RNA sequencing processed data).

ETHICS STATEMENT

The studies involving human participants were reviewed and approved by Institutional review board (IRB) approval for human subjects research was obtained *via* the University of California San Francisco institutional review board (# 16-20204; reference #227030). Written informed consent for participation was not required for this study in accordance with the national legislation and the institutional requirements

AUTHOR CONTRIBUTIONS

EM: Investigation, Project Administration, Methodology, Formal Analysis, Funding Acquisition, Writing (original draft, review and editing), Supervision Validation, and Visualization. SG: Data curation, Methodology, and Investigation. AR: Conceptualization, Methodology, and Supervision. KS: Investigation. NM: Investigation and Validation. CT: Investigation. AK: Methodology, Investigation, and Resources. PK: Project Administration, Supervision, and Writing (original draft, review and editing). JF: Conceptualization, Resources, Funding Acquisition, Supervision, and Writing (original draft, review and editing). LZ: Resources. YK: Conceptualization, Resources, Supervision, Funding Acquisition, and Writing (original draft, review and editing). All authors contributed to the article and approved the submitted version.

FUNDING

This work was supported by funding from NIH (R01 DE025225 to YK and JF; F30 DE027598 to EM).

ACKNOWLEDGMENTS

The authors of this paper want to acknowledge the contributions of the Bush Lab in assistance performing the live imaging experiments. We also want to acknowledge Cesar Diaz and Kristina Guardino for the contributions they made to this paper.

SUPPLEMENTARY MATERIAL

The Supplementary Material for this article can be found online at: https://www.frontiersin.org/articles/10.3389/fcimb.2021.671968/full#supplementary-material

Supplementary Figure 1 | *T. denticola* interaction negatively influences PDL cell actin filament functioning. Approximately 1.0x10^5 PDL cells per well were plated in a 4-well glass bottom culture plate. SiR-Actin dye (1:5000) and Hoechst (1:3000) stain were added to each well 4 hours before imaging. *T. denticola* was pre-incubated in a 15mL falcon tube with Syto9 (1:500) fluorescent dye for 20 mins. Bacteria were washed and centrifuged twice to remove unbound Syto9 and cells were reconstituted with αMEM media. Syto9-labelled *T. denticola* (50 MOI) was added to plated PDL cells. Control cells contained no *T. denticola.* Culture plates were imaged in a sterile chamber containing 5% CO2 and connected to a scanning laser confocal microscope. Images were set to image every 15 minutes for 24 hours. Maximum projections (representative image) and each individual image were analyzed in FIJI software. Hoechst, SiR-Actin, and Syto9 were assigned blue, cyan, and green filters, respectively. Images were combined to create the imaging video. Link to high resolution videos are under the data availability statement.

Supplementary Figure 2 | *T. denticola* interaction does not affect viability of PDL Cells. PDL cells were plated in 96 well plate (approximately 3x 10^4 cell per well) unchallenged (control) or challenged with *T. denticola* (10, 50, or 100 MOI) for 24 h and Calcein AM assays were performed according to manufacturer's instructions. Data represent mean ± SD from three independent experiments containing 10 wells per sample. Data was compared using One-way ANOVA Tukey's Multiple comparisons test. *= $p<0.05$; N.S.= not significant

Supplementary Figure 3 | *T. denticola* interaction reflects an effect on actin and cytoskeletal biological processes. Gene ontology enrichment was performed from RNAseq data previously described. Gene ontology for PDL cells challenged for 5 h with *T. denticola* versus control (unchallenged PDL cells) showed a significant differential expression. Top differentially expressed biological processes include: regulation of actin filament organization and actin filament-based process, actin filament organization, regulation of cytoskeletal organization, regulation of actin organization, extracellular matrix organization.

REFERENCES

Amin, M., Ho, A. C., Lin, J. Y., Batista da Silva, A. P., Glogauer, M., and Ellen, R. P. (2004). Induction of De Novo Subcortical Actin Filament Assembly by *Treponema Denticola* Major Outer Sheath Protein. *Infect. Immun.* 72 (6), 3650–3654. doi: 10.1128/IAI.72.6.3650-3654.2004

Armitage, G. C. (2004). Periodontal Diagnoses and Classification of Periodontal Diseases. *Periodontol* 2000 34, 9–21. doi: 10.1046/j.0906-6713.2002.003421.x

Ateia, I. M., Sutthiboonyapan, P., Kamarajan, P., Jin, T., Godovikova, V., Kapila, Y. L., et al. (2018). *Treponema* Denticola Increases MMP-2 Expression and Activation in the Periodontium Via Reversible DNA and Histone Modifications. *Cell Microbiol.* 20 (4), 10.1111/cmi.12815. doi: 10.1111/cmi.12815

Baehni, P. C., Song, M., McCulloch, C. A., and Ellen, R. P. (1992). *Treponema Denticola* Induces Actin Rearrangement and Detachment of Human Gingival Fibroblasts. *Infect. Immun.* 60 (8), 3360–3368. doi: 10.1128/IAI.60.8.3360-3368.1992

Bildyug, N. (2016). Matrix Metalloproteinases: An Emerging Role in Regulation of Actin Microfilament System. *Biomol. Concepts* 7 (5-6), 321–329. doi: 10.1515/bmc-2016-0022

Chintala, S. K., Sawaya, R., Aggarwal, B. B., Majumder, S., Giri, D. K., Kyritsis, A. P., et al. (1998). Induction of Matrix Metalloproteinase-9 Requires a Polymerized Actin Cytoskeleton in Human Malignant Glioma Cells. *J. Biol. Chem.* 273 (22), 13545–13551. doi: 10.1074/jbc.273.22.13545

Choi, C., and Helfman, D. M. (2014). The Ras-ERK Pathway Modulates Cytoskeleton Organization, Cell Motility and Lung Metastasis Signature Genes in MDA-MB-231 LM2. *Oncogene* 33 (28), 3668–3676. doi: 10.1038/onc.2013.341

Chukkapalli, S. S., and Lele, T. P. (2018). Periodontal Cell Mechanotransduction. *Open Biol.* 8 (9), 180053. doi: 10.1098/rsob.180053

de Araujo, R. M., Oba, Y., Kuroda, S., Tanaka, E., and Moriyama, K. (2014). Rhoe Regulates Actin Cytoskeleton Organization in Human Periodontal Ligament Cells Under Mechanical Stress. *Arch. Oral. Biol.* 59 (2), 187–192. doi: 10.1016/j.archoralbio.2013.11.010

Ding, Y., Uitto, V.-J., Haapasalo, M., Lounatmaa, K., Konttinen, Y. T., Salo, T., et al. (1996). Membrane Components of *Treponema Denticola* Trigger Proteinase Release From Human Polymorphonuclear Leukocytes. *J. Dental Res.* 75 (12), 1986–1993. doi: 10.1177/00220345960750121101

Fenno, J. C., Hannam, P. M., Leung, W. K., Tamura, M., Uitto, V. J., and McBride, B. C. (1998). Cytopathic Effects of the Major Surface Protein and the Chymotrypsinlike Protease of *Treponema Denticola*. *Infect. Immun.* 66 (5), 1869–1877. doi: 10.1128/IAI.66.5.1869-1877.1998

Fenno, J. C., Wong, G. W., Hannam, P. M., Müller, K. H., Leung, W. K., and McBride, B. C. (1997). Conservation of *Msp*, the Gene Encoding the Major Outer Membrane Protein of Oral *Treponema* Spp. *J. Bacteriol.* 179 (4), 1082–1089. doi: 10.1128/JB.179.4.1082-1089.1997

Fernández, A., Cárdenas, A. M., Astorga, J., Veloso, P., Alvarado, A., Merino, P., et al. (2019). Expression of Toll-Like Receptors 2 and 4 and Its Association With Matrix Metalloproteinases in Symptomatic and Asymptomatic Apical Periodontitis. *Clin. Oral. Investig.* 23 (12), 4205–4212. doi: 10.1007/s00784-019-02861-9

Gaibani, P., Caroli, F., Nucci, C., and Sambri, V. (2010). Major Surface Protein Complex of *Treponema Denticola* Induces the Production of Tumor Necrosis Factor Alpha, Interleukin-1 Beta, Interleukin-6 and Matrix Metalloproteinase 9 by Primary Human Peripheral Blood Monocytes. *J. Periodontal Res.* 45 (3), 361–366. doi: 10.1111/j.1600-0765.2009.01246.x

Godovikova, V., Wang, H. T., Goetting-Minesky, M. P., Ning, Y., Capone, R. F., Slater, C. K., et al. (2010). Treponema Denticola Prcb is Required for Expression and Activity of the Prca-Prtp (Dentilisin) Complex. *J. Bacteriol.* 192 (13), 3337–3344. doi: 10.1128/JB.00274-10

Gursoy, U. K., Könönen, E., and Uitto, V. J. (2008). Stimulation of Epithelial Cell Matrix Metalloproteinase (MMP-2, -9, -13) and Interleukin-8 Secretion by Fusobacteria. *Oral. Microbiol. Immunol.* 23 (5), 432–434. doi: 10.1111/j.1399-302X.2008.00453.x

Gutiérrez-Venegas, G., Kawasaki-Cárdenas, P., Garcés, C. P., Román-Alvárez, P., Barajas-Torres, C., and Contreras-Marmolejo, L. A. (2007). *Actinobacillus Actinomycetemcomitans* Adheres to Human Gingival Fibroblasts and Modifies Cytoskeletal Organization. *Cell Biol. Int.* 31 (9), 1063–1068. doi: 10.1016/j.cellbi.2007.03.028

Hasegawa, Y., Tribble, G. D., Baker, H. V., Mans, J. J., Handfield, M., and Lamont, R. J. (2008). Role of *Porphyromonas Gingivalis* Serb in Gingival Epithelial Cell Cytoskeletal Remodeling and Cytokine Production. *Infect. Immun.* 76 (6), 2420–2427. doi: 10.1128/IAI.00156-08

Hassell, T. M., Baehni, P., Harris, E. L., Walker, C., Gabbiani, G., and Geinoz, A. (1997). Evidence for Genetic Control of Changes in F-Actin Polymerization Caused by Pathogenic Microorganisms: *in Vitro* Assessment Using Gingival Fibroblasts From Human Twins. *J. Periodontal Res.* 32 (1 Pt 2), 90–98. doi: 10.1111/j.1600-0765.1997.tb01387.x

Humphrey, J. D., Dufresne, E. R., and Schwartz, M. A. (2014). Mechanotransduction and Extracellular Matrix Homeostasis. *Nat. Rev. Mol. Cell Biol.* 15 (12), 802–812. doi: 10.1038/nrm3896

Huynh, Q. N., Wang, S., Tafolla, E., Gansky, S. A., Kapila, S., Armitage, G. C., et al. (2002). Specific Fibronectin Fragments as Markers of Periodontal Disease Status. *J. Period.* 73 (10), 1101–1110. doi: 10.1902/jop.2002.73.10.1101

Jang, A. T., Chen, L., Shimotake, A. R., Landis, W., Altoe, V., Aloni, S., et al. (2018). a Force on the Crown and Tug of War in the Periodontal Complex. *J. Dent. Res.* 97 (3), 241–250. doi: 10.1177/0022034517744556

Jin, H., Wang, X., Ying, J., Wong, A. H., Cui, Y., Srivastava, G., et al. (2007). Epigenetic Silencing of a Ca(2+)-Regulated Ras Gtpase-Activating Protein RASAL Defines a New Mechanism of Ras Activation in Human Cancers. *Proc. Natl. Acad. Sci. U.S.A.* 104 (30), 12353–12358. doi: 10.1073/pnas.0700153104

Jobin, M. C., Virdee, I., McCulloch, C. A., and Ellen, R. P. (2007). Activation of MAPK in Fibroblasts by Treponema Denticola Major Outer Sheath Protein. *Biochem. Biophys. Res. Commun.* 356 (1), 213–218. doi: 10.1016/j.bbrc.2007.02.111

Kang, Y. G., Nam, J. H., Kim, K. H., and Lee, K. S. (2010). FAK Pathway Regulates PGE(2) Production in Compressed Periodontal Ligament Cells. *J. Dent. Res.* 89 (12), 1444–1449. doi: 10.1177/0022034510378521

Kanzaki, H., Chiba, M., Shimizu, Y., and Mitani, H. (2002). Periodontal Ligament Cells Under Mechanical Stress Induce Osteoclastogenesis by Receptor Activator of Nuclear Factor Kappab Ligand Up-Regulation Via Prostaglandin E2 Synthesis. *J. Bone Miner Res.* 17 (2), 210–220. doi: 10.1359/jbmr.2002.17.2.210

Kapila, Y. L., Kapila, S., and Johnson, P. W. (1996). Fibronectin and Fibronectin Fragments Modulate the Expression of Proteinases and Proteinase Inhibitors in Human Periodontal Ligament Cells. *Matrix Biol.* 15 (4), 251–261. doi: 10.1016/S0945-053X(96)90116-X

Kapoor, P., and Shen, X. (2014). Mechanisms of Nuclear Actin in Chromatin-Remodeling Complexes. *Trends Cell Biol.* 24 (4), 238–246. doi: 10.1016/j.tcb.2013.10.007

Kinane, J. A., Benakanakere, M. R., Zhao, J., Hosur, K. B., and Kinane, D. F. (2012). *Porphyromonas Gingivalis* Influences Actin Degradation Within Epithelial Cells During Invasion and Apoptosis. *Cell Microbiol.* 14 (7), 1085–1096. doi: 10.1111/j.1462-5822.2012.01780.x

Ko, K. S., Glogauer, M., McCulloch, C. A., and Ellen, R. P. (1998). *Treponema Denticola* Outer Membrane Inhibits Calcium Flux in Gingival Fibroblasts. *Infect. Immun.* 66 (2), 703–709. doi: 10.1128/IAI.66.2.703-709.1998

Letra, A., Ghaneh, G., Zhao, M., Ray, H.Jr., Francisconi, C. F., Garlet, G. P., et al. (2013). MMP-7 and TIMP-1, New Targets in Predicting Poor Wound Healing in Apical Periodontitis. *J. Endod.* 39 (9), 1141–1146. doi: 10.1016/j.joen.2013.06.015

Li, L., Zeng, T. T., Zhang, B. Z., Li, Y., Zhu, Y. H., and Guan, X. Y. (2017). Overexpression of HN1L Promotes Cell Malignant Proliferation in Non-Small Cell Lung Cancer. *Cancer Biol. Ther.* 18 (11), 904–915. doi: 10.1080/15384047.2017.1385678

Manokawinchoke, J., Limjeerajarus, N., Limjeerajarus, C., Sastravaha, P., Everts, V., and Pavasant, P. (2015). Mechanical Force-Induced TGFB1 Increases Expression of SOST/POSTN by Hpdl Cells. *J. Dent. Res.* 94 (7), 983–989. doi: 10.1177/0022034515581372

Miao, D., Fenno, J. C., Timm, J. C., Joo, N. E., and Kapila, Y. L. (2011). the *Treponema Denticola* Chymotrypsin-Like Protease Dentilisin Induces Matrix Metalloproteinase-2-Dependent Fibronectin Fragmentation in Periodontal Ligament Cells. *Infect. Immun.* 79 (2), 806–811. doi: 10.1128/IAI.01001-10

Miao, D., Godovikova, V., Qian, X., Seshadrinathan, S., Kapila, Y. L., and Fenno, J. C. (2014). *Treponema Denticola* Upregulates MMP-2 Activation in Periodontal Ligament Cells: Interplay Between Epigenetics and Periodontal Infection. *Arch. Oral. Biol.* 59 (10), 1056–1064. doi: 10.1016/j.archoralbio.2014.06.003

Misu, S., Takebayashi, M., and Miyamoto, K. (2017). Nuclear Actin in Development and Transcriptional Reprogramming. *Front. Genet.* 8, 27. doi: 10.3389/fgene.2017.00027

Munshi, H. G., Wu, Y. I., Ariztia, E. V., and Stack, M. S. (2002). Calcium Regulation of Matrix Metalloproteinase-Mediated Migration in Oral Squamous Cell Carcinoma Cells. *J. Biol. Chem.* 277 (44), 41480–41488. doi: 10.1074/jbc.M207695200

Nieminen, M. T., Listyarifah, D., Hagström, J., Haglund, C., Grenier, D., Nordström, D., et al. (2018). *Treponema Denticola* Chymotrypsin-Like Proteinase May Contribute to Orodigestive Carcinogenesis Through Immunomodulation. *Br. J. Cancer* 118 (3), 428–434. doi: 10.1038/bjc.2017.409

Osorio, C., Cavalla, F., Paula-Lima, A., Díaz-Araya, G., Vernal, R., Ahumada, P., et al. (2015). H2 O2 Activates Matrix Metalloproteinases Through the Nuclear Factor Kappa B Pathway and Ca(2+) Signals in Human Periodontal Fibroblasts. *J. Periodontal Res.* 50 (6), 798–806. doi: 10.1111/jre.12267

Pattamapun, K., Tiranathanagul, S., Yongchaitrakul, T., Kuwatanasuchat, J., and Pavasant, P. (2003). Activation of MMP-2 by Porphyromonas Gingivalis in Human Periodontal Ligament Cells. *J. Periodontal Res.* 38 (2), 115–121. doi: 10.1034/j.1600-0765.2003.01650.x

Ruby, J., Martin, M., Passineau, M. J., Godovikova, V., Fenno, J. C., and Wu, H. (2018). Activation of the Innate Immune System by *Treponema Denticola* Periplasmic Flagella Through Toll-Like Receptor 2. *Infect. Immun.* 86 (1), e00573–17. doi: 10.1128/IAI.00573-17

Sadhukhan, S., Sarkar, K., Taylor, M., Candotti, F., and Vyas, Y. M. (2014). Nuclear Role of Wasp in Gene Transcription is Uncoupled From Its ARP2/3-Dependent Cytoplasmic Role in Actin Polymerization. *J. Immunol.* 193 (1), 150–160. doi: 10.4049/jimmunol.1302923

Sanka, K., Maddala, R., Epstein, D. L., and Rao, P. V. (2007). Influence of Actin Cytoskeletal Integrity on Matrix Metalloproteinase-2 Activation in Cultured Human Trabecular Meshwork Cells. *Invest. Ophthalmol. Vis. Sci.* 48 (5), 2105–2114. doi: 10.1167/iovs.06-1089

Serebryannyy, L. A., Cruz, C. M., and de Lanerolle, P. (2016). a Role for Nuclear Actin in HDAC 1 and 2 Regulation. *Sci. Rep.* 6, 28460. doi: 10.1038/srep28460

Socransky, S. S., Haffajee, A. D., Cugini, M. A., Smith, C., and Kent, R. L.Jr. (1998). Microbial Complexes in Subgingival Plaque. *J. Clin. Periodontol.* 25 (2), 134–144. doi: 10.1111/j.1600-051X.1998.tb02419.x

Takeuchi, Y., Umeda, M., Sakamoto, M., Benno, Y., Huang, Y., and Ishikawa, I. (2001). *Treponema Socranskii, Treponema Denticola, and Porphyromonas Gingivalis* are Associated With Severity of Periodontal Tissue Destruction. *J. Periodontol.* 72 (10), 1354–1363. doi: 10.1902/jop.2001.72.10.1354

Tiranathanagul, S., Pattamapun, K., Yongchaitrakul, T., and Pavasant, P. (2004). MMP-2 Activation by *Actinobacillus Actinomycetemcomitans* Supernatant in Human PDL Cells was Corresponded With Reduction of TIMP-2. *Oral. Dis.* 10 (6), 383–388. doi: 10.1111/j.1601-0825.2004.01044.x

Tsuji, K., Uno, K., Zhang, G. X., and Tamura, M. (2004). Periodontal Ligament Cells Under Intermittent Tensile Stress Regulate Mrna Expression of Osteoprotegerin and Tissue Inhibitor of Matrix Metalloprotease-1 and -2. *J. Bone Miner Metab.* 22 (2), 94–103. doi: 10.1007/s00774-003-0456-0

Visa, N., and Percipalle, P. (2010). Nuclear Functions of Actin. *Cold Spring Harb. Perspect. Biol.* 2 (4), a000620. doi: 10.1101/cshperspect.a000620

Visser, M. B., Koh, A., Glogauer, M., and Ellen, R. P. (2011). *Treponema Denticola* Major Outer Sheath Protein Induces Actin Assembly At Free Barbed Ends by a PIP2-Dependent Uncapping Mechanism in Fibroblasts. *PloS One* 6 (8), e23736. doi: 10.1371/journal.pone.0023736

Wang, W. Y., Davidson, C. D., Lin, D., and Baker, B. M. (2019). Actomyosin Contractility-Dependent Matrix Stretch and Recoil Induces Rapid Cell Migration. *Nat. Commun.* 10 (1), 1186. doi: 10.1038/s41467-019-09121-0

Wang, Q., Ko, K. S., Kapus, A., McCulloch, C. A., and Ellen, R. P. (2001). a Spirochete Surface Protein Uncouples Store-Operated Calcium Channels in Fibroblasts: A Novel Cytotoxic Mechanism. *J. Biol. Chem.* 276 (25), 23056–23064. doi: 10.1074/jbc.M011735200

Yakob, M., Meurman, J. H., Sorsa, T., and Söder, B. (2013). *Treponema Denticola* Associates With Increased Levels of MMP-8 and MMP-9 in Gingival Crevicular Fluid. *Oral. Dis.* 19 (7), 694–701. doi: 10.1111/odi.12057

Yamada, M., Ikegami, A., and Kuramitsu, H. K. (2005). Synergistic Biofilm Formation by *Treponema Denticola and Porphyromonas Gingivalis*. *FEMS Microbiol. Lett.* 250 (2), 271–277. doi: 10.1016/j.femsle.2005.07.019

Yang, P. F., Song, M., Grove, D. A., and Ellen, R. P. (1998). Filamentous Actin Disruption and Diminished Inositol Phosphate Response in Gingival Fibroblasts Caused by Treponema Denticola. *Infect. Immun.* 66 (2), 696–702. doi: 10.1128/IAI.66.2.696-702.1998

Yilmaz, O., Young, P. A., Lamont, R. J., and Kenny, G. E. (2003). Gingival Epithelial Cell Signalling and Cytoskeletal Responses to *Porphyromonas Gingivalis* Invasion. *Microbiol. (Reading)* 149 (Pt 9), 2417–2426. doi: 10.1099/mic.0.26483-0

Zhang, J., Guo, J., Dzhagalov, I., and He, Y. W. (2005). an Essential Function for the Calcium-Promoted Ras Inactivator in Fcgamma Receptor-Mediated Phagocytosis. *Nat. Immunol.* 6 (9), 911–919. doi: 10.1038/ni1232

Zhang, W., Ju, J., Rigney, T., and Tribble, G. (2013). Integrin Alpha5beta1-Fimbriae Binding and Actin Rearrangement are Essential for *Porphyromonas Gingivalis* Invasion of Osteoblasts and Subsequent Activation of the JNK Pathway. *BMC Microbiol.* 13, 5. doi: 10.1186/1471-2180-13-5

Zhao, K., Wang, W., Rando, O. J., Xue, Y., Swiderek, K., Kuo, A., et al. (1998). Rapid and Phosphoinositol-Dependent Binding of the SWI/SNF-Like BAF Complex to Chromatin After T Lymphocyte Receptor Signaling. *Cell* 95 (5), 625–636. doi: 10.1016/S0092-8674(00)81633-5

Conflict of Interest: The authors declare that the research was conducted in the absence of any commercial or financial relationships that could be construed as a potential conflict of interest.

frontiers in Cellular and Infection Microbiology

ORIGINAL RESEARCH
published: 28 May 2021
doi: 10.3389/fcimb.2021.658203

Association Between Oral Microbiota and Cigarette Smoking in the Chinese Population

Yi-Jing Jia[1,2†], Ying Liao[2†], Yong-Qiao He[2], Mei-Qi Zheng[2], Xia-Ting Tong[1,2], Wen-Qiong Xue[2], Jiang-Bo Zhang[2], Lei-Lei Yuan[1,2], Wen-Li Zhang[2] and Wei-Hua Jia[1,2]*

[1] School of Public Health, Sun Yat-sen University, Guangzhou, China, [2] State Key Laboratory of Oncology in South China, Collaborative Innovation Center for Cancer Medicine, Guangdong Key Laboratory of Nasopharyngeal Carcinoma Diagnosis and Therapy, Sun Yat-sen University Cancer Center, Guangzhou, China

The oral microbiota has been observed to be influenced by cigarette smoking and linked to several human diseases. However, research on the effect of cigarette smoking on the oral microbiota has not been systematically conducted in the Chinese population. We profiled the oral microbiota of 316 healthy subjects in the Chinese population by 16S rRNA gene sequencing. The alpha diversity of oral microbiota was different between never smokers and smokers (P = 0.002). Several bacterial taxa were first reported to be associated with cigarette smoking by LEfSe analysis, including *Moryella* (q = 1.56E-04), *Bulleidia* (q = 1.65E-06), and *Moraxella* (q = 3.52E-02) at the genus level and *Rothia dentocariosa* (q = 1.55E-02), *Prevotella melaninogenica* (q = 8.48E-08), *Prevotella pallens* (q = 4.13E-03), *Bulleidia moorei* (q = 1.79E-06), *Rothia aeria* (q = 3.83E-06), *Actinobacillus parahaemolyticus* (q = 2.28E-04), and *Haemophilus parainfluenzae* (q = 4.82E-02) at the species level. Two nitrite-producing bacteria that can increase the acidity of the oral cavity, *Actinomyces* and *Veillonella*, were also enriched in smokers with FDR-adjusted q-values of 3.62E-06 and 1.10E-06, respectively. Notably, we observed that two acid production-related pathways, amino acid-related enzymes (q = 6.19E-05) and amino sugar and nucleotide sugar metabolism (q = 2.63E-06), were increased in smokers by PICRUSt analysis. Finally, the co-occurrence analysis demonstrated that smoker-enriched bacteria were significantly positively associated with each other and were negatively correlated with the bacteria decreased in smokers. Our results suggested that cigarette smoking may affect oral health by creating a different environment by altering bacterial abundance, connections among oral microbiota, and the microbiota and their metabolic function.

Keywords: oral microbiota, cigarette smoking, 16S rRNA gene sequencing, China, saliva

OPEN ACCESS

Edited by:
Sinem Esra Sahingur, University of Pennsylvania, United States

Reviewed by:
Oleh Andrukov, University Dental Clinic Vienna, Austria
Laura de Freitas, University of São Paulo, Brazil

***Correspondence:**
Wei-Hua Jia
jiawh@sysucc.org.cn

†These authors have contributed equally to this work and share first authorship

Specialty section:
This article was submitted to Bacteria and Host, a section of the journal Frontiers in Cellular and Infection Microbiology

Received: *25 January 2021*
Accepted: *19 April 2021*
Published: *28 May 2021*

Citation:
Jia Y-J, Liao Y, He Y-Q, Zheng M-Q, Tong X-T, Xue W-Q, Zhang J-B, Yuan L-L, Zhang W-L and Jia W-H (2021) Association Between Oral Microbiota and Cigarette Smoking in the Chinese Population. Front. Cell. Infect. Microbiol. 11:658203. doi: 10.3389/fcimb.2021.658203

INTRODUCTION

The human oral cavity is colonized by more than 600 different bacterial species together with viruses and fungi, which collectively compose the oral microbiota (Dewhirst et al., 2010). The balance of the oral microbiota is essential to maintaining human health. Oral dysbiosis is related not only to oral health issues, such as dental caries, periodontal diseases, and tooth loss (Yang et al., 2012; Teles et al., 2013), but

also to systemic diseases, such as cardiovascular disease, diabetes, and even cancer (Koren et al., 2011; Galvão-Moreira and da Cruz, 2016; Long et al., 2017). Thus, maintaining normal and healthy oral microbiota is important for human health.

China is the largest producer and consumer of tobacco in the world. Cigarette smoking is a common risk factor affecting public health (Hu et al., 2006). Cigarette smoke contains numerous toxic substances. The oral cavity is the first part of the body that comes into contact with smoke. Thus, the oral microbiota has the greatest potential to be affected by smoke. The toxicants in cigarette smoke can interfere with oral microbial ecology *via* antibiotic effects and oxygen deprivation (Macgregor, 1989).

Cigarette smoking is a cause of oral dysbiosis that affects the diversity of oral microbiota and their functional potential (Mason et al., 2015; Wu et al., 2016; Yu et al., 2017; Yang et al., 2019). In addition, Wu et al. studied the effects of cigarette smoking on oral wash samples among American adults and observed that smoking may affect oral microbiota by promoting an anaerobic oral environment (Wu et al., 2016). Yang et al. investigated cigarette smoking in relation to the oral microbiota of mouth rinse samples in low-income and African-American populations, and they observed that changes in oral microbiota caused by cigarette smoking were recovered after smoking cessation (Yang et al., 2019). Sato et al. observed in East Asians that tongue microbiota and related metagenomic pathways of current smokers differ from those of never smokers (Sato et al., 2020b).

The oral ecological environment is affected by many external factors and exhibits considerable individual differences. For instance, a study determined the distinctiveness of the saliva microbiome of humans living under different climatic conditions (Li et al., 2014). Genetic variations of the host were also reported to influence the oral microbiota (Demmitt et al., 2017). Therefore, the effect of cigarette smoking on the overall oral microbiota may depend on geographic or ethnic background. Epidemiological studies exploring the effect of cigarette smoking on the composition of the oral microbiota in Chinese people remain lacking. Therefore, the relationship between the oral microbiota and cigarette smoking in China warrants further investigation.

The aim of this study was to improve our understanding of the impact of cigarette smoking on the oral microbiota in the Chinese population. In this work, we employed saliva bacterial 16S rRNA gene sequencing to conduct an oral microbial study of 316 subjects from three areas of China. We recruited individuals from three areas in southern, northern and northeastern China with large latitude differences, distinct dietary habits, and different life habits. This study may provide a useful opportunity to further assess the consistent relationship between cigarette smoking and the oral microbiota and add findings from the Chinese population.

MATERIALS AND METHODS

Study Population and Saliva Sample Collection

Three populations from (1) Guangdong Province (defined as the GD population), (2) Yangquan city in Shanxi Province (defined as the YQ population), and (3) Mishan city in Heilongjiang Province (defined as the MS population) were included in our study. These populations have been previously described in detail (He et al., 2019). Briefly, 1223 adults with a mean age (± SD) of 46.89 ± 11.47 years were recruited between 1 October 2015 and 1 August 2016 in the GD population. A total of 2416 adults with a mean age (± SD) of 46.74 ± 11.16 years were recruited between 1 May and 1 October 2014 in the YQ population. A total of 1279 adults with a mean age (± SD) of 46.17 ± 11.48 years were recruited between 1 May and 1 September 2015 in the MS population. At the enrollment step, saliva samples were collected. Informed consent was signed by every subject before the interview, and the Human Ethics Committee of Sun Yat-sen University Cancer Center reviewed and approved the proposal for the study (the approval number: GZR2013-008).

In the present study, we conducted stratified random sampling by age and sex from three populations. A subset of 316 subjects were included in the present study, including 150 from the GD population, 81 from the YQ population, and 85 from the MS population. Comprehensive demographic and lifestyle information was collected using face-to-face interviews conducted by well-trained investigators. Current smokers were defined as subjects who smoked at least one cigarette every one to three days in the past year. Former smokers were defined as subjects who smoked at least one cigarette every one to three days but had quit smoking for at least a year. Never smokers were defined as subjects who had never smoked at least one cigarette every one to three days. We found former and current smokers overlapped on the principal coordinate analysis plot (**Supplementary Figure 1A**). The overall microbiota composition of former smokers tended to be more similar to current smokers than never smokers (**Supplementary Figure 1B**). And given the number of ever smokers in this study is small, in order to increase the statistical power, we combined ever smokers and current smokers into one smokers group. Unstimulated whole saliva samples were collected from participants during study enrollment. All participants were asked not to eat or drink for half an hour before providing samples. Five milliliters of saliva were collected into a 50-ml centrifuge tube. We added an equal volume of salivary lysate to the saliva to facilitate subsequent nucleic acid extraction. The salivary lysate included Tris-HCL (pH=8.0), EDTA, sucrose, NaCl and 10% SDS. Then the saliva samples were divided into 2-ml EP tubes and were subsequently stored at −80°C until use.

DNA Extraction and 16S rRNA Gene Sequencing

Bacterial genomic DNA was extracted from saliva samples using the Powersoil DNA isolation kit (Qiagen, Duesseldorf, Hilden, Germany) with the bead-beating method according to the manufacturer's instructions. Amplicon libraries were generated following an optimized protocol based on a previously described method (Gohl et al., 2016) with slight modifications. Briefly, the V4 variable region of the 16S rRNA gene was amplified with forward and reverse primers containing common adapter sequences and 12-bp barcodes: [barcode] +

[overhang] + 515F/806R (GTGCCAGCMGCCGCGGTAA/GGACTACHVGGGTWTCTAAT) (Caporaso et al., 2011) with 20 cycles. Next, the Illumina flow cell adapters and dual indices (6 bp) were added in a secondary amplification with 10 cycles of amplification. PCR products were visualized with nucleic acid gel electrophoresis, purified using Agencourt AMPure XP (Beckman Coulter, Brea, CA, USA), and quantified using the Qubit HS kit (Invitrogen, Carlsbad, MA, USA). Pooled amplicon libraries were sequenced using the Illumina MiSeq 250-bp paired-end strategy.

Sequencing Data Processing and Quality Controls

QIIME2 version 2019.4 was utilized to process and analyze 16S rRNA gene amplicon sequences (Bolyen et al., 2019). Multiplexed libraries were deconvoluted based on the barcodes assigned to each sample. After demultiplexing, quality control and paired-end read joining were performed with DADA2 (Callahan et al., 2016). Pre-processed sequences were clustered into amplicon sequence variants (ASVs). ASVs observed in fewer than three samples and with total abundances of less than five were excluded. All quality-checked reads were mapped to each OTU with > 99% identity using the Greengenes database 13.8 (McDonald et al., 2012) predefined taxonomy map of reference sequences. To detect possible bacteria in reagents and environmental contamination obtained in the course of the experiment, we used negative control samples in the processes of DNA extraction and construction of the PCR library. After the above steps with QIIME2, read counts from negative control samples were negligible compared to saliva samples (**Supplementary Figure 2**).

Statistical Analysis

We used chi-square tests for categorical variables and Student's t tests for continuous variables. A P-value < 0.05 was considered to be significant. For the diversity analysis of 16S rRNA data, samples were rarefied to 10000 sequences per sample. The alpha diversity of the saliva microbiota between never smokers and smokers was measured by the Shannon's diversity index (Lozupone and Knight, 2008). The beta diversity was assessed using weighted UniFrac distance matrices (Lozupone et al., 2007). Permutational multivariate analysis of variance (PERMANOVA; adonis function, vegan package, R) of the weighted UniFrac distance was employed to test differences in overall oral microbiome composition across smoking and nonsmoking groups. Principal coordinate analysis (PCoA) was performed to obtain principal coordinates and visualize complex, multidimensional data. The significance level was $P < 0.05$.

The detection of the difference in the relative abundance of features at the phylum, class, order, family, genus, and species levels between never smokers and smokers was performed using the linear discriminant analysis effect size (LEfSe) method (Segata et al., 2011). We used the online galaxy server (https://huttenhower.sph.harvard.edu/galaxy/) to identify differentially abundant bacterial taxa between never smokers and smokers. Features with logarithmic LDA scores for discriminative features > 2.0 and false discovery rate (FDR)-adjusted q-values < 0.05 were considered to be significant. Next, we investigated potential interactions of features at the genus and species levels by network analysis of taxa co-occurrence patterns using SparCC (Friedman and Alm, 2012). Cytoscape (version 3.7.1) was employed to establish the genus-genus and species-species networks. Only Spearman's correlation coefficients > 0.4 or < −0.4 and with P-values < 0.05 are shown.

Phylogenetic Investigation of Communities by Reconstruction of Unobserved States (PICRUSt) (http://galaxy.morganlangille.com/) was used to infer the functional shifts in the microbiota of never smokers and smokers. PICRUSt can predict the Kyoto Encyclopedia of Genes and Genomes (KEGG) pathway functional profiles of microbial communities *via* 16S rRNA gene sequences (Langille et al., 2013). Statistical Analysis of Metagenomic Profiles (STAMP) was employed to compute the abundance differences of KEGG pathways. False discovery rate (FDR)-adjusted q-values less than 0.05 were considered to be significant. Next, we used Spearman's rank correlation to examine the associations between pathways and genera and species that were significantly associated with smoking status. Pathways with average relative abundance > 1% were included.

All statistical tests were two-sided, and all statistical analyses were performed using R version 3.6.3.

RESULTS

Characteristics of the Study Participants

Our study included 316 subjects from China who provided valid informed consent, a completed questionnaire on smoking status, and a saliva sample. Our population was recruited from three areas in China, which included 150 from the GD population, 81 from the YQ population, and 85 from the MS population. Demographic characteristics of the subjects in each region were shown in **Supplementary Table 1**. Age, gender, and smoking status were equally comparable among three populations. The education level was significantly different and more people were under high school in GD population.

Bacterial Diversity and Community Structure of Saliva Microbiota

To investigate the effects of smoking status on oral microbiota diversity, we examined the bacterial diversity of salivary microbiota in different smoking statuses. The Shannon diversity index, an alpha diversity estimator, was significantly higher in smokers than in never smokers ($P = 0.002$) (**Figure 1A**). Next, we performed a principal coordinate analysis based on weighted UniFrac distances to determine whether the overall microbiota composition differed according to smoking status. **Figure 1B** presents a PCoA plot based on the weighted UniFrac distances. Although there was no significant difference between never smokers and smokers in the overall bacterial community structure of saliva according to ANOSIM ($P = 0.456$), we observed separate trends between the two groups.

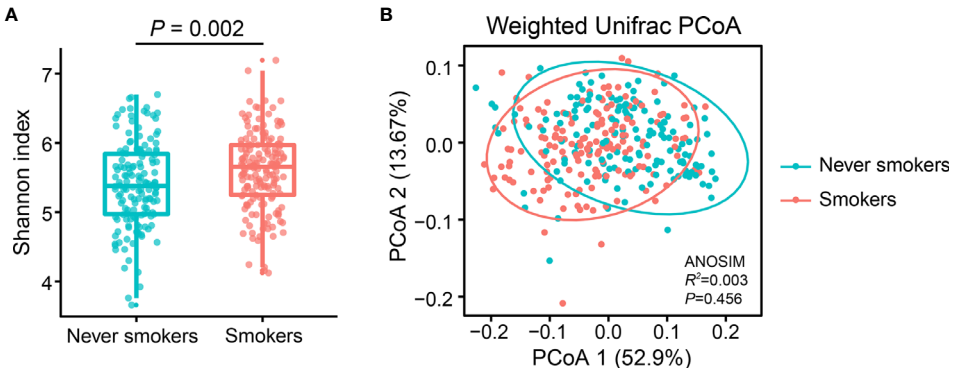

FIGURE 1 | Alpha and beta diversity estimates of the oral microbial community. **(A)** Comparison of Shannon index in the oral microbiota between never smokers and smokers (P = 0.002). **(B)** PCoA based on the weighted UniFrac distances of the oral microbial communities between never smokers and smokers.

Bacterial Taxa With a Significant Differential Abundance Between Never Smokers and Smokers

To further explore the effects of smoking status on specific bacteria, LEfSe analysis was performed to investigate the differentially abundant taxa between never smokers and smokers. We observed 53 differentially abundant taxa between never smokers and smokers that reached significance with a log LDA score > 2.0 and FDR q-value < 0.05 in the total population (**Supplementary Table 2**). Among these taxa, there were 18 differentially abundant taxa at the genus level and 10 differentially abundant taxa at the species level (**Table 1** and **Figure 2**).

At the genus level, *Actinomyces, Atopobium, Prevotella, Moryella, Oribacterium, Megasphaera, Veillonella, Bulleidia*, and *Campylobacter* were significantly enriched in smokers. *Peptococcus, Lautropia, Eikenella, Kingella, Neisseria, Cardiobacterium, Aggregatibacter, Haemophilus*, and *Moraxella* were significantly depleted in smokers. Among these genera, *Moryella, Bulleidia*, and *Moraxella* were first observed to be significantly different in smoking status. In addition, at the species level, *Rothia dentocariosa, Prevotella melaninogenica, Prevotella pallens, Veillonella dispar*, and *Bulleidia moorei* were determined to be significantly enriched in smokers. *Rothia aeria, Neisseria oralis, Neisseria subflava, Actinobacillus parahaemolyticus*, and *Haemophilus parainfluenzae* were significantly depleted in smokers. These species, except for *Veillonella dispar, Neisseria oralis*, and *Neisseria subflava*, were first found to have significant differences in smoking status. The bacteria enriched in smokers primarily belonged to the phyla *Actinobacteria, Bacteroidetes*, and *Firmicutes*. Conversely, the bacteria that decreased in smokers primarily belonged to the *Proteobacteria* phylum.

We analyzed the distribution of these bacteria in three populations separately to identify whether the oral taxa consistently altered by cigarette smoking were independent of climate environment and lifestyle (**Supplementary Table 2** and **Figure 2**). For 18 differentially abundant genera and 10 differentially abundant species in the total population, these bacteria showed consistent abundance changes in all three areas. Taking P < 0.05 as the standard, 11 genera and 7 species exhibited significant differences in at least two areas. Taking q < 0.05 as the standard, 4 genera and 5 species exhibited significant differences in at least two areas. Among these bacteria, *Atopobium* remained significantly different (q < 0.05) in the three populations. *Actinomyces*, *Veillonella*, *Bulleidia*, *Rothia aeria*, *Prevotella melaninogenica*, *Veillonella dispar*, *Bulleidia moorei*, and *Neisseria oralis* maintained (q < 0.05) significant differences in the two populations. Although the results were not completely consistent across the three different populations, the trend was the same. This finding may be attributable to the small number of people in independent areas, as no significant difference was observed.

Co-Occurrence Network of the Bacteria in the Saliva Microbiota

We used SparCC and Cytoscape to construct network structures to analyze co-occurrence and co-excluding relationships at the genus and species levels. Genera and species correlations that met the threshold of Spearman's r > 0.4 and P < 0.05 are shown in the networks (**Figure 3**). At the genus level (**Figure 3A**), there were 29 nodes and 58 edges (including 48 positive correlations and 10 negative correlations). At the species level (**Figure 3B**), there were 15 nodes and 16 edges (14 positive correlations and 2 negative correlations). Analysis of the bacterial correlation coefficients showed distinct clusters separated by smoking status. From the co-occurrence network, we observed that the bacteria that were significantly enriched in smokers had a strong positive correlation but a negative correlation with the bacteria that were decreased in smokers. At the genus level, *Prevotella*, *Veillonella*, *Atopobium*, *Megasphaera*, and *Bulleidia* were the top five genera with hubs with more than 6 linkers. Notably, all of these genera were smoker-enriched taxa (**Figure 3A**). *Veillonella* showed the strongest correlation with *Actinomyces* (r = 0.70). At the species level, *Prevotella melaninogenica*, *Prevotella pallens*, *Bulleidia moorei*, *Lachnoanaerobaculum orale*, and *Neisseria subflava* were the top five hubs with more than 2 linkers.

TABLE 1 | Differentially abundant taxa at the genus and species level between never smokers and smokers.

Taxa	Detectable rate (%)		Average relative abundance (%)		LDA score	*q*-value[a]
	Never smokers (n=150)	Smokers (n=166)	Never smokers (n=150)	Smokers (n=166)		
Phylum Actinobacteria						
Genus Actinomyces	100.00	100.00	1.56	2.33	3.60	3.62E-06
Species Rothia aeria	96.67	82.00	0.42	0.21	3.04	3.83E-06
Species Rothia dentocariosa	80.67	88.00	0.26	0.33	2.60	1.55E-02
Genus Atopobium	88.00	97.33	0.23	0.58	3.25	1.87E-11
Phylum Bacteroidetes						
Genus Prevotella	100.00	100.00	10.96	15.06	4.30	1.84E-05
Species Prevotella melaninogenica	100.00	100.00	4.80	8.07	4.19	8.48E-08
Species Prevotella pallens	98.67	100.00	1.23	1.69	3.30	4.13E-03
Phylum Firmicutes						
Genus Moryella	85.33	96.67	0.16	0.25	2.69	1.56E-04
Genus Oribacterium	98.67	100.00	0.44	0.53	2.63	1.72E-03
Genus Peptococcus	83.33	72.67	0.05	0.03	2.10	3.07E-03
Genus Megasphaera	84.00	96.67	0.38	0.82	3.34	3.29E-09
Genus Veillonella	100.00	100.00	5.36	7.79	4.07	1.10E-06
Species Veillonella dispar	90.67	93.33	2.20	3.69	3.86	8.22E-05
Genus Bulleidia	98.67	98.67	0.30	0.44	2.85	1.65E-06
Species Bulleidia moorei	98.67	98.67	0.29	0.42	2.82	1.79E-06
Phylum Proteobacteria						
Genus Lautropia	98.00	96.00	1.06	0.70	3.25	5.59E-04
Genus Eikenella	99.33	100.00	1.06	0.69	3.30	1.65E-02
Genus Kingella	69.33	58.00	0.07	0.04	2.11	3.48E-02
Genus Neisseria	100.00	100.00	19.43	15.25	4.31	3.38E-04
Species Neisseria oralis	93.33	78.67	0.70	0.25	3.36	3.97E-09
Species Neisseria subflava	100.00	100.00	14.96	12.11	4.16	1.18E-02
Genus Campylobacter	100.00	100.00	0.78	0.93	2.87	2.54E-02
Genus Cardiobacterium	88.00	78.00	0.11	0.05	2.43	3.74E-06
Species Actinobacillus parahaemolyticus	64.67	40.00	0.48	0.18	3.17	2.28E-04
Genus Aggregatibacter	98.00	98.00	1.82	1.53	3.18	3.85E-02
Genus Haemophilus	100.00	100.00	8.14	6.53	3.91	7.16E-03
Species Haemophilus parainfluenzae	100.00	100.00	7.19	5.97	3.79	4.82E-02
Genus Moraxella	43.33	20.67	0.54	0.19	3.29	3.52E-02

[a]*False discovery rate adjusted q-values were calcualated based based on P-values from the LefSe analysis.*

Among these species, *Prevotella melaninogenica* showed the strongest correlation with *Prevotella pallens* (r = 0.72).

Correlation Between Saliva Microbiota and Predictive Functional Pathways

To investigate the functional role of the oral microbiota in different smoking statuses, PICRUSt analysis was performed to explore microbiome function based on inferred metagenomes. Of 328 KEGG pathways identified, we excluded pathways that occurred in less than 30% of participants and with an average relative abundance below 1%. Twelve discernible microbiota pathways were clearly different between never smokers and smokers (q < 0.01, **Supplementary Table 3**). These pathways included pathways related to environmental information processing, genetic information processing, and metabolism. We found that smokers showed a higher abundance of most pathways from genetic information processing and metabolism but showed a lower abundance of pathways associated with environmental information processing (**Figure 4A**). Notably, pathways related to acid production (amino acid-related enzymes and amino sugar and nucleotide sugar metabolism, q = 6.19E-05 and q = 2.63E-06, respectively) were all enriched in smokers. Next, we analyzed the correlation between differentially abundant pathways and genera/species to explore whether the bacteria altered by cigarette smoking were necessarily related to many of these pathways (**Figures 4B, C**). We observed that genera and species enriched in smokers were positively associated with the KEGG pathways increased in smokers. The bacteria significantly enriched in smokers had similar functions but had a distinct difference in function from those decreased in smokers.

DISCUSSION

In this study, we compared the saliva microbiota composition of never smokers and smokers, as well as the functional profiles of the saliva samples, using 16S rRNA sequencing data. We observed a clear difference in the saliva microbiota and related metagenomic pathways between never smokers and smokers. Previous studies on the association between cigarette smoking and oral microbiota have primarily focused on non-Asian populations. To the best of our knowledge, this report describes the first relatively systematic study to demonstrate cigarette smoking-associated oral microbial alterations in a Chinese population.

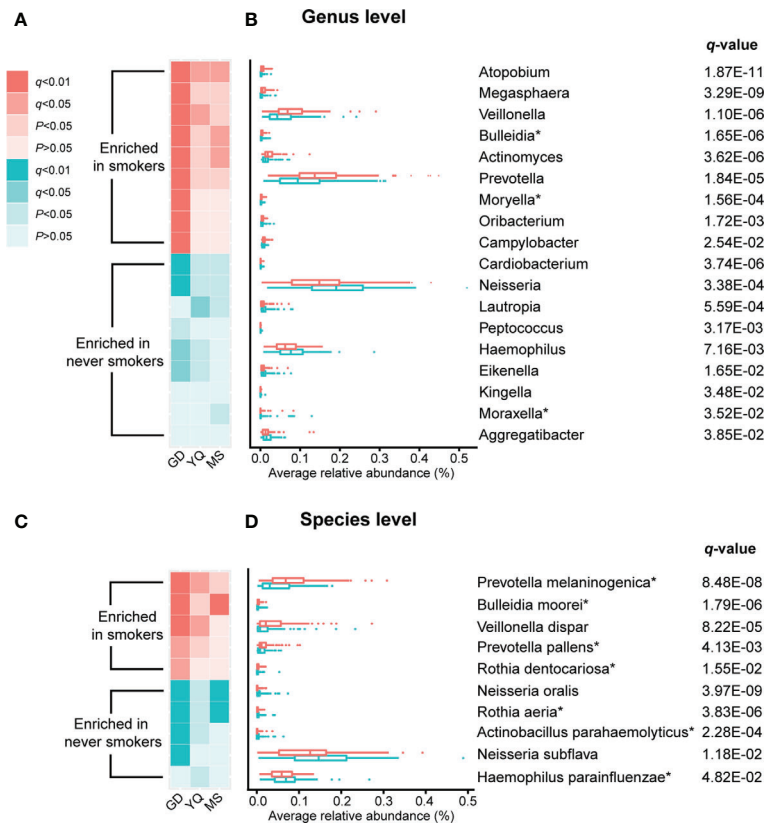

FIGURE 2 | The result of comparison of bacterial abundance at the genus level and species level. **(A, C)** The heatmaps show the *q*-value and *P*-value of these differentially abundant taxa in Guangdong, Yangquan, and Mishan populations. **(B, D)** The box plots show the average relative abundances of differentially abundant taxa in total populations. * Means bacterium has been found firstly to differ significantly between never smokers and smokers in our study.

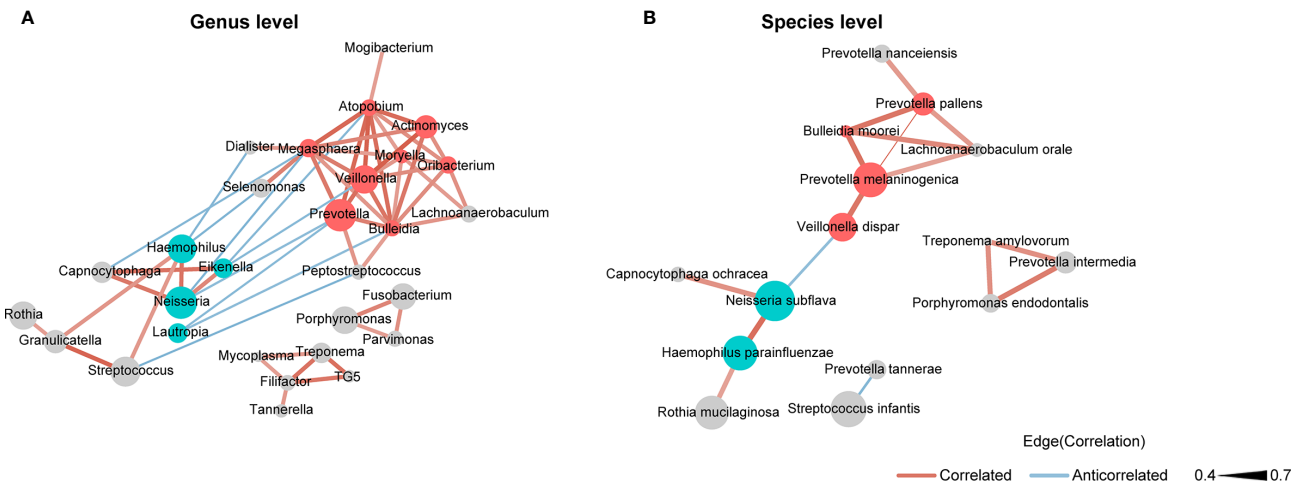

FIGURE 3 | Co-occurrence network of **(A)** the genera and **(B)** the species in oral microbiota. The sizes of the nodes indicate the mean relative abundance of the corresponding bacteria. The red nodes represent bacteria that were enriched in smokers. The blue nodes represent bacteria that were decreased in smokers. The gray nodes represent bacteria that were not identified as being significantly associated to smokers or never smokers. The width of the lines reflects the strength of correlation and the color of the lines, red or blue, indicates a positive or negative correlation, respectively.

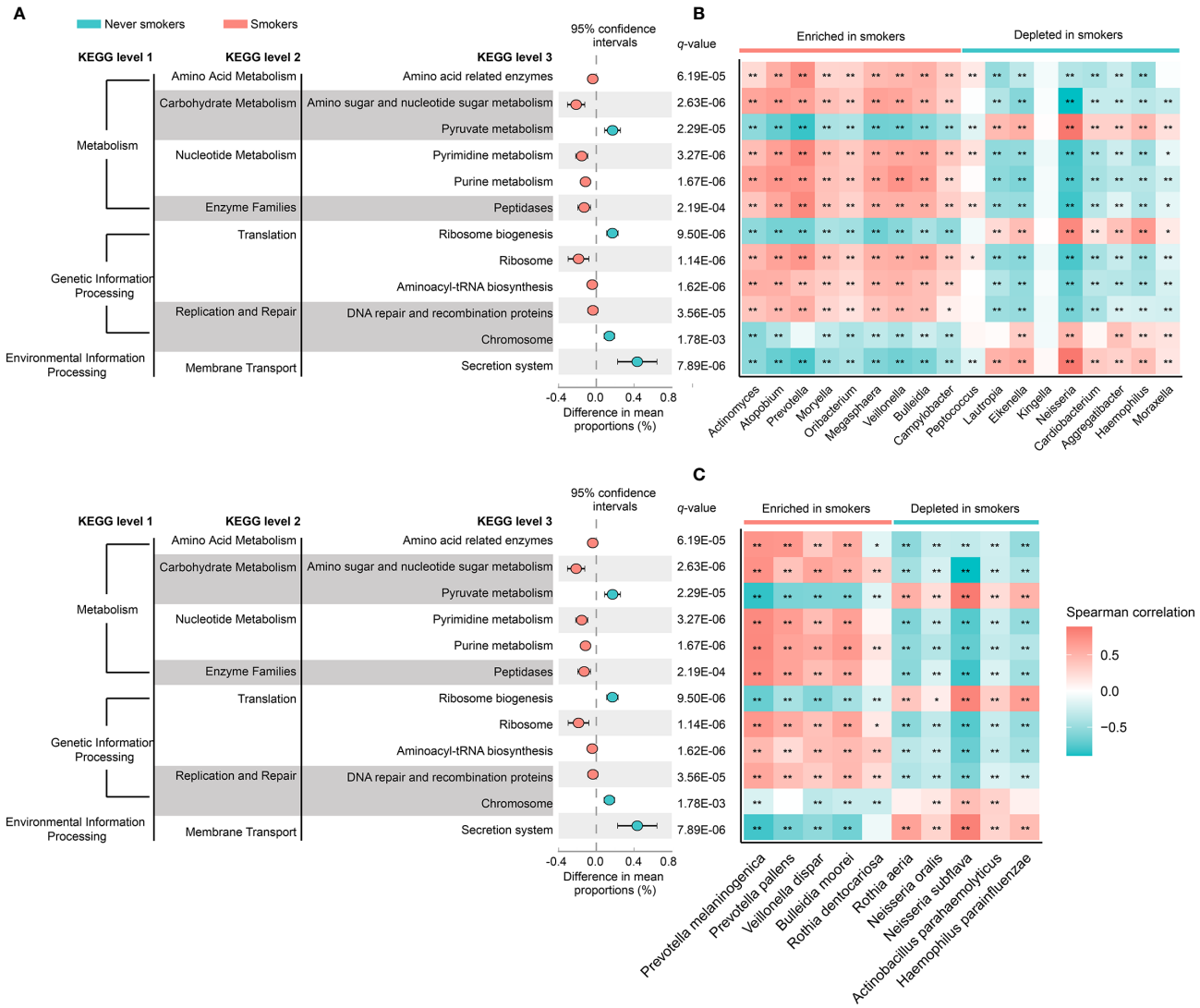

FIGURE 4 | **(A)** The different analysis of microbial community functions between never smokers and smokers (KEGG pathways average relative abundance > 1%). Difference in mean proportion for pathways showing significant difference in abundance are shown. The 95% confidence intervals and statistical significance (FDR *q*-value) are indicated as well. **(B)** Heatmap of spearman correlation between differentially abundant genera and above-mentioned pathways. **(C)** Heatmap of spearman correlation between differentially abundant species and above-mentioned pathways. The strength of the color depicts the Spearman's correlation coefficients (negative score, blue; positive score, red). $^{*}P < 0.05$, $^{**}P < 0.01$.

In the present study, the influence of cigarette smoking on the diversity and overall composition of oral microbiota was analyzed. We found that the Shannon diversity index was different between never smokers and smokers, and the difference was significant. This result indicated differences in richness and evenness between never smokers and smokers. Beta diversity exhibited separate trends but no significant difference between the two groups. Our findings suggested that the oral microbiota of former smokers was more similar to that of current smokers than never smokers. This suggested that the effects of cigarette smoking on oral microbiota may persist for years. In addition, we found that the majority of the observed taxa were present in both the never smoker and smoker groups, albeit at different frequencies of detection. Fifty-three taxa were found to be significantly different between never smokers and smokers, including 18 genera and 10 species. These taxa were primarily distributed in four bacterial phyla: *Actinobacteria*, *Bacteroidetes*, *Firmicutes*, and *Proteobacteria*. This observation was in accordance with previous studies (Wu et al., 2016; Yang et al., 2019). At the genus level, most of the differentially abundant taxa that we identified were consistent with those observed in previous studies (Camelo-Castillo et al., 2015; Wu et al., 2016; Yang et al., 2019; Sato et al., 2020b; Wirth et al., 2020), except for *Moryella, Bulleidia*, and *Moraxella*. The previous 16S rRNA gene sequences on cigarette smoking and oral microbiota have been less thoroughly investigated at the species level. *Rothia aeria*,

Rothia dentocariosa, *Prevotella melaninogenica*, *Prevotella pallens*, *Bulleidia moorei*, *Actinobacillus parahaemolyticus*, and *Haemophilus parainfluenzae* were all first identified in our study, and *Veillonella dispar* (Sato et al., 2020a), *Neisseria oralis*, and *Neisseria subflava* (Yang et al., 2019) were not.

To further explore whether the influence of cigarette smoking on saliva microbiota was stable in different populations from distinct environments, we performed LEfSe analysis in GD, YQ, and MS populations separately. We found a consistent alteration trend of the abundance of taxa according to smoking status, although some of them could not reach a significant *P*-value. We still found that 11 genera and 7 species had significant differences in at least two areas at the standard of $P < 0.05$, indicating that the effect of cigarette smoking on oral microbiota was stable even under different climatic conditions and living habits. *Atopobium* remained significantly different in all three populations with $q < 0.05$, indicating that *Atopobium* may be the bacterium that is most affected by cigarette smoking.

The relationships between diseases and oral microbiota were previously investigated in several studies. We found that the bacteria associated with diseases were primarily increased in smokers. For example, *Actinomyces* contributed to the development of oral diseases, such as caries and periodontitis (Kolenbrander, 2000). *Actinomyces* in saliva microbiota was also reported to be related to liver cancer progression. (Li et al., 2020). A previous study showed the association between *Atopobium* in tissue and oral squamous cell carcinoma (Perera et al., 2018). Another study showed that *Actinomyces* and *Atopobium* in saliva were both related to a high risk of esophageal squamous cell carcinoma (Wang et al., 2019). In pancreatic head carcinoma (Lu et al., 2019), *Actinomyces* and *Atopobium* were overrepresented in the tongue coating. By studying the saliva microbiota of inflammatory bowel disease patients, *Atopobium* was significantly increased (Qi et al., 2020). The abundances of *Prevotella*, *Veillonella*, *Megasphaera*, *Atopobium*, and *Oribacterium* were all increased in saliva samples from reflux esophagitis patients (Wang et al., 2020). In addition, at the species level, *Prevotella melaninogenica* and *Prevotella pallens* were associated with oral squamous cell carcinoma (Pushalkar et al., 2012). *Veillonella dispar* was significantly increased in the intestinal flora of sporadic nasopharyngeal carcinoma patients (Jiang et al., 2019). Cigarette smoking may affect the health of smokers by affecting these bacteria.

Notably, bacteria that significantly increased in smokers were anaerobes, and those that decreased were aerobes. This phenomenon might be related to the formation of an oral oxygen deprivation state caused by cigarette smoking (Macgregor, 1989). Cigarette smoking may create an oxygen-free environment in the mouth. This effect would influence the oxygen availability of microbes in the oral cavity, ultimately altering the oral microbial ecology. Oral bacteria can convert nitrate, which is abundant in vegetables, to nitrite, which may make the oral cavity more acidic (Li et al., 2007). Anaerobic bacteria promote this conversion, especially *Actinomyces* and *Veillonella* (Hyde et al., 2014). Notably, Actinomyces and Veillonella were found to be significantly enriched in smokers and had the strongest correlation at the genus level in our study. The acid environment promotes the development of biofilms in the oral cavity and is related to disease of the oral cavity (Krzyściak et al., 2013).

The oral microbiota also plays a key role in the metabolism and degradation of amino acids and carbohydrates. Analysis of inferred metagenomes indicated that pathways with significant differences between never smokers and smokers mainly belong to the metabolism category. Additionally, we found that bacteria that were significantly enriched in smokers had opposite functions to those bacteria depleted in smokers. This finding suggested that cigarette smoking may affect oral health by altering the microbiota and their metabolic functions. We found positive correlations between bacteria enriched in smokers and amino acid-related enzymes and pathways of amino sugar and nucleotide sugar metabolism pathways, which would increase the acidity of the oral cavity environment. Consistent with our findings, Li et al. also found that ribosome, DNA repair and recombination proteins, and purine metabolism were increased in the mouse lower respiratory tract microbiome when exposed to cigarette smoke (Li et al., 2019). This finding suggests that cigarette smoking could affect the microbiota not only in the oral cavity but also in the lower respiratory tract along the respiratory tract.

Co-occurrence networks can provide insights into the potential interactions in oral microbiota communities. In this study, we found that the bacteria enriched in smokers promoted each other and directly or indirectly suppressed the bacteria depleted in smokers. This finding is probably observed because cigarette smoking creates different oral cavity environments that are better for the bacteria that are enriched in smokers. It is also possible that the bacteria enriched in smokers by other biological mechanisms inhibit the proliferation of bacteria depleted in smokers. Cigarette smoking may affect the oral microbiota by affecting the complex relationships between bacteria.

To the best of our knowledge, our study is the first relatively systematic report to demonstrate the effects of cigarette smoking on the oral microbiota composition in a Chinese population. Our methods relied on high-throughput next-generation sequencing of the 16S rRNA marker gene determined in unstimulated saliva samples. The results of our study are largely consistent with previous studies, although different studies used different oral samples, including oral wash samples, subgingival plaques, and tongue-coating samples, (Camelo-Castillo et al., 2015; Wu et al., 2016; Sato et al., 2020b). The microbiota from different oral cavity sites were reported to be highly similar, although differences exist with a small effect size (Hall et al., 2017). Another study also found no differences in the effects of cigarette smoking on the oral cavity and nasal cavity microbiota compositions (Yu et al., 2017). In fecal samples, we found that the effects of cigarette smoking on the gut microbiota were similar to those on the oral microbiota (Capurso and Lahner, 2017; Nolan-Kenney et al., 2019). Whether the harmful substances in cigarettes directly affect the microbiota of different body parts or whether the bacteria in the oral cavity

migrate to other locations along with the respiratory tract or digestive tract needs further research.

A limitation of our study is the small sample size, limiting our ability to detect potential differences in overall oral microbiome composition. Due to the small sample size of former smokers, we combined them with current smokers into one group of smokers to increase statistical power. This made us unable to further discover the effects of smoking cessation on oral microbiota. Future studies should investigate the effects of cigarette smoking on oral microbiota in a larger sample size. Additionally, although our findings suggested that cigarette smoking may make the oral environment more acidic, it is unable to objectively measure salivary pH to test our hypothesis due to the addition of lysates that can affect the pH of saliva. Further studies are needed to confirm this hypothesis through a better research design.

In summary, in this study of the oral microbiota in a Chinese population, we observed that cigarette smoking influenced the overall oral microbiota community composition and the abundance of specific oral taxa. Our study suggested that cigarette smoking may affect health by creating a different environment in the oral cavity by affecting complex relationships between bacteria and by altering certain metabolic pathways. Future studies are still warranted to investigate the impact of cigarette smoking on the metagenomic content of the microbiome in multiple parts of the body under a relatively larger sample size to enhance our understanding of the systematic microbiota-related effects of cigarette smoking, which might provide new evidence for microbiota-targeted approaches for disease prevention.

DATA AVAILABILITY STATEMENT

The data presented in the study are deposited in the NCBI BioProject repository, accession numbers: PRJNA720269 and PRJNA721325.

ETHICS STATEMENT

The studies involving human participants were reviewed and approved by the Human Ethics Committee of Sun Yat-sen University Cancer Center (the approval number: GZR2013-008). An informed consent was signed by every subject before the interview.

AUTHOR CONTRIBUTIONS

W-HJ, YL, and Y-JJ conceived and designed the study. W-HJ, J-BZ, W-QX, and Y-QH supported the administrative work of the study. W-HJ, W-QX, Y-QH, M-QZ, X-TT, L-LY, and W-LZ contributed to population enrollment and data collection. YL and Y-JJ contributed to data analysis. All authors contributed to the article and approved the submitted version.

FUNDING

This work was supported by the National Key Research and Development Program of China (grant number 2016YFC1302700), the National Natural Science Foundation of China (grant number 81973131), the Science and Technology Planning Project of Guangzhou, China (grant number 201904010467), the Science and Technology Planning Project of Guangdong Province, China (grant number 2019B030316031), and the Sino-Sweden Joint Research Program (grant number 81861138006).

ACKNOWLEDGMENTS

We are grateful to Qi-Hong Huang (Sihui Institute for Cancer Prevention and Control), Hui-Jun Li (First General Hospital of Yangquan city), Hong-Shen (General Hospital of Mishan city), and Xiu-Hua Yu (General Hospital of Mishan city) for their contributions in the recruitment of the study population.

SUPPLEMENTARY MATERIAL

The Supplementary Material for this article can be found online at: https://www.frontiersin.org/articles/10.3389/fcimb.2021.658203/full#supplementary-material

REFERENCES

Bolyen, E., Rideout, J. R., Dillon, M. R., Bokulich, N. A., Abnet, C. C., Al-Ghalith, G. A., et al. (2019). Reproducible, Interactive, Scalable and Extensible Microbiome Data Science Using Qiime 2. *Nat. Biotechnol.* 37 (8), 852–857. doi: 10.1038/s41587-019-0209-9

Callahan, B. J., McMurdie, P. J., Rosen, M. J., Han, A. W., Johnson, A. J., and Holmes, S. P. (2016). Dada2: High-Resolution Sample Inference From Illumina Amplicon Data. *Nat. Methods* 13 (7), 581–583. doi: 10.1038/nmeth.3869

Camelo-Castillo, A. J., Mira, A., Pico, A., Nibali, L., Henderson, B., Donos, N., et al. (2015). Subgingival Microbiota in Health Compared to Periodontitis and the Influence of Smoking. *Front. Microbiol.* 6, 119. doi: 10.3389/fmicb.2015.00119

Caporaso, J. G., Lauber, C. L., Walters, W. A., Berg-Lyons, D., Lozupone, C. A., Turnbaugh, P. J., et al. (2011). Global Patterns of 16S Rrna Diversity At a Depth of Millions of Sequences Per Sample. *Proc. Natl. Acad. Sci. U. S. A.* 108 Suppl 1, 4516–4522. doi: 10.1073/pnas.1000080107

Capurso, G., and Lahner, E. (2017). The Interaction Between Smoking, Alcohol and the Gut Microbiome. *Best Pract. Res. Clin. Gastroenterol.* 31 (5), 579–588. doi: 10.1016/j.bpg.2017.10.006

Demmitt, B. A., Corley, R. P., Huibregtse, B. M., Keller, M. C., Hewitt, J. K., McQueen, M. B., et al. (2017). Genetic Influences on the Human Oral Microbiome. *BMC Genomics* 18 (1), 659. doi: 10.1186/s12864-017-4008-8

Dewhirst, F. E., Chen, T., Izard, J., Paster, B. J., Tanner, A. C., Yu, W. H., et al. (2010). The Human Oral Microbiome. *J. Bacteriol.* 192 (19), 5002–5017. doi: 10.1128/jb.00542-10

Friedman, J., and Alm, E. J. (2012). Inferring Correlation Networks From Genomic Survey Data. *PloS Comput. Biol.* 8 (9), e1002687. doi: 10.1371/journal.pcbi.1002687

Galvão-Moreira, L. V., and da Cruz, M. C. (2016). Oral Microbiome, Periodontitis and Risk of Head and Neck Cancer. *Oral. Oncol.* 53, 17–19. doi: 10.1016/j.oraloncology.2015.11.013

Gohl, D. M., Vangay, P., Garbe, J., MacLean, A., Hauge, A., Becker, A., et al. (2016). Systematic Improvement of Amplicon Marker Gene Methods for

Increased Accuracy in Microbiome Studies. *Nat. Biotechnol.* 34 (9), 942–949. doi: 10.1038/nbt.3601

Hall, M. W., Singh, N., Ng, K. F., Lam, D. K., Goldberg, M. B., Tenenbaum, H. C., et al. (2017). Inter-Personal Diversity and Temporal Dynamics of Dental, Tongue, and Salivary Microbiota in the Healthy Oral Cavity. *NPJ Biofilms Microbiomes* 3, 2. doi: 10.1038/s41522-016-0011-0

He, Y. Q., Liao, X. Y., Xue, W. Q., Xu, Y. F., Xu, F. H., Li, F. F., et al. (2019). Association Between Environmental Factors and Oral Epstein-Barr Virus DNA Loads: A Multicenter Cross-sectional Study in China. *J. Infect. Dis.* 219 (3), 400–409. doi: 10.1093/infdis/jiy542

Hu, T. W., Mao, Z., Ong, M., Tong, E., Tao, M., Jiang, H., et al. (2006). China At the Crossroads: The Economics of Tobacco and Health. *Tob Control* 15 (Suppl 1), i37–i41. doi: 10.1136/tc.2005.014621. (Suppl 1).

Hyde, E. R., Andrade, F., Vaksman, Z., Parthasarathy, K., Jiang, H., Parthasarathy, D. K., et al. (2014). Metagenomic Analysis of Nitrate-Reducing Bacteria in the Oral Cavity: Implications for Nitric Oxide Homeostasis. *PloS One* 9 (3), e88645. doi: 10.1371/journal.pone.0088645

Jiang, H., Li, J., Zhang, B., Huang, R., Zhang, J., Chen, Z., et al. (2019). Intestinal Flora Disruption and Novel Biomarkers Associated With Nasopharyngeal Carcinoma. *Front. Oncol.* 9, 1346. doi: 10.3389/fonc.2019.01346

Kolenbrander, P. E. (2000). Oral Microbial Communities: Biofilms, Interactions, and Genetic Systems. *Annu. Rev. Microbiol.* 54, 413–437. doi: 10.1146/annurev.micro.54.1.413

Koren, O., Spor, A., Felin, J., Fåk, F., Stombaugh, J., Tremaroli, V., et al. (2011). Human Oral, Gut, and Plaque Microbiota in Patients With Atherosclerosis. *Proc. Natl. Acad. Sci. U. S. A.* 108 Suppl 1, 4592–4598. doi: 10.1073/pnas.1011383107

Krzyściak, W., Jurczak, A., Kościelniak, D., Bystrowska, B., and Skalniak, A. (2013). The Virulence of Streptococcus Mutans and the Ability to Form Biofilms. *Eur. J. Clin. Microbiol. Infect. Dis.* 33 (4), 499–515. doi: 10.1007/s10096-013-1993-7

Langille, M. G., Zaneveld, J., Caporaso, J. G., McDonald, D., Knights, D., Reyes, J. A., et al. (2013). Predictive Functional Profiling of Microbial Communities Using 16S Rrna Marker Gene Sequences. *Nat. Biotechnol.* 31 (9), 814–821. doi: 10.1038/nbt.2676

Li, K. J., Chen, Z. L., Huang, Y., Zhang, R., Luan, X. Q., Lei, T. T., et al. (2019). Dysbiosis of Lower Respiratory Tract Microbiome Are Associated With Inflammation and Microbial Function Variety. *Respir. Res.* 20 (1), 272. doi: 10.1186/s12931-019-1246-0

Li, J., Quinque, D., Horz, H. P., Li, M., Rzhetskaya, M., Raff, J. A., et al. (2014). Comparative Analysis of the Human Saliva Microbiome From Different Climate Zones: Alaska, Germany, and Africa. *BMC Microbiol.* 14, 316. doi: 10.1186/s12866-014-0316-1

Li, H., Thompson, I., Carter, P., Whiteley, A., Bailey, M., Leifert, C., et al. (2007). Salivary Nitrate–An Ecological Factor in Reducing Oral Acidity. *Oral. Microbiol. Immunol.* 22 (1), 67–71. doi: 10.1111/j.1399-302X.2007.00313.x

Li, D., Xi, W., Zhang, Z., Ren, L., Deng, C., Chen, J., et al. (2020). Oral Microbial Community Analysis of the Patients in the Progression of Liver Cancer. *Microb. Pathog.* 149, 104479. doi: 10.1016/j.micpath.2020.104479

Long, J., Cai, Q., Steinwandel, M., Hargreaves, M. K., Bordenstein, S. R., Blot, W. J., et al. (2017). Association of Oral Microbiome With Type 2 Diabetes Risk. *J. Periodontal Res.* 52 (3), 636–643. doi: 10.1111/jre.12432

Lozupone, C. A., Hamady, M., Kelley, S. T., and Knight, R. (2007). Quantitative and Qualitative Beta Diversity Measures Lead to Different Insights Into Factors That Structure Microbial Communities. *Appl. Environ. Microbiol.* 73 (5), 1576–1585. doi: 10.1128/aem.01996-06

Lozupone, C. A., and Knight, R. (2008). Species Divergence and the Measurement of Microbial Diversity. *FEMS Microbiol. Rev.* 32 (4), 557–578. doi: 10.1111/j.1574-6976.2008.00111.x

Lu, H., Ren, Z., Li, A., Li, J., Xu, S., Zhang, H., et al. (2019). Tongue Coating Microbiome Data Distinguish Patients With Pancreatic Head Cancer From Healthy Controls. *J. Oral. Microbiol.* 11 (1), 1563409. doi: 10.1080/20002297.2018.1563409

Macgregor, I. D. (1989). Effects of Smoking on Oral Ecology. A Review of the Literature. *Clin. Prev. Dent* 11 (1), 3–7.

Mason, M. R., Preshaw, P. M., Nagaraja, H. N., Dabdoub, S. M., Rahman, A., and Kumar, P. S. (2015). The Subgingival Microbiome of Clinically Healthy Current and Never Smokers. *ISME J.* 9 (1), 268–272. doi: 10.1038/ismej.2014.114

McDonald, D., Price, M. N., Goodrich, J., Nawrocki, E. P., DeSantis, T. Z., Probst, A., et al. (2012). An Improved Greengenes Taxonomy With Explicit Ranks for Ecological and Evolutionary Analyses of Bacteria and Archaea. *ISME J.* 6 (3), 610–618. doi: 10.1038/ismej.2011.139

Nolan-Kenney, R., Wu, F., Hu, J., Yang, L., Kelly, D., Li, H., et al. (2019). The Association Between Smoking and Gut Microbiome in Bangladesh. *Nicotine Tob Res.* 22 (8), 1339–1346. doi: 10.1093/ntr/ntz220

Perera, M., Al-Hebshi, N. N., Perera, I., Ipe, D., Ulett, G. C., Speicher, D. J., et al. (2018). Inflammatory Bacteriome and Oral Squamous Cell Carcinoma. *J. Dent Res.* 97 (6), 725–732. doi: 10.1177/0022034518767118

Pushalkar, S., Ji, X., Li, Y., Estilo, C., Yegnanarayana, R., Singh, B., et al. (2012). Comparison of Oral Microbiota in Tumor and Non-Tumor Tissues of Patients With Oral Squamous Cell Carcinoma. *BMC Microbiol.* 12, 144. doi: 10.1186/1471-2180-12-144

Qi, Y., Zang, S. Q., Wei, J., Yu, H. C., Yang, Z., Wu, H. M., et al. (2020). High-Throughput Sequencing Provides Insights Into Oral Microbiota Dysbiosis in Association With Inflammatory Bowel Disease. *Genomics* 113 (1 Pt 2), 664–676. doi: 10.1016/j.ygeno.2020.09.063

Sato, N., Kakuta, M., Hasegawa, T., Yamaguchi, R., Uchino, E., Kobayashi, W., et al. (2020a). Metagenomic Analysis of Bacterial Species in Tongue Microbiome of Current and Never Smokers. *NPJ Biofilms Microbiomes* 6 (1), 11. doi: 10.1038/s41522-020-0121-6

Sato, N., Kakuta, M., Uchino, E., Hasegawa, T., Kojima, R., Kobayashi, W., et al. (2020b). The Relationship Between Cigarette Smoking and the Tongue Microbiome in an East Asian Population. *J. Oral. Microbiol.* 12 (1), 1742527. doi: 10.1080/20002297.2020.1742527

Segata, N., Izard, J., Waldron, L., Gevers, D., Miropolsky, L., Garrett, W. S., et al. (2011). Metagenomic Biomarker Discovery and Explanation. *Genome Biol.* 12 (6), R60. doi: 10.1186/gb-2011-12-6-r60

Teles, R., Teles, F., Frias-Lopez, J., Paster, B., and Haffajee, A. (2013). Lessons Learned and Unlearned in Periodontal Microbiology. *Periodontol. 2000* 62 (1), 95–162. doi: 10.1111/prd.12010

Wang, Q., Rao, Y., Guo, X., Liu, N., Liu, S., Wen, P., et al. (2019). Oral Microbiome in Patients With Oesophageal Squamous Cell Carcinoma. *Sci. Rep.* 9 (1), 19055. doi: 10.1038/s41598-019-55667-w

Wang, B., Zhang, Y., Zhao, Q., Yan, Y., Yang, T., Xia, Y., et al. (2020). Patients With Reflux Esophagitis Possess a Possible Different Oral Microbiota Compared With Healthy Controls. *Front. Pharmacol.* 11, 1000. doi: 10.3389/fphar.2020.01000

Wirth, R., Maróti, G., Mihók, R., Simon-Fiala, D., Antal, M., Pap, B., et al. (2020). A Case Study of Salivary Microbiome in Smokers and Non-Smokers in Hungary: Analysis by Shotgun Metagenome Sequencing. *J. Oral. Microbiol.* 12 (1), 1773067. doi: 10.1080/20002297.2020.1773067

Wu, J., Peters, B. A., Dominianni, C., Zhang, Y., Pei, Z., Yang, L., et al. (2016). Cigarette Smoking and the Oral Microbiome in a Large Study of American Adults. *ISME J.* 10 (10), 2435–2446. doi: 10.1038/ismej.2016.37

Yang, F., Zeng, X., Ning, K., Liu, K. L., Lo, C. C., Wang, W., et al. (2012). Saliva Microbiomes Distinguish Caries-Active From Healthy Human Populations. *ISME J.* 6 (1), 1–10. doi: 10.1038/ismej.2011.71

Yang, Y., Zheng, W., Cai, Q. Y., Shrubsole, M. J., Pei, Z., Brucker, R., et al. (2019). Cigarette Smoking and Oral Microbiota in Low-Income and African-American Populations. *J. Epidemiol. Community Health* 73 (12), 1108–1115. doi: 10.1136/jech-2019-212474

Yu, G., Phillips, S., Gail, M. H., Goedert, J. J., Humphrys, M. S., Ravel, J., et al. (2017). The Effect of Cigarette Smoking on the Oral and Nasal Microbiota. *Microbiome* 5 (1), 3. doi: 10.1186/s40168-016-0226-6

Conflict of Interest: The authors declare that the research was conducted in the absence of any commercial or financial relationships that could be construed as a potential conflict of interest.

frontiers in Cellular and Infection Microbiology

ORIGINAL RESEARCH
published: 01 June 2021
doi: 10.3389/fcimb.2021.669989

Porphyromonas gingivalis Provokes Exosome Secretion and Paracrine Immune Senescence in Bystander Dendritic Cells

Ranya Elsayed[1], *Mahmoud Elashiry*[1], *Yutao Liu*[2], *Ahmed El-Awady*[1], *Mark Hamrick*[2] *and Christopher W. Cutler*[1]*

[1] Department of Periodontics, Dental College of Georgia, Augusta University, Augusta, GA, United States, [2] Department of Cellular Biology and Anatomy, Medical College of Georgia, Augusta, GA, United States

Periodontitis is a disease of ageing or inflammaging, and is comorbid with other more severe age-related chronic diseases. With advanced age comes an increase in accumulation of senescent cells that release soluble and insoluble pro-inflammatory factors collectively termed the senescence associated secretory phenotype (SASP). In the present report, we examined whether immune cells typical of those at the oral mucosa-microbe interface, are vulnerable to cellular senescence (CS) and the role of dysbiotic oral pathogen *Porphyromonas gingivalis*. Bone marrow-derived dendritic cells (DCs) from young (yDCs) and old (oDCs) mice were co-cultured *in vitro* with CS inducer doxorubicin or *P.gingivalis (Pg)*, plus or minus senolytic agent rapamycin. CS profiling revealed elevated CS mediators SA-β-Gal, p16 ^{INK4A}, p53, and p21$^{Waf1/Clip1}$ in oDCs, or yDCs in response to doxorubicin or *P. gingivalis*, reversible with rapamycin. Functional studies indicate impaired maturation function of oDCs, and yDC exposed to *P. gingivalis*; moreover, OVA-driven proliferation of CD4+ T cells from young OTII transgenic mice was impaired by oDCs or yDCs+Pg. The SASP of DCs, consisting of secreted exosomes and inflammasome-related cytokines was further analyzed. Exosomes of DCs cocultured with *P. gingivalis* (PgDCexo) were purified, quantitated and characterized. Though typical in terms of size, shape and phenotype, PgDCexo were 2-fold greater in number than control DCs, with several important distinctions. Namely, PgDCexo were enriched in age-related miRNAs, and miRNAs reported to disrupt immune homeostasis through negative regulation of apoptosis and autophagy functions. We further show that PgDCexo were enriched in *P. gingivalis* fimbrial adhesin protein mfa1 and in inflammasome related cytokines IL-1β, TNFα and IL-6. Functionally PgDCexo were readily endocytosed by recipient yDCs, amplifying functional impairment in maturation and ability to promote Ova-driven proliferation of OTII CD4+ T cells from young mice. In conclusion *P. gingivalis* induces premature (autocrine) senescence in DCs by direct cellular invasion and greatly amplifies senescence, in paracrine, of bystander DCs by secretion of inflammatory exosomes. The implications of this pathological pathway for periodontal disease *in vivo* is under investigation in mouse models.

Keywords: (MeSH): dendritic cells, exosomes, immune senescence, periodontitis, *Porphyromonas gingivalis*

OPEN ACCESS

Edited by:
Sinem Esra Sahingur, University of Pennsylvania, United States

Reviewed by:
Zhao Lin, Virginia Commonwealth University, United States
Nicolas Dutzan, University of Chile, Chile

***Correspondence:**
Christopher W. Cutler
chcutler@augusta.edu

Specialty section:
This article was submitted to Bacteria and Host, a section of the journal Frontiers in Cellular and Infection Microbiology

Received: *19 February 2021*
Accepted: *11 May 2021*
Published: *01 June 2021*

Citation:
Elsayed R, Elashiry M, Liu Y, El-Awady A, Hamrick M and Cutler CW (2021) Porphyromonas gingivalis *Provokes Exosome Secretion and Paracrine Immune Senescence in Bystander Dendritic Cells. Front. Cell. Infect. Microbiol. 11:669989. doi: 10.3389/fcimb.2021.669989*

INTRODUCTION

Periodontitis (PD) in adults is a chronic inflammatory disease of ageing or inflammaging (Ebersole et al., 2018; Qin et al., 2020). This is particularly striking when the National Health and Nutrition Examination Survey (NHANES) data from 2009-2010 are stratified by patient age, with PD prevalence increasing from 24.4% in adults aged 30-34 yrs., to 70.1% in those aged 65 yrs. and over (Eke et al., 2012). Periodontitis has been linked to other age-related diseases with more serious mortality and morbidity profiles such as cancer (Michaud et al., 2017), Alzheimer's disease (Teixeira et al., 2017), and atherosclerosis (Carrion et al., 2012). *Porphyromonas gingivalis (P.gingivalis)* is considered a "keystone" pathogen in PD due to its outsized influence on the local microflora. *P. gingivalis* induces a dysbiosis by disruption of innate immunity, wherein symbiotic commensals become accessory pathogens (Hajishengallis et al., 2011; Hajishengallis et al., 2012; Dutzan et al., 2018) through unclear mechanisms. The antigen presenting cells dendritic cells (DCs), responsible for bridging innate and adaptive immunity, infiltrate the gingiva in PD (Jotwani et al., 2001; Jotwani and Cutler, 2003; Jotwani et al., 2003; Jotwani et al., 2004), where *P. gingivalis* and other microbes are taken up *in vivo* (Carrion et al., 2012; El-Awady et al., 2019; Rajendran et al., 2019). *P.gingivalis* also invades epithelial, endothelial and smooth muscle cells (Li et al., 2008). Invasion of DCs by *P.gingivalis* occurs through coordinate regulation of its minor (mfa-1) and major (fimA) fimbriae (Zeituni et al., 2009; Zeituni et al., 2010; El-Awady et al., 2015; El-Awady et al., 2015; El-Awady et al., 2019). *P.gingivalis'* viability in DCs depends on an mTORC1-dependent anti-autophagosomal/lysosomal pathway (Arjunan et al., 2016; Arjunan et al., 2018; Meghil et al., 2019), while viability of the host DCs is preserved by an anti-apoptotic signaling pathway involving hyperactivation of Akt1 (Arjunan et al., 2016; Arjunan et al., 2018; Meghil et al., 2019). Hyperactivation of Akt1 and antiapoptotic pathways (Meghil et al., 2019) have recently been linked to premature cellular senescence (CS) (Nogueira et al., 2008).

CS is typified by irreversible cell cycle arrest (in replicative cells), increased apoptosis resistance and activation of the senescence-associated secretory phenotype or SASP (Acosta et al., 2013). CS, first reported by Hayflick and colleagues (Hayflick and Moorhead, 1961) as cell cycle arrest after a finite number of cell divisions, (also known as Hayflick limit), is now recognized as a more complex phenomenon. CS can be caused by a variety of stressors which can lead to different types of senescence. In addition to replicative senescence, oncogene-induced senescence, genotoxic-induced senescence, developmental senescence and tissue repair senescence have been described (Gorgoulis et al., 2019). Fundamentally, CS is a defense mechanism to prevent dissemination of tissue damage and protect against tumorigenesis; however, accumulation of senescent cells can be harmful to the host environment. Although senescent cells are quiescent, they are metabolically active and have the capacity to release a plethora of pro-inflammatory mediators collectively known as SASP. The SASP can promote paracrine senescence in neighboring cells and elicit a chronic inflammatory status known as inflammaging. The SASP consist of a distinct profile of inflammatory cytokines and extracellular vesicles (EV), e.g. exosomes, collectively called the secretome. Exosomes are nano-sized EV of endosomal origin secreted by all cells (Jakhar and Crasta, 2019), and contain proteins, RNAs and other moieties reflective of the homeostatic or pathologic state of the donor cells. Exosomal microribonucleic acids (miRNA) have emerged as novel biological biomarkers of aging (Machida et al., 2015). Saliva exosomes (Murillo et al., 2019) for example, are being studied for molecular clues about cancer initiation/progression (Nonaka and Wong, 2017). From a functional standpoint exosomes can amplify CS signaling in an autocrine fashion, or transmit CS to non-aged cells in paracrine (Acosta et al., 2013). Advanced age-associated alveolar bone loss, reported in mice, is attenuated by senolytic agent rapamycin (An et al., 2017).

Keratinocytes (Moffatt-Jauregui et al., 2013) and DCs (Jotwani et al., 2001; Jotwani and Cutler, 2003; Jotwani et al., 2004), both resident cells at the front line of the oral mucosal-microbe interface, may be particularly vulnerable to CS induction. Indeed, we show here by CS profiling, DCs derived from bone marrow of young mice (yDCs) are readily provoked to CS by exposure to canonical CS stressor doxorubicin and *P. gingivalis* 381. The response of yDCs to these stressors included elevated IL-1β and TNFa mRNA levels, but impaired maturation response, and impaired antigen presentation to OTII CD4 T cells, consistent with immune senescence. Moreover, DCs from old mice (oDCs) are similarly impaired at baseline. *P. gingivalis* has been identified inside DCs *in vitro* and *in vivo* in PD patients (Carrion et al., 2012; El-Awady et al., 2019; Rajendran et al., 2019). Here we show that *P. gingivalis* invasion of yDCs is a predicate of robust senescence; moreover, resultant yDCs had a 2-fold greater secretion of exosomes. These *P. gingivalis*-induced DC exosomes (PgDCexo) while morphologically typical exosomes, are enriched in anti-apoptosis and anti-autophagy miRNAs, inflammasome proteins IL-6 and mature IL-1b, and unexpectedly, the minor mfa1 fimbrial protein of *P. gingivalis;* moreover, PgDCexo *are* taken up by recipient yDCs, promoting immune senescence in recipient young DCs. Overall the results support *P. gingivalis* as a potent cell stressor of CS, both directly through infection of cells and indirectly through induction of the exosomal SASP; thereby promoting immune senescence in paracrine to bystander cells.

MATERIALS AND METHODS

Ethics Statement

The Institutional Animal Care and Use Committee (IACUC) of Augusta University (protocol # 2013-0586) approved all experimental procedures on C57BL/6 mice.

Generation and Culture of Bone Marrow Derived Dendritic Cells From Young (yDCs) and Old (oDCs) Mice

Generation of BMDCs was performed as previously described (Elashiry et al., 2020; Elsayed et al., 2020). Briefly, bone marrow was isolated from femurs and tibiae of young (2 months) and old

(22-24 months) C57B6 mice. Red blood cells were lysed using ACK cell lysis buffer (Invitrogen, Thermofisher scientific, and Columbia, SC, USA). Cells were cultured in complete media (RPMI 1640 containing 10% FBS and 100 IU/mL penicillin/streptomycin) in the presence of murine GM-CSF (20 ng/ml) and IL-4(20 ng/ml) (Peprotech, Rocky Hill, NJ, USA). Culture media was changed every 2 days with the addition of fresh growth factors. Cells were re-incubated on day 6 in EXO depleted complete media to generate iDCs or in the presence of 1μg/ml LPS (Sigma, St. Louis, M.O., USA) to generate mature stimDCs for 48 hours. On day 8, cells were washed and re-incubated in EXO free media for 24 h and on day 9, cells were isolated and, culture supernatants were collected for EXO purification. In some of the experiments, bone marrow derived dendritic cells (DCs) were treated at day 6 of culture with Doxorubicin (Sigma Aldrich, St Louise, MO, USA) at a dose of 50nM, Ecoli LPS (Sigma Aldrich, St Louise, MO, USA) at 100ng/ml. *P.gingivalis* LPS (Invivogen Inc., San Diego, CA, USA) at 100ng/ml, Rapamycin 1μM(R8781)(Sigma Aldrich, St Louise, MO, USA) or PgDCexo, StimDCexo, iDCexo 108 particles/ml (Elashiry et al., 2020).

P.gingivalis Bacterial Culture and DCs Infection

P.gingivalis 381 (Pg) was maintained anaerobically in (10%, H2, 10% CO2, and 80% N2) in a Coy lab vinyl anaerobic chamber (Coy Laboratory Products, Inc., Grass Lake, MI) at 37∘C in Wilkins-Chalgren anaerobe broth. Bacterial cells were maintained until mid-log phase. Bacterial CFU were calculated based on a spectrophotometer OD 660 reading of 0.11, previously determined to equal 5x10^7 CFU (El-Awady et al., 2015; Meghil et al., 2019). At day 6 of DC culture, cells were pulsed with *P.gingivalis* at a multiplicity of infection (MOI) of 10 for 48 hours. On day 8, cells were washed and incubated for 24 hrs and on day 9, cells were isolated and, culture supernatants were collected for EXO purification.

Exosome Isolation and Purification

Exosome isolation was performed as previously described (Kim et al., 2005; Elashiry et al., 2020). Briefly, supernatants from DC cultures were subjected to differential centrifugation (successive centrifugations at 500 g for (5 min), 2000g for (20 min), and 10,000 g for (30 min) to eliminate cells and debris. This was followed by ultrafiltration 2x with 0.2 μm and 2x with 100 kDA filters (to remove microvesicles and free proteins) and ultracentrifugation for 90 min at 120,000 g. Then EXO pellets were washed with PBS and ultra-centrifuged 2x at 120,000 g for 90 min, and finally re-suspended in 100 μl of PBS, stored in -80 for further analysis and experiments.

Nanotracking Analysis of DC-Derived Exosomes

For quantification of size and count of nanoparticles in suspension, Nano tracking analysis (NTA) was performed using Zeta view PMX 110 (Particle Metrix, Meerbusch, Germany) as previously described (Helwa et al., 2017; Elashiry et al., 2020). Briefly, 10 μl of the sample was diluted in 1xPBS and loaded into the sample chamber, then size and concentration of the sample were automatically calculated by the software (ZetaView 8.02.28).

Electron Microscopy

As described previously (Helwa et al., 2017; Elashiry et al., 2020) exosome sample was fixed in 4% paraformaldehyde in 0.1M cacodylate buffer ph 7.4 overnight. Twenty microliter (20ul) of suspended exosome preparation was applied to a carbon-Formvar coated 200 mesh nickel grid and allowed to stand 30 minutes. The excess sample was wicked off onto Whatman filter paper. Grids were floated exosome side down onto a 20 μl drop of 1M Ammonium Chloride for 30 minutes to quench aldehyde groups from the fixation step. Grids were floated on drops of blocking buffer (0.4% BSA in PBS) for 2 hours. Then rinsed 3 X 5 minutes each with PBS. Grids were set up as follows and allowed to incubate in blocking buffer or the primary antibody (anti CD63, anti CD81, anti Mfa1) for 1 hour. Grids were floated on drops of 1.4 nm secondary antibody nanogold (Nanoprobes, Inc.) diluted 1:1000 in blocking buffer for 1 hour. Grids were rinsed 3 X 5 minutes each with PBS. Grids were rinsed 3 X 5 minutes each with DI H_2O. For double labelling, grids were enhanced 12 minutes (for Mfa1 antibody) and 3 minutes (for CD81 antibody) in Gold Enhance EM (gold enhancement reagent, Nanoprobes, Inc.) and rinsed in ice cold DI H_2O to stop enhancement. The different times for enhancement allows for the gold particles labeling the first primary antibody to be enhanced twice producing larger size gold particles between 20 and 30 nm in size. The gold particles labeling the second primary antibody is enhanced only once and for a much shorter time to produce gold particles which are smaller in size, between 10 and 12 nm in size. Then grids were negatively stained in 2% aqueous Uranyl Acetate and wicked dry. Grids were allowed to air dry before being examined in a JEM 1230 transmission electron microscope (JEOL USA inc., Peabody MA) at 110 kV and imaged with an UltraScan 4000 CCD camera & First Light Digital Camera Controller (Gatan Inc., Pleasanton, CA.)

miRNA Microarray of DC-Derived Exosomes

Total EXO RNA Kit (4478545), (Thermofisher Scientific, Waltham MA, USA) was used to isolate miRNAs from exosomes according to manufacturer's instructions. The concentration of miRNA was measured using a NanoDrop spectrophotometer (Thermo Scientific) and analysis of the quality of miRNA was performed using an Agilent 2100 Bioanalyzer. Analysis of miRNAs was performed using an Affymetrix GeneChip® miRNA 4.0 Array at the Integrated Genomics Core, Augusta University, GA. A P-value cut-off of 0.05 and the miRNAs with a fold change above 1.5 were considered differentially expressed. Bioinformatic analysis was performed using ClastVist software and TargetScan software was used to detect computationally predicted miRNA-mRNA target relationships.

Senescence Associated β Galactosidase (SA-β-Gal) Histochemical Staining Kit

DCs suspension were subjected to cytospins on a microscopic slide before fixation and staining. SA-β-gal histochemical staining kit (CS0030) (Sigma Aldrich, St Louise, MO, USA) was used according to the manufacturer's instructions. Briefly, cells were fixed with fixation buffer supplied with the kit (20% formaldehyde, 2% glutaraldehyde, 70.4 mM Na2HPO4, 14.7 mM KH2PO4, 1.37 M NaCl, and 26.8 mM KCl), for 6-8 minutes then washed 3x with PBS. This was followed by adding staining solution containing X-Gal and incubated for 12 hours at 37°C with no CO2. Cells were then washed with PBS and visualized under EVOS cell imaging system (Evos FL Auto Imaging System, Thermofisher) and at least 5 random pictures were taken per sample with 60x objective lens.

SA-β-Gal Flow Cytometry Staining Kit

Cell Event Senescence Green flow cytometry assay kit (Thermofisher Scientific, Waltham MA, USA) was used according to the manufacturer's instruction. Briefly DCs were first stained for cell surface marker CD11c using regular staining protocol discussed in detail in the following sections. After the last wash, cells were fixed with 4% paraformaldehyde (PFA) for 10 minutes at room temperature followed by washing to remove the fixative solution. Cells were then incubated with Cell Event Senescence Green probe (Thermofisher Scientific, Waltham MA, USA) at 1:500 dilution for 2 hours at 37°C with no CO2. Cells were then washed with PBS, 2% FBS and data acquired by MACSQuant analyzer machine and MACSQuantify software (Miltenyi Biotech Auburn, CA, USA).

Exosome Uptake *In Vitro*

Analysis of exosome uptake consisted of labelling exosomes with Dil (D282, Thermofisher Scientific, Waltham MA, USA), then coculturing them with recipient DCs for 24h. Cells were subjected to cytospins, fixed and stained on glass slides with Alex flour 647 phalloidin (A22287) and DAPI (D1306) (Invitrogen, Thermofisher scientific West Columbia, SC, USA). Slides were then visualized by Zeiss upright confocal microscope (Carl Zeiss AG, Oberkochen, Germany) and images were taken with 40x objective lens.

P.gingivalis Uptake by DCs In Vitro

P.gingivalis was labeled with 10 μM carboxyfluoresceine succinimidyl ester (CFSE ebioscience, Invitrogen, Thermofisher Scientific West Columbia, SC, USA) for 1 hour at 37 degree with shaking, then residual stain removed by successive washings and bacterium suspended at 10 MOI for uptake experiments, with/without Cytochalasin D 1uM (Sigma Aldrich, St Louise, MO, USA) for 48 hours, after which cells were harvested and analyzed by flow cytometry and SA-B-gal staining. Cells were harvested, thoroughly washed and then fixed with 4% paraformaldehyde, permeabilized with 0.1% Triton X-100 in PBS and stained with actin ActinRed 555 ReadyProbes Reagent and nuclear counterstaining using DAPI mounting medium; ProLong Gold Antifade Mountant (Invitrogen, Thermofisher scientific, Waltham MA, USA), then images were taken using Zeiss 780 upright confocal microscope (Carl Zeiss AG, Oberkochen, Germany).

Flow Cytometry and Antibodies

FACS Staining Buffer (Thermofisher Scientific, Waltham MA, USA) was used to stain cells on ice. FC receptors (FcR) were blocked using mouse FcR blocking reagent (Miltenyi Biotec, Auburn, CA, USA) for 15 minutes protected from light followed by incubation with conjugated antibodies on ice for 30 minutes. Cells were then washed and re-suspended in FACS buffer and data was acquired using MACSQuant analyzer machine and MACSQuantify software (Miltenyi Biotech Auburn, CA, USA). Antibodies used: CD11c APC; clone N418 (Affymetrix, eBioscience, Thermofisher Scientific, Waltham MA, USA)., CD86 (B7-2) PE; clone GL1(Affymetrix, eBioscience, Thermofisher Scientific, Waltham MA, USA)., CD80 FITC; clone 16-10A1(Invitrogen, Thermofisher Scientific, Waltham MA, USA), CD4 Vioblue; clone GK1.5 (Invitrogen, Thermofisher Scientific, Waltham MA, USA), MHCII Viogreen; clone M5/114.15.2, (Miltenyi Biotech Auburn, CA, USA).

Real Time PCR

Total RNA was isolated using QIAGEN RNeasy mini kit (Qiagen, Inc., Valencia, CA, and USA). RNA purity and concentration were measured using Nanodrop (NanoDrop 1000 UV-VIS Spectrophotometer Software Ver.3.8.1, Thermofisher Scientific). Ratio of 260/280 of 2.0 was considered adequate for analysis. Reverse transcription to cDNA was performed using the High-Capacity cDNA Reverse Transcription Kit (Applied Biosystem, Thermofisher Scientific, Waltham MA, USA) in total reaction of 20 μL. Quantitative real-time PCR was performed using TaqMan fast advanced master mix (Applied Biosystem, Thermofisher Scientific, Waltham MA, USA) and Taq-Man Gene Expression assay (Applied Biosystem, Foster City, CA, USA) specific for: IL6 (Mm00446190_m1), TNF (Mm00443258_m1) and IL1B (Mm00434228_m1), internal control Glyceraldehyde-3-phosphate dehydrogenase (GAPDH Mm99999915_m1). RT-PCR was run in StepOnePlus Real-Time PCR System. Calculation of relative mRNA expression was performed using delta-delta CT and presented as relative fold-change.

Western Blotting Analysis, Antibodies

Cells or exosomes were lysed using RIPA buffer with the addition of protease/phosphatase inhibitor cocktail and incubated for 20 minutes on ice, then protein lysates stored at -80° till further use. After denaturation of proteins lysates, equal protein concentrations and volumes were loaded and separated by 10-15% Mini-PROTEAN TGX Precast Protein Gel (Bio-Rad Laboratories, Hercules, CA), and transferred onto PVDF membranes (Sigma-Aldrich). Membranes were blocked with 5% nonfat dry milk in TBST, then incubated with primary antibodies at 4° overnight. After washing with TBST, membranes were incubated with HRP-conjugated secondary antibodies for 1 h at room temperature. Membranes were then

washed and developed by ECL kit and imaged with ChemiDoc MP Imaging Gel (Bio-Rad Laboratories, Hercules, CA). Antibodies used: anti-Beta-actin (8H10D10) as loading control (Cell Signaling Technology, Danvers, MA, USA). Anti-mouse anti $p21^{Waf1/Clip1}$ (#64016) (Cell Signaling Technology, Danvers, MA, USA). Anti-mouse anti $p16^{INK4A}$ PA1030670 (Thermofisher Scientific, Waltham MA, USA) and anti p53 (#2524) (Cell Signaling Technology, Danvers, MA, USA), anti-TSG101 (MA1-23296) (Thermofisher Scientific, Waltham MA, USA), anti-Alix (MA1-83977) (Thermofisher Scientific, Waltham MA, USA), anti CD81(#10037) (Cell Signaling Technology, Danvers, MA, USA) Anti IL6(12912) (Cell Signaling Technology, Danvers, MA, USA), anti cleaved-IL-1ββ (#52718) (Cell Signaling Technology, Danvers, MA, USA), anti TNFa (#11948) (Cell Signaling Technology, Danvers, MA, USA), anti-Mfa1 (mAb 89.15 against the native minor fimbriae (Zeituni et al., 2010), generated at the Cell Culture/Hybridoma Facility at Stony Brook University, as reported (Carrion et al., 2012)), secondary antibodies: anti-mouse IgG HRP-linked (#7076) (Cell Signaling Technology, Danvers, MA, USA), anti-rabbit IgG HRP-linked (# 7074) (Cell Signaling Technology, Danvers, MA, USA).

T Cell Isolation and Antigen Presentation

OVA antigen-specific T cells were isolated from OT-II transgenic mice (B6.Cg-Tg(TcraTcrb)425Cbn/J; Jackson Laboratory) using negative selection with Mouse T-cell Enrichment Kit (MagniSort; Thermofisher Scientific, West Columbia, SC, USA). T cell purity was assessed by flow cytometry analysis, using CD4 antibody. OT-II T cells were stained with 0.5 μM CFSE (ebioscience, Invitrogen, Thermofisher Scientific West Columbia, SC, USA) for 15 minutes at 37°C, after which cells were washed 2 times. DCs pretreated with PgDCexo, iDCexo, or StimDCexo, or infected with *P.gingivalis* (10 MOI) ± Rapamycin were harvested, washed thoroughly and pulsed with 3 μg/mL OVA323-339 peptide (Sigma Aldrich, St Louise, MO, USA) for 24 hours. Cells were then harvested, thoroughly washed and co-cultured with T cells at 1:10 DC: T cell ratio in 96-well round-bottom plates with complete RPMI 1640 (10% fetal bovine serum FBS,1% Pen Strep, 1x non-essential amino acids, 0.1% b-mercaptoetanol). After a 72-hours incubation at 37°C with 5% CO2, the proliferation of CFSE-labeled CD4+ T cells was then assessed by flow cytometry.

Magnetic Separation of CD81, CD9, CD63 Positive EXO

PgDCEXO were incubated with microbeads that recognize CD81, CD9 and CD63 positive exosomes (pan EXO) (Miltenyi Biotech Auburn, CA, USA). Magnetic separation of labeled EXO was performed by loading it onto a μ column placed in a magnetic field of μMACS separator (Miltenyi Biotech Auburn, CA, USA). The magnetically labeled EXO are retained within the column and the unlabeled vesicles run through the column. The positively selected retained EXO are then eluted from the column. The number of particles in the run through (passage1) of unlabeled extracellular vesicles (EV) fraction was then counted using NTA. Magnetic separation of the run through was repeated (passage 2) to completely deplete pan EXO from the run through and then particles counted in the final run through of unlabeled EV and a percentage to the total number of EV was calculated. The eluate (CD81, CD9 and CD63 positive exosomes) and the run through were then analyzed using WB.

Statistical Analysis

Data was analyzed using GraphPad Prism 6 (GraphPad Software, La Jolla, CA). Data analysis was performed by two-way or one ANOVA with significance defined as $P < 0.05$, and confidence level of 95% confidence interval followed by Tukey's multiple-comparisons test. Values are expressed as mean ± standard deviation (SD) and experiments were repeated 3 times.

RESULTS

Murine DCs From Old Mice, or Young Mice Exposed to *P. gingivalis*, Are Senescent

DCs are resident sentinel immune cells in oral mucosa and the bloodstream, previously shown to contain *P. gingivalis* microbial signatures in periodontitis (PD) patients (Carrion et al., 2012; El-Awady et al., 2019; Rajendran et al., 2019). Here, bone marrow derived DCs (DCs) from young (yDCs) or old (oDCs) mice were cocultured with *P. gingivalis* or doxorubicin and subjected to CS-profiling. Both *P. gingivalis* and doxorubicin stimulated an increase in $p16^{INK4A}$, p53 and $p21^{Waf1/Clip1}$ in yDCs (**Figures 1A, B**). oDCs had a trend towards constitutively higher levels of senescence markers than yDCs shown by immunoblot analysis of induced $p16^{INK4A}$, p53 and $p21^{Waf1/Clip1}$, however, it only reached significance level in P53 upregulation. Chromogenic staining (**Figure 1C**) and FACS analysis (**Figure 1D**) confirmed SA-β-Gal induction in yDCs and oDCs in response to *P. gingivalis* or doxorubicin. Senolytic agent rapamycin (Sargiacomo et al., 2020) reversed *P. gingivalis*-induced $p16^{INK4A}$, p53 and $p21^{Waf1/Clip1}$ and *P.gingivalis*-induced SA-β-Gal in in yDCs and oDCs. *P.gingivalis* LPS induced increased expression of p53 and $p21^{Waf1/Clip1}$, but not $p16^{INK4A}$ and SA-β-Gal in yDCs compared to control yDCs with no infection. IL-1β, TNFa, and IL6 are known to be major constituents of the SASP. Here we show that *P. gingivalis* was the most potent inducer of IL-1b, and TNFa transcripts in yDCs and oDCs while increasing IL-6 relative mRNA expression only in yDCs. Rapamycin ablated TNFa, and reduced IL-1b but did not influence IL-6 induction by *P. gingivalis* in yDCs (**Figure 1E**).

Impairment of Maturation Function in oDCs or yDCs Exposed to *P. gingivalis*

In view of CS profiling results, we examined the phenotype and maturation functions of oDCs and yDCs before and after co-culture with *P. gingivalis* or LPS by FACS analysis (**Figure 2A**). Constitutive expression of CD86 and MHCII was lower in oDCs than yDCs. E. coli LPS elicited a strong DC maturation response,

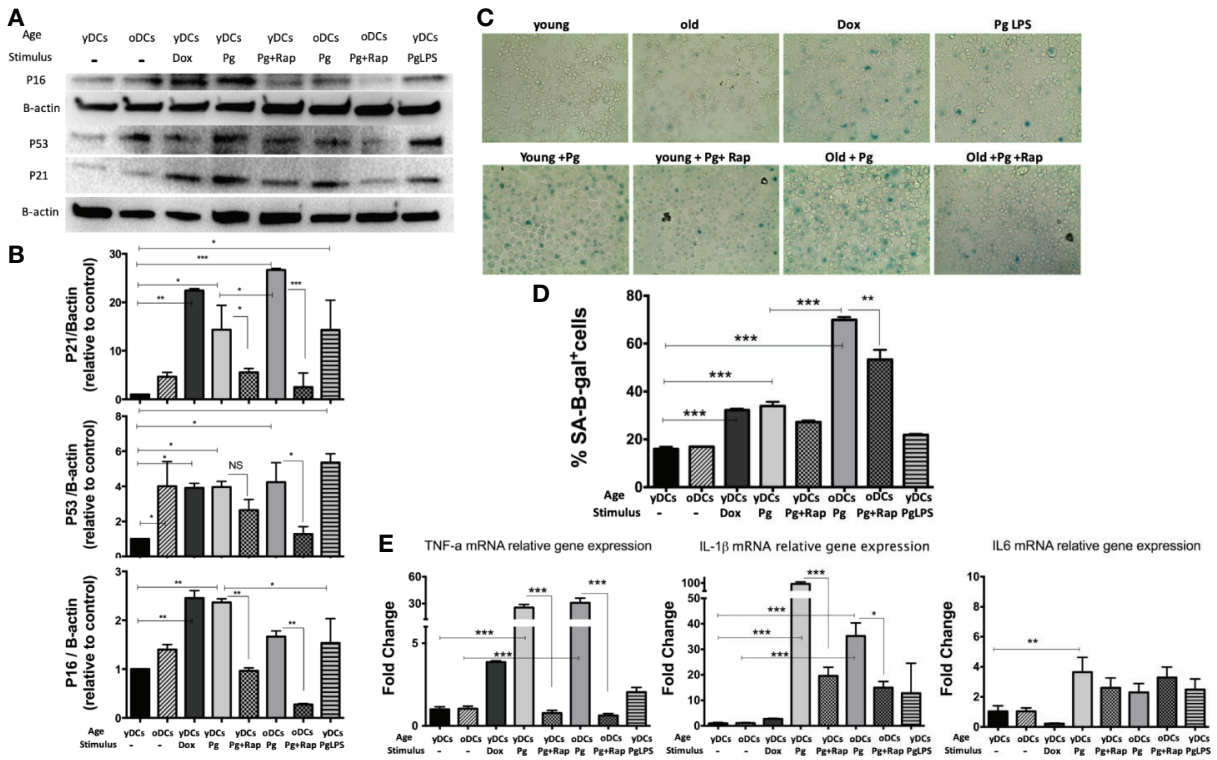

FIGURE 1 | *P.gingivalis* induces immune senescence in murine bone marrow derived DCs (DCs): At day 6, DCs from young (yDCs) and old (oDCs) mice were co-cultured with *P.gingivalis* (10 MOI) ± Rapamycin (1μM), yDCs were treated with Dox (50nM) or *P.gingivalis* LPS (100ng/ml) and CS profiling was performed at day 8. **(A)** Representative western blot images for p16 ^{INK4A}, p53, and p21$^{Waf1/Clip1}$ protein expression in BMDCS treated with *P.gingivalis* ± Rapamycin, Dox or LPS. **(B)** Densitometric analysis of p16 ^{INK4A}, p53, and p21$^{Waf1/Clip1}$ protein expression in BMDCs. β-actin was used as a loading control. Band densities were normalized to β-actin, and data presented as fold change relative to the control (yDCs with no stimulus). **(C)** Representative images of SA-β-gal staining of BMDCs at PH 6, blue stain indicates senescence **(D)** Quantification of SA-β-gal positive cells using FACS analysis. **(E)** qPCR analysis showing relative mRNA expression of TNFa, IL-1β- and IL6 in BMDCs treated with *P.gingivalis* ± Rapamycin, Dox or LPS. Relative gene expression was calculated using delta-delta CT method and presented as fold change relative to the control (yDCs.). Analysis was done using one-way ANOVA and Tukey multiple comparison *post hoc* test (Data are expressed as means ± SD, *p<0.05, **p<0.01, ***p<0.001). NS, not significant.

relative to PgLPS in yDCs, but oDCs were less responsive to either stimulant. *P.gingivalis* did not induce maturation of yDCs or oDCs, relative to control and levels were significantly lower than that induced by E.coli LPS, and CD86 and MHCII significantly lower than that induced by Pg LPS. Interestingly, *P.gingivalis* significantly reduced constitutive CD86, and CD80 levels in oDCs (51.06%, 47.8%) compared to control oDCs with no infection (27.6% and 33.9%) respectively (**Figures 2B, C**). Rapamycin reversed *P.gingivalis*-induced deficit in maturation as shown by a significant increase in expression of MHCII, CD86 and CD80 in yDCs and oDCs.

P. gingivalis Invasion for Robust Immune Senescence in yDCs

We hypothesized that active invasion of DCs by *P. gingivalis* (Zeituni et al., 2009; Zeituni et al., 2010; Zeituni et al., 2010; Acosta et al., 2013) was a critical factor in robust immune senescence. Accordingly, yDCs were cocultured with CFSE-labeled *P. gingivalis* in the presence or absence of cytochalasin D. Invasion was imaged by confocal microscopy, with SA-β-Gal, MHCII, CD80 and CD86 expression assessed by flow cytometry. Images show internalized *P. gingivalis* (**Figure 3A**), associated with increased SA-β-Gal expression on yDCs, and unresponsiveness in MHCII, CD80 and CD86 expression (**Figures 3B, C**). Pre-treatment of yDCs with cytochalasin D reduced *P. gingivalis* invasion, reversed SA-β-Gal response and restored the MHCII, CD86 and CD80 responsiveness (**Figures 3B, C**). E coli LPS control established that yDCs were fully capable of maturation.

PgDCexo Are Typical Exosomes With Distinctive Characteristics

CS is a complex cellular inflammatory process in non-immune (Naylor et al., 2013), and immune cells (Mondal et al., 2013; Salminen, 2020); most notable feature being induction of the SASP. Exosomes have emerged as an important characteristic of the SASP (Acosta et al., 2013). Here, exosomes released by *P.gingivalis* infected yDCs (PgDCexo), relative to uninfected control DCs were isolated, characterized and quantitated. Correct size distribution (30-150 nm) was confirmed by nanotracking analysis (**Figure 4A**). Enumeration of secreted exosomes indicate 2-fold greater number of exosomes from

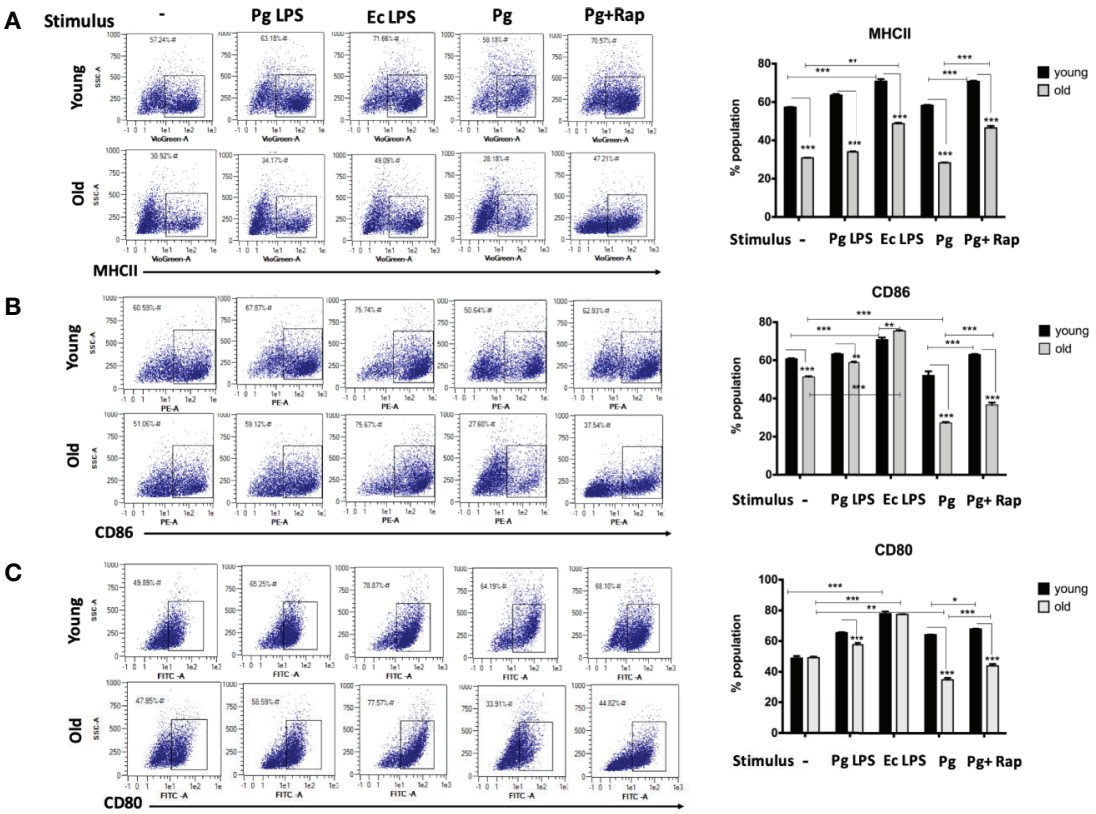

FIGURE 2 | *P.gingivalis* impairs maturation of bone marrow derived dendritic cells(DCs) from young and old mice. At day 6, DCs from young (yDCs) and old (oDCs) mice were co-cultured with *P.gingivalis* (10 MOI) ± Rapamycin (1μM), Pg LPS (100ng/ml) or Ecoli LPS (100ng/ml). Cells were harvested at day 8 and analyzed by flow cytometry for the expression of maturation markers, MHCII and co stimulatory molecules CD80 and CD86. **(A)** Flow cytometry scatter gram and its corresponding bar graph showing % of MHCII positive cells in young (upper panel) and old (lower panel), DCs gated on $CD11c^+$ cells (gate not shown). **(B)** Flow cytometry scatter gram and its corresponding bar graph showing % of CD86 positive cells in young (upper panel) and old (lower panel), DCs gated on $CD11c^+$ cells (gate not shown).**(C)** Flow cytometry scatter gram and its corresponding bar graph showing % of CD80 positive cells in young (upper panel) and old (lower panel), DCs gated on $CD11c^+$ cells (gate not shown). Analysis was done using Two-way ANOVA and Dunn's correction test. (Data are expressed as means ± SD, *p<0.05, **p<0.01, ***p<0.001). NS, not significant.

P. gingivalis-infected yDCs (=4.2 x 10^8 per 10^6 DCs) than control DCs (ctl DC) (=2 x 10^8). This increase was ablated by senolytic agent rapamycin (=2.2 x 10^8) (**Figure 4B**). Correct phenotype of typical DC exosomes was confirmed by immunogold TEM for CD63 (**Figure 4C**) and SEM showing characteristic cup-shaped morphology (**Figure 4D**). Western blotting analysis (**Figure 4F**) establishes typical exosomal markers CD81, Alix and TSG101 on PgDCexo and control iDC exo and stim DCexo (Elashiry et al., 2020). PgDCexo also express the minor Mfa1 fimbrial protein, an adhesin used by *P.gingivalis* to invade DCs *in vitro* (Zeituni et al., 2010) and *in vivo* (Carrion et al., 2012; El-Awady et al., 2015; El-Awady et al., 2019). Co-localization of Mfa1 fimbrial protein with the tetraspanin CD81, a eukaryotic exosomal marker was confirmed using TEM immuno-gold double labeling (**Figure 4E**). Passage of PgDC exo over a Pan exo magnetic bead column 1x and 2x removed 99.9% and 99.99% of particles, respectively. Column eluate was enriched in Mfa1, CD81, Alix, TSG101 and CD9, consistent with bona fide exosomes, while run-through contained trace levels of Mfa1, Alix, TSG101 and CD9 (**Supplementary Figure 1**). PgDCexo also contain IL-6 and mature IL-1β, consistent with inflammasome activation and the SASP (Acosta et al., 2013). StimDCexo, from donor yDCs treated with LPS, also expressed IL-6 and IL-1β, as previously reported (Elashiry et al., 2020), albeit at lower levels than PgDCexo (**Figure 4F**). Bioinformatics analysis of miRNA content of exosomes (**Figure 4G**) show miRNAs upregulated (red) and down regulated (blue) in PgDCexo, relative to control exosomes from imDCs or LPS-matured DCs (stimDC). Distinct pattern of blue/red miRNAs in PgDCexo versus controls is particularly striking. Of particular note are miRNAs involved in disruption of immune homeostasis, through anti-apoptosis and anti-autophagy functions, including miR106b, miR-17-5p, miR378a-3p, miR-324-5p, miR-132-3p. MiR17-5p was 1.71-fold upregulated in PgDCexo vs. imDCexo, and 1.2-fold downregulated in mDCexo vs imDCexo (**Figure 4G**). MiRNA 132-3p was 4-fold upregulated ($p<0.05$) in Pg-induced exo, consistent with that previously observed in aged BMDCs (Park et al., 2013).

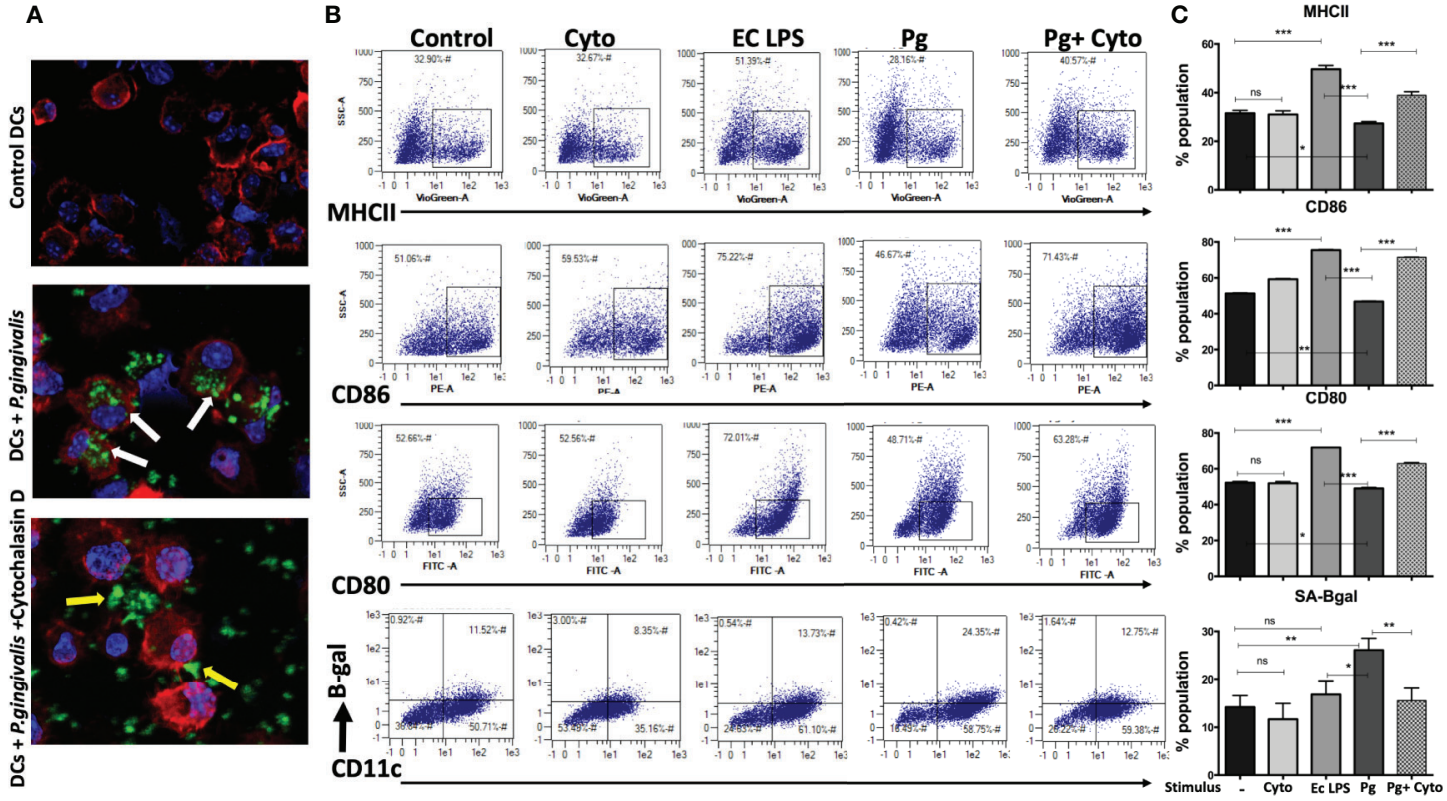

FIGURE 3 | *P.gingivalis*-induced senescence and impaired maturation in yDCs is abrogated by inhibition of its uptake by DCs. At day 6, yDCs were co-cultured with *P.gingivalis* (10MOI) ± Cytochalasin D (1ug/ml), or cytochalasin D alone, or E-coli LPS. Cells were harvested at day 8 and analyzed by flow cytometry for the expression of maturation markers, MHCII and co stimulatory molecules CD80 and CD86 and SA-β-gal. **(A)** Representative confocal microscopy images showing uptake (white arrows) of CFSE labeled *P.gingivalis* (green) into DCs with labeled actin (red) and counterstained with DAPI for nuclear staining (blue). Yellow arrows indicating the inhibition of uptake and accumulation of CFSE labeled *P.gingivalis* on the outer surface of the cell. **(B)** Flow cytometry scattergrams showing effect of inhibition of *P.gingivalis* uptake using cytochalasin D on expression of maturation markers, measured by % population of MHCII(first panel), CD86 (second panel) and CD80 (third panel) and activation of senescence marker SA-β-gal (fourth panel). All gated on $CD11c^{+}$ cells (gate not shown). **(C)** Summary bar graphs of the flow cytometry data). Analysis was done using one-way ANOVA and Tukey multiple comparison *post hoc* test (Data are expressed as means ± SD, *p<0.05, **p<0.01, ***p<0.001). NS, not significant.

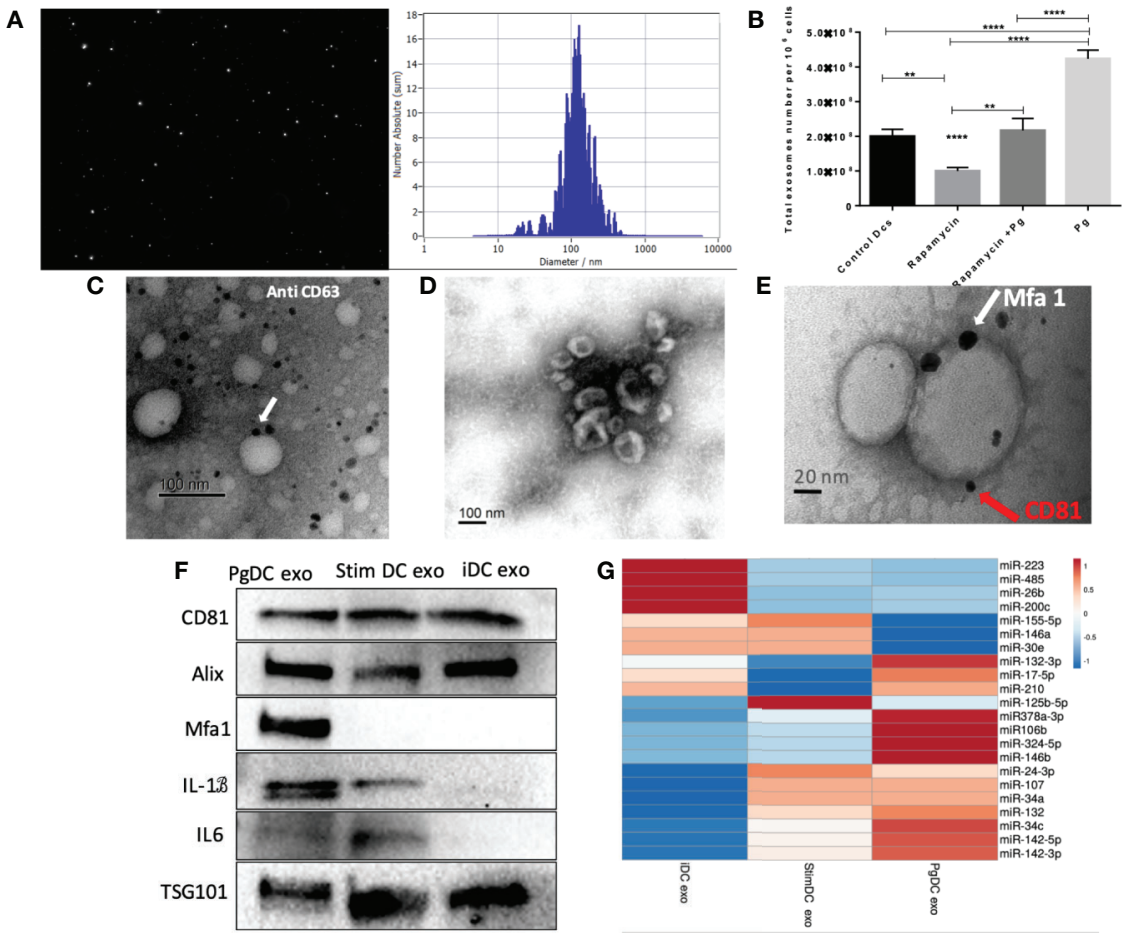

FIGURE 4 | Characterization of exosomes released from DCs infected with *P.gingivalis* (PgDCexo): **(A)** Nano tracking analysis (NTA) to determine Exo number and size distribution in nanometer (nm). **(B)** Total number of Exo released per 10^6 cells as determined by NTA from DCs treated or non-treated with Pg and/or Rapamycin **(C)** Immuno-gold TEM showing EXO marker, tetraspanin CD63. **(D)** SEM showing characteristic Exo morphology. **(E)** Co-localization of Mfa1 bacterial protein (large- sized gold Nano particle indicated with white arrow) with the eukaryotic cellular exosomal marker, CD81 (small-sized gold Nano particle indicated with red arrow) using TEM immune-gold double labeling **(F)** Western blot showing Exo-related markers TSG101, Alix, and tetraspanin CD81 and proinflammatory cytokines IL6, TNFa and IL-1b and Mfa1 in exosomes released from control immature DCs (iDCs), Ecoli LPS-stimulated mature DCs (StimDCexo) and Pg infected DCs (PgDCexo). **(G)** miRNA analysis of Pg or Ecoli LPS-induced DCs Exo (PgDC exo and StimDCexo respectively) compared to immature control DCs exo; (iDCexo). (iDCs), control immature DCs exo, (StimDCexo), Ecoli LPS-stimulated mature DCs exo; (PgDCexo), Pg-infected DCs. **p<0.01, ****p<0.001, 1 Way ANOVA.

DC Exosomal SASP Induced by *P. gingivalis* Amplifies Paracrine Immune Senescence in Recipient yDC

We hypothesized PgDCexo would be potent inducers of immune senescence in non-senescent recipient yDCs. Co-culture of DiI-labeled PgDCexo with recipient yDCs confirmed their uptake as shown by confocal microscopy (**Figure 5A**). CS profiling of recipient yDCs indicate activation of SA-β-Gal, by chromogenic staining (**Figure 5B**) and confirmed by flow cytometry using fluorescent SA-β-Gal staining (**Figure 5C**). Moreover, this increase was significant compared to control yDCs and yDCs treated with exosomes from immature DCs (iDCexo). A significant increase in SA-β-Gal$^+$ DCs was also induced directly by doxorubicin and Pg LPS, while stimDCexo induced a non-significant trend for increased SA-β-Gal$^+$ DCs (**Figure 5C**). Western blot analysis of PgDCexo recipient DCs (**Figures 5D, E**) showed a significant upregulated expression of p16 ^{INK4A}, p53 and p21$^{Waf1/Clip1}$ relative to non-treated DCs and similar to Dox-treated yDCs. No effect on p16 ^{INK4A}, p53 and p21$^{Waf1/Clip1}$ expression was observed with iDCexo treatment, while stimDCexo induced upregulation which was not statistically significant. Pg LPS showed an upregulation in p16 ^{INK4A} with no significant effect on p53 and p21$^{Waf1/Clip1}$ expression. Rapamycin reversed PgDCexo-induced senescence (**Figures 5C, E**).

Maturation and Antigen Presenting Functions of Recipient DCs Shut Down by PgDCexo

The maturation and antigen presentation functions of yDCs cocultured with PgDCexo were examined. FACS analysis

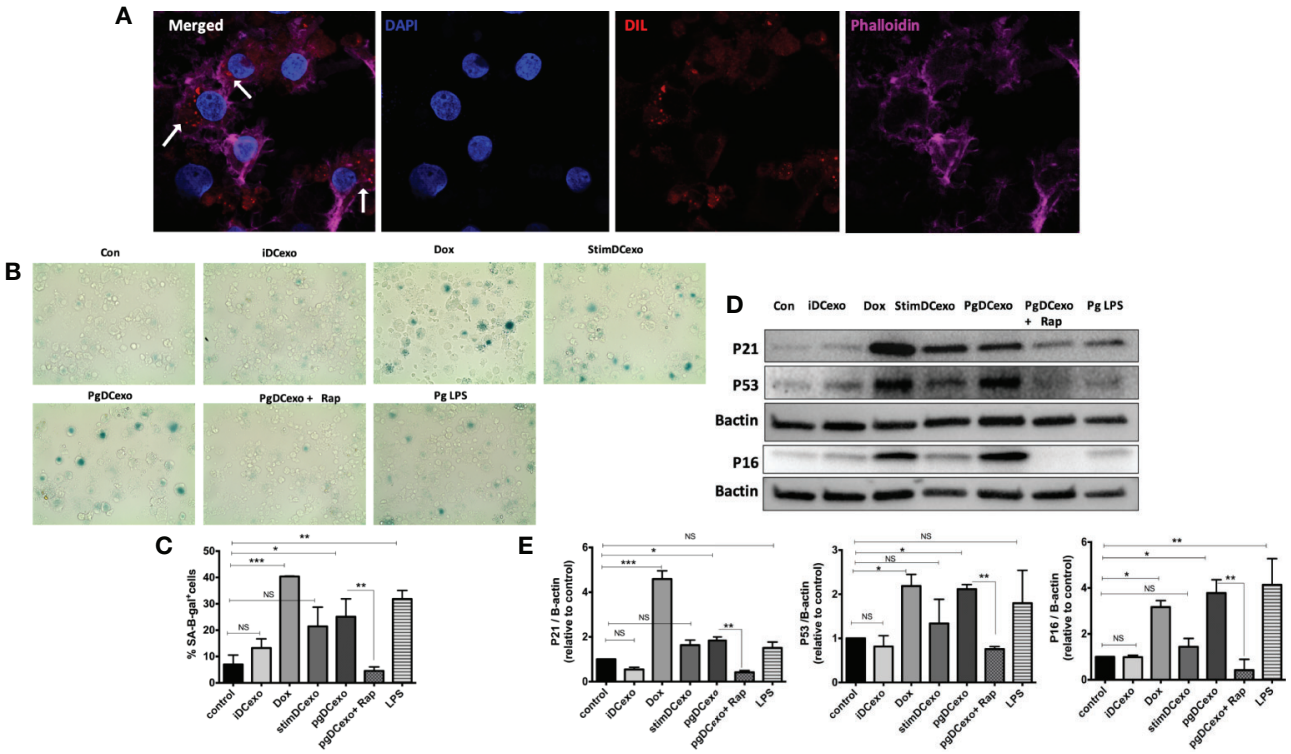

FIGURE 5 | PgDCexo induces paracrine immune senescence in yDCs: **(A)** Confocal microscopy images showing uptake of DiI-labelled EXO (red) by yDCs with phalloidin actin staining (magenta) and counter stained with blue nuclear stain DAPI (white arrows indicating EXO internalization by yDCs). **(B)** Representative images of SA-β-gal staining of yDCs treated with PgDCexo ± Rapamycin, Stim DCexo, iDCexo, Dox, Pg LPS or received no treatment (Con) at PH 6, blue stain indicates senescence. **(C)** Quantification of % population of SA-β-gal^{+} DCs using FACS analysis. **(D)** Representative immunoblot image of p16 ^{INK4A}, p53, and p21$^{Waf1/Clip1}$ expression in yDCs with different treatments. **(E)** Densitometric analysis of p16 ^{INK4A}, p53, and p21$^{Waf1/Clip1}$ protein expression in yDCs with different treatments. β-actin was used as a loading control. Band densities were normalized to β-actin, and data presented as fold change relative to the control. Analysis was done using one-way ANOVA and Tukey multiple comparison *post hoc* test (Data are expressed as means ± SD, *p<0.05, **p<0.001, ***p<0.0001). (iDCs), control immature DCs exo; (StimDCexo), Ecoli LPS-stimulated mature DCs exo; (PgDCexo), Pg-infected DCs. NS, not significant.

revealed ablation of maturation function of PgDCexo recipient yDCs as shown by a significant decrease in maturation markers MHCII, CD86 and CD80 (**Figures 6A, B**), which was restored by rapamycin treatment. Positive control LPS and stimDCexo, but not iDCexo, promoted yDC maturation,. Ability of yDCs treated with PgDCexo to engage in antigen presentation was assessed by coculture of DCs with Ova peptide and CFSE labeled splenic CD4+ T cells from OTII mice. T cell proliferation was assessed by percentage loss of CFSE with each T cell generation, with gating shown in **Figure 7A**). Negative controls for proliferation include T cells only, yDC/T cells only, Ova/T cells, and Rap/T cells, none of which supported proliferation (**Figure 7C**). Robust proliferation of T cells (=84.4%) was induced by yDCs pulsed with Ova. Coculture of yDCs with PgDCexo ablated T cell proliferation by 51%. This was reversed with rapamycin. Direct infection of yDCs with *P. gingivalis* inhibited T cell proliferation to Ova by 30%, which was restored with rapamycin. Control iDC exo from immature yDCs did not alter T cell proliferation (**Figure 7B**). Summary graphs are shown in **Figure 7D**.

DISCUSSION

Periodontitis (PD), a disease of inflammaging, is comorbid with other age-related diseases (Eke et al., [[NoYear]]; Carrion et al., 2012; Michaud et al., 2017; Teixeira et al., 2017; Zhang et al., 2019) but underlying mechanisms remain to be elucidated. The goals of the present report were to examine whether immune cells, representative of those at the oral mucosal-microbe interface in PD (Cutler and Teng, 2007; Hovav, 2014; Dutzan et al., 2016), are vulnerable to CS *in vitro*, as induced by the dysbiotic pathogen *P. gingivalis* (Hajishengallis et al., 2011; Hajishengallis et al., 2012; Dutzan et al., 2018), and whether this occurs by both direct means (i.e. through infection of target cells) and indirect means (i.e. through induction of the exosomal SASP.

Inflammatory DCs convey *P.gingivalis* and other microbes to distant sites (Carrion et al., 2012; Rajendran et al., 2019), which may have profound implications for age-related comorbid diseases associated with PD. *P. gingivalis* directly invades DCs, hyperactivating the Akt-1/Foxo1 pathway (Arjunan et al., 2016; Arjunan et al., 2018; Meghil et al., 2019). This pathway: Akt1,

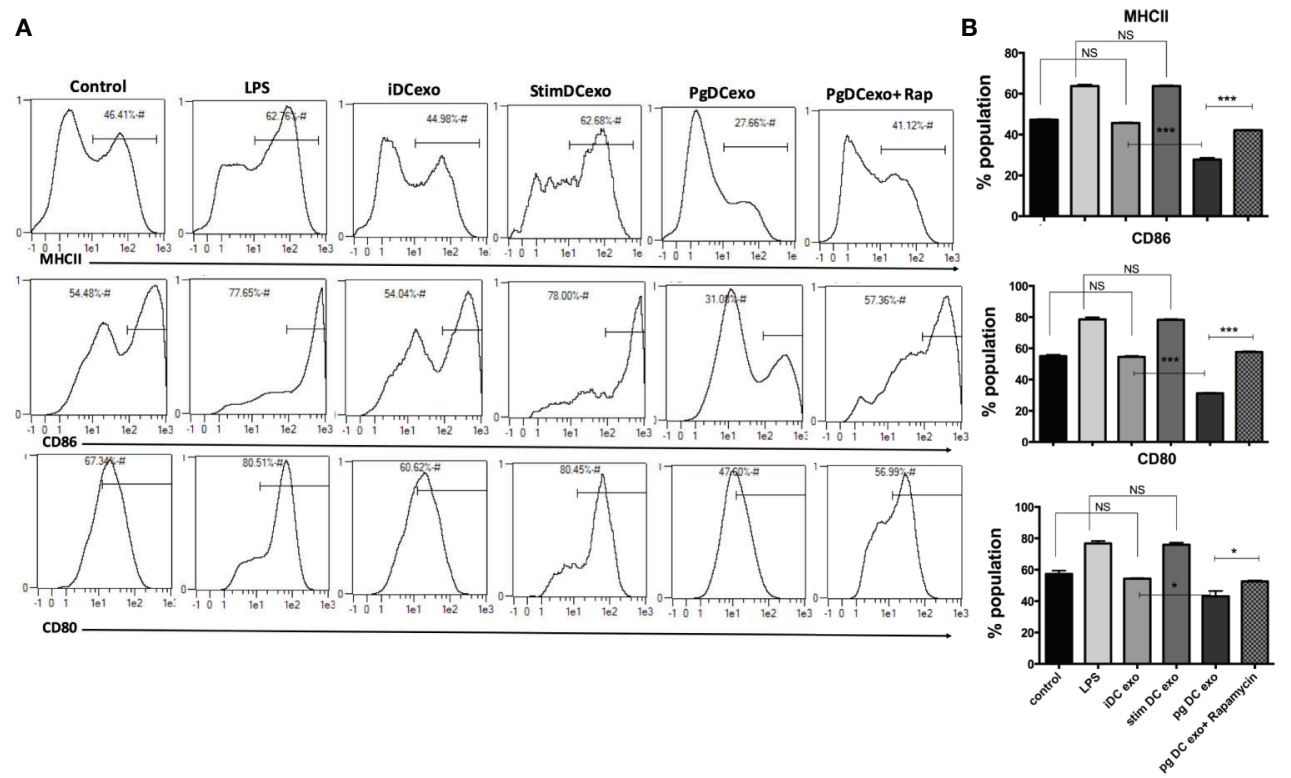

FIGURE 6 | PgDCexo impairs maturation of recipient yDCs: At day 6, yDCs were treated with PgDCexo ± Rapamycin, StimDCexo, iDCexo, Dox, E-coli LPS or received no treatment (Con) and incubated for 48 hrs. Cells were harvested at day 8 and analyzed by flow cytometry for the expression of maturation markers MHCII and co stimulatory molecules CD80 and CD86. **(A)** Representative flow cytometry histograms showing % of MHCII^{+} population in yDCs (upper panel) %CD86^{+} (middle panel) and %CD80+ (lower panel) gated on CD11c^{+} cells (gate not shown). **(B)** Summary bar graphs for flow cytometry data shown in **(A)**. Analysis was done using one-way ANOVA and Tukey multiple comparison *post hoc* test (Data are expressed as means ± SD, *p<0.05, ***p<0.001). (iDCs), control immature DCs exo; (StimDCexo), Ecoli LPS-stimulated mature DCs exo; (PgDCexo) Pg-infected DCs. NS, not significant.

pFOXO1, FOXP3, IDO1, BIM and Bcl-2, is hyperactivated in PD in humans (Arjunan et al., 2018) and in mice (Song et al., 2017), and has been recognized for its anti-apoptotic, immunosuppressive functions in DCs, leading to disruption of immune homeostasis in PD (Arjunan et al., 2018). However, the link to premature senescence (Nogueira et al., 2008) vis á vis *P.gingivalis* infection was not appreciated at the time. Accordingly, the focus here was on analysis of bone marrow derived DCs from young (yDCs) and old (oDCs) mice, by subjecting them to coculture with prototypic CS inducer doxorubicin or *P.gingivalis* 381, followed by CS profiling (Gorgoulis et al., 2019). Interestingly, yDCs were provoked to premature CS, evidenced by significant activation of SA-B-Gal, p16 ^{INK4A}, p53, and p21$^{Waf1/Clip1}$. Further, our data suggest that direct 'premature aging' of yDCs is mediated by invasion of *P.gingivalis*. This was confirmed by pre-treatment of yDCs with cytochalasin D, which reduced invasion, reversed SA-B-Gal response and restored the MHCII, CD86 and CD80 response.

Age-related impairment of the immune response (Hajishengallis, 2010; Boots et al., 2013; Ebersole et al., 2016; Preshaw et al., 2017) is known as immune senescence, and has been reported in monocytes, macrophages, DCs and T cells [reviewed in (Linton and Thoman, 2014)]. This is coupled with the constitutive release of inflammatory mediators, cytokines, and chemokines, leading to elevated basal inflammation or "inflammaging" (Ebersole et al., 2016). DCs from aged mice have impaired antigen-presenting function (Moretto et al., 2008; Pereira et al., 2011; Li et al., 2012), decreased migratory capacity (Wu et al., 2016), and increased production of inflammatory cytokines (Agrawal et al., 2012; Ebersole et al., 2016). However, the role of aged DCs in immune senescence in response to etiological agents of PD are presently unclear. Results revealed elevated basal levels of senescence markers in oDCs relative to yDCs. However, it only reached significance level in P53 marker. Nonetheless, these elevations in the basal levels were sufficient to induce a more exaggerated response of oDCs to *P.gingivalis* induction of P21 and SA-B-gal. Moreover, significant lower constitutive expression of basal levels of MHCII and co-stimulatory molecule CD86 in oDCs relative to yDCs shown here are consistent with DC immune senescence accompanied with aging (Shurin et al., 2007). Interestingly, *P.gingivalis*-induced SA-B-gal and p21$^{Waf1/Clip1}$ and impaired maturation were more aggravated in oDCs relative to yDCs, abrogated with a senotherapeutic agent, Rapamycin. This suggests that a bidirectional relationship of PD and CS might exist,

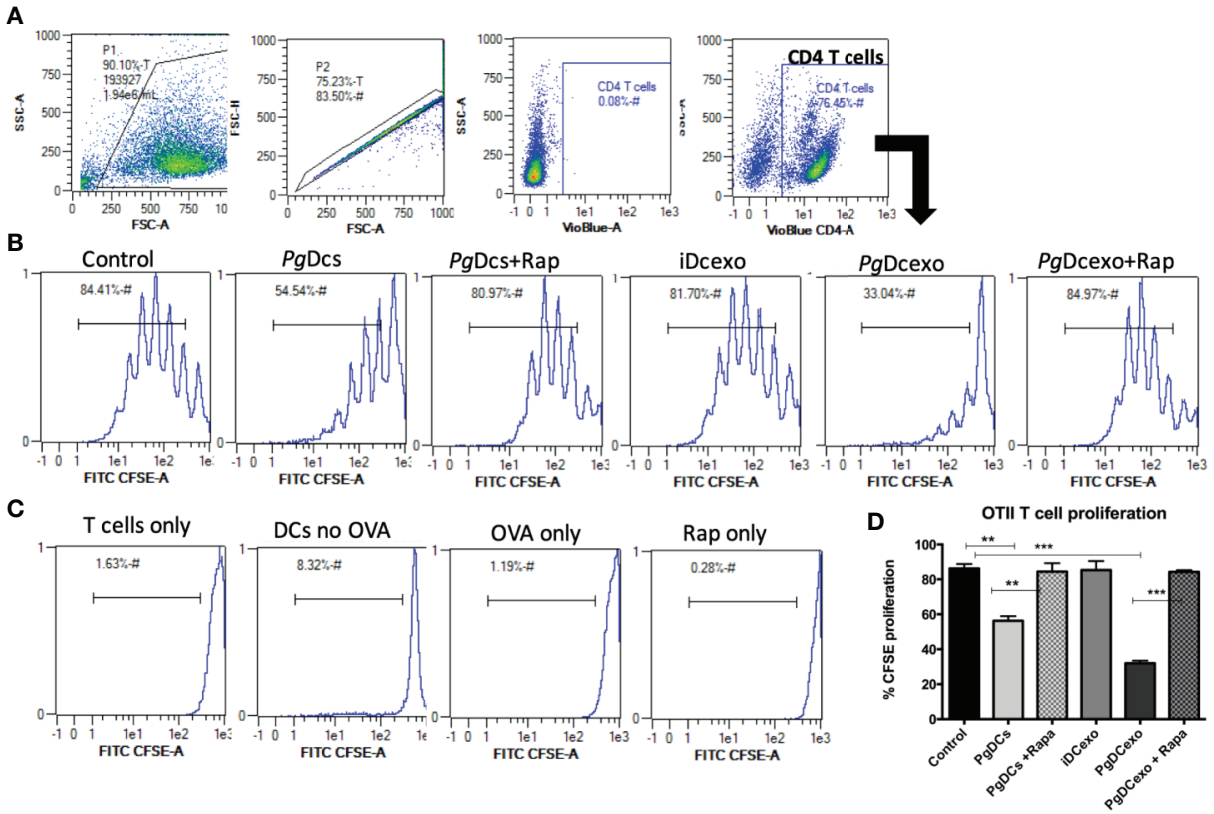

FIGURE 7 | PgDCexo impairs antigen presentation of recipient yDCs: **(A)** Flow cytometry scatter grams showing Gating strategy. **(B)** Representative flow cytometry histograms showing % proliferation of CFSE labeled splenic ovalbumin specific CD4 T cells from OTII mice co-cultured with pre-treated yDCs. **(C)** Flow cytometry histograms showing % of CFSE proliferation in negative controls for proliferation which include T cells only, yDC/T cells only, Ova/T cells, and Rap/T cells. **(D)** Summary bar graphs for flow cytometry data shown in **(B)**. Analysis was done using one-way ANOVA and Tukey multiple comparison *post hoc* test (Data are expressed as means ± SD, **p<0.01, ***p<0.001). (iDCs), control immature DCs exo; (StimDCexo), Ecoli LPS-stimulated mature DCs exo; (PgDCexo), Pg-infected DCs.

wherein inducers of PD can promote CS and CS accompanied with aging can promote PD.

CS is traditionally ascribed to cell cycle arrest in proliferating cells, but can also occur in terminally differentiated cells (Herranz and Gil, 2018; Sapieha and Mallette, 2018; Wengerodt et al., 2019) such as neurons (Jurk et al., 2012), hepatocytes (Kang et al., 2011), osteocytes (Aquino-Martinez et al., 2020), and macrophages (Hall et al., 2016). Macrophages from aged mice upregulate expression of p16 ^{INK4A} and SA-B-gal (Hall et al., 2016), as do macrophages isolated from peritoneal inflammation (Liu et al., 2019). However, macrophages can express elevated p16 ^{INK4A} and SA-B-gal due to physiological stimuli which do not necessarily indicate senescence (Hall et al., 2017), thus necessitating that a more comprehensive analysis of senescence be conducted. Thus, a functional analysis of yDCs 'prematurely aged' by *P. gingivalis* was performed, revealing a profound impairment of maturation functions, and inability to stimulate antigen specific T cell proliferation, similarly to oDCs.

Microbial-induced senescence has been variously attributed to DNA damage by bacterial genotoxins (Aquino-Martinez et al., 2020), oxidative stress induction and ROS production (Aquino-Martinez et al., 2020; Humphreys et al., 2020) or persistent activation of TLR4-NF-KB-P21-P53 pathway (Feng et al., 2014). In the present study, the impairment of maturation of yDCs and oDCs, was accompanied by a robust IL-1b, TNFa and IL6 response, consistent with an inflammasome mediated response to *P.gingivalis* (Arjunan et al., 2016; Tyagi et al., 2017). NLR pyrin domain-containing 3 (NLRP3) inflammasome activation is involved in senescence induction (Luo et al., 2019; Shi et al., 2019) and its inhibition suppresses CS in mesenchymal stromal cells (Shi et al., 2019). NLRP3 inflammasome could play a potential role in *P.gingivalis*-induced immune senescence in DCs, however, further analysis of caspase-1 and/or caspase 11 (Paroli et al., 2018) activation are required to examine such a role.

Induction of the exosomal SASP is an indirect, yet more powerful mechanism by which *P. gingivalis* amplifies senescence in bystander cells. The SASP consists of secreted inflammatory cytokines, chemokines, growth factors and extracellular vesicles (EV) (e.g. exosomes), collectively called the secretome. The secretome can amplify CS signaling in an autocrine fashion or can transmit CS to bystander cells in a paracrine fashion (Acosta

et al., 2013). Senescent fibroblasts *via* the SASP transmit an immunosuppressive tumorigenic response in mice (Ruhland et al., 2016). Exosomes are a particularly active component of SASP (Jakhar and Crasta, 2019). Infection alters the exosome biogenesis and number from the host cell (Zhang et al., 2018). Indeed, an increase in the number of generated exosomes was observed from DCs infected with *P.gingivalis*, through as yet unclear mechanisms. Presumably, this involves deployment of endocytic pathways of exosome biogenesis by pathogenic bacteria. Autophagy inhibition promotes an increase in exosome secretion to compensate for the accumulation of damaged proteins or organelles, whilst activation of autophagy reduces exosome release due to the fusion of MVB and autophagosomes (Tian et al., 2019). Consistent with this notion is our observation that *P.gingivalis*-induced exosome release was ablated by senolytic (and pro-autophagy agent) rapamycin.

Exosomes derived from infected cells carry bacterial RNA and protein (Zhang et al., 2018), and can contribute to spread of infection and disease pathologies (Zhang et al., 2018). The DC invasin Mfa1 fimbrial protein (Zeituni et al., 2009; Zeituni et al., 2010) was detected on PgDCexo by immunoblot and confirmed by immuno-gold transmission electron microscopy. Colocalization of Mfa1 with the tetraspanin CD81, a well-defined eukaryotic exosomal marker, suggests a common pathway of biogenesis. Studies have shown that outer membrane vesicles (OMV) secreted by bacteria range from 50-250 nm (Xie, 2015) and contribute to the virulence of the bacteria by carrying a number of antigenic proteins from the parent cell (Schwechheimer and Kuehn, 2015). Thus, a minor contribution of outer membrane vesicles (OMV) from Pg cannot be ruled out. However, based on results of anti- CD81, CD9, and CD63-linked magnetic bead separation of PgDC exo (**Figure S1**) only 0.01% of the total particles could potentially be Pg OMVs. Moreover, immunoblot analysis indicates that the Mfa-1 protein incorporated in the eluate while barely detectable in the run through (**Figure S1C**). These results indicate that the majority of PgDC exo are DC-derived exosomes that contain Pg Mfa-1 fimbrial adhesin, through an as yet undefined biogenesis pathway. Whether the Mfa-1 is present on the surface membrane of the exosome and/or present inside the exosomal lumen remains to be determined. Previously, our group has shown that exosomes protect their protein cargo against proteolytic degradation (Elashiry et al., 2020). *P.gingivalis*, through its glycosylated mfa1 fimbriae, binds to C-type lectin receptor CD209 to invade DCs (Zeituni et al., 2009; Zeituni et al., 2010; El-Awady et al., 2015; El-Awady et al., 2015; El-Awady et al., 2019). This activates mTORC1 dependent anti-autophagy signaling pathway (El-Awady et al., 2015; Arjunan et al., 2016; Arjunan et al., 2018; Meghil et al., 2019). Thus, the presence of Mfa-1 on/in DC exosomes should confer distinct functional advantage for penetration into tissues and blood for enhanced and sustainable bacterial virulence.

Perhaps most significantly, PgDCexo were taken up by recipient (bystander) yDCs, promoting their senescence induction, by shutting down maturation and antigen presenting functions. Further studies are required to dissect the mechanisms involved, presumably by a combination of direct surface receptor binding, endocytosis, and intracellular signaling (Jakhar and Crasta, 2019; Elashiry et al., 2020). In this context, the microRNA (miRNA) content of PgDCexo, is worth mentioning, as it results from a complex sorting process during cellular biogenesis and export (Villarroya-Beltri et al., 2013). MiRNAs are especially active in post transcriptional regulation of genes (Stark et al., 2008) of CS and aging (reviewed in (Smith-Vikos and Slack, 2012)). Reported functions of miRNAs induced in PgDCexo include inhibition of beclin-mediated autophagy (Chatterjee et al., 2014), repression of ULK1 and LC3I/II (Duan et al., 2015) (miR17-5p), prevention of autophagy-dependent eradication of intracellular bacteria (Lu et al., 2014) (miR106B). Four-fold upregulation of miRNA 132-3p in PgDCexo ($p<0.05$), is consistent with aged bone-marrow derived DCs (BMDC). Other miRNAs in aged BMDC under normal and activated conditions include miR-155, miR-223, miR-146a, miR-146b, miR-132, miR-142-5p, and miR-142-3p. A frequently identified miRNA in PgDCexo was miR-24-3p, also identified in saliva exosomes of those with advanced age ($p = 0.042$), and with periodontal disease progression (Machida et al., 2015). Ten miRNAs recently identified to be deregulated early, in another disease of aging Alzheimer's disease (Swarbrick et al., 2019), recently linked to *P.gingivalis* infections and periodontitis (Ryder, 2020). These include hsa-mir-107, hsa-mir-26b, hsa-mir-30e, hsa-mir-34a, hsa-mir-485, hsa-mir200c, hsa-mir-210, hsa-mir-146a, hsa-mir-34c and hsa-mir-125b.

In conclusion, *P. gingivalis* induces premature senescence through direct cellular invasion(autocrine) and by stimulating secretion of inflammatory exosomes that amplify immune senescence in paracrine to bystander cells. Our study signifies a potential role of exosome-mediated signaling in the pathogenesis of periodontal disease. In vivo studies are underway to evaluate such role and further dissect the mechanism of PgDCexo-induced paracrine senescence in PD.

DATA AVAILABILITY STATEMENT

The raw data supporting the conclusions of this article will be made available by the authors, in response to a detailed written request.

ETHICS STATEMENT

The Institutional Animal Care and Use Committee (IACUC) of Augusta University (protocol # 2013-0586) approved all experimental procedures on C57BL/6 mice.

AUTHOR CONTRIBUTIONS

Study design (CC, RE, and ME). Data generation, analysis, and interpretation (RE, ME, CC, and YL). Intellectual input (AE, YL, and MH). Manuscript preparation (CC and RE). All authors contributed to the article and approved the submitted version.

FUNDING

This project was supported by a grant from the Carlos and Marguerite Mason Trust and by an Intramural grant from the Office of the Vice President for Research, Augusta University.

ACKNOWLEDGMENTS

We would like to thank the Electron microscopy core at Augusta University for conducting the TEM and immunogold plating.

SUPPLEMENTARY MATERIAL

The Supplementary Material for this article can be found online at: https://www.frontiersin.org/articles/10.3389/fcimb.2021.669989/full#supplementary-material

Supplementary Figure 1 | (A) Schematic diagram showing the work flow of magnetic separation of EXO labeled with CD81, CD9 and CD63. **(B)** Nano tracking analysis (NTA) to determine Exo number and size distribution in nanometer(nm) within the run through. Y-axis is linear in all three histograms, with the range being, from left to right: 10^{11}, 10^{8}, 10^{7}. **(C)** WB analysis of proteins in the eluate and the run through after magnetic separation.

REFERENCES

Acosta, J. C., Banito, A., Wuestefeld, T., Georgilis, A., Janich, P., Morton, J. P., et al. (2013). A Complex Secretory Program Orchestrated by the Inflammasome Controls Paracrine Senescence. *Nat. Cell Biol.* 15, 978–990. doi: 10.1038/ncb2784

Agrawal, A., Sridharan, A., Prakash, S., and Agrawal, H. (2012). Dendritic Cells and Aging: Consequences for Autoimmunity. *Expert Rev. Clin. Immunol.* 8, 73–80. doi: 10.1586/eci.11.77

An, J. Y., Quarles, E. K., Mekvanich, S., Kang, A., Liu, A., Santos, D., et al. (2017). Rapamycin Treatment Attenuates Age-Associated Periodontitis in Mice. *Geroscience* 39, 457–463. doi: 10.1007/s11357-017-9994-6

Aquino-Martinez, R., Khosla, S., Farr, J. N., and Monroe, D. G. (2020). Periodontal Disease and Senescent Cells: New Players for an Old Oral Health Problem? *Int. J. Mol. Sci.* 21 (20), 7441. doi: 10.3390/ijms21207441

Aquino-Martinez, R., Rowsey, J. L., Fraser, D. G., Eckhardt, B. A., Khosla, S., Farr, J. N., et al. (2020). LPS-Induced Premature Osteocyte Senescence: Implications in Inflammatory Alveolar Bone Loss and Periodontal Disease Pathogenesis. *Bone* 132, 115220. doi: 10.1016/j.bone.2019.115220

Arjunan, P., El-Awady, A., Dannebaum, R. O., Kunde-Ramamoorthy, G., and Cutler, C. W. (2016). High-Throughput Sequencing Reveals Key Genes and Immune Homeostatic Pathways Activated in Myeloid Dendritic Cells by Porphyromonas Gingivalis 381 and Its Fimbrial Mutants. *Mol. Oral. Microbiol.* 31, 78–93. doi: 10.1111/omi.12131

Arjunan, P., Meghil, M. M., Pi, W., Xu, J., Lang, L., El-Awady, A., et al. (2018). Oral Pathobiont Activates Anti-Apoptotic Pathway, Promoting Both Immune Suppression and Oncogenic Cell Proliferation. *Sci. Rep.* 8, 16607. doi: 10.1038/s41598-018-35126-8

Boots, A. M., Maier, A. B., Stinissen, P., Masson, P., Lories, R. J., and De Keyser, F. (2013). The Influence of Ageing on the Development and Management of Rheumatoid Arthritis. *Nat. Rev. Rheumatol.* 9, 604–613. doi: 10.1038/nrrheum.2013.92

Carrion, J., Scisci, E., Miles, B., Sabino, G. J., Zeituni, A. E., Gu, Y., et al. (2012). Microbial Carriage State of Peripheral Blood Dendritic Cells (Dcs) in Chronic Periodontitis Influences DC Differentiation, Atherogenic Potential. *J. Immunol.* 189, 3178–3187. doi: 10.4049/jimmunol.1201053

Chatterjee, A., Chattopadhyay, D., and Chakrabarti, G. (2014). miR-17-5p Downregulation Contributes to Paclitaxel Resistance of Lung Cancer Cells Through Altering Beclin1 Expression. *PloS One* 9, e95716. doi: 10.1371/journal.pone.0095716

Cutler, C. W., and Teng, Y. T. (2007). Oral Mucosal Dendritic Cells and Periodontitis: Many Sides of the Same Coin With New Twists. *Periodontol* 2000 45, 35–50. doi: 10.1111/j.1600-0757.2007.00222.x

Duan, X., Zhang, T., Ding, S., Wei, J., Su, C., Liu, H., et al. (2015). Microrna-17-5p Modulates Bacille Calmette-Guerin Growth in RAW264.7 Cells by Targeting Ulk1. *PloS One* 10, e0138011. doi: 10.1371/journal.pone.0138011

Dutzan, N., Kajikawa, T., Abusleme, L., Greenwell-Wild, T., Zuazo, C. E., Ikeuchi, T., et al. (2018). A Dysbiotic Microbiome Triggers TH17 Cells to Mediate Oral Mucosal Immunopathology in Mice and Humans. *Sci. Transl. Med.* 10 (463), eaat0797. doi: 10.1126/scitranslmed.aat0797

Dutzan, N., Konkel, J. E., Greenwell-Wild, T., and Moutsopoulos, N. M. (2016). Characterization of the Human Immune Cell Network at the Gingival Barrier. *Mucosal Immunol.* 9, 1163–1172. doi: 10.1038/mi.2015.136

Ebersole, J. L., Dawson, D. A., Emecen Huja, P., Pandruvada, S., Basu, A., Nguyen, L., et al. (2018). Age and Periodontal Health - Immunological View. *Curr. Oral. Health Rep.* 5, 229–241. doi: 10.1007/s40496-018-0202-2

Ebersole, J. L., Graves, C. L., Gonzalez, O. A., Dawson, D.,. 3., Morford, L. A., Huja, P. E., et al. (2016). Aging, Inflammation, Immunity and Periodontal Disease. *Periodontol 2000* 72, 54–75. doi: 10.1111/prd.12135

Eke, P. I., Dye, B. A., Wei, L., Thornton-Evans, G. O., and Genco, R. J. Prevalence of Periodontitis in Adults in the United States: 2009 and 2010. *J. Dent. Res.* 91, 914–920. doi: 10.1177/0022034512457373

Eke, P. I., Dye, B. A., Wei, L., Thornton-Evans, G. O., Genco, R. J.Cdc Periodontal Disease Surveillance workgroup: James Beck, G. D. R. P. (2012). Prevalence of Periodontitis in Adults in the United States: 2009 and 2010. *J. Dent. Res.* 91 (10), 914–920. doi: 10.1177/0022034512457373

Elashiry, M., Elashiry, M. M., Elsayed, R., Rajendran, M., Auersvald, C., Zeitoun, R., et al. (2020). Dendritic Cell Derived Exosomes Loaded With Immunoregulatory Cargo Reprogram Local Immune Responses and Inhibit Degenerative Bone Disease In Vivo. *J. Extracell Vesicles* 9, 1795362. doi: 10.1080/20013078.2020.1795362

El-Awady, A. R., Arce, R. M., and Cutler, C. W. (2015). Dendritic Cells: Microbial Clearance Via Autophagy and Potential Immunobiological Consequences for Periodontal Disease. *Periodontol* 2000 (69), 160–180. doi: 10.1111/prd.12096

El-Awady, A., de Sousa Rabelo, M., Meghil, M. M., Rajendran, M., Elashiry, M., Stadler, A. F., et al. (2019). Polymicrobial Synergy Within Oral Biofilm Promotes Invasion of Dendritic Cells and Survival of Consortia Members. *NPJ Biofilms Microbiomes* 5, 11. doi: 10.1038/s41522-019-0084-7

El-Awady, A. R., Miles, B., Scisci, E., Kurago, Z. B., Palani, C. D., Arce, R. M., et al. (2015). Porphyromonas Gingivalis Evasion of Autophagy and Intracellular Killing by Human Myeloid Dendritic Cells Involves DC-SIGN-TLR2 Crosstalk. *PloS Pathog.* 10, e1004647. doi: 10.1371/journal.ppat.1004647

Elsayed, R., Kurago, Z., Cutler, C. W., Arce, R. M., Gerber, J., Celis, E., et al. (2020). Role of Dendritic Cell-Mediated Immune Response in Oral Homeostasis: A New Mechanism of Osteonecrosis of the Jaw. *FASEB J.* 34, 2595–2608. doi: 10.1096/fj.201901819RR

Feng, X., Feng, G., Xing, J., Shen, B., Tan, W., Huang, D., et al. (2014). Repeated Lipopolysaccharide Stimulation Promotes Cellular Senescence in Human Dental Pulp Stem Cells (Dpscs). *Cell Tissue Res.* 356, 369–380. doi: 10.1007/s00441-014-1799-7

Gorgoulis, V., Adams, P. D., Alimonti, A., Bennett, D. C., Bischof, O., Bishop, C., et al. (2019). Cellular Senescence: Defining a Path Forward. *Cell* 179, 813–827. doi: 10.1016/j.cell.2019.10.005

Hajishengallis, G. (2010). Too Old to Fight? Aging and Its Toll on Innate Immunity. *Mol. Oral. Microbiol.* 25, 25–37. doi: 10.1111/j.2041-1014.2009.00562.x

Hajishengallis, G., Darveau, R. P., and Curtis, M. A. (2012). The Keystone-Pathogen Hypothesis. *Nat. Rev. Microbiol.* 10, 717–725. doi: 10.1038/nrmicro2873

Hajishengallis, G., Liang, S., Payne, M. A., Hashim, A., Jotwani, R., Eskan, M. A., et al. (2011). Low-Abundance Biofilm Species Orchestrates Inflammatory Periodontal Disease Through the Commensal Microbiota and Complement. *Cell Host Microbe* 10, 497–506. doi: 10.1016/j.chom.2011.10.006

Hall, B. M., Balan, V., Gleiberman, A. S., Strom, E., Krasnov, P., Virtuoso, L. P., et al. (2017). p16(Ink4a) and Senescence-Associated β-Galactosidase Can Be

Induced in Macrophages as Part of a Reversible Response to Physiological Stimuli. *Aging (Albany NY)* 9, 1867–1884. doi: 10.18632/aging.101268

Hall, B. M., Balan, V., Gleiberman, A. S., Strom, E., Krasnov, P., Virtuoso, L. P., et al. (2016). Aging of Mice is Associated With p16(Ink4a)- and β-Galactosidase-Positive Macrophage Accumulation That can be Induced in Young Mice by Senescent Cells. *Aging (Albany NY)* 8, 1294–1315. doi: 10.18632/aging.100991

Hayflick, L., and Moorhead, P. S. (1961). The Serial Cultivation of Human Diploid Cell Strains. *Exp. Cell Res.* 25, 585–621. doi: 10.1016/0014-4827(61)90192-6

Helwa, I., Cai, J., Drewry, M. D., Zimmerman, A., Dinkins, M. B., Khaled, M. L., et al. (2017). A Comparative Study of Serum Exosome Isolation Using Differential Ultracentrifugation and Three Commercial Reagents. *PloS One* 12, e0170628. doi: 10.1371/journal.pone.0170628

Herranz, N., and Gil, J. (2018). Mechanisms and Functions of Cellular Senescence. *J. Clin. Invest* 128, 1238–1246. doi: 10.1172/JCI95148

Hovav, A. H. (2014). Dendritic Cells of the Oral Mucosa. *Mucosal Immunol.* 7, 27–37. doi: 10.1038/mi.2013.42

Humphreys, D., ElGhazaly, M., and Frisan, T. (2020). Senescence and Host-Pathogen Interactions. *Cells* 9 (7), 1747. doi: 10.3390/cells9071747

Jakhar, R., and Crasta, K. (2019). Exosomes as Emerging Pro-Tumorigenic Mediators of the Senescence-Associated Secretory Phenotype. *Int. J. Mol. Sci.* 20 (10), 2547. doi: 10.3390/ijms20102547

Jotwani, R., and Cutler, C. W. (2003). Multiple Dendritic Cell (DC) Subpopulations in Human Gingiva and Association of Mature DCs With CD4+ T-Cells in Situ. *J. Dent. Res.* 82, 736–741. doi: 10.1177/154405910308200915

Jotwani, R., Muthukuru, M., and Cutler, C. W. (2004). Increase in HIV Receptors/Co-Receptors/Alpha-Defensins in Inflamed Human Gingiva. *J. Dent. Res.* 83, 371–377. doi: 10.1177/154405910408300504

Jotwani, R., Palucka, A. K., Al-Quotub, M., Nouri-Shirazi, M., Kim, J., Bell, D., et al. (2001). Mature Dendritic Cells Infiltrate the T Cell-Rich Region of Oral Mucosa in Chronic Periodontitis: in Situ, In Vivo, and In Vitro Studies. *J. Immunol.* 167, 4693–4700. doi: 10.4049/jimmunol.167.8.4693

Jotwani, R., Pulendran, B., Agrawal, S., and Cutler, C. W. (2003). Human Dendritic Cells Respond to Porphyromonas Gingivalis LPS by Promoting a Th2 Effector Response In Vitro. *Eur. J. Immunol.* 33, 2980–2986. doi: 10.1002/eji.200324392

Jurk, D., Wang, C., Miwa, S., Maddick, M., Korolchuk, V., Tsolou, A., et al. (2012). Postmitotic Neurons Develop a p21-Dependent Senescence-Like Phenotype Driven by a DNA Damage Response. *Aging Cell* 11, 996–1004. doi: 10.1111/j.1474-9726.2012.00870.x

Kang, T.-W., Yevsa, T., Woller, N., Hoenicke, L., Wuestefeld, T., Dauch, D., et al. (2011). Senescence Surveillance of Pre-Malignant Hepatocytes Limits Liver Cancer Development. *Nature* 479, 547–551. doi: 10.1038/nature10599

Kim, S. H., Lechman, E. R., Bianco, N., Menon, R., Keravala, A., Nash, J., et al. (2005). Exosomes Derived From IL-10-Treated Dendritic Cells can Suppress Inflammation and Collagen-Induced Arthritis. *J. Immunol. (Baltimore Md 1950)* 174, 6440–6448. doi: 10.4049/jimmunol.174.10.6440

Li, L., Michel, R., Cohen, J., Decarlo, A., and Kozarov, E. (2008). Intracellular Survival and Vascular Cell-to-Cell Transmission of Porphyromonas Gingivalis. *BMC Microbiol.* 8, 26. doi: 10.1186/1471-2180-8-26

Linton, P. J., and Thoman, M. L. (2014). Immunosenescence in Monocytes, Macrophages, and Dendritic Cells: Lessons Learned From the Lung and Heart. *Immunol. Lett.* 162, 290–297. doi: 10.1016/j.imlet.2014.06.017

Li, G., Smithey, M. J., Rudd, B. D., and Nikolich-Žugich, J. (2012). Age-Associated Alterations in CD8α+ Dendritic Cells Impair CD8 T-Cell Expansion in Response to an Intracellular Bacterium. *Aging Cell* 11, 968–977. doi: 10.1111/j.1474-9726.2012.00867.x

Liu, J. Y., Souroullas, G. P., Diekman, B. O., Krishnamurthy, J., Hall, B. M., Sorrentino, J. A., et al. (2019). Cells Exhibiting Strong p16 (INK4a) Promoter Activation In Vivo Display Features of Senescence. *Proc. Natl. Acad. Sci. U.S.A.* 116, 2603–2611. doi: 10.1073/pnas.1818313116

Lu, C., Chen, J., Xu, H. G., Zhou, X., He, Q., Li, Y. L., et al. (2014). MIR106B and MIR93 Prevent Removal of Bacteria From Epithelial Cells by Disrupting ATG16L1-mediated Autophagy. *Gastroenterology* 146, 188–199. doi: 10.1053/j.gastro.2013.09.006

Luo, H., Mu, W. C., Karki, R., Chiang, H. H., Mohrin, M., Shin, J. J., et al. (2019). Mitochondrial Stress-Initiated Aberrant Activation of the NLRP3 Inflammasome Regulates the Functional Deterioration of Hematopoietic Stem Cell Aging. *Cell Rep.* 26, 945–954.e944. doi: 10.1016/j.celrep.2018.12.101

Machida, T., Tomofuji, T., Ekuni, D., Maruyama, T., Yoneda, T., Kawabata, Y., et al. (2015). MicroRNAs in Salivary Exosome as Potential Biomarkers of Aging. *Int. J. Mol. Sci.* 16, 21294–21309. doi: 10.3390/ijms160921294

Meghil, M. M., Tawfik, O. K., Elashiry, M., Rajendran, M., Arce, R. M., Fulton, D. J., et al. (2019). Disruption of Immune Homeostasis in Human Dendritic Cells Via Regulation of Autophagy and Apoptosis by Porphyromonas Gingivalis. *Front. Immunol.* 10, 2286. doi: 10.3389/fimmu.2019.02286

Michaud, D. S., Fu, Z., Shi, J., and Chung, M. (2017). Periodontal Disease, Tooth Loss, and Cancer Risk. *Epidemiol. Rev.* 39, 49–58. doi: 10.1093/epirev/mxx006

Moffatt-Jauregui, C. E., Robinson, B., de Moya, A. V., Brockman, R. D., Roman, A. V., Cash, M. N., et al. (2013). Establishment and Characterization of a Telomerase Immortalized Human Gingival Epithelial Cell Line. *J. Periodontal Res.* 48, 713–721. doi: 10.1111/jre.12059

Mondal, A. M., Horikawa, I., Pine, S. R., Fujita, K., Morgan, K. M., Vera, E., et al. (2013). p53 Isoforms Regulate Aging- and Tumor-Associated Replicative Senescence in T Lymphocytes. *J. Clin. Invest.* 123, 5247–5257. doi: 10.1172/JCI70355

Moretto, M. M., Lawlor, E. M., and Khan, I. A. (2008). Aging Mice Exhibit a Functional Defect in Mucosal Dendritic Cell Response Against an Intracellular Pathogen. *J. Immunol.* 181, 7977–7984. doi: 10.4049/jimmunol.181.11.7977

Murillo, O. D., Thistlethwaite, W., Rozowsky, J., Subramanian, S. L., Lucero, R., Shah, N., et al. (2019). Exrna Atlas Analysis Reveals Distinct Extracellular Rna Cargo Types and Their Carriers Present Across Human Biofluids. *Cell* 177, 463–477.e415. doi: 10.1016/j.cell.2019.02.018

Naylor, R. M., Baker, D. J., and van Deursen, J. M. (2013). Senescent Cells: A Novel Therapeutic Target for Aging and Age-Related Diseases. *Clin. Pharmacol. Ther.* 93, 105–116. doi: 10.1038/clpt.2012.193

Nogueira, V., Park, Y., Chen, C. C., Xu, P. Z., Chen, M. L., Tonic, I., et al. (2008). Akt Determines Replicative Senescence and Oxidative or Oncogenic Premature Senescence and Sensitizes Cells to Oxidative Apoptosis. *Cancer Cell* 14, 458–470. doi: 10.1016/j.ccr.2008.11.003

Nonaka, T., and Wong, D. T. W. (2017). Saliva-Exosomics in Cancer: Molecular Characterization of Cancer-Derived Exosomes in Saliva. *Enzymes* 42, 125–151. doi: 10.1016/bs.enz.2017.08.002

Park, S., Kang, S., Min, K. H., Woo Hwang, K., and Min, H. (2013). Age-Associated Changes in microRNA Expression in Bone Marrow Derived Dendritic Cells. *Immunol. Invest.* 42, 179–190. doi: 10.3109/08820139.2012.717328

Paroli, A. F., Gonzalez, P. V., Díaz-Luján, C., Onofrio, L. I., Arocena, A., Cano, R. C., et al. (2018). Nlrp3 Inflammasome and Caspase-1/11 Pathway Orchestrate Different Outcomes in the Host Protection Against Trypanosoma Cruzi Acute Infection. *Front. Immunol.* 9, 913. doi: 10.3389/fimmu.2018.00913

Pereira, L. F., de Souza, A. P., Borges, T. J., and Bonorino, C. (2011). Impaired In Vivo Cd4+ T Cell Expansion and Differentiation in Aged Mice is Not Solely Due to T Cell Defects: Decreased Stimulation by Aged Dendritic Cells. *Mech. Ageing Dev.* 132, 187–194. doi: 10.1016/j.mad.2011.03.005

Preshaw, P. M., Henne, K., Taylor, J. J., Valentine, R. A., and Conrads, G. (2017). Age-Related Changes in Immune Function (Immune Senescence) in Caries and Periodontal Diseases: A Systematic Review. *J. Clin. Periodontol.* 44 Suppl 18, S153–S177. doi: 10.1111/jcpe.12675

Qin, Z. Y., Gu, X., Chen, Y. L., Liu, J. B., Hou, C. X., Lin, S. Y., et al. (2020). Tolllike Receptor 4 Activates the NLRP3 Inflammasome Pathway and Periodontal Inflammaging by Inhibiting Bmi1 Expression. *Int. J. Mol. Med.* 47 (1), 137–150. doi: 10.3892/ijmm.2020.4787

Rajendran, M., Looney, S., Singh, N., Elashiry, M., Meghil, M. M., El-Awady, A. R., et al. (2019). Systemic Antibiotic Therapy Reduces Circulating Inflammatory Dendritic Cells and Treg-Th17 Plasticity in Periodontitis. *J. Immunol.* 202, 2690–2699. doi: 10.4049/jimmunol.1900046

Ruhland, M. K., Loza, A. J., Capietto, A. H., Luo, X., Knolhoff, B. L., Flanagan, K. C., et al. (2016). Stromal Senescence Establishes an Immunosuppressive Microenvironment That Drives Tumorigenesis. *Nat. Commun.* 7, 11762. doi: 10.1038/ncomms11762

Ryder, M. I. (2020). Porphyromonas Gingivalis and Alzheimer Disease: Recent Findings and Potential Therapies. *J. Periodontol.* 91 Suppl 1, S45–S49. doi: 10.1002/JPER.20-0104

Salminen, A. (2020). Activation of Immunosuppressive Network in the Aging Process. *Ageing Res. Rev.* 57, 100998. doi: 10.1016/j.arr.2019.100998

Sapieha, P., and Mallette, F. A. (2018). Cellular Senescence in Postmitotic Cells: Beyond Growth Arrest. *Trends Cell Biol.* 28, 595–607. doi: 10.1016/j.tcb.2018.03.003

Sargiacomo, C., Sotgia, F., and Lisanti, M. P. (2020). Covid-19 and Chronological Aging: Senolytics and Other Anti-Aging Drugs for the Treatment or Prevention of Corona Virus Infection? *Aging (Albany NY).* 12 (8), 6511–6517. doi: 10.18632/aging.103001

Schwechheimer, C., and Kuehn, M. J. (2015). Outer-Membrane Vesicles From Gram-negative Bacteria: Biogenesis and Functions. *Nat. Rev. Microbiol.* 13, 605–619. doi: 10.1038/nrmicro3525

Shi, L., Zhao, Y., Fei, C., Guo, J., Jia, Y., Wu, D., et al. (2019). Cellular Senescence Induced by S100A9 in Mesenchymal Stromal Cells Through NLRP3 Inflammasome Activation. *Aging (Albany NY)* 11, 9626–9642. doi: 10.18632/aging.102409

Shurin, M. R., Shurin, G. V., and Chatta, G. S. (2007). Aging and the Dendritic Cell System: Implications for Cancer. *Crit. Rev. Oncol. Hematol.* 64, 90–105. doi: 10.1016/j.critrevonc.2007.03.002

Smith-Vikos, T., and Slack, F. J. (2012). MicroRNAs and Their Roles in Aging. *J. Cell Sci.* 125, 7–17. doi: 10.1242/jcs.099200

Song, L., Dong, G., Guo, L., and Graves, D. T. (2017). The Function of Dendritic Cells in Modulating the Host Response. *Mol. Oral. Microbiol.* 33 (1), 13–21. doi: 10.1111/omi.12195

Stark, A., Bushati, N., Jan, C. H., Kheradpour, P., Hodges, E., Brennecke, J., et al. (2008). A Single Hox Locus in Drosophila Produces Functional microRNAs From Opposite DNA Strands. *Genes Dev.* 22, 8–13. doi: 10.1101/gad.1613108

Swarbrick, S., Wragg, N., Ghosh, S., and Stolzing, A. (2019). Systematic Review of miRNA as Biomarkers in Alzheimer's Disease. *Mol. Neurobiol.* 56, 6156–6167. doi: 10.1007/s12035-019-1500-y

Teixeira, F. B., Saito, M. T., Matheus, F. C., Prediger, R. D., Yamada, E. S., Maia, C. S. F., et al. (2017). Periodontitis and Alzheimer's Disease: A Possible Comorbidity Between Oral Chronic Inflammatory Condition and Neuroinflammation. *Front. Aging Neurosci.* 9, 327. doi: 10.3389/fnagi.2017.00327

Tian, J., Popal, M. S., Zhao, Y., Liu, Y., Chen, K., and Liu, Y. (2019). Interplay Between Exosomes and Autophagy in Cardiovascular Diseases: Novel Promising Target for Diagnostic and Therapeutic Application. *Aging Dis.* 10, 1302–1310. doi: 10.14336/AD.2018.1020

Tyagi, R. K., Miles, B., Parmar, R., Garg, N. K., Dalai, S. K., Baban, B., et al. (2017). Human IDO-Competent, Long-Lived Immunoregulatory Dendritic Cells Induced by Intracellular Pathogen, and Their Fate in Humanized Mice. *Sci. Rep.* 7, 41083. doi: 10.1038/srep41083

Villarroya-Beltri, C., Gutierrez-Vazquez, C., Sanchez-Cabo, F., Perez-Hernandez, D., Vazquez, J., Martin-Cofreces, N., et al. (2013). Sumoylated hnRNPA2B1 Controls the Sorting of miRNAs Into Exosomes Through Binding to Specific Motifs. *Nat. Commun.* 4, 2980. doi: 10.1038/ncomms3980

Wengerodt, D., Schmeer, C., Witte, O. W., and Kretz, A. (2019). Amitosenescence and Pseudomitosenescence: Putative New Players in the Aging Process. *Cells* 8 (12), 1546. doi: 10.3390/cells8121546

Wu, Y., Dong, G., Xiao, W., Xiao, E., Miao, F., Syverson, A., et al. (2016). Effect of Aging on Periodontal Inflammation, Microbial Colonization, and Disease Susceptibility. *J. Dent Res.* 95, 460–466. doi: 10.1177/0022034515625962

Xie, H. (2015). Biogenesis and Function of Porphyromonas Gingivalis Outer Membrane Vesicles. *Future Microbiol.* 10, 1517–1527. doi: 10.2217/fmb.15.63

Zeituni, A. E., Carrion, J., and Cutler, C. W. (2010). Porphyromonas Ginigvalis-Dendritic Cell Interactions: Consequences for Coronary Artery Disease. *J. Oral. Microbiol.* 2, 5782. doi: 10.3402/jom.v2i0.5782

Zeituni, A. E., Jotwani, R., Carrion, J., and Cutler, C. W. (2009). Targeting of DC-SIGN on Human Dendritic Cells by Minor Fimbriated Porphyromonas Gingivalis Strains Elicits a Distinct Effector T Cell Response. *J. Immunol.* 183, 5694–5704. doi: 10.4049/jimmunol.0901030

Zeituni, A. E., McCaig, W., Scisci, E., Thanassi, D. G., and Cutler, C. W. (2010). The Native 67-Kilodalton Minor Fimbria of Porphyromonas Gingivalis Is a Novel Glycoprotein With DC-SIGN-targeting Motifs. *J. Bacteriol* 192, 4103–4110. doi: 10.1128/JB.00275-10

Zhang, W., Jiang, X., Bao, J., Wang, Y., Liu, H., and Tang, L. (2018). Exosomes in Pathogen Infections: A Bridge to Deliver Molecules and Link Functions. *Front. Immunol.* 9, 90. doi: 10.3389/fimmu.2018.00090

Zhang, P., Wang, Q., Nie, L., Zhu, R., Zhou, X., Zhao, P., et al. (2019). Hyperglycemia-Induced Inflamm-Aging Accelerates Gingival Senescence Via NLRC4 Phosphorylation. *J. Biol. Chem.* 294, 18807–18819. doi: 10.1074/jbc.RA119.010648

Conflict of Interest: The authors declare that the research was conducted in the absence of any commercial or financial relationships that could be construed as a potential conflict of interest.

frontiers in Cellular and Infection Microbiology

ORIGINAL RESEARCH
published: 13 September 2021
doi: 10.3389/fcimb.2021.714366

Tetracycline, an Appropriate Reagent for Measuring Bone-Formation Activity in the Murine Model of the *Streptococcus mutans*-Induced Bone Loss

Yuna Hirohashi[1†], *Shingo Kamijo*[1†], *Masud Khan*[1], *Masaomi Ikeda*[2], *Meiko Oki*[1], *Khairul Matin*[3,4], *Fatma Rashed*[1,5] *and Kazuhiro Aoki*[1*]

[1] *Department of Basic Oral Health Engineering, Graduate School of Medical and Dental Sciences, Tokyo Medical and Dental University, Tokyo, Japan,* [2] *Department of Oral Prosthetic Engineering, Graduate School of Medical and Dental Sciences, Tokyo Medical and Dental University, Tokyo, Japan,* [3] *Department of Cariology and Operative Dentistry, Graduate School of Medical and Dental Sciences, Tokyo Medical and Dental University, Tokyo, Japan,* [4] *Endowed Department of International Oral Health Science, Tsurumi University School of Dental Medicine, Tsurumi, Yokohama, Japan,* [5] *Department of Oral Biology, Faculty of Dentistry, Damanhour University, El Behera, Egypt*

OPEN ACCESS

Edited by:
Tomomi Hashizume-Takizawa, Nihon University, Japan

Reviewed by:
Yineng Han, Peking University School and Hospital of Stomatology, China
Natalie A Sims, University of Melbourne, Australia

***Correspondence:**
Kazuhiro Aoki
kazu.hpha@tmd.ac.jp

[†]*These authors have contributed equally to this work and share first authorship*

Specialty section:
This article was submitted to Microbiome in Health and Disease, a section of the journal Frontiers in Cellular and Infection Microbiology

Received: *25 May 2021*
Accepted: *20 August 2021*
Published: *13 September 2021*

Citation:
Hirohashi Y, Kamijo S, Khan M, Ikeda M, Oki M, Matin K, Rashed F and Aoki K (2021) Tetracycline, an Appropriate Reagent for Measuring Bone-Formation Activity in the Murine Model of the Streptococcus mutans-Induced Bone Loss. Front. Cell. Infect. Microbiol. 11:714366. doi: 10.3389/fcimb.2021.714366

Tetracycline is used as a fluorescent reagent to measure bone formation activity in bone histomorphometric analyses. However, there is a possibility to lead a different conclusion when it is used in a bacteria-infected murine model since the tetracycline is considered to work as an antibiotic reagent. There are non-antibiotic fluorescent reagents such as alizarin and calcein for measuring bone formation activity. The purpose of this study was to clarify whether tetracycline could be an appropriate reagent to measure bone formation activity in a murine bacterial model in the same way as a non-antibiotic fluorescent reagent. We used *Streptococcus mutans* (*S. mutans*), a normal inhabitant in the oral cavity and tetracycline-sensitive bacteria, for inducing the bacterial model. The murine bacterial model was generated by intravenously inoculating *S. mutans* to the tail vein, followed immediately by the injection of the first fluorescent reagent, and the second one was injected 2 days prior to euthanization. After one day of inoculation with *S. mutans*, the subcutaneously injected alizarin had a similar colony count derived from the liver and the bone marrow tissue compared to the phosphate buffered saline (PBS)-injected control group. On the other hand, subcutaneous injection of tetracycline led to a significantly lower colony count from the liver compared to alizarin- or calcein-injected group. However, on day seven, after *S. mutans* intravenous injections, bone mineral density of distal femurs was significantly reduced by the bacteria inoculation regardless of which fluorescent reagents were injected subcutaneously. Finally, *S. mutans* inoculation reduced bone-formation-activity indices in both the tetracycline-alizarin double-injected mice and the calcein-alizarin double-injected mice. These results suggested that a one-time injection of tetracycline did not affect bone formation indices in the *S. mutans*-induced bone loss model. Tetracycline could be used for measuring bone formation activity in the

same way as non-antibiotic fluorescent reagent such as calcein and alizarin, even in a tetracycline-sensitive bacterium-infected model.

Keywords: tetracycline, bone formation indices, fluorescent labeling, *Streptococcus. mutans*, bone loss

1 INTRODUCTION

Bone and immune cells share the same microenvironment and interact with each other in the bone marrow, and the bone itself provides a unique harbor for microorganisms (Tsukasaki and Takayanagi, 2019). Recently, a bacteriological challenge was reported to reduce bone mineral density and bone formation activity in cecal ligation and puncture model (Terashima et al., 2016). Although several lines of evidence showed the relationship between bone remodeling and *Porphyromonas gingivalis*, a periodontal disease-related bacteria (Kajiya et al., 2010; Zhang et al., 2014), the relationship between cariogenic bacteria and bone disorders has not yet been widely elucidated. *Streptococcus mutans* (*S. mutans*) is the most common facultative anaerobic gram-positive cocci found in the human oral cavity. It is considered to be the major cariogenic bacterium (Forssten et al., 2010) associated with pyogenic and other infections in various sites, including the mouth, heart, joints, skin, muscle, and central nervous system (Bergy and Holt, 1994). In addition, *S. mutans* have been reported as the most frequently detected species in cardiovascular patients with high detection rates in the heart valve and aneurysm wall specimens of 42.7% and 62.8%, respectively, when compared among oral bacteria (Nakano et al., 2009). It may also be associated with the development of deep cerebral microbleeds, intracerebral hemorrhage, and stroke, with a mechanism linked to chronic inflammation (Tonomura et al., 2016). On the other hand, the bone organ is now known to be interconnected with the nervous, endocrine, and immune system. The latter is closely related to the formation of osteoclasts and osteoblasts and their function (Okamoto et al., 2017). Therefore, it could be an interesting field of work to study the relationship between oral bacteria and bone metabolism, bone formation, and bone resorption. However, there is no established procedure in bone histomorphometric analyses to detect changes in bone formation activity, which can be measured using fluorescent reagents in a bacterium-infected model.

Bone histomorphometry was developed in the 1960s to quantify the balance between bone resorption and bone formation using human iliac biopsy samples administered with fluorescent material (Frost, 1969). Among the bone histomorphometric parameters that quantify bone remodeling using undecalcified sections, the bone formation parameters are considered to be the most reliable indices with minor inter-observer variation (Compston et al., 1986). Usually, tetracycline, a fluorescent reagent, has been long-time used as a clinical bone formation marker that is generally administered to clarify bone formation activity in the morphological analyses using the undecalcified bone specimen (Weinstein et al., 1997; Parfitt, 2002). The measurement of bone formation activity utilizes the fact that a fluorescent reagent is deposited on the calcification front. Various indices of bone formation activity are calculated by measuring the distance between the double fluorescent labels of tetracycline administered at different time points (Dempster et al., 2013). Tetracycline is also applied to animal studies in bone histomorphometric analyses. Since tetracycline is an antibacterial drug, it cannot be ruled out the possibility that the results of experiments using bacteria may be misinterpreted. Over the past several decades, green and red fluorescence have become standard fluorescent reagents in a cell biological study using a confocal laser scanning microscope since a special filter set is necessary to detect tetracycline. Therefore, calcein, green fluorescence, and alizarin, a red fluorescence are preferably used compared to tetracycline, a yellow fluorescence. However, tetracycline is still used in animal studies for measuring bone formation activities, and it has not yet been investigated which fluorescent reagent is suitable for bacterial-infection experiments. Therefore, the purpose of this study was to examine fluorescent reagents suitable for evaluating bone formation activity using infected mice inoculated with *S. mutans* that are considered to be sensitive to tetracycline (Jarvinen et al., 1993). In addition, the effects of *S. mutans* inoculation on bone remodeling were also investigated.

2 MATERIALS AND METHODS

2.1 Preparation of *S. mutans* Suspension

A laboratory strain of cariogenic bacteria, *S. mutans* MT8148 strain (Biosafety level 1), was used for this *S. mutans*-infected model. After 16 hrs of preculture, fresh *S. mutans* were cultured with 5 ml of brain heart-infusion broth (BHI; Becton, Dickinson and Company, Sparks, MD, USA) at 37°C under anaerobic conditions using O_2-absorbing and CO_2-generating AnaeroPouch (Mitsubishi Gas Chemical Co., Inc., Tokyo, Japan) for 16 hrs, then centrifuged at 3,500 rpm (1330g), 4°C for 10 minutes as described elsewhere (Gyo et al., 2008). The pellet was dissolved with sterile phosphate buffer saline (PBS). The optical density of the bacterial suspension was adjusted by adding up PBS until an optical density of 490 nm (OD_{490}) = 1.0 [approximately 3.3×10^7 colony-forming unit (CFU)/ml]. The optical density was recorded using a spectrophotometer (Model 680 Microplate Reader: Bio-Rad, Hercules, CA, USA).

2.2 Experimental Design

Thirty-five twelve-week-old male BALB/c mice (Sankyo Labo Service Corporation, INC., Tokyo, Japan) were used. All animals were given a week to adapt to a 12-hour dark/light cycle under constant temperature (21 ± 1°C) with *ad libitum* access to food and water. All mice cages used were sterilized with the sterilized filtered top, and all procedures for feeding and cleaning mice

were performed inside a biological safety cabinet. Experimental procedures were approved by the Animal Care and Use Committee of Tokyo Medical and Dental University (Tokyo, Japan, authorization numbers: A2019-216C2). After one week adaptation period, the mice were inoculated with 0.3 ml of above *S. mutans* suspension intravenously into the tail vein of mice sedated with medetomidine hydrochloride (0.75 mg/kg; Domitor®, Zenoaq, Fukushima, Japan) subcutaneously injected into the back at a dose of 0.1 ml/10 g mice. The experimental protocol was schematically shown in **Figure 1**; one-day experiment (**Figure 1A**), seven-day experiment (**Figure 1B**).

2.2.1 One-Day Experiment

Fifteen mice were divided into five groups: 1) subcutaneously PBS-injected group immediately after intravenous PBS injection from the tail vein (negative control) (n = 3), 2) alizarin complexone (alizarin; Dojindo, Kumamoto, Japan) -injected group (n = 3), 3) calcein (Sigma-Aldrich) -injected group (n = 3), 4) tetracycline hydrochloride (tetracycline; FUJIFILM Wako Pure Chemical Corp., Osaka, Japan)-injected group (n = 3), and 5) demeclocycline hydrochloride (demeclocycline; Sigma-Aldrich, St. Luis, MO, USA) -injected group (n = 3) (**Figure 1A**). Later four groups received subcutaneous injections of fluorescent reagents using a 27 G needle and a 1 ml syringe (Terumo Corporation, Tokyo, Japan) at a dose of 20 mg/kg immediately after intravenous *S. mutans* inoculation to the tail vein. All mice were sedated and then sacrificed by cervical dislocation 24 hrs after intravenous PBS injection or *S. mutans* inoculation. The mice were immersed in 70% ethyl alcohol for several seconds, and then right femurs and liver were dissected for bacteriological analyses. The comparison between alizarin and PBS subcutaneous injections on the colony formation was shown in the **Supplementary Section**.

2.2.2 Seven-Day Experiment

Twenty mice were divided into four groups: 1) calcein and alizarin double-injected group with the intravenous PBS injection (n = 5), 2) tetracycline and alizarin double-injected group with the intravenous PBS injection (n = 5), 3) calcein and alizarin double-injected group with intravenous *S. mutans* inoculation (n = 5), and 4) tetracycline and alizarin double-injected group with intravenous *S. mutans* inoculation (n = 5) (**Figure 1B**). The first fluorescent reagent was subcutaneously injected immediately after intravenous PBS injection or the *S. mutans* inoculation on day 0. The second fluorescent injection was performed on day 5 after the intravenous PBS injection *S. mutans* inoculation at a dose of 20 mg/kg. On day 7, after the intravenous PBS injection or the

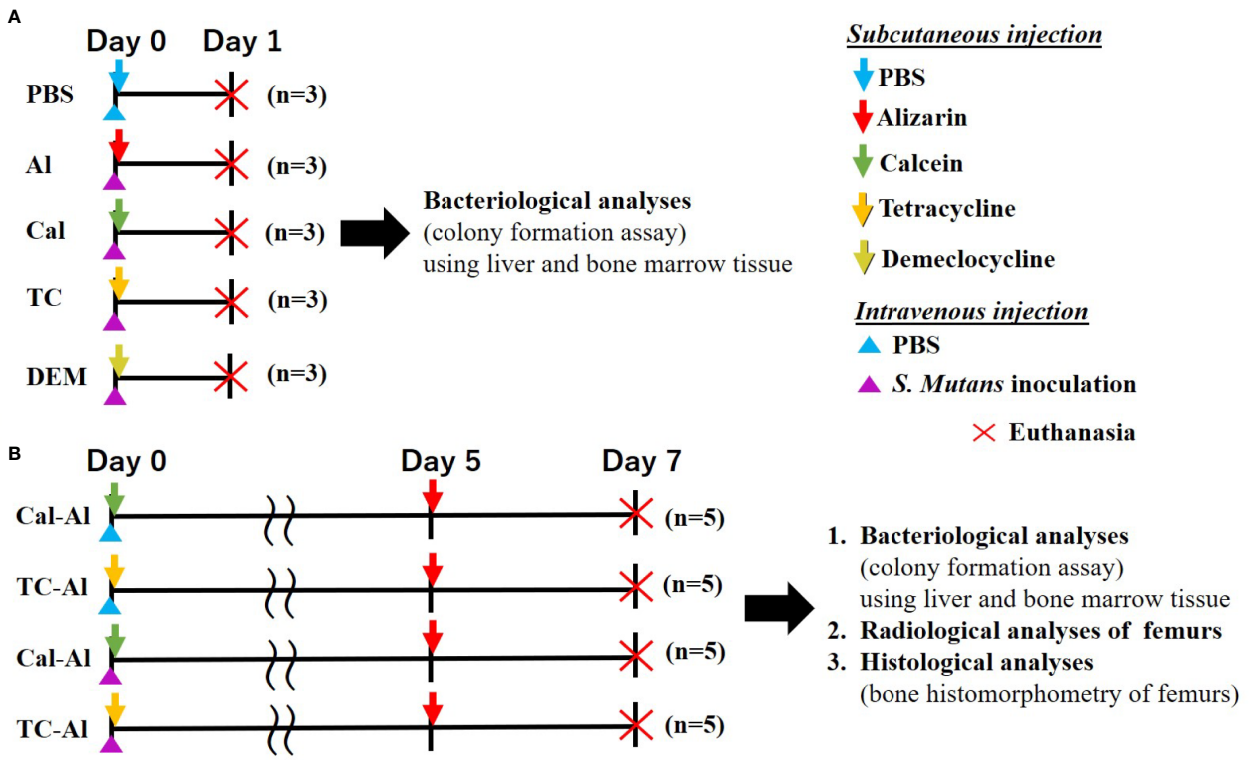

FIGURE 1 | Experimental design. **(A)** One-day experiment comparing the effects of 4 different fluorescent reagents on bacterial colony formation in *S. mutans*-infected mice. Subcutaneous injection of PBS to the intravenously injected mice used as a control **(B)** Seven-day experiment examining the effects of tetracycline versus calcein as a fluorescent reagent bacteriologically, radiologically, and histologically in the *S. mutans*-infected model comparing to the mice received an intravenous injection of PBS.

intravenous *S. mutans* inoculation, all mice were sedated and sacrificed by cervical dislocation. The right femurs and liver were dissected for bacteriological analyses in the same way as performed in the one-day experiment. The left femurs were also dissected for radiological and histological analyses.

The procedures of dissecting organs and tissues were all performed inside a biological safety cabinet to ensure an aseptic environment and prevent other bacterial contamination.

2.3 Bacteriological Analyses of Liver and Bone Marrow Tissue

The dissected liver and right femurs were used for colony measurement. The left lateral lobe of the liver tissue was taken and weighed. The tissue was suspended in 1 ml of PBS and then crushed in PBS with a homogenizer (UP100H, DKSH Japan K.K., Tokyo, Japan). Bone marrow was flushed out from the right femur using a syringe using 1 ml of PBS. The suspension (appx. 50μl each) of liver or bone marrow tissue was seeded on Difco™ Mitis-Salivarius Agar (Becton, Dickinson and Company) plate by using a spiral machine (EDDY JET, Central Science Trading Co., Ltd., Tokyo, Japan). Plates were grown under anaerobic conditions for 48 hrs at 37°C, and colony number was counted in microscopic images according to the manufacturer's protocol and presented as colony forming units (CFU/ml/mg).

2.4 Radiological Analyses

The dissected left femurs were fixed overnight in 3.7% phosphate-buffered formalin solution (pH 7.4) (FUJIFILM Wako Pure Chemical Corp.) at 4°C under constant shaking motion. All samples were then washed with PBS to remove formalin as much as possible. Soft X-ray images were taken with a cabinet X-ray apparatus (type SRO-M50, Sofron, Tokyo, Japan) under the conditions of 28 kV, 4 mA, to preliminarily visualize the calcified tissue and to observe the structural changes of the cancellous region of distal femur diaphysis.

Three-dimensional reconstruction images of femurs were obtained by microfocal computed tomography (μCT) (Scan Xmate-E090; Comscan, Kanagawa, Japan). Microarchitectural changes were then observed using a three-dimensional bone structure reconstruction system (TRI/3D-View; RATOC System Engineering, Tokyo, Japan).

Three-dimensional cross-sectional scanning was performed at 1.5-2.1 mm proximal starting from the distal end of femurs using peripheral quantitative computed tomography (pQCT; XCT Research SA +, Stratec Medizintechnik GmbH, Pforzheim, Germany). The total bone mineral density (BMD), trabecular BMD, and cortical bone thickness at the diaphysis of femurs were obtained from the average of 3 slices of each sample. We used 395 and 690 mg/cm^3 as thresholds of the trabecular BMD (peel mode 2) and cortical BMD, respectively.

2.5 Histological Assessments and Bone Histomorphometry

The dissected left femurs were embedded in Super Cryoembedding Medium compound (SCEM; Section-Lab Co. Ltd, Hiroshima, Japan) and frozen into blocks at −100°C in a freezing machine (UT2000F; Leica Microsystems, Tokyo, Japan). Micro CT images guided the direction of the section cuts of the embedded bone samples. The undecalcified frozen blocks were then cut into slices of 5 μm in thickness using a microtome (CM3050sIV; Leica Microsystems) and the adhesive film (Cryofilm type 2C, Section-Lab, Co., Ltd) for applying the Kawamoto method (Kawamoto, 2003).

The fluorescence-labeled sections were observed under an inverted fluorescence microscope (FSX100; Olympus, Tokyo, Japan), and histomorphometric analyses were performed using an image analyzing system (ImageJ software program, version 1.53i; NIH, Bethesda, MD, USA). All bone histomorphometric measurements were performed according to the standard protocols updated by the American Society of Bone and Mineral Research (Dempster et al., 2013). The region of interest (ROI) for the histomorphometric analyses was set in the secondary spongiosa of the 0.72 mm2 area (1.2 x 0.6 mm) rectangle starting from 0.6 mm proximal femur's growth plate from the growth plate of the distal femur. Measured parameters were shown as follows; structural parameters: bone volume per tissue volume (BV/TV), trabecular thickness (Tb.Th), trabecular number (Tb.N), and the trabecular separation (Tb.Sp); Bone formation parameters: mineral apposition rate (MAR), mineralizing surface (MS/BS), and bone formation rate (BFR) as bone surface reference. Bone resorption parameter: osteoclast number (N.Oc/BS). Some sections were stained with tartrate-resistant acid phosphatase (TRAP) and counterstained with methyl green to identify osteoclasts. TRAP-positive cells on the bone surface of the trabeculae with two or more nuclei were identified as osteoclasts.

2.6 Statistical Analysis

The number of mice of day-seven experiment was determined using the following formula based on the calculated number from the data of trabecular BMD in our pilot study.

$$n = 2(Z\alpha/2 + Z\beta)2\ SD2/\Delta 2$$

n, number of specimens, which was expected to get a significant difference in each experimental group

Zα/2 = 1.96: fixed number in the case of Significance = 5%

Zβ =0.84: the fixed number in the case of Power = 80%

SD, Standard deviation

Δ: The difference between the mean value; Av1 and Av2

The difference between the average and standard deviation was determined by the pilot study

$$n = \frac{2 * (1.96 + 0.84)^2 * (SD)^2}{(Av_1 - Av_2)^2}$$

Standard deviations and mean difference (SD=14, Av1 - Av2 = 25) were obtained for Total BMD from the results of the pilot study.

$$4.917 = \frac{2 * (1.96 + 0.84)^2 * (14)^2}{(25)^2}$$

And also, the effect size was calculated by statistical software (G*power 3.1.9.2) after statistical analysis (Faul et al., 2007;

Erdfelder et al., 2009). Effect size indicated 1.111 from the result of statistical analysis for ANOVA. This value indicates a strong statistical effect.

Regarding the one-day experiment, the number of mice was determined based on the data of colony counting in our pilot study in the same way as described above. The detail of the calculation for one-day experiment is shown in the **Supplementary Section**.

The distribution of data was analyzed by the Shapiro-Wilk test. The variance of data was analyzed by the Levene test. The comparison among the colony formation experimental groups was analyzed by the Kruskal Wallis test and the Wilcoxon rank-sum test. The comparison of the rest of the results was analyzed by the ANOVA and Tukey HSD test. P-value was performed with $p<0.05$ as having a significant difference. The data were expressed as mean ± standard deviation. Statistical procedures were performed using SPSS ver.27.0 (IBM, Chicago, USA).

3 RESULTS

3.1 Tetracycline Injection With the *S. mutans* Inoculation Affected the Colony Formation of Liver and Bone Marrow Tissue on Day One, but Calcein and Alizarin Did Not

We used a bacterial model induced by *S. mutans* to evaluate whether a tetracycline could be an appropriate fluorescent reagent for clarifying the changes of bone formation activity under an infected condition with the tetracycline-sensitive bacteria. Four kinds of fluorescent reagents, which have been often used in bone histomorphometric analyses, were injected in the *S. mutans*-infected model (**Figure 1A**). The dose of fluorescent reagents was the standard dose for bone histomorphometry in a mouse model.

Before starting the experiment shown in **Figure 1A**, we had preliminarily tested the effects of subcutaneous injection of alizarin, one of the representative fluorescent reagents to evaluate bone formation activity, on colony formation of liver and bone marrow tissue on day one after *S. mutans* intravenous inoculation compared to those of subcutaneous PBS injection. Similar numbers of colonies derived from liver and bone marrow tissue appeared in alizarin- and PBS- injected groups after one day of intravenous inoculation of *S. mutans*. Quantitative analyses of the number of colonies derived from the liver and bone marrow tissue showed no significant difference between alizarin- and PBS-injected groups ($p>0.05$, **Supplementary Figure 1**).

Tetracycline and demeclocycline injections immediately after the *S. mutans* inoculation lowered the number of colonies derived from liver and bone marrow tissue after one day of *S. mutans* intravenous inoculation (**Figures 2A, B**). Quantitative analyses of the number of colonies from the liver in the tetracycline-injected group showed a significant reduction compared to alizarin-single and calcein-single injected groups ($p<0.05$, **Figure 2C**). The culture plate of both liver and bone marrow tissues obtained from intravenously PBS-injected mice showed no colony formation on one day after subcutaneous PBS-injections, which was performed immediately after the intravenous *S. mutans* injections. The number of colonies derived from bone marrow similarly appeared as the number of colonies derived from the liver, although there was no significant reduction in the number of colonies due to the tetracycline injection (**Figures 2B, D**).

Liver-derived colonies after 7 days of *S. mutans* inoculation with subcutaneous injection of tetracycline on day zero and alizarin on day 5 after *S. mutans* inoculation also reduced compared to the calcein-alizarin double injected group. However, there was no significant difference between tetracycline-alizarin double injected and calcein-alizarin double injected groups ($p>0.05$, **Figure 3A**). In the observation of colonies derived from bone marrow tissue in mice injected with calcein-alizarin on day 7, one sample out of 5 samples showed colony formation and, while no colony formation was observed in the tetracycline-alizarin double injected group (**Figure 3B**). There was no colony formation appeared in both calcein-alizarin and tetracycline-alizarin injected groups on day 7 after the PBS-intravenously injection (**Figures 3A, B**).

3.2 *S. mutans* Inoculation Reduced Bone Mineral Density in the Tetracycline-Injected Group to the Same Extent as in the Calcein-Injected Group

Soft X-ray images showed a reduced radio-opacity at the cancellous bone region of distal femurs in the *S. mutans*-inoculated group compared to the PBS control group (**Figure 4A**). Nevertheless, we could not find apparent changes at the cancellous bone region in the tetracycline-alizarin double injected mice compared to the calcein-alizarin double injected mice among the *S. mutans*-inoculation mice (**Figure 4A**). Micro CT images revealed that the *S. mutans*-inoculated groups showed a clear reduction in the cancellous bone region in the distal diaphysis of femurs compared to the PBS-injected control groups (**Figure 4B**). On the other hand, no apparent difference was found between the calcein-alizarin and tetracycline-alizarin double injected groups (**Figure 4B**).

pQCT analyses confirmed these observations (**Figures 5A, B**). On day 7, after intravenous injection of PBS or *S. mutans*, total BMD, which includes both cancellous and cortical bone regions at the distal diaphysis of femurs, showed a significant decrease in the *S. mutans*-injected group compared to the PBS-injected group in the calcein-alizarin double injected mice ($p<0.05$). The trabecular BMD and cortical thickness also showed similar changes to the total BMD (**Figure 5B**). However, no significant difference between calcein-alizarin and tetracycline-alizarin double-injected groups in both PBS and *S. mutans*-injected groups ($p>0.05$, **Figure 5B**).

3.3 A Reduction of Bone Formation Activity in the *S. mutans*-Infected Model Occurred Regardless of the Tetracycline or Calcein Injection

We used undecalcified thin sections of femurs to clarify the effects of tetracycline fluorescence injection on bone structure,

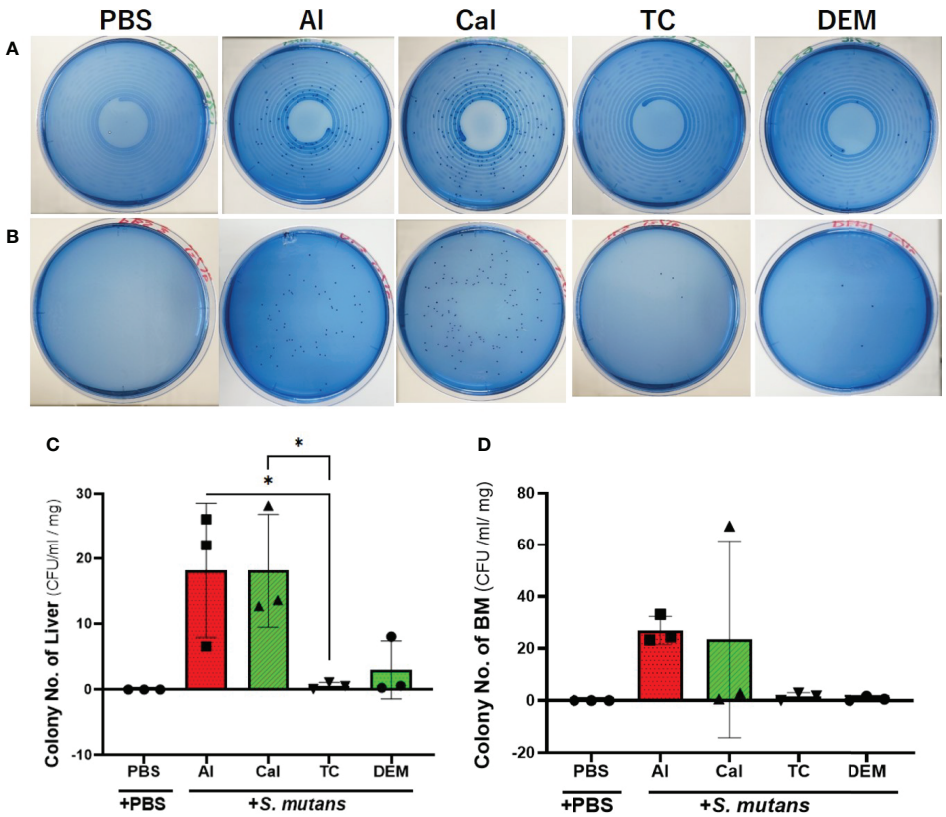

FIGURE 2 | Tetracycline-related fluorescent reagents affected colony formation. Bacteriological analysis of one-day experiment comparing the effects of 4 different fluorescent reagents on the bacterial colony formation in *S. mutans*-infected mice. **(A)** Culture-plate images of liver-derived colonies after one day of *S. mutans* inoculation. **(B)** Culture-plate images of bone marrow (BM)-derived colonies after one day of *S. mutans* inoculation. **(C)** The number of colonies derived from liver. **(D)** The number of colonies derived from bone marrow tissue. PBS, phosphate buffer saline; Al, alizarin; Ca, calcein; TC, tetracycline; DEM, demeclocycline. +PBS, intravenously PBS-injected group; +*S. mutans*, intravenously *S. mutans*-inoculated groups. The variance of data was analyzed by the Levene test. The comparison between groups was analyzed by the Kruskal Wallis test and the Wilcoxon rank-sum test. Values are expressed as the mean ± SD, *p < 0.05.

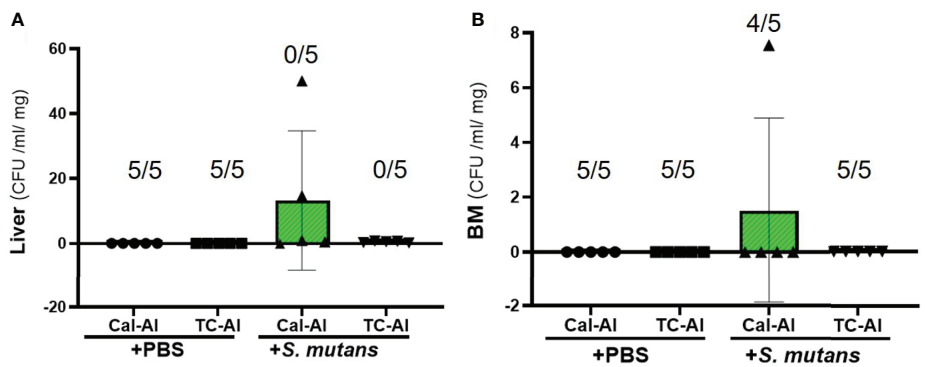

FIGURE 3 | Colony formation from the liver and bone marrow tissue on day 7 after intravenous injection of PBS or *S. mutans* inoculation. Comparison of the number of colonies derived from liver and bone marrow tissue after seven days of *S. mutans* inoculation. **(A)** The number of colonies derived from liver. **(B)** The number of colonies derived from bone marrow tissue. Cal-Al, mice received double injections of calcein and alizarin; TC-Al, mice received double injections of tetracycline and alizarin; +PBS, intravenously PBS-injected groups; +*S. mutans*, intravenously *S. mutans*-inoculated groups. The numerator and denominator numbers inside the bracket represent the numbers of the sample, which shows zero value and the number of all samples, respectively, i.e.: (5/5) means that 5 out of 5 have zero value. The variance of data was analyzed by the Levene test. The comparison between groups was analyzed by the Kruskal Wallis test and the Wilcoxon rank-sum test. Values are expressed as the mean ± SD.

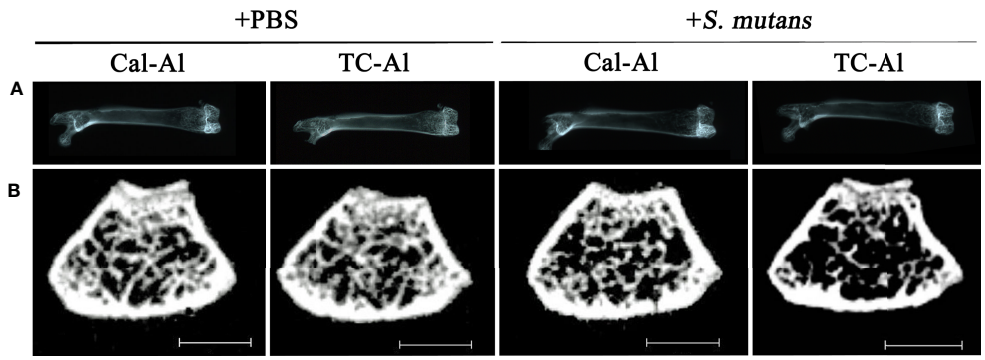

FIGURE 4 | Representative radiological examination of the femur. Radiological analyses of the femurs after seven days of intravenous injections of PBS or *S. mutans* inoculation. **(A)** Representative soft X-ray photographic images of femurs. **(B)** Representative μCT images of a cross-section at the diaphysis of the distal end of the femurs. Cal-Al, mice received double injections of calcein and alizarin; TC-Al, mice received double injections of tetracycline and alizarin; +PBS, intravenously PBS-injected groups; +*S. mutans*, intravenously *S. mutans*-inoculated groups. Scale bar = 1 mm.

bone formation, and resorption in the *S. mutans*-infected model using the bone histomorphometric analysis. On day 7 after intravenous inoculation of *S. mutans* or PBS injection, bone volume (BV/TV) and trabecular thickness (Tb.Th) were reduced significantly in the *S. mutans*-inoculated groups compared to the PBS-injected groups ($p<0.05$). However, no significant difference of these parameters was detected between calcein-alizarin and tetracycline-alizarin double injected groups ($p>0.05$, **Figures 6A, B**). The trabecular number showed a similar tendency to the two structural parameters mentioned above (**Figure 6C**). Trabecular separation showed a significant increase in the *S. mutans*-inoculated groups compared to the PBS-injected groups ($p<0.05$). However, no significant difference between calcein and tetracycline injections was appeared in the *S. mutans*-inoculated group ($p>0.05$, **Figure 6D**).

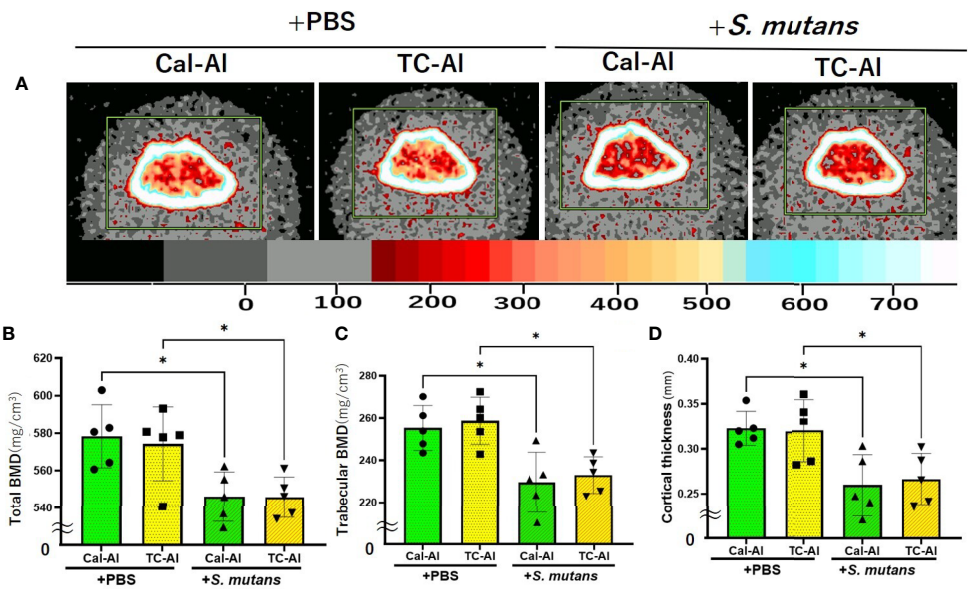

FIGURE 5 | *S. mutans* inoculation reduced bone mineral density. Quantitative analyses of the bone mineral content of the diaphysis of distal femurs after seven days of intravenous injection of PBS or *S. mutans* inoculation. **(A)** Representative pQCT image of the distal femurs for quantitative analyses. The color palette for bone mineral density is shown in the lower bar. **(B)** Total bone mineral density (Total density) of the distal femur; **(C)** Trabecular bone mineral density (Trabecular density) of the distal femur; **(D)** Cortical bone thickness (Cortical thickness) of the distal femur. Cal-Al, mice received double injections of calcein and alizarin; TC-Al, mice received double injections of tetracycline and alizarin; +PBS, intravenously PBS-injected groups; +*S. mutans*, intravenously *S. mutans*-inoculated groups. The variance of data was analyzed by the Levene test. The comparison between groups was analyzed by the ANOVA and Tukey HSD test. Values are expressed as the mean ± SD, *$p < 0.05$.

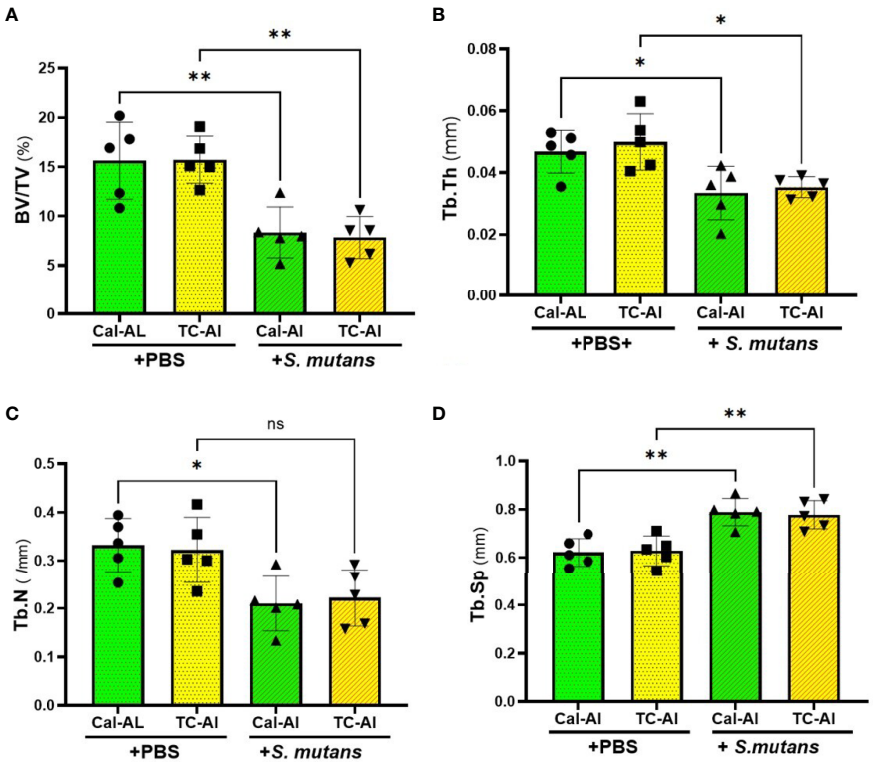

FIGURE 6 | *S. mutans* inoculation decreased structural parameters of bone. Quantitative analyses of the bone structural parameters of the distal femur after seven days of intravenous injection of PBS or *S. mutans* inoculation. **(A)** The ratio of bone volume (BV) to tissue volume (TV), **(B)** Trabecular thickness (Tb.Th), **(C)** Trabecular number (Tb.N), **(D)** Trabecular separation (Tb.Sp). Cal-Al, mice received double injections of calcein and alizarin; TC-Al, mice received double injections of tetracycline and alizarin; +PBS, intravenously PBS-injected groups; +*S. mutans*, intravenously *S. mutans*-inoculated groups. The variance of data was analyzed by the Levene test. The comparison between groups was analyzed by the ANOVA and Tukey HSD test. Values are expressed as the mean ± SD, *p < 0.05, **p < 0.01, ns, no statistically significant difference (p > 0.05).

Fluorescence images of undecalcified sections revealed that the double fluorescence labeling appeared to be reduced in the *S. mutans*-injected groups compared to the PBS-injected control groups regardless of calcein or tetracycline injections (**Figure 7A**). Quantitative analyses confirmed these observations (**Figures 7B, C**). A significant reduction of MAR, which is calculated from the intra-distance between double fluorescence labeling and shows a function of osteoblasts to form calcified tissues, was detected regardless of calcein or tetracycline injection (p<0.05, **Figure 7B**). The significant reduction of MS/BS, which indicates the active bone formation surface and reflects the number of active osteoblasts, was also detected (p<0.05, **Supplementary Figure 2**). In the same manner, as MAR and MS/BS, BFR, which indicates an amount of bone formed in a day in the ROI of the distal femurs, was significantly reduced compared to the PBS-injected group (p<0.05, **Figure 7C**). There was no significant difference on N.Oc/BS, which indicates a ratio of osteoclasts number per bone surface and a frequency to initiate bone remodeling among examined groups (p>0.05, **Figure 7D** and **Supplementary Figure 3**). As we observed the effects of tetracycline injection on the BMD and the structural parameters, all these bone formation and bone resorption-related parameters did not show any significant difference between the tetracycline-alizarin double injected groups and the calcein-alizarin double injected groups in both the PBS-injected and the *S. mutans*-inoculated groups (p>0.05, **Figures 6** and **7**).

4 DISCUSSION

We investigated the feasibility of using tetracycline to measure bone formation activity in a bacteria-infected mice model. The effects of four different fluorescent reagents on the colony formation of liver and bone marrow tissues were compared in the *S. mutans*-infected model. The tetracycline injection reduced the number of colonies derived from the liver after one day of *S. mutans* inoculation (**Figure 2C**). Radiological analyses of the femurs revealed that the *S. mutans* inoculation reduced the total and trabecular BMD in both the calcein-alizarin and the tetracycline-alizarin double injected groups. However, there was no significant difference in these radiological indices between calcein and tetracycline (**Figure 5**). The *S. mutans*-inoculated groups showed an osteopenic phenotype, a significantly lower in structural parameters such as bone volume and trabecular thickness, associated with a significantly

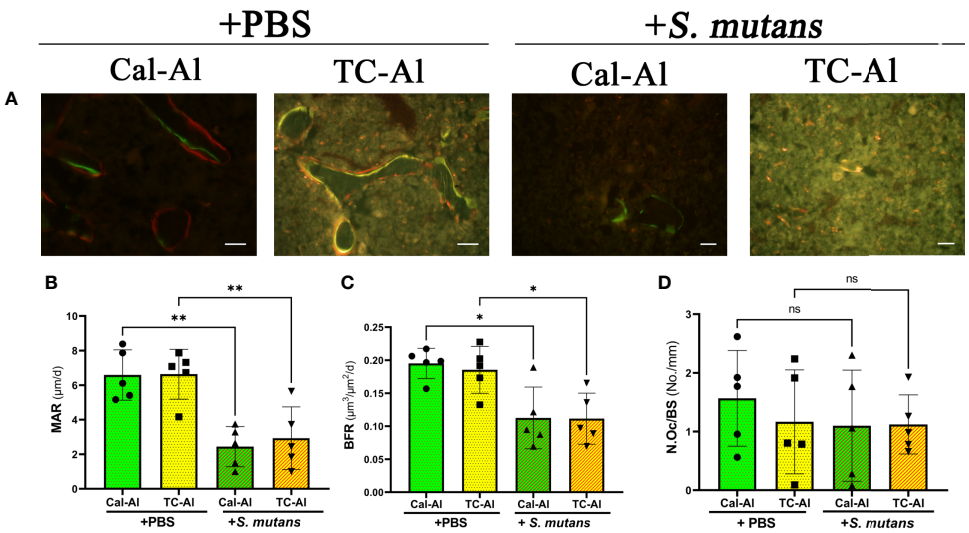

FIGURE 7 | *S. mutans* inoculation decreased structural bone formation parameters. Histological images and bone histomorphometry after seven days of intravenous injection of PBS or *S. mutans* inoculation. **(A)** Representative fluorescence images of undecalcified frozen sections: calcein (green), tetracycline (yellow), and alizarin (red). Scale bar = 50 μm. Quantitative analyses of bone formation activity were performed using standard bone histomorphometric measurement techniques based on the calcein/tetracycline- and alizarin-labeled surface in the ROI, which was described in the *Materials and Methods* section. **(B)** Mineral apposition rate (MAR), **(C)** Bone formation rate (BFR), **(D)** Number of osteoclast per bone surface (N.Oc/BS). Cal-Al, mice received double injections of calcein and alizarin; TC-Al, mice received double injections of tetracycline and alizarin; +PBS, intravenously PBS-injected groups; +*S. mutans*, intravenously *S. mutans*-inoculated groups. The variance of data was analyzed by the Levene test. The comparison between groups was analyzed by the ANOVA and Tukey HSD test. Values are expressed as the mean ± SD, *$p < 0.05$, **$p < 0.01$, ns, no significant difference.

higher value in trabecular separation (**Figure 6**) compared to the PBS-injected groups. Then again, no significant difference in these structural parameters was found between the calcein-alizarin and the tetracycline-alizarin double injected groups (**Figure 6**). Finally, fluorescence images of undecalcified sections revealed that bone formation activity was significantly lower in the *S. mutans* groups compared to the PBS control groups. It had no significant difference between the calcein- and tetracycline-injected groups (**Figures 7A–C**). Bone resorption parameter showed similar values regardless of calcein- or tetracycline-injection (**Figure 7D**). These results suggest that one-time injection of tetracycline to measure bone formation indices did not affect bone formation and resorption in the bacterial model induced by tetracycline-sensitive bacteria even though it could reduce the live bacteria derived from the liver of the infected mice (**Figure 2C**).

As described above, a one-time injection of tetracycline did not ameliorate the reduction of BMD and bone formation caused by *S. mutans*, despite its ability to kill bacteria shown in **Figure 2**, suggesting that tetracycline might not interfere with the inhibitory effects of *S. mutans* on bone formation in this study. We might explain this discrepancy from the pharmacological point of view. When the estimated blood concentration of tetracycline was calculated from the usual fluoresce dose for bone histomorphometry, it would be around 200 μg/ml if the injection was performed intravenously. In this study, we performed a subcutaneous injection, which was thought to deliver less than one-third (66.7 μg/ml) of the maximum blood concentration in case of intravenous injection. The estimated concentration was still considerably higher than the minimum inhibitory concentration (MIC) of tetracycline for *S. mutans* (Jarvinen et al., 1993). This estimated concentration of tetracycline might explain the inhibitory effects on colony formation of the tissues on day one (**Figure 2**). However, antibiotics are usually administered periodically to maintain the blood concentration above MIC, having antibacterial effects *in vivo*. In this study, we injected tetracycline only once simultaneously with the *S. mutans* inoculation and did not inject it periodically. This tetracycline-injection schedule to measure the bone formation activity might not affect bone remodeling because tetracycline injection could not recover the *S. mutans*-induced decrease of BMD and bone formation (**Figures 5** and **7**).

On the other hand, there was a possibility that tetracycline might directly affect osteoblasts and osteoclasts since tetracycline is reported to promote osteoblast differentiation (Sasaki et al., 1991) and inhibit osteoclastogenesis *via* MMP-9 inhibition (Kim et al., 2019). This study did not show any tetracycline-induced increase of bone formation and decreased osteoclast number regardless of the PBS or the *S. mutans* injection. Therefore, from our results, we conclude that tetracycline could be an appropriate fluorescent reagent for investigating bone formation activity, and it could be used even in a tetracycline-sensitive bacterium-induced model. From the histomorphometric point of view, tetracycline could also be explained as an appropriate fluorescence to clarify bone formation activity. The main concern when tetracycline is used in the younger age of mice compared to our study is the discoloration of the teeth in the dental field of work, and stronger effects of tetracycline as antibiotics (Cohlan and Bevelander, 1963). However, we

assumed the effects of tetracycline in the younger mice on bone remodeling could not be discussed since the remodeling activity in the growing stage appears much lower than that in the adult stage and the higher rate of bone modeling at the growing stage would definitely affect the bone remodeling indices, which could not lead the evidence to show the effects of the antibiotic, tetracycline by using younger mice than 12 week-old. Usually, two kinds of fluorescent reagents are administered at least several days apart to measure bone formation of the bone specimen. If only one type of reagent is used and injected twice, it would sometimes be difficult to distinguish the two-fluorescent labeling along the bone surface to measure MAR since the clarification of the order of the fluorescent injections and the direction of forming bone is necessary to measure MAR. In our study, tetracycline was administered only once on the day of *S. mutans* injection, indicating that the effects of the antibiotic are very limited. Therefore, tetracycline injection could scarcely matter so long as it is injected only once during the experimental period for the histomorphometric analyses.

Several concerns remain in this study to clarify the effects of the *S. mutans* injection on the colony formation of liver and bone marrow tissues. First, we did not perform any tests to confirm whether the colonies formed were *S. mutans*. However, the colonies we observed could be mainly derived from *S. mutans* since the PBS-injected control group under the condition of no *S. mutans* inoculation did not show any colony formation (**Figures 2** and **3**). Of course, it is necessary to perform the polymerase chain reaction (PCR) following the sequence reading of the PCR products or to use the modified *S. mutans*, such as *S. mutans* inserted a luciferase gene cassette to determine whether the colony we observed was *S. mutans*. Second, we could not clarify whether the bacteria remaining in the liver on day one would grow again until the day of sacrifice. As shown in **Figure 3A**, the colony formation derived from the liver was observed even though the numbers of the colonies were limited on the plate from both the calcein-alizarin double injected and the tetracycline-alizarin double injected groups on day seven after *S. mutans* inoculation. Still, we could not determine whether these colonies on day seven were also derived from *S. mutans* for the same reason described above. Therefore, time-course studies should be examined at shorter time intervals, like three or five days other than performing the PCR analyses, and the recovery of *S. mutans* might be detected. Third, we could not explain why the colonies derived from bone marrow tissue varied very much, and the number of the colonies was less compared to the liver tissue (**Figures 2** and **3**). In this study, bone marrow tissue was examined as it is the origin of bone cells and subsequently reflects the bacterial cell's effect on bone metabolism. The liver tissue was selected for clarifying the growth of the bacteria as it is known to work as a lymphoid tissue in response to the bacterial attack, and it plays a major role in rapidly clearing bacteria from the bloodstream (Gregory et al., 1996). Further studies are necessary to clarify the immune response and/or the ability of the tissue on the clearance of bacteria, comparing bone marrow tissue with the liver.

In this study, we found a significant reduction of the BMD of femurs on day seven after the intravenous injection of 1×10^7 CFU *S. mutans*. Although the amount of the bacteria injected was determined according to a recent study (Naka et al., 2016), still, we do not know how much amount of *S. mutans* could reduce the BMD of femurs and whether the amount of the bacteria we used in this study reflects a low-hygiene circumstance of the oral cavity in humans. Furthermore, there is currently no data available that accurately represents the average amount of *S. mutans*, which enters the bloodstream after a dental procedure or daily tooth brushing. Continuous investigation is necessary to establish a new mice model to clarify the relationship between oral bacteria and systemic diseases. On the other hand, the reduction of the BMD induced in the other bacterial model was reported (Terashima et al., 2016). Their results support our present data, showing that the mechanism of the BMD reduction in their bacterial model is explained by reducing bone formation activity and no significant changes of bone resorption index (**Figure 7**). Since MS/BS reflects the active bone-forming surface per bone surface, the values of MS/BS are closely related to the osteoblast number or osteoblast surface per bone surface. As we showed the reduced MS/BS compared to the PBS control group (**Supplementary Figure 2**), osteoblast number might be reduced in our bacterial model. Terashima et al. also proposed the importance of osteoblasts, which produced interleukin 7 to maintain common lymphocyte precursors in the bone marrow tissue. Since these lymphocyte precursors are responsible for producing both T cells and B cells, the reduced osteoblasts might lead to immunosuppression in our *S. mutans*-infected model by reducing the number of lymphocytes. Regarding the relationship between *S. mutans* and bone resorption, we did not observe any significant increase in bone resorption index, as shown in **Figure 7D** although it was reported that Mutan, a protein extract from *S. mutans*, induced osteoclast differentiation and promoted alveolar bone loss (Kwon et al., 2016). Additional studies are necessary to clarify whether the *S. mutans*-induced immune response causes an increase of osteoclasts or *S. mutans* directly affect osteoclast differentiation.

5 CONCLUSIONS

Tetracycline was shown to be an appropriate fluorescent reagent to measure a bone formation activity even in the tetracycline-sensitive bacterium-induced animal model when it was injected once during an experimental period. In addition, intravenous inoculation of *S. mutans* led to the reduction of bone volume, probably by reducing the bone formation activity without changing osteoclastogenesis.

DATA AVAILABILITY STATEMENT

The raw data supporting the conclusions of this article will be made available by the authors, without undue reservation.

ETHICS STATEMENT

The animal study was reviewed and approved by The Animal Care and Use Committee of Tokyo Medical and Dental University (Tokyo, Japan, authorization numbers: A2019-216C2.

AUTHOR CONTRIBUTIONS

YH performed all experiments and drafted the manuscript. SK helped in all experiments, including radiological analyses and statistics of the data, and revised the manuscript. They have contributed equally to this work and share the first authorship. MK contributed to all animal experiments especially helping intravenous injections to the tail vein, taking soft X-ray images, and making undecalcified sections. MI performed the statistics required for this paper. MO provided suggestions and significantly revised and refined the manuscript. KM supervised the bacterial culture section. FR contributed to the experimental part, analyzed data, and wrote the manuscript. KA received a grant for this project, conceived the idea, reviewed the drafts, supervised the writing process, and edited this manuscript. All authors contributed to the article and approved the submitted version.

FUNDING

This work was supported in part by the Company of Biologists' grants-Travelling Fellowship - 232 Number: JCSTF1908265 to FR; Nakatani Foundation for Advancement of Measuring Technologies 233 in Biomedical Engineering, Technical Exchange Grant (study in Japan) to KA; and the Japan Society for the 234 Promotion of Science (18K19637 and 19H01068 to KA).

ACKNOWLEDGMENTS

We would like to express our gratitude to Dr. Yukihiko Tamura (Section of Pharmacology, Department of Hard Tissue Engineering, Graduate School of Medical and Dental Sciences, Tokyo Medical and Dental University), Satowa Nakamura, Mana Abe, and everyone who cooperated regarding this experiment in the course of Oral Health Engineering, Faculty of Dentistry, Tokyo Medical and Dental University.

SUPPLEMENTARY MATERIAL

The Supplementary Material for this article can be found online at: https://www.frontiersin.org/articles/10.3389/fcimb.2021.714366/full#supplementary-material

REFERENCES

Bergy, D., and Holt, J. (1994). *Bergey's Manual of Determinative Bacteriology (9th Ed)* (Baltimore: Williams & Wilkins).

Cohlan, S. Q., and Bevelander G, T. T. (1963). Growth Inhibition of Premature Receiving Tetracycline: A Clinical and Laboratory Investigation of Tetracycline-Induced Bone Fluorescence. *Am. J. Dis. Children* 105 (5), 453–461. doi: 10.1001/archpedi.1963.02080040455005

Compston, J. E., Vedi, S., and Stellon, A. J. (1986). Inter-Observer and Intra-Observer Variation in Bone Histomorphometry. *Calcif. Tissue Int.* 38 (2), 67–70. doi: 10.1007/BF02556831

Dempster, D. W., Compston, J. E., Drezner, M. K., Glorieux, F. H., Kanis, J. A., Malluche, H., et al. (2013). Standardized Nomenclature, Symbols, and Units For Bone Histomorphometry: A 2012 Update of the Report of the ASBMR Histomorphometry Nomenclature Committee. *J. Bone Miner. Res.* 28 (1), 2–17. doi: 10.1002/jbmr.1805

Erdfelder, E., FAul, F., Buchner, A., and Lang, A. G. (2009). Statistical Power Analyses Using G*Power 3.1: Tests for Correlation and Regression Analyses. *Behav. Res. Methods* 41 (4), 1149–1160. doi: 10.3758/BRM.41.4.1149

Faul, F., Erdfelder, E., Lang, A.-G., and Buchner, A. (2007). G * Power 3 : A Flexible Statistical Power Analysis Program for the Social, Behavioral, and Biomedical Sciences. *Behav. Res. Method* 39 (2), 175–191. doi: 10.3758/BF03193146

Forssten, S. D., Björklund, M., and Ouwehand, A. C. (2010). Streptococcus Mutans, Caries and Simulation Models. *Nutrients* 2 (3), 290–298. doi: 10.3390/nu2030290

Frost, H. M. (1969). Tetracycline-Based Histological Analysis of Bone Remodeling. *Calcified Tissue Res.* 3 (1), 211–237. doi: 10.1007/BF02058664

Gregory, S. H., Sagnimeni, A. J., and Wing, E. J. (1996). Bacteria in the Bloodstream Are Trapped in the Liver and Killed by Immigrating Neutrophils. *J. Immunol.* 157 (6), 2514–2520.

Gyo, M., Nikaido, T., Okada, K., Yamauchi, J., Tagami, J., and Matin, K. (2008). Surface Response of Fluorine Polymer-Incorporated Resin Composites to Cariogenic Biofilm Adherence. *Appl. Environ. Microbiol.* 74 (5), 1428–1435. doi: 10.1128/AEM.02039-07

Jarvinen, H., Tenovuo, J., and Huovinen, P. (1993). *In Vitro* Susceptibility of Streptococcus Mutans to Chlorhexidine and Six Other Antimicrobial Agents. *Antimicrobial Agents Chemother.* 37 (5), 1158–1159. doi: 10.1128/AAC.37.5.1158

Kajiya, M., Giro, G., Taubman, M. A., Han, X., Mayer, M. P. A., and Kawai, T. (2010). Role of Periodontal Pathogenic Bacteria in RANKL-Mediated Bone Destruction in Periodontal Disease. *J. Oral. Microbiol.* (1-16) 5532. doi: 10.3402/jom.v2i0.5532

Kawamoto, T. (2003). Use of A New Adhesive Film for The Preparation of Multi-Purpose Fresh-Frozen Sections From Hard Tissues, Whole-Animals, Insects And Plants. *Arch. Histol. Cytol.* 66 (2), 123–143. doi: 10.1679/aohc.66.123

Kim, Y., Kim, J., Lee, H., Shin, W. R., Lee, S., Lee, J., et al. (2019). Tetracycline Analogs Inhibit Osteoclast Differentiation by Suppressing MMP-9-Mediated Histone H3 Cleavage. *Int. J. Mol. Sci.* 20 (16), 4038. doi: 10.3390/ijms20164038

Kwon, H. J., Kim, J. M., Han, K. I., Jung, E. G., Kim, Y. H., Patnaik, B. B., et al. (2016). Mutan: A Mixed Linkage α-[(1, 3)-and (1, 6)]-D-Glucan From Streptococcus Mutans, That Induces Osteoclast Differentiation and Promotes Alveolar Bone Loss. *Carbohydr. Polym.* 137, 561–569. doi: 10.1039/C8RA10263E

Naka, S., Hatakeyama, R., Takashima, Y., Matsumoto-Nakano, M., Nomura, R., and Nakano, K. (2016). Contributions of Streptococcus Mutans Cnm and PA Antigens to Aggravation of Non-Alcoholic Steatohepatitis in Mice. *Sci. Rep.* 6 (1), 1–13. doi: 10.1371/journal.pone.0159613

Nakano, K., Nemoto, H., Nomura, R., Inaba, H., Yoshioka, H., Taniguchi, K., et al. (2009). Detection of Oral Bacteria in Cardiovascular Specimens. *Oral. Microbiol. Immunol.* 24 (1), 64–68. doi: 10.1111/j.1399-302X.2008.00479.x

Okamoto, K., Nakashima, T., Shinohara, M., Negishi-Koga, T., Komatsu, N., Terashima, A., et al. (2017). Osteoimmunology: The Conceptual Framework Unifying the Immune and Skeletal Systems. *Physiol. Rev.* 97 (4), 1295–1349. doi: 10.1152/physrev.00036.2016

Parfitt, A. M. (2002). Misconceptions (2): Turnover Is Always Higher in Cancellous Than in Cortical Bone. *Bone* 30 (6), 807–809. doi: 10.1016/S8756-3282(02)00735-4

Sasaki, T., Kaneko, H., Ramamurthy, N. S., and Golub, L. M. (1991). Tetracycline Administration Restores Osteoblast Structure And Function During Experimental Diabetes. *Anat. Rec.* 231 (1), 25–34. doi: 10.1002/ar.1092310105

Terashima, A., Okamoto, K., Nakashima, T., Akira, S., Ikuta, K., and Takayanagi, H. (2016). Sepsis-Induced Osteoblast Ablation Causes Immunodeficiency. *Immunity* 44 (6), 1434–1443. doi: 10.1016/j.immuni.2016.05.012

Tonomura, S., Ihara, M., Kawano, T., Tanaka, T., Okuno, Y., Saito, S., et al. (2016). Intracerebral Hemorrhage and Deep Microbleeds Associated With Cnm-Positive Streptococcus Mutans; A Hospital Cohort Study. *Sci. Rep.* 6, 1–8. doi: 10.1038/srep20074

Tsukasaki, M., and Takayanagi, H. (2019). Osteoimmunology: Evolving Concepts in Bone–Immune Interactions in Health and Disease. *Nat. Rev. Immunol.* 19 (10), 626–642. doi: 10.1038/s41577-019-0178-8

Weinstein, R. S., Jilka, R. L., Michael Parfitt, A., and Manolagas, S. C. (1997). The Effects of Androgen Deficiency on Murine Bone Remodeling and Bone Mineral Density are Mediated *via* Cells of the Osteoblastic Lineage. *Endocrinology* 138 (9), 4013–4021. doi: 10.1210/endo.138.9.5359

Zhang, W., Ju, J., Rigney, T., and Tribble, G. (2014). Porphyromonas Gingivalis Infection Increases Osteoclastic Bone Resorption and Osteoblastic Bone Formation in a Periodontitis Mouse Model. *BMC Oral. Health* 14 (1), 1–9. doi: 10.1186/1472-6831-14-89

Conflict of Interest: The authors declare that the research was conducted in the absence of any commercial or financial relationships that could be construed as a potential conflict of interest.

Publisher's Note: All claims expressed in this article are solely those of the authors and do not necessarily represent those of their affiliated organizations, or those of the publisher, the editors and the reviewers. Any product that may be evaluated in this article, or claim that may be made by its manufacturer, is not guaranteed or endorsed by the publisher.

Advantages of publishing in Frontiers

OPEN ACCESS
Articles are free to read for greatest visibility and readership

FAST PUBLICATION
Around 90 days from submission to decision

HIGH QUALITY PEER-REVIEW
Rigorous, collaborative, and constructive peer-review

TRANSPARENT PEER-REVIEW
Editors and reviewers acknowledged by name on published articles

Frontiers
Avenue du Tribunal-Fédéral 34
1005 Lausanne | Switzerland

Visit us: www.frontiersin.org
Contact us: frontiersin.org/about/contact

REPRODUCIBILITY OF RESEARCH
Support open data and methods to enhance research reproducibility

DIGITAL PUBLISHING
Articles designed for optimal readership across devices

FOLLOW US
@frontiersin

IMPACT METRICS
Advanced article metrics track visibility across digital media

EXTENSIVE PROMOTION
Marketing and promotion of impactful research

LOOP RESEARCH NETWORK
Our network increases your article's readership